frontiers | Research Topics

Placental dysfunction in pregnancy: endocrine and metabolic mechanisms in preeclampsia, FGR, diabetes, and hypertension

Edited by
Sruthi Alahari and Leonardo Ermini

Published in
Frontiers in Endocrinology

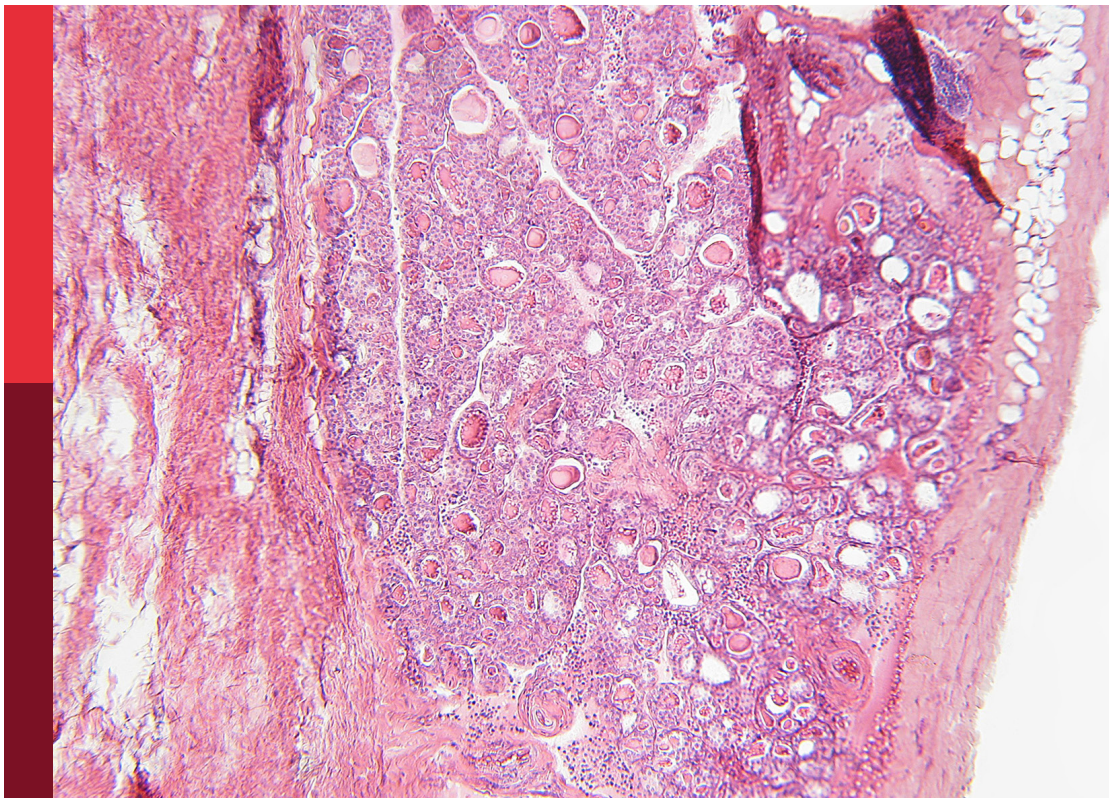

ISSN 1664-8714
ISBN 978-2-8325-7349-5
DOI 10.3389/978-2-8325-7349-5

Generative AI statement
Any alternative text (Alt text) provided alongside figures in the articles in this ebook has been generated by Frontiers with the support of artificial intelligence and reasonable efforts have been made to ensure accuracy, including review by the authors wherever possible. If you identify any issues, please contact us.

About Frontiers

Frontiers is more than just an open access publisher of scholarly articles: it is a pioneering approach to the world of academia, radically improving the way scholarly research is managed. The grand vision of Frontiers is a world where all people have an equal opportunity to seek, share and generate knowledge. Frontiers provides immediate and permanent online open access to all its publications, but this alone is not enough to realize our grand goals.

Frontiers journal series

The Frontiers journal series is a multi-tier and interdisciplinary set of open-access, online journals, promising a paradigm shift from the current review, selection and dissemination processes in academic publishing. All Frontiers journals are driven by researchers for researchers; therefore, they constitute a service to the scholarly community. At the same time, the *Frontiers journal series* operates on a revolutionary invention, the tiered publishing system, initially addressing specific communities of scholars, and gradually climbing up to broader public understanding, thus serving the interests of the lay society, too.

Dedication to quality

Each Frontiers article is a landmark of the highest quality, thanks to genuinely collaborative interactions between authors and review editors, who include some of the world's best academicians. Research must be certified by peers before entering a stream of knowledge that may eventually reach the public - and shape society; therefore, Frontiers only applies the most rigorous and unbiased reviews. Frontiers revolutionizes research publishing by freely delivering the most outstanding research, evaluated with no bias from both the academic and social point of view. By applying the most advanced information technologies, Frontiers is catapulting scholarly publishing into a new generation.

What are Frontiers Research Topics?

Frontiers Research Topics are very popular trademarks of the *Frontiers journals series*: they are collections of at least ten articles, all centered on a particular subject. With their unique mix of varied contributions from Original Research to Review Articles, Frontiers Research Topics unify the most influential researchers, the latest key findings and historical advances in a hot research area.

Find out more on how to host your own Frontiers Research Topic or contribute to one as an author by contacting the Frontiers editorial office: frontiersin.org/about/contact

Placental dysfunction in pregnancy: endocrine and metabolic mechanisms in preeclampsia, FGR, diabetes, and hypertension

Topic editors
Sruthi Alahari — University of Toronto, Canada
Leonardo Ermini — University of Siena, Italy

Citation
Alahari, S., Ermini, L., eds. (2026). *Placental dysfunction in pregnancy: endocrine and metabolic mechanisms in preeclampsia, FGR, diabetes, and hypertension*. Lausanne: Frontiers Media SA. doi: 10.3389/978-2-8325-7349-5

Table of contents

04 Editorial: Placental dysfunction in pregnancy: endocrine and metabolic mechanisms in preeclampsia, FGR, diabetes, and hypertension
Sruthi Alahari and Leonardo Ermini

07 Perinatal outcomes and predictors of placental abruption: a retrospective study in an Ethiopian tertiary care center
Mesfin Tadese, Gebresenbet Getachew, Tirusew Nigussie Kebede, Toyba Ebrahim Yesuf, Saba Desta Tessema, Wogene Asefa Damesa and Gebeyehu Shumet Solomon

16 Maternal diabetes disrupts early corticogenesis through altered mitotic gene regulation: a transcriptomic analysis
Rocío Valle-Bautista, Diana S. de la Merced-García, Dafne A. Díaz-Piña, Néstor Fabián Díaz, Daniela Ávila-González and Anayansi Molina-Hernández

31 Explainable machine learning reveals ribosome biogenesis biomarkers in preeclampsia risk prediction
Jingjing Chen, Dan Zhang, Chengxiu Zhu, Lin Lin, Kejun Ye, Ying Hua and Mengjia Peng

49 Effects of pre-eclampsia/eclampsia on platelet parameters in small for gestational age preterm infants
Huiling Huang, Jing Zhao, Jichong Huang, Yuan Ai and Tingting Zhu

56 Progesterone decline threshold in predicting early pregnancy loss: a retrospective study
Yanling Wei, Xiaoyu Xin, Fangxiang Mu and Fang Wang

65 Dual specificity phosphatase 1 as a non-invasive circulating biomarker candidate in preeclampsia
Jonatane Andrieu, Agathe Donet, Jean-François Cocallemen, Guillaume Charbonnier, Noémie Resseguier, Julien Paganini, Jean-Louis Mège, Soraya Mezouar and Florence Bretelle

78 Association of Placental Growth Factor with the risk of adverse pregnancy outcomes: a prospective cohort study in Chinese pregnant women
Tai-Shun Li, Yuan Wang, Ya Wang, Hui-Rong Tang, Hong-Lei Duan, Guang-Feng Zhao, Jie Li and Ya-Li Hu

89 Melatonin modulates the gene expression of WEE1 kinase and clock genes: a crosstalk between the molecular clocks of the placenta?
Carlos Venegas, Kevins Jara-Medina, Nicole Cueto, Gerardo Cabello-Guzmán, Constanza Lagunas, Luis Lillo and Francisco J. Valenzuela-Melgarejo

103 Estradiol trajectories and early pregnancy loss: a retrospective study
Yanling Wei, Xue Wei, Fangxiang Mu and Fang Wang

frontiers | Frontiers in Endocrinology

TYPE Editorial
PUBLISHED 19 December 2025
DOI 10.3389/fendo.2025.1756523

OPEN ACCESS

EDITED AND REVIEWED BY
Wei Ge,
University of Macau, China

*CORRESPONDENCE
Sruthi Alahari
alahari@lunenfeld.ca

RECEIVED 28 November 2025
ACCEPTED 10 December 2025
PUBLISHED 19 December 2025

CITATION
Alahari S and Ermini L (2025) Editorial: Placental dysfunction in pregnancy: endocrine and metabolic mechanisms in preeclampsia, FGR, diabetes, and hypertension.
Front. Endocrinol. 16:1756523.
doi: 10.3389/fendo.2025.1756523

Editorial: Placental dysfunction in pregnancy: endocrine and metabolic mechanisms in preeclampsia, FGR, diabetes, and hypertension

Sruthi Alahari[1]* and Leonardo Ermini[2]

[1]Lunenfeld-Tanenbaum Research Institute, Mount Sinai Hospital, University of Toronto, Toronto, ON, Canada, [2]Department of Life Sciences, Universita degli Studi di Siena, Siena, Italy

KEYWORDS

adverse pregnancy, fetal growth restriction (FGR), gestational diabètes, placenta, preeclampsia, pregnancy

Editorial on the Research Topic

Placental dysfunction in pregnancy: endocrine and metabolic mechanisms in preeclampsia, FGR, diabetes, and hypertension

Pregnancy complications such as preeclampsia, fetal growth restriction (FGR), gestational diabetes, and hypertensive disorders remain leading causes of maternal and perinatal morbidity worldwide, underscoring the urgent need to better understand the biological mechanisms that drive these conditions. Central to these syndromes is the placenta, a dynamic endocrine and metabolic organ that orchestrates maternal–fetal exchange, hormonal communication, immune modulation, and vascular adaptation. Disruptions in placental signaling can impair these tightly regulated processes and contribute to poor pregnancy outcomes. This Research Topic, *Placental Dysfunction in Pregnancy: Endocrine and Metabolic Mechanisms in Preeclampsia, FGR, Diabetes, and Hypertension*, brings together nine original research articles that collectively advance our mechanistic understanding of placental dysfunction and highlight emerging biomarkers and molecular pathways with diagnostic and therapeutic potential. Together, these studies address key knowledge gaps in how endocrine, metabolic, vascular, and immunologic disturbances converge to produce clinically significant pregnancy disorders.

A central theme across several contributions is the identification of early circulating biomarkers that reflect underlying placental pathology. In a large prospective cohort of nearly 6,000 pregnancies, Li et al. demonstrated that maternal serum placental growth factor (PlGF) measured in early gestation is strongly and inversely associated with the risk of preeclampsia and small-for-gestational-age neonates, supporting its value for gestational age–specific risk stratification across modes of conception. Complementing these angiogenic insights, Wei et al. analyzed endocrine trajectories and showed that women with a "high and steadily rising" estradiol trajectory during early pregnancy had a significantly lower risk of early miscarriage compared with those with low and slowly increasing levels, underscoring the prognostic significance of dynamic hormonal patterns rather than isolated measurements. In a related retrospective analysis from the same group,

repeated-measures modeling of progesterone identified decline thresholds that were strongly associated with early pregnancy loss, demonstrating a dose–response relationship between the number of threshold crossings and miscarriage risk. These findings highlight the clinical relevance of monitoring progesterone changes over time for early risk assessment (Wei et al.). Taken together, the PlGF, estradiol, and progesterone studies illustrate how dynamic hormonal and angiogenic profiling may open earlier diagnostic windows for placental dysfunction.

Another major focus of this Research Topic is the molecular and cellular regulation of placental function, including circadian signaling, translational control, and mitotic fidelity. Venegas et al. characterized circadian oscillations within human placental explants and identified rhythmic expression patterns of BMAL1, PER genes, and the cell-cycle regulator WEE1. Intriguingly, exogenous melatonin suppressed these oscillations without altering the placenta's endogenous melatonin production, suggesting a selective modulatory effect on the placental molecular clock and its links to trophoblast proliferation. Complementing this temporal dimension, Chen et al. applied explainable machine learning to integrated placental transcriptomic datasets and revealed dysregulated ribosome biogenesis as a central pathway in preeclampsia. Their model identified six predictive biomarkers: GLUL, DDX28, NCL, RIOK1, SUV39H1, and RRS1, with strong diagnostic performance and mechanistic associations with immune microenvironment alterations. This systems-level approach underscores the potential of interpretable artificial intelligence for identifying clinically meaningful biomarkers grounded in underlying biology. Together, these molecular studies highlight the importance of cellular homeostasis—including circadian regulation, translational machinery, and cell-cycle fidelity—in the pathogenesis of placental dysfunction.

Translational applications are further strengthened by the identification of non-invasive molecular indicators of placental pathology. Andrieu et al. reported that circulating dual specificity phosphatase 1 (DUSP1) is elevated at the time of preeclampsia diagnosis but normalizes postpartum, emphasizing its potential as a disease-specific and temporally resolved biomarker. Their work suggests that DUSP1 captures an aspect of active placental dysfunction and merits validation in prospective cohorts. Such markers may help distinguish current disease activity from residual risk, advancing precision monitoring strategies in pregnancy.

The downstream neonatal consequences of impaired placental function are highlighted in the work by Huang et al., who examined platelet indices in small-for-gestational-age preterm infants born to mothers with or without preeclampsia. Although neonates of preeclamptic pregnancies exhibited lower platelet counts on Day 7, the overall pattern suggested that SGA status itself may be the stronger determinant of platelet abnormalities, emphasizing the enduring hematologic effects of restricted fetal growth. In a complementary population-driven perspective from Ethiopia, Tadese et al. reported on perinatal outcomes associated with placental abruption and found that nearly 40% of affected pregnancies resulted in adverse neonatal outcomes. Severity of abruption and preterm presentation emerged as dominant predictors, highlighting the need for early recognition, patient-centered counseling, and context-specific interventions to mitigate risk in resource-limited settings. Together, these neonatal studies underscore the lasting clinical impact of placental pathology on infant health trajectories.

Finally, the developmental implications of maternal metabolic disease are illustrated by Valle-Bautista et al., who profiled early corticogenesis in embryos of diabetic dams. Their transcriptomic analysis revealed perturbations in mitotic regulation, microtubule organization, and chromosome segregation, with upregulation of AURKB and NUMA1 and corresponding structural abnormalities in neural stem cell mitosis. These alterations suggest an accelerated shift toward neurogenesis that may deplete progenitor pools and compromise cortical development, offering mechanistic insight into the neurodevelopmental vulnerabilities observed in offspring of diabetic mothers.

Together, the articles in this Research Topic offer a multidimensional exploration of placental dysfunction, spanning endocrine trajectories, molecular clocks, ribosome biology, immune contexture, clinical biomarkers, developmental pathways, and neonatal outcomes. They collectively reinforce the concept that pregnancy complications arise from a complex interplay of metabolic, vascular, immunologic, and endocrine signals that converge on placental health. As placental biology increasingly integrates multi-omics, longitudinal biomarker profiling, advanced computational modeling, and translational clinical research, future studies will be poised to identify earlier diagnostic windows and test mechanism-based therapies aimed at restoring placental function. These advances are essential for reducing the global burden of preeclampsia, FGR, gestational diabetes, and hypertensive disorders, and for improving the lifelong health trajectories of mothers and their children.

We thank all authors, reviewers, and Topic Editors for their contributions to this important field.

Author contributions

SA: Writing – original draft, Writing – review & editing. LE: Writing – review & editing.

Conflict of interest

The authors declared that this work was conducted in the absence of any commercial or financial relationships that could be construed as a potential conflict of interest.

Generative AI statement

The author(s) declared that generative AI was not used in the creation of this manuscript.

Any alternative text (alt text) provided alongside figures in this article has been generated by Frontiers with the support of artificial intelligence and reasonable efforts have been made to ensure accuracy, including review by the authors wherever possible. If you identify any issues, please contact us.

Publisher's note

frontiers | Frontiers in Public Health

TYPE Original Research
PUBLISHED 07 January 2025
DOI 10.3389/fpubh.2024.1453117

OPEN ACCESS

EDITED BY
Sruthi Alahari,
University of Toronto, Canada

REVIEWED BY
Paul Eze,
The Pennsylvania State University (PSU), United States
Ali Çetin,
University of Health Sciences, Türkiye

*CORRESPONDENCE
Mesfin Tadese
mesitad031@gmail.com

RECEIVED 22 June 2024
ACCEPTED 18 December 2024
PUBLISHED 07 January 2025

CITATION
Tadese M, Getachew G, Kebede TN, Yesuf TE, Tessema SD, Damesa WA and Solomon GS (2025) Perinatal outcomes and predictors of placental abruption: a retrospective study in an Ethiopian tertiary care center.
Front. Public Health 12:1453117.
doi: 10.3389/fpubh.2024.1453117

Perinatal outcomes and predictors of placental abruption: a retrospective study in an Ethiopian tertiary care center

Mesfin Tadese[1]*, Gebresenbet Getachew[2], Tirusew Nigussie Kebede[1], Toyba Ebrahim Yesuf[1], Saba Desta Tessema[1], Wogene Asefa Damesa[3] and Gebeyehu Shumet Solomon[4]

[1]Department of Midwifery, School of Nursing and Midwifery, Asrat Woldeyes Health Science Campus, Debre Berhan University, Debre Berhan, Ethiopia, [2]Department of Medicine, Obstetrician and Gynecologist, College of Medicine and Health Science, University of Gondar, Gondar, Ethiopia, [3]Department of Medicine, Obstetrician and Gynecologist, Abebech Gobena Mothers and Childrens Health Hospital, Addis Ababa, Ethiopia, [4]Department of Epidemiology, St. Peter Specialized Hospital, Addis Ababa, Ethiopia

Background: Placental abruption is a critical obstetric condition characterized by the premature separation of the placenta from the uterus, leading to severe maternal and fetal complications. In Ethiopia, the maternal and perinatal morbidity and mortality rates are alarmingly high, and placental abruption significantly contributes to these adverse outcomes. Despite its severity, there is a lack of comprehensive data on the burden, risk factors, and outcomes associated with placental abruption in the Ethiopian context. Thus, the study aimed to investigate the adverse perinatal outcomes of placental abruption and the factors associated with these outcomes among pregnant women admitted to the University of Gondar Comprehensive Specialized Hospital in Ethiopia.

Method: An institution-based retrospective cross-sectional study was conducted among 367 pregnant women who were admitted and managed for placental abruption from January 1, 2021, to January 1, 2023, at the University of Gondar Comprehensive Specialized Hospital. A simple random sample method was employed to choose the medical records. Data was collected using a checklist prepared with the KOBO collect tool and then exported to SPSS version 25.0. Variables having a *p*-value of less than 0.05 were deemed significant in the multivariable logistic regression analysis that was done. The adjusted odds ratio with a 95% confidence interval was reported.

Result: The prevalence of adverse perinatal outcome of placental abruption was 39.2, 95% CI: 34.3–44.1. The most common adverse outcomes were prematurity (25.6%), low birth weight (25.6%), and NICU admission (13.9%). Severe placental abruption [AOR (CI) = 8.82 (4.48–17.31)] and abruption at preterm gestation [AOR (CI) = 18.71 (9.59–36.42)] were significant predictors of adverse perinatal outcomes.

Conclusion: The adverse perinatal outcomes of pregnancies complicated by placental abruption in this study were higher compared to other studies in Ethiopia. The degree of placental abruption and gestational age at diagnosis were significant associates of adverse perinatal outcomes. The study highlights the critical need for patient-centered counseling on antenatal bleeding to encourage early healthcare-seeking behavior, close follow up for those

undergoing expectant management and the early detection and management of placental abruption to improve perinatal outcomes.

KEYWORDS

placental abruption, adverse perinatal outcome, factors, Ethiopia, antepartum hemorrhage

Background

Placental abruption, also known as abruption placentae, occurs when bleeding at the decidual-placental interface leads to partial or complete detachment of the placenta before the fetus is delivered. This condition is typically diagnosed in pregnancies beyond 28 weeks of gestation. Major clinical symptoms include vaginal bleeding and abdominal pain, which are often accompanied by hypertonic uterine contractions, uterine tenderness, and a non-reassuring fetal heart rate pattern (1). Abruption occurs in approximately 0.6 to 1.2% of all pregnancies, with nearly half of cases happening at term gestations (1).

Abruption is a serious obstetric complication that poses significant risks for maternal and perinatal morbidity as well as perinatal mortality. The perinatal mortality rate is about 20 times higher in pregnancies with abruption compared to those without (12% versus 0.6%, respectively) (2). In Japan, placental abruption accounted for 9% of all stillbirths (3). It also led to preterm birth, perinatal asphyxia, intrauterine growth restriction, and low birth weight (1). The woman is at risk of severe hemorrhage, necessitating blood transfusions and potentially leading to complications such as hysterectomy, bleeding disorders like disseminated intravascular coagulopathy, and renal failure. These complications can lead to Sheehan syndrome or postpartum pituitary gland necrosis (4). In numerous countries, the occurrence of placental abruption has been on the rise despite advancements in obstetrical care and monitoring methods. This trend highlights a multifactorial etiology that remains poorly understood (5, 6). However, placental abruption is believed to result from a disruption of the maternal-fetal interface, specifically the decidual-placental junction. This disruption can be caused by various factors, including uteroplacental under perfusion, placental inflammation, or mechanical forces, leading to bleeding and subsequent separation of the placenta from the uterine wall (1). Identifying and managing the risk factors for placental abruption is crucial in mitigating these adverse outcomes.

The precise cause of placental abruption is unknown; however, various factors are associated with its occurrence. Placental abruption occurs in 40% of smokers, 14.1% of women with vasculoplacental disorders, and 42.2% of women with pre-eclampsia (7). Maternal age over 35 years, short umbilical cord, sudden decompression of the uterus, previous abruption, and trauma are also the strongest risk factors for abruption (4). Additionally, significant risk factors for placental abruption include frequent motorbike transportation, a history of infertility, and marginal cord insertion (8).

In Ethiopia, 30% of women with antepartum hemorrhage experienced adverse perinatal outcomes. Factors significantly associated with adverse maternal and perinatal outcomes include hemodynamic status, parity, antenatal care, duration of bleeding, gestational age, and the amount of vaginal bleeding (9). Uterine malformations, preterm premature rupture of membranes, and oligohydramnios significantly increased the risk of adverse perinatal outcomes of placental abruption (10). Additionally, maternal age of 20 years or younger, preeclampsia/eclampsia, and chronic hypertensive disorders during pregnancy were associated with adverse perinatal outcomes (11).

In Ethiopia, perinatal mortality rates remain high, and complications related to placental abruption contribute substantially to these adverse outcomes. Despite its severity, there is a lack of comprehensive data on the prevalence, risk factors, and outcomes associated with placental abruption in the Ethiopian healthcare settings. Thus, the study aims to examine the adverse perinatal outcomes associated with placental abruption and identify the factors contributing to these outcomes among pregnant women. Understanding these factors can inform clinical practices and policy interventions to improve maternal and neonatal health in Ethiopia.

Method

Study design, area, and period

From January 1, 2021, to January 1, 2023, an institution-based retrospective cross-sectional study was conducted at the University of Gondar Comprehensive Specialized Hospital (UOGCSH). UOGCSH is situated in Gondar, 741 kilometers away from Ethiopia's capital, Addis Ababa. The hospital is a tertiary-level teaching and referral hospital in the Amhara region, which is one of the biggest and oldest medical schools in Ethiopia established as the Public Health College in 1954. UOGCSH provides various health services, including surgery, internal medicine, pathology, dermatology, obstetrics and gynecology, pediatric care, laboratory services, pharmacy, and physiotherapy. The labor and maternity ward is staffed by 8 gynecologic oncology subspecialists, 5 maternal-fetal medicine subspecialists, 4 urogynecology subspecialists, 7 subspecialist fellows, 5 obstetrics and gynecology specialists, 199 midwives, and 71 residents (20 first-year, 19 s-year, 23 third-year, and 13 fourth-year residents).

Population and eligibility criteria

All randomly selected pregnant women admitted and managed for the diagnosis of placental abruption were the study population. Pregnant women with multiple gestation and lethal fetal congenital anomaly were excluded.

Abbreviations: APGAR, Appearance, Pulse, Grimace, Activity, and Respiration; BP, Blood pressure; CS, Cesarean section; LBW, Low birth weight; NICU, Neonatal Intensive Care Unit; UOGCSH, University of Gondar Comprehensive Specialized Hospital.

Sample size and sampling techniques

The required sample size was determined using single population proportion formula for the first and second objective. Taking an assumption of power 80%, margin of error 5, 95% two-sided confidence level, and stillbirth in abruption 66% (12). After adding 10% missing records the final sample size was 380.

Computer-generated simple random sampling was used based on a sampling frame prepared by arranging medical record numbers in order from the maternity triage registration book. A total of 517 pregnant women were admitted with the diagnosis of placental abruption at UOGCSH from January 1, 2021, to January 1, 2023. Using simple random sampling, 380 pregnant women were selected, but 13 charts were missing, incomplete, or damaged.

Covariates

Adverse perinatal outcome was the dependent variable. Socio demographic status included age, residency, marital status, and distance traveled to arrive the study hospital. Details of past and present obstetric factors included prior abortion, prior stillbirth, prior cesarean section, parity, gravidity, interpregnancy interval, ANC follow up, gestation age at diagnosis, polyhydramnios, oligohydramnios, preeclampsia, premature rupture of membrane, and gestational diabetes mellitus. Maternal characteristics included duration of bleeding, degree of placental abruption, blood pressure, anemia, onset of labor, and mode of delivery.

Definition of terms

Placental abruption

Placental abruption was identified from participant medical records if there was a physician documented diagnosis of antepartum or intrapartum placental abruption, if it was noted as the indication for cesarean delivery, or if there was a discharge code indicating abruption.

Mild placental abruption

Clinically asymptomatic before delivery and typically detected by the existence of a retro-placental clotting and characterized by no vaginal bleeding to mild vaginal bleeding, slightly tender uterus, normal maternal BP and heart rate, no coagulopathy, and reassuring fetal heart rate (9).

Severe placental abruption

The presence of one or more of the following maternal or fetal complication in a patient diagnosed with placental abruption. Maternal: disseminated intravascular coagulation, hypovolemic shock, need for blood transfusion, hysterectomy, renal failure, and death. Fetal: non-reassuring fetal heart rate, intrauterine growth restriction, need for preterm birth, and death (13, 14).

Adverse perinatal outcome

The presence of at least one or more of the following: preterm birth (delivery before 37 completed weeks, but after 28 or more weeks of gestation), stillbirth (death of a fetus after 28 weeks of gestation, but before or during birth), low APGAR score (5^{th} minute APGAR is less than 7), low birth weight (<2,500 gm), IUGR (a birth weight of below 10^{th} percentile for gestational age and fetal sex), NICU admission, and need for resuscitation (15, 16).

Interpregnancy interval (IPI)

IPI is the period between the end of one pregnancy and the beginning of the next pregnancy. The IPI was categorized as short if <24 months, Optimal if 24 to <60 months, and long if more than or equal to 60 months (17).

Anemia

Anemia is a decrease in the concentration of erythrocytes or hemoglobin less than 11.0 g/dL / Hct 33%. Categorized into; Mild (10 to 10.9 g/dL), Moderate (7 to 9.9 g/dL), and Severe (7 g/dL) (18).

Data collection tool and quality assurance

Data was collected using a structured checklist prepared with the KOBO collect tool. The checklist included demographic information (age, residence), obstetric history (parity, previous abruption), clinical presentation (gestational age at diagnosis, degree of abruption), and perinatal outcomes (birth weight, APGAR scores, NICU admission). A data extraction tool was developed after reviewing previous literature on the subject and validated by a reproductive health expert. A pre-test was conducted with 5% of the total sample size at Debre Berhan Comprehensive Specialized hospital and required modifications were considered. Three research midwife data collectors and two obstetrics and gynecology resident supervisors were included in the data collection process. Data collectors received 1 day of training on the study's objectives, using the KOBO collect digital data extraction tool, accessing records, data handling, and maintaining participant confidentiality. The principal investigator checked the extracted data for completeness on a daily basis.

Data processing and analysis

The data collected using KOBO collect was exported to SPSS version 25.0. Descriptive statistics were presented through frequency tables, graphs, and text. Binary logistic regression was employed to examine the association between dependent and independent variables. Multivariable logistic regression analysis was performed to identify independent predictors of adverse perinatal outcomes. Variables with $p < 0.25$ in the bivariate analysis were included in the multivariable model. The Hosmer-Lemeshow test was used to assess the goodness-of-fit of the model. Adjusted odds ratios (AOR) with 95% confidence intervals (CI) were calculated, and variables with $p < 0.05$ in the final model were considered statistically significant.

Results

Baseline characteristics

A total of 367 pregnant women diagnosed with placental abruption were included, representing 96.6% of the final sample

TABLE 1 Baseline characteristics of pregnant women admitted and managed for the diagnosis of placental abruption at University of Gondar Comprehensive Specialized Hospital (UOGCSH), Ethiopia, 2023.

Variables	Category	Frequency	Percent (%)
Age	<20	31	8.4%
	20–34	269	73.3%
	≥35	67	18.3%
Residence	Rural	148	40.3%
	Urban	219	59.7%
Marital status	Married	324	98.9%
	Others*	24	1.1%
Distance traveled to the UOGCSH	<15 min	206	56.1%
	15–30 min	14	3.8%
	≥30 min	147	40.1%

*Single, divorced, and widowed.

size. The participants' ages ranged from 17 to 40 years, with a mean age of 27.91 ± 5.5 years. Most participants (73.3%) were aged between 20 and 34, and 60% were urban residents (Table 1).

Reproductive and obstetric characteristics

More than half (72%) of the women were multigravida, and 56.7% had a short interpregnancy interval. Additionally, 21.5% had previously experienced an abortion, and 4.4% had a history of stillbirth. The majority (93.7%) of participants had antenatal care (ANC) contact for the index pregnancy. Preeclampsia (6.8%), oligohydramnios (5.7%), and premature rupture of membrane (4.9%) were the commonest obstetrics complication identified during the index pregnancy (Table 2).

Maternal condition at admission and delivery

Upon admission, 61% of the women reported bleeding for a duration of 12 h or less, and 58.6% presented at term. More than one-third (70.6%) did not have anemia at the time of admission. Additionally, among the mothers with placental abruption, 25.6% delivered preterm, and 34.1% underwent an emergency cesarean section (Table 3).

Prevalence of adverse perinatal outcome

In this study, 39.2% ($N = 144$) (95% CI: 34.3–44.1) of participants had one or more adverse perinatal outcome of placental abruption. As illustrated in Figure 1, the adverse perinatal outcomes varied in frequency. Prematurity and low birth weight were equally prevalent, each affecting 25.6% of cases. NICU admission was necessary for 13.9% of newborns, while 5.4% exhibited a low APGAR score at 5 min. Stillbirth occurred in 4.9% of cases, and 3.5% required neonatal resuscitation. These findings underscore the significant impact of placental abruption on neonatal health (Figure 1).

Factors of adverse perinatal outcome

Bivariable and multivariable logistic regression analysis were conducted to identify factors associated with adverse perinatal outcomes. In the bivariable analysis, variables such as age, residence, parity, ANC follow-up, distance traveled, premature rupture of membranes, duration of bleeding, degree of placental abruption, systolic blood pressure, anemia, and gestational age at diagnosis had p-values <0.25 and were included in the multivariable model. The multivariable logistic regression analysis revealed that the degree of placental abruption and gestational age at diagnosis were significantly associated with adverse perinatal outcomes.

Women who developed severe placental abruption were eight times more likely to experience adverse perinatal outcomes compared to those with mild placental abruption [AOR (CI) = 8.82 (4.48–17.31)]. Additionally, women with placental abruption during preterm pregnancy were 18 times more likely to face adverse perinatal outcomes compared to those whose placental abruption occurred at term [AOR (CI) = 18.71 (9.59–36.42)] (Table 4).

Discussion

In this study, 39.2, 95% CI: 34.3–44.1 of pregnant women had developed at least one adverse perinatal outcome. The degree of placental abruption and gestational age at diagnosis were significantly associated with adverse perinatal outcomes.

The prevalence of adverse perinatal outcome among women admitted and managed for placental abruption was 39.2%. From these, 25.6% are premature, 25.6% are low birth weight (LBW), and 14% are referred to NICU. Similarly, in the United States, abruption was associated with an elevated risk of newborn resuscitation, asphyxia, respiratory distress syndrome, NICU admission, and stillbirth (19). It is also consistent with the study conducted in Nepal, where placental abruption is associated with preterm labor, low birth weight, and NICU admission (20). Chronic conditions such as thrombosis, inflammation, infection, and uteroplacental and decidual

TABLE 2 Reproductive and obstetric characteristics of pregnant women admitted and managed for the diagnosis of placental abruption at UOGCSH, Ethiopia, 2023.

Variables	Category	Frequency	Percent (%)
Gravidity	Primigravida	103	28.1%
	Multigravida	264	71.9%
Parity	Nulliparous (0)	136	37.1%
	Multiparous (1 – 4)	178	48.5%
	Grand multiparous (≥5)	53	14.4%
Interpregnancy interval	Short (<24 months)	208	56.7%
	Optimal (24–59 months)	132	36.0%
	Long (≥ 60 months)	27	7.3%
History of abortion	No	288	78.5%
	Yes	79	21.5%
Number of abortion (n = 79)	One	68	86.1%
	Two or more	11	13.9%
History of stillbirth	No	351	95.6%
	Yes	16	4.4%
History of early neonatal death	No	340	92.6%
	Yes	27	7.4%
Previous cesarean section (CS)	No	347	94.6%
	Yes	20	5.4%
ANC follow up	No	23	6.3%
	Yes	344	93.7%
Preeclampsia	No	342	93.2%
	Yes	25	6.8%
Gestational diabetes mellitus	No	364	99.2%
	Yes	3	0.8%
Premature rupture of membrane	No	349	95.1%
	Yes	18	4.9%
Polyhydramnios	No	350	95.4%
	Yes	17	4.6%
Oligohydramnios	No	346	94.3%
	Yes	21	5.7%
HIV/AIDS	No	358	97.5%
	Yes	9	2.5%
RH status	Negative	27	7.4%
	Positive	340	92.6%

vasculopathy predispose to placental abruption. Placental hypoperfusion, impaired spiral artery remodeling, placental infarction, and shallow trophoblast invasion are the outcomes of these processes. These long-term changes heighten the risk of abruption and other placental-related complications, such as low birth weight (LBW), preterm birth, and fetal growth restriction (1).

However, this study has shown a higher prevalence of adverse perinatal outcomes than the study conducted at Southwest Ethiopia, where 30% of women with antepartum hemorrhage experienced adverse perinatal outcomes (9). This may be due to the ongoing conflict in the study area throughout the study period. This conflict could have caused transportation problems, preventing women from accessing maternity care when experiencing signs of vaginal bleeding. Consequently, women might present with major placental abruption and severe complications. Similarly, a systematic review and meta-analysis of studies in 12 conflict-zone countries reported an increased risk

10.3389/fpubh.2024.1453117

TABLE 3 Maternal conditions of pregnant women admitted and managed for the diagnosis of placental abruption at UOGCSH, Ethiopia, 2023.

Variables	Category	Frequency	Percent (%)
Duration of bleeding/symptoms of abruption	≤ 12 h	224	61.0%
	> 12 h	143	39.0%
Degree of placental abruption	Mild	184	50.1%
	Severe	183	49.9%
Gestational age at diagnosis	Preterm	140	38.1%
	Term	215	58.6%
	Post-term	12	3.3%
Systolic blood pressure (BP) at admission	<90 mmHg	4	1.1%
	90–139 mmHg	344	93.7%
	≥140 mmHg	19	5.2%
Diastolic BP at admission	<60 mmHg	7	1.9%
	60–89 mmHg	330	89.9%
	≥90 mmHg	30	8.2%
Anemia (Hemoglobin)	No anemia	259	70.6%
	Mild anemia	49	13.4%
	Moderate	45	12.2%
	Severe anemia	14	3.8%
Gestational age at delivery	Preterm	94	25.6%
	Term	259	70.6%
	Post-term	14	3.8%
Onset of labor	Elective CS	14	3.8%
	Induced	55	15.0%
	Spontaneous	298	81.2%
Mode of delivery	Elective CS	14	3.8%
	Emergency CS	125	34.1%
	Vaginal delivery	228	62.1%

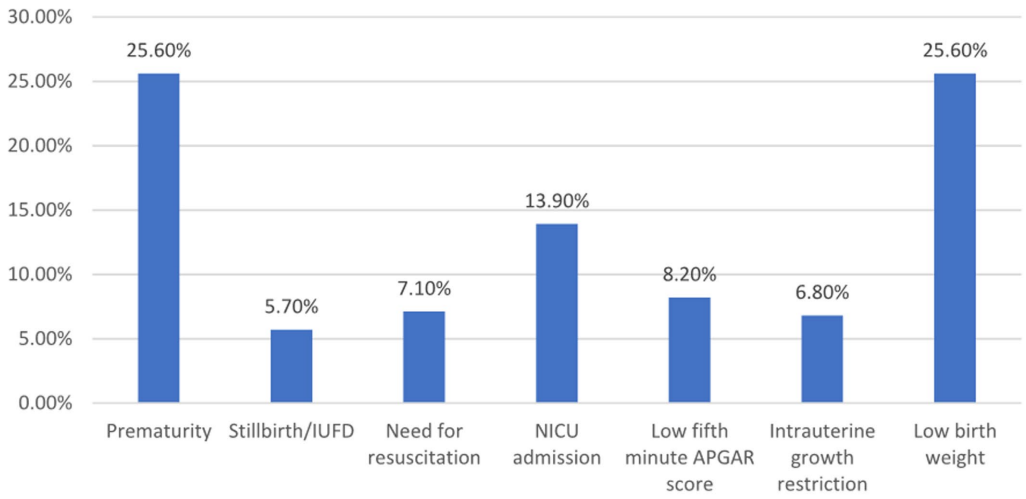

FIGURE 1
Adverse perinatal outcome among women admitted and managed for diagnosis of placental abruption at UOGCSII, Ethiopia, 2023. APGAR, Appearance, Pulse, Grimace, Activity, and Respiration; NICU, Neonatal intensive care unit; IUFD, Intrauterine fetal death.

10.3389/fpubh.2024.1453117

TABLE 4 Factors associated with adverse perinatal outcome among women admitted and managed for diagnosis of placental abruption at UOGCSH, Ethiopia, 2023.

Variables	Adverse perinatal outcome		COR (95% CI)	AOR (95% CI)
	No	Yes		
Age				
<20	23	8	1	1
20–34	161	108	1.92 (0.83–4.47)	1.36 (0.38–4.86)
≥35	39	28	2.06 (0.81–5.28)	0.88 (0.18–4.33)
Residence				
Rural	70	78	2.58 (1.67–3.98)	0.95 (0.30–3.04)
Urba	153	66	1	1
Parity				
Primipara	85	51	1	1
Multipara	113	65	0.96 (0.60–1.52)	0.53 (0.25–1.14)
Grand multipara	25	28	1.87 (0.98–3.55)	0.64 (0.18–2.34)
ANC follow up				
No	8	15	3.13 (1.29–7.58)	3.31 (0.76–14.5)
Yes	215	129	1	1
Premature rupture of membrane (PROM)				
No	217	132	1	1
Yes	6	12	3.29 (1.21–8.97)	3.46 (0.73–16.3)
Duration of bleeding				
≤ 12 h.	142	82	1	1
> 12 h.	81	62	1.33 (0.86–2.03)	0.91 (0.46–1.78)
Degree of placental abruption				
Mild	161	23	1	1
Severe	62	121	13.6 (8.01–23.3)	8.82 (4.48–17.3)*
Systolic BP at admission				
<140 mmHg	214	134	1	1
≥140 mmHg	9	10	1.77 (0.70–4.48)	0.95 (0.24–3.80)
Anemia at admission				
No anemia	171	88	1	1
Anemia	52	56	1.46 (0.78–2.71)	1.24 (0.62–2.47)
Gestational age at diagnosis				
<37 weeks	28	112	24.4 (13.9–42.5)	18.7 (9.59–36.4)*
≥37 weeks	195	32	1	1
Distance of the hospital				
<15 min	148	58	1	1
15–30 min	7	7	2.55 (0.86–7.60)	2.05 (0.29–14.6)
≥30 min	68	79	2.96 (1.90–4.62)	1.76 (0.58–5.36)

BP, Blood pressure; * statistically significant at p-value < 0.05.

of small-for-gestational-age births, low 5th-minute APGAR scores, stillbirth, and perinatal mortality (21).

Additionally, our findings indicated a higher prevalence of placental abruption compared to a study conducted in Addis Ababa, where the prevalence was reported at 2.3% (22). This discrepancy may be attributed to the lower institutional delivery rate in the Amhara region, which stands at 54.2%, compared to 94.8% in Addis Ababa, according to the 2019 EDHS report.

Similarly, 81.8% of pregnant women in Addis Ababa had four or more ANC visits, whereas only 50.8% in the Amhara region attended that many visits (23).

Preterm placental abruption at the time of admission increased the likelihood of adverse outcomes by 18 times compared to term abruption. Additionally, in this study, 38.1% of pregnant women presented before 37 weeks of gestation, and 25.6% delivered preterm. Patients with preterm abruption are typically managed expectantly if the fetomaternal condition is stable, with delivery planned for 37 to 38 weeks (13). However, these patients remain at risk of maternal or fetal complications due to progressive or recurrent placental separation, leading to relatively high neonatal morbidity and mortality. Partial abruption can suddenly and unpredictably progress to total abruption. Preventing preterm birth in pregnancies complicated by abruption is challenging. Consequently, urgent preterm operative delivery may be required without adequate preparation for neonatal care. Therefore, to reduce adverse perinatal outcome, it is recommended that most patients with acute abruption be delivered at 34 to 36 weeks of gestation, with continuous monitoring, optimal care, and thorough preparation.

Compared to women with mild placental abruption, those with severe abruption had an eight-fold increased risk of adverse perinatal outcomes. Similarly, a retrospective cohort research conducted in the United States found that women who experienced severe placental abruption had a 4.29-fold increased risk of serious maternal and neonatal complications, while women who experienced mild abruption had a 1.52-fold increased risk (14). Severe placental abruption might be characterized by heavy vaginal bleeding, total placental separation, tetanic uterus/ board-like consistency, hypofibrinogenemia and coagulopathy (4). This may aggravate the adverse obstetric and perinatal outcomes.

Our findings emphasize the critical need for vigilant monitoring of pregnancies complicated by placental abruption, particularly those presenting before term. The high rates of prematurity and low birth weight suggest that early detection and management of abruption may be crucial in improving perinatal outcomes. Furthermore, the increased risk associated with severe abruption highlights the importance of prompt recognition and intervention in these cases. These results may inform clinical protocols for the management of placental abruption, potentially including more frequent fetal monitoring and earlier consideration of delivery in cases of severe abruption.

Limitation

This study has several limitations that should be considered when interpreting the results. First, as a retrospective study, it is subject to inherent biases, including potential inaccuracies in medical records and missing data. Second, the single-center design may limit the generalizability of our findings to other settings, particularly those with different resources or patient populations. Third, we were unable to assess long-term neonatal outcomes beyond the immediate perinatal period, which may underestimate the full impact of placental abruption. Finally, while we identified significant predictors of adverse outcomes, the observational nature of our study precludes causal inferences. Furthermore, the limited number of similar studies makes it challenging to engage in a comprehensive discussion.

Conclusion and implication

The prevalence of adverse perinatal outcome of pregnancy complicated with placental abruption is this study was high compared to the study done in similar setting. The degree of placental abruption and gestational age at diagnosis were significant associates of adverse perinatal outcomes. The study highlights the critical need for patient-centered counseling on antenatal bleeding to encourage early healthcare-seeking behavior, close follow up for those undergoing expectant management and the early detection and management of placental abruption to improve perinatal outcomes.

Our research indicates that placental abruption is associated with a higher risk of low birth weight, preterm delivery, neonatal resuscitation, and NICU admission. This suggests a possible link between abruption and physiological underdevelopment. Additionally, patients under expectant management may experience hypoxia and a gradual worsening of the condition. It is important to have the recommended antenatal care contact for improving the overall maternal and fetal outcomes.

Data availability statement

The raw data supporting the conclusions of this article will be made available by the authors, without undue reservation.

Ethics statement

Ethical clearance was obtained from the Ethical Review Committee of the University of Gondar, College of Medicine and Health Sciences with reference number SOM 702/2023. Patient confidentiality and privacy were maintained by excluding names from the data extraction forms. Written informed consent from the [patients/participants OR patients/participants legal guardian/next of kin] was not required to participate in this study in accordance with the national legislation and the institutional requirements.

Author contributions

MT: Conceptualization, Data curation, Formal analysis, Funding acquisition, Investigation, Methodology, Project administration, Resources, Software, Supervision, Validation, Visualization, Writing – original draft, Writing – review & editing. GG: Conceptualization, Data curation, Investigation, Methodology, Project administration, Resources, Supervision, Visualization, Writing – original draft. TK: Data curation, Methodology, Project administration, Resources, Supervision, Validation, Visualization, Writing – review & editing. TY: Conceptualization, Data curation, Methodology, Project administration, Resources, Supervision, Validation, Visualization, Writing – review & editing. ST: Conceptualization, Data curation,

Methodology, Project administration, Resources, Validation, Visualization, Writing – review & editing. WD: Resources, Software, Validation, Visualization, Writing – review & editing, Conceptualization, Data curation, Investigation, Methodology, Project administration. GS: Conceptualization, Data curation, Investigation, Methodology, Project administration, Resources, Validation, Visualization, Writing – review & editing.

Funding

The author(s) declare that no financial support was received for the research, authorship, and/or publication of this article.

Acknowledgments

The authors would like to thank the data collectors, supervisors, and the study participants for providing genuine information. We also extend our thanks to University of Gondar, College of Medicine and Health Sciences for approving the study.

Conflict of interest

The authors declare that the research was conducted in the absence of any commercial or financial relationships that could be construed as a potential conflict of interest.

Publisher's note

References

1. Brandt JS, Ananth CV. Placental abruption at near-term and term gestations: pathophysiology, epidemiology, diagnosis, and management. *Am J Obstet Gynecol*. (2023) 228:S1313–29. doi: 10.1016/j.ajog.2022.06.059

2. Tikkanen M, Luukkaala T, Gissler M, Ritvanen A, Ylikorkala O, Paavonen J, et al. Decreasing perinatal mortality in placental abruption. *Acta Obstet Gynecol Scand*. (2013) 92:298–305. doi: 10.1111/aogs.12030

3. Kasahara M, Koshida S, Tokoro S, Katsura D, Tsuji S, Murakami T, et al. Potential prevention of stillbirth caused by placental abruption: a regional population-based study in Japan. *J Matern Fetal Neonatal Med*. (2024) 37:2321485. doi: 10.1080/14767058.2024.2321485

4. Schmidt P, Skelly CL, Raines DA. Placental abruption. Treasure Island, FL: StatPearls Publishing (2022).

5. Miller C, Grynspan D, Gaudet L, Ferretti E, Lawrence S, Moretti F, et al. Maternal and neonatal characteristics of a Canadian urban cohort receiving treatment for opioid use disorder during pregnancy. *J Dev Orig Health Dis*. (2019) 10:132–7. doi: 10.1017/S2040174418000478

6. Workalemahu T, Enquobahrie DA, Gelaye B, Sanchez SE, Garcia PJ, Tekola-Ayele F, et al. Genetic variations and risk of placental abruption: a genome-wide association study and meta-analysis of genome-wide association studies. *Placenta*. (2018) 66:8–16. doi: 10.1016/j.placenta.2018.04.008

7. de Moreuil C, Hannigsberg J, Chauvet J, Remoue A, Tremouilhac C, Merviel P, et al. Factors associated with poor fetal outcome in placental abruption. *Pregnancy Hypertens*. (2021) 23:59–65. doi: 10.1016/j.preghy.2020.11.004

8. Nkwabong E, Tchomguie Moussi OS, Fouedjio J. Risk factors for placental abruption. *Trop Dr*. (2023) 53:37–40. doi: 10.1177/00494755221116716

9. Gelan M, Bekela T, Angasu K, Ebisa M. Adverse perinatal and maternal outcomes and associated factors among women with antepartum hemorrhage in Jimma University medical center, Southwest Ethiopia, 2020. *Obstet Gynecol Int*. (2022) 2022:1–7. doi: 10.1155/2022/4594136

10. Bączkowska M, Kosińska-Kaczyńska K, Zgliczyńska M, Brawura-Biskupski-Samaha R, Rebizant B, Ciebiera M. Epidemiology, risk factors, and perinatal outcomes of placental abruption—detailed annual data and clinical perspectives from polish tertiary center. *Int J Environ Res Public Health*. (2022) 19:5148. doi: 10.3390/ijerph19095148

11. Anyanwu M, Amuzu C, Bittaye M. A longitudinal study of incidence and pregnancy outcome of abruption placenta at the–tertiary hospital in Gambia. *Int J Pregn Child Birth*. (2019) 5:57–61. doi: 10.15406/ipcb.2019.05.00147

12. Nethaji DT, Hurakadli KM, Duggavathi SP. Maternal and perinatal outcome in abruption placenta in tertiary care center: a record based case series study. *Int J Reprod Contracept Obstet Gynecol*. (2023) 12:1270–4. doi: 10.18203/2320-1770.ijrcog20231208

13. Oyelese Y, Annath C V. (2016). Placental abruption: management. Available at: http://www.uptodate.com/contents/placental-abruptionmanagement (Accessed June 3, 2024).

14. Ananth CV, Lavery JA, Vintzileos AM, Skupski DW, Varner M, Saade G, et al. Severe placental abruption: clinical definition and associations with maternal complications. *Am J Obstet Gynecol*. (2016) 214:272.e1–9. doi: 10.1016/j.ajog.2015.09.069

15. Jaleta DD, Abdisa DK. Predictors of adverse perinatal outcome among women who gave birth at medical Center of Southwest Ethiopia: a retrospective cohort study. *BMJ Open*. (2022) 12:e053881. doi: 10.1136/bmjopen-2021-053881

16. Tadese M, Damesa WA, Solomon GS, Fitie GW, Mitiku YM, Tessema SD, et al. Prevalence and determinants of adverse perinatal outcomes of preeclampsia with severe features at two selected public hospitals in Addis Ababa, Ethiopia. *Front Pediatr*. (2024) 12:12. doi: 10.3389/fped.2024.1345055

17. Agrawal S, Chaudhary M, Das V, Agarwal A, Pandey A, Kumar N, et al. Association of long and short interpregnancy intervals with maternal outcomes. *J Fam Med Prim Care*. (2022) 11:2917–22. doi: 10.4103/jfmpc.jfmpc_2231_21

18. Auerbach M, Landy HJ, Barss VA. (2020). Anemia in pregnancy. Available at: https://www.uptodate.com/contents/anemia-in-pregnancy (Accessed June 15, 2024).

19. Downes KL, Shenassa ED, Grantz KL. Neonatal outcomes associated with placental abruption. *Am J Epidemiol*. (2017) 186:1319–28. doi: 10.1093/aje/kwx202

20. Maharjan S, Thapa M, Chaudhary B, Shakya S. Abruptio placenta among pregnant women admitted to the Department of Obstetrics and Gynaecology in a tertiary care Centre: a descriptive cross-sectional study. *JNMA J Nepal Med Assoc*. (2022) 60:918–21. doi: 10.31729/jnma.7796

21. Behboudi-Gandevani S, Bidhendi-Yarandi R, Panahi MH, Mardani A, Prinds C, Vaismoradi M. Perinatal and neonatal outcomes in immigrants from conflict-zone countries: a systematic review and meta-analysis of observational studies. *Front Public Health*. (2022) 10:766943. doi: 10.3389/fpubh.2022.766943

22. Assefa A, Fantahun Y, Mesfin E. Maternal and perinatal outcome of antepartum hemorrhage at three teaching hospitals in Addis Ababa, Ethiopia. *Ethiopia J Reprod Health*. (2020) 12:12–9. doi: 10.69614/ejrh.v12i3.395

23. ICF EPHI. Ethiopia mini demographic and health survey 2019: key indicators. Maryland, USA: EPHI ICF (2019).

frontiers | Frontiers in Endocrinology

TYPE Original Research
PUBLISHED 13 May 2025
DOI 10.3389/fendo.2025.1564441

OPEN ACCESS

EDITED BY
Sruthi Alahari,
University of Toronto, Canada

REVIEWED BY
Megha Kumar,
Centre for Cellular & Molecular Biology (CCMB), India
Vishi Sharma,
National Centre for Cell Science, India
Binod Timalsina,
Institute for Basic Science (IBS), Republic of Korea

*CORRESPONDENCE
Anayansi Molina-Hernández
anayansimolina@gmail.com

RECEIVED 21 January 2025
ACCEPTED 11 April 2025
PUBLISHED 13 May 2025

CITATION
Valle-Bautista R, de la Merced-García DS, Díaz-Piña DA, Díaz NF, Ávila-González D and Molina-Hernández A (2025) Maternal diabetes disrupts early corticogenesis through altered mitotic gene regulation: a transcriptomic analysis.
Front. Endocrinol. 16:1564441.
doi: 10.3389/fendo.2025.1564441

Maternal diabetes disrupts early corticogenesis through altered mitotic gene regulation: a transcriptomic analysis

Rocío Valle-Bautista, Diana S. de la Merced-García, Dafne A. Díaz-Piña, Néstor Fabián Díaz, Daniela Ávila-González and Anayansi Molina-Hernández*

Departamento de Fisiología y Desarrollo Celular, Instituto Nacional de Perinatología "Isidro Espinosa de los Reyes", Mexico City, Mexico

Maternal diabetes is linked to neurodevelopmental impairments in offspring, but the underlying molecular mechanisms remain unclear. Early cortical neurogenesis is a critical window vulnerable to maternal metabolic disturbances. Here, we analyzed global gene expression by RNA sequencing in dorsal prosencephalon tissue from 12-day-old embryos without neural tube defects. Gene ontology (GO) enrichment identified key candidates, validated by qRT-PCR, Western blotting, and immunofluorescence. We found 247 differentially expressed genes (111 upregulated, 136 downregulated), with upregulated genes enriched in mitosis, microtubule organization, and chromosome segregation pathways. Aurkb and Numa1 emerged as central regulators and were confirmed upregulated by qRT-PCR. Although Western blotting showed no protein-level changes, immunofluorescence revealed altered subcellular localization, disrupted spindle architecture, monopolar spindles, and increased asymmetric divisions in neural stem cells. These results suggest maternal diabetes disrupts mitotic regulation, accelerates neurogenic differentiation, and depletes the neural stem cell pool, potentially contributing to cortical defects and neurodevelopmental impairments in offspring. This study provides new insight into the developmental origins of neurodevelopmental disorders in the context of maternal diabetes, highlighting mitotic dysregulation as a potential mechanistic link in fetal programming.

KEYWORDS

maternal diabetes, embryo cortical transcriptome, corticogenesis, neural stem cells mitosis, achromatic spindle

1 Introduction

Maternal diabetes is associated with cognitive impairments in offspring, including verbal and nonverbal IQ scores, working memory and cognitive flexibility, and attention deficit hyperactivity disorder (ADHD) (1–5). The prefrontal cortex is essential in mediating these cognitive and executive functions, as it integrates information from various brain regions to support complex cognitive processes (6).

During corticogenesis, several alterations have been reported in embryos of diabetic rodents, including precocious and enhanced neurogenesis, reduced proliferation, a thinner cerebral cortex with impaired cytoarchitecture, and decreased excitability of deep-layer cortical neurons in 21-day-old pups (7–10). Furthermore, 14-day-old embryos (E14) from diabetic rats exhibited increased nuclear localization of FOXP2, a transcription factor implicated in speech and language development. During cortical development, FOXP2 promotes the transition from NSC population to intermediate progenitor (IP) and, ultimately, neuronal differentiation (7, 11). Among the targets of FOXP2 are genes involved in neurogenesis, cell death, and cell migration (12). The above suggests an accelerated NSC-to-IP transition.

Cortigogenesis is precisely regulated by intrinsic and extrinsic factors (13–15). Initially, multipotent epithelial stem cells proliferate to form a semi-stratified neuroepithelium, generating the first neurons, Cajal-Retzius cells, which delineate the basal side of the developing cortex. Within the semi-stratified neuroepithelium, radial glial cells (RGCs), a type of bipolar NSCs, undergo symmetrical and asymmetrical division to expand its pool or to produce neurons, astrocytes, and oligodendrocytes in a temporally controlled manner to determine the size and function of the brain (16). Neurons are the earliest specialized cells to arise, originating directly from NSCs or indirectly via IPs, and to establish the characteristic laminar structure of the cerebral cortex, they migrate in an inside-out pattern manner, with the deeper layer neurons born first and the more superficial layers at the end (13, 17–19). Typical in rodents, IPs undergo a terminal division, yielding two neurons. However, IP cells that undergo two successive divisions in the dorsal cortex are found at low frequencies (20).

During the NSC cell cycle, the nucleus undergoes interkinetic nuclear migration, moving between the apical and basal sides of the ventricular zone (VZ), moving basally during G1, undergoing the S-phase on the basal side, migrating apically during G2, and finally, on the apical surface, mitosis occurs (21).

Axis polarity, spindle orientation, and cleavage plane orientation are critical factors influencing whether divisions are symmetric or asymmetric. When the mitotic spindle aligns parallel to the cell's apical-basal axis, asymmetric divisions are favored. Conversely, when it is perpendicular, division tends to be symmetric. Another factor regulating the transition from neuroepithelial cells to RGCs and from proliferative to neurogenic divisions is the length of the NSCs cycle, specifically an elongation of the G1 phase (22, 23). Intrinsic differences in mitotic spindle architecture at different neurogenic stages have also been documented. While in the early stages, an astral spindle morphology, with numerous and longer microtubules contacting the cellular cortex, in later stages, it loses its astral morphology and exhibits an increased density of inner spindle microtubules (24).

Although previous studies have provided insight into how maternal diabetes affects embryonic nervous system development, many investigations have not distinguished between embryos with and without neural tube defects. This lack of distinction makes it challenging to identify the underlying mechanism involved in postnatal neurodevelopment impairments in "normally" developing embryos. Nonetheless, valuable information has emerged, indicating changes in DNA methylation and the expression of genes associated with synaptic plasticity, neurotransmitter signaling, mitochondrial metabolism, neuroinflammation, neuronal development, synaptic function, cell proliferation, cytoskeletal remodeling, and oxidative phosphorylation (8, 25–28). To address part of these gaps, we separate embryos without neural tube defects and examine how high glucose influences the neural tube before the onset of the neurogenic peak, thereby focusing on the early cellular events that may affect cell fate determination.

Here, we analyzed the transcriptome from pooled total RNA samples obtained at E12 from the dorsal prosencephalon of control (Ctl) and diabetic (Db) pregnant rats. Our results showed that in the Db group, 247 genes were differentially expressed (111 up-regulated and 136 down-regulated) compared to the Ctl. Gene Ontology (GO) analysis of biological processes and cellular components revealed significant enrichment in pathways related to mitosis, microtubule organization, catalytic activity, and nuclear lumen. Notably, the genes Numa and Aurkb were listed in more than half of the enriched categories. Given their pivotal roles in the cell cycle and mitosis (29, 30), we validated their expression and evaluated protein levels. While qRT-PCR confirmed up-regulation of Numa and Aurkb in the Db group, no changes in total protein content were detected. However, immunofluorescence revealed altered distribution patterns of NUMA, phosphorylated AURKB (AURKBph), and α-tubulin (α-TUB) in the VZ. Furthermore, alterations in mitotic spindle architecture and an increase in asymmetric cell division in the Db group were also observed, underscoring the impact of maternal diabetes on early corticogenesis.

The findings presented here might advance our understanding of the molecular basis of neurological disorders associated with maternal diabetes. Article types

2 Materials and methods

All animal experiments and procedures followed ARRIVE guidelines 2.0 (31) and Mexican NOM-062-ZOO-1999. The protocol was approved by the Instituto Nacional de Perinatología committees of Research and Animal Care (CICUAL), Biosecurity, and Ethics (protocol number 2018-1-146).

2.1 Diabetes induction and embryonic tissue recovery

Adult female Wistar rats (250–310 g) were housed under standard conditions (12:12 h light/dark cycle, 21 ± 2°C and 40% relative humidity) with ad libitum access to food and water. Females were mated with fertile male rats during the dark cycle, and the presence of spermatozoids in a vaginal smear within the first four hours of the light cycle was considered E0.5. Pregnant rats were then housed in groups of five.

Pregnant rats were housed in groups of five and randomly assigned to Ctl or Db groups. At E5, the Ctl group received a single

intraperitoneal injection of citrate buffer (pH 6.4, 250 µL), while the Db received a single injection of streptozotocin (STZ; 50 mg/kg in 250 µl vehicle; Sigma Aldrich, MO, USA). After 48 h, plasma glucose was measured from tail vein blood using an electronic glucometer (ACCU-Check Performa, Roche Diagnostics, Basel, CH). Only rats injected with STZ with blood glucose levels higher than 200 mg/dL at euthanasia were included in the Db group, and those that received the vehicle with glucose levels between 96-120 mg/dL were included in the Ctl group. Db pregnant rats in the study exhibited blood glucose levels of 428.3 ± 14.9 mg/dL, whereas control animals showed levels of 109 ± 10.2 mg/dL.

At E12, pregnant rats were euthanized by decapitation following anesthesia induction with sevoflurane; embryos were collected by cesarian and washed in cold phosphate-buffered saline (PBS, pH 7.4). Only embryos without neural tube defects were included in further analyses (Figure 1A). Embryos with neural tube defects were identified under a stereomicroscope and excluded if they exhibited anencephalia, brain vesicle abnormalities (malformed or asymmetrical), aberrant neural tube closure in the forebrain or spinal cord, or abnormal and brain embryos with brains showing folding.

Embryos of both sexes were used without distinction in all experiments. As previously reported, the dorsal telencephalon of E14 embryos from diabetic pregnant rats exhibits increased neurogenesis, presumably due to an early shift in NSC differentiation either directly or via IP generation (7, 9). We selected E12 as it marks the onset of the cortical laminar neurogenic phase in rats, characterized by the initiation of asymmetric NSC division alongside ongoing active symmetric division. This developmental window is critical for establishing the initial cortical architecture and the neural progenitor pool, making it a relevant time point to evaluate the effects of maternal diabetes on early neurodevelopmental processes.

For RNA-seq (n = 3), qRT-PCR (n = 4), and Western Blot (WB), 30 dorsal prosencephalons per experimental unit for a total of an n = 3 were dissected under a stereoscopic microscope (Olympus Corporation S7X2-ILLT, Tokyo, JPN) and frozen at -70°C until used. For the immunofluorescence analyses, three embryos per litter per experimental unit (n = 3) were fixed in 4% paraformaldehyde (in PBS, pH 7.4) and processed for histology. For cell culture experiments, the dorsal prosencephalon from non-neural tube defective embryos of an entire litter or two litters, for control and diabetic groups, respectively (n = 1), were mechanically dissociated, and a total of 3 experiments were performed in passage one, as described below. The total number of animals used was 83 female and six male rats for mating.

2.2 RNA-seq and bioinformatic analysis

Total RNA was obtained using TRIZOL® reagent (Thermo Fisher Scientific, MA, USA) following provider's instructions. RNA quality and purity were determined (Nanodrop, Thermo Fisher Scientific), and only 260/230 ≥ 1.0 and 260/280 ≥ 1.8 samples were

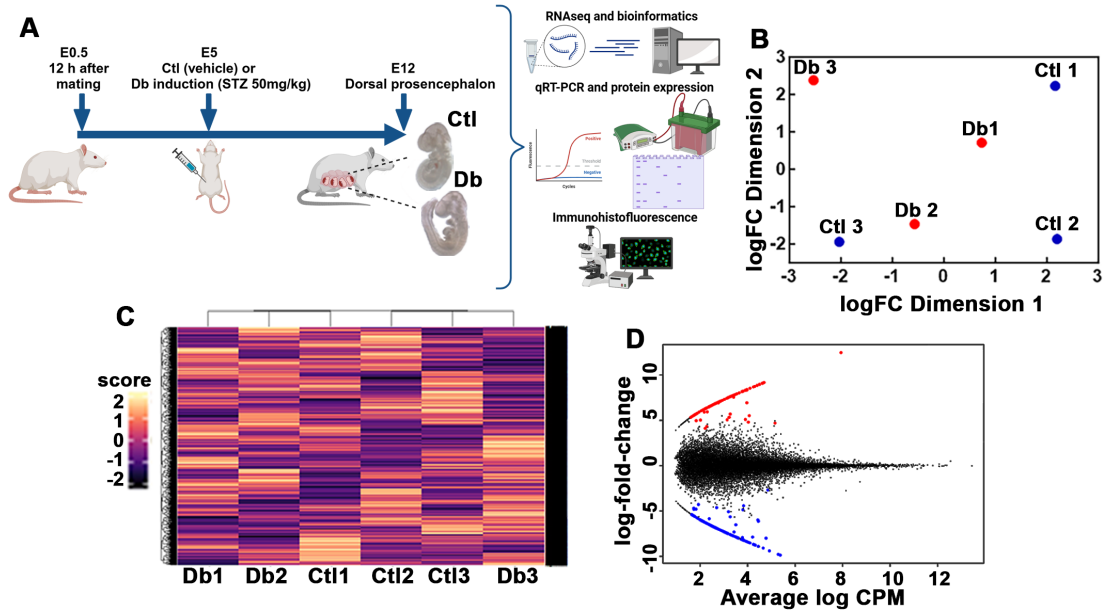

FIGURE 1
Experimental strategy and transcriptomic analysis of control (Ctl) and diabetic (Db) groups. **(A)** Schematic representation of the experimental strategy for analyzing transcriptomic differences between 12-day-old embryos (E12) from control (Ctl) and diabetic (Db) rats. Only embryos without neural tube defects were included. **(B)** Principal Component Analysis (PCA) plot showing distinct clustering of transcriptome data from Ctl (blue dots) and Db (red dots) groups of E12 dorsal prosencephalon tissue. **(C)** Hierarchical clustering heatmap of the transcriptomic data from Ctl and Db groups. Rows represent individual genes, and columns represent samples. Color intensity corresponds to expression levels, with distinct clustering reflecting differential gene expression between groups. **(D)** MA/SMEAR plot showing differential gene expression análisis between E12 tissue from Ctl and Db groups. Up-regulated (red dots) and down-regulated genes (blue dots) are highlighted (p-value < 0.05, and log2 fold change > 1.5).

used. RNA Integrity Number (RIN) was obtained by using a BioAnalyzer (Agilent 2100 BioAnalyzer, CA, USA). The mean RIN was 9.04 ± 0.44.

RNA-seq libraries were prepared using the Truseq Stranded mRNA library prep kit from (Illumina, CA, USA) according to the manufacturer's instructions. Sequencing was conducted on the Illumina Nextseq 500 platform with paired-end two lectures ×75 bp reads, cycles paired-end to generate approximately 30 million reads per sample.

Quality control of raw reads was performed with FastQC (32), and adapters were removed using Cutadapt (33). Trimmed reads were aligned to the Rattus_norvegicus reference genome (mRATBN7.2) using the Bowtie2 (34). Gene-level quantification was performed using RSEM v1.3.3 (35). Total counts for each sample were merged; a matrix was generated using the "abundance_estimates_to_matrix.pl" included in the Trinity pipeline (34).

Differential expression analysis was performed with edgeR (36). The abundance of all genes was calculated using the mapped reads by the Fragments per Kilobase of transcript per Million fragments mapped (FPKM) method, combined with RSEM to measure and normalize gene expression levels and to identify genes with significant differences in expression in the Db versus (vs) the Ctl group. For the up- and down-regulated genes, an ontology (GO) enrichment analysis was performed using the ShinyGO (v0.741) (37).

2.3 qRT-PCR analysis

cDNA was synthesized from one microgram of total RNA (Promega, WI, USA). PCRs were performed using a 10 µL mix containing cDNA (500 ng), forward and reverse primers (0.8 pmol), and NZYSpeedy qPCR Green Master Mix 2× (NZYTech, Lisbon, PRT. Primer sequences were: Aurkb, forward 5'-GTAGGTTCTCCGGTGTACGA-3' and reverse 5'-AGGTGTTCAGGCCAGATTGA-3'; Numa, forward 5'-GGGGGATATGGAACGATGGG-3' and reverse 5'-TAGTTAGAGACAGGGGCCAGA; and actin, forward 5'-CCGCGAGTACAACCTTCTTGC-3' and reverse 5'-GTACTTCAGGGTCAGGATGCC-3'.

The PCRs conditions were: 10 min denaturalization at 95°C, 35 cycles of denaturalization (30 s at 95 °C), aligning (15 s; Aurkb 60°C, Numa 56°C, and actin 63°C), and extension (30 s at 72 °C). Actin was used as internal control, whereas total RNA and the PCR mix without cDNA were negative controls.

End-point PCR products were recovered using the ZymocleanTM Gel DNA Recovery Kit (Zymo Research, Irvine, CA, USA) and sequenced. Using BLAST® (standard nucleotide BLAST), a 100% identity was obtained for each product (nucleotides 25-254 of NM_053749.2, 7036-7257 of NM_031144.3, and 18-285 of NM_031144.3 for Aurkb, Numa, and actin, respectively).

Efficiency and threshold values for each qPCR product were obtained from dynamic ranges using a Rotor-Gene thermocycler (QIAGEN, Venlo, NLD). Melting curves were performed to ensure a single amplified product. The $2^{-\Delta\Delta CT}$ relative expression method was used to evaluate changes in gene expression between groups (24).

2.4 Western blot analysis

The tissue was homogenated in lysis buffer (20 mM HEPES, 1.5 mM MgCl2, 10 mM KCl, 1 mM DTT, and protease/phosphatase (Thermo Fisher Scientific; A32961). After centrifugation (10 min, 13000× rpm), the supernatant was collected, and protein concentration was determined by the Bradford method (38). The protein (60 µg) was separated in 10% SDS-PAGE gels using the MiniProtean II system (Bio-Rad, Hercules, CA, USA) and transferred to nitrocellulose membranes (AmershamTM Hybond TM-ECL, Buckinghamshire, UK) using a semi-dry transfer cell system (Bio-Rad) (39).

Membranes were blocked with TBS blocking buffer (LI-COR, Lincoln, NE, USA), incubated overnight at 4°C with rabbit anti-NUMA (1:500, GTX64368, GeneTex, Irvine, CA, USA), rabbit anti-AURK (1:1000, ab287960, Abcam, Cambridge, UK), and rabbit anti-AURKT232ph (1:1000, ab115793, Abcam), and mouse anti-actin as internal control (1:2000; GTX82559) antibodies, and incubated with IRDye 800CW donkey anti-rabbit and 680RD donkey anti-mouse (1:1000, P/N: 926-32213 and 926-68073, LI-CORbio, Lincoln, NE, United States) secondary antibodies. Bands were visualized using an Odyssey infrared scanner and analyzed using Image Studio ver.4.0 (LI-CORbio). The fluorescence rate of each protein was obtained, along with that of Actin.

2.5 Neural stem cell culture

Embryo tissue was mechanically dissociated in 1:1 N2 (DMEM/F12 (ATCC, Manassas, VA, USA), GlutaMAX, N2 supplement, 0.1 mM non-essential amino acids, 0.1 mM 2-mercaptoethanol, and 50 U/ml penicillin/streptomycin) and Neurobasal/B27 media (B27 supplement, two mM glutamine, and 50 U/ml penicillin-streptomycin), seeded (120,000 cells/well; 24-well plates) onto plates coated with 15 µg/ml poly-L-ornithine (Sigma-Aldrich) and 1 µg/ml fibronectin (Thermo Fisher), maintained at 37°C, 5% C02 and FGFb (R&D, Minneapolis, MN, USA), and the medium changed every third day until 80% confluency. Cells were passaged (150,000 cells/well) and, after 24 hours, fixed with 4% paraformaldehyde.

2.6 Immunofluorescence

Paraformaldehyde fixed consecutive coronal sections (10 µm thick) placed on poly-L-lysine coated slides from paraffin-embedded embryonic brains containing the dorsal prosencephalon obtained in a microtome (HM320, Thermo Fisher/Micron), dorsal prosencephalon explants, and cultured

NSCs were used for immunofluorescence. Samples were permeabilized and blocked in PBS containing 0.3% Triton-X100 and 10% normal goat serum or 5% bovine serum albumin for 30 min, incubated overnight at 4°C with primary antibodies (rabbit anti-NUMA, 1:50; rabbit anti-AURKB, 1:250; rabbit anti-α-AURKT232ph, 1:250; and mouse anti-α-Tubulin, ab7291, 1:250), one hour with Alexa Fluor IgG 488 anti-rabbit and 568 anti-mouse (1:1000; A-11008 and A-11004, Thermo Fisher Scientific) secondary antibodies, nuclei were stained with DAPI (one ng/mL; Sigma-Aldrich), and mounted in AquaPolymount. Controls omitting the primary antibody were included. Explants were placed in an en-face view (40). Confocal images were obtained using a Leica TCS-SP8 DM6000 (Leica, Leitz, DEU) microscopy with a 40× (N.A. 1.3) objective for slices and a Leica TCS-SPE DMI4000 (Leica) microscope with a 63× (N.A.1.2) objective for explants. Representative images are shown as single confocal z-stack images. NSC images were obtained using an Olympus IX81 epifluorescence microscope and a Hamamatsu ORCA-Flash 2.8 CCD camera (Hamamatsu, JPN), deconvoluted using ImageJ. Representative images were processed using Adobe Photoshop CS6 (Adobe Inc., San Jose, CA, USA).

2.7 Achromatic spindle measurement

The length of achromatic spindles in cultured E12 NSC was measured using FIJI software (ImageJ) with the Analyze Skeleton plugin (https://imagej.net/plugins/analyze-skeleton/). Micrographs (40×) were converted to binary, scale set in μm, and the following steps were performed: Analyze>Skeleton>Classify particles using skeleton. AURKBT232ph mark was selected for the particle image and the α-TUB for the skeletonizable mask parameters. MaxEntropy was used to detect auto-threshold particles (41). The resulting skeleton structure for each achromatic spindle was used to obtain the total size and the "Longest-Shortest Path". As the mitotic spindles showed a complex skeleton with numerous "branches", the tagged skeleton was represented as an undirected and weighted graph, where the nodes are the end-point and junction pixels, and the weighted edges are the summed Euclidean distances between every slab pixel and its neighbor in the edge (42). For our purpose, the longest-shortest path was used to obtain the size of the mitotic spindle.

2.8 Statistics analysis and graphs

Differentially expressed genes were identified with a false discovery rate (FDR) < 0.05 and at least a 1.5-fold change in FPKM values between groups. Data are mean ± standard error of the mean (SEM). Differences between groups were assessed by unpaired Student's *t*-test ($P<0.05$ considered significant). Statistics and graphs were performed in GraphPad Prism version 9 (GraphPad Software, Inc., San Diego, CA, USA).

3 Results

3.1 Bioinformatic analysis

All samples showed FastQC scores above 28. Principal component analysis (PCA) indicated that two samples from each group clustered closely together, highlighting the variability in gene expression among E12 embryos (Figure 1B). Hierarchical clustering analysis further supported these findings, showing that two diabetics and two control samples grouped together while one sample from each group diverged from the main cluster (Figure 1C). Despite the heterogeneity, all samples passed quality control, and thus, all were included in the differential gene expression and subsequent analysis.

Differentially expression analysis identified 247 genes (out of 24170) with significant changes: 111 were up-regulated and 136 down-regulated (Figure 1D; Supplementary Tables 1, 2). GO analysis of the biological process for the up-regulated genes revealed 21 enriched terms, primarily related to cell cycle and division. The most enriched terms included multicellular organism development (GO:0007275), microtubule cytoskeleton organization (GO:0000226), and positive regulation of DNA metabolic process (GO:0051054; Figure 2A, Supplementary Table 3). A network analysis showed that these terms were interconnected (Figure 2C). Notably, 57% and 85% of the enriched biological processes included Numa1 and Aurkb, respectively.

To refine the analysis, a STRING functional protein association network was generated for the second-most enriched process. In rats, this network revealed a node comprising six of the eleven proteins, excluding Numa1 and Aurkb (Figure 2E). However, in humans, a node containing only NUMA1 and AURKB was evident (Figure 2F).

GO analysis for cellular components identified 17 enriched terms, with the top three being mitotic spindle midzone (GO:1990023), chromosomal region (GO:0098687), and chromosome centromeric region (GO:0000775; Figure 2B, Supplementary Table 4). Numa1 and Aurkb were present in 53% and 82% of these terms, respectively. The resultant network demonstrated that the centrosome and spindle pole centrosome acted as key hubs. Interestingly, Numa1 and Aurkb were the only genes associated with the spindle pole centrosome (Figure 2D, Supplementary Table 4).

In rats, STRING analysis for mitotic spindle midzone term (GO:1990023) excluded Numa1 (Figure 2G). However, in humans, a unified network included the three up-regulated genes listed associated with this term (Figure 2H).

For the down-regulated genes, GO analysis of biological process identified five affected terms: microtubule depolymerization (GO:0007019), cellular protein modification (GO:0006464), organelle organization (GO:0006996), protein modification (GO:0036211), and macromolecule modification (GO:0043412; Figure 3A). These terms included genes such as Kif18a, Kif2c,

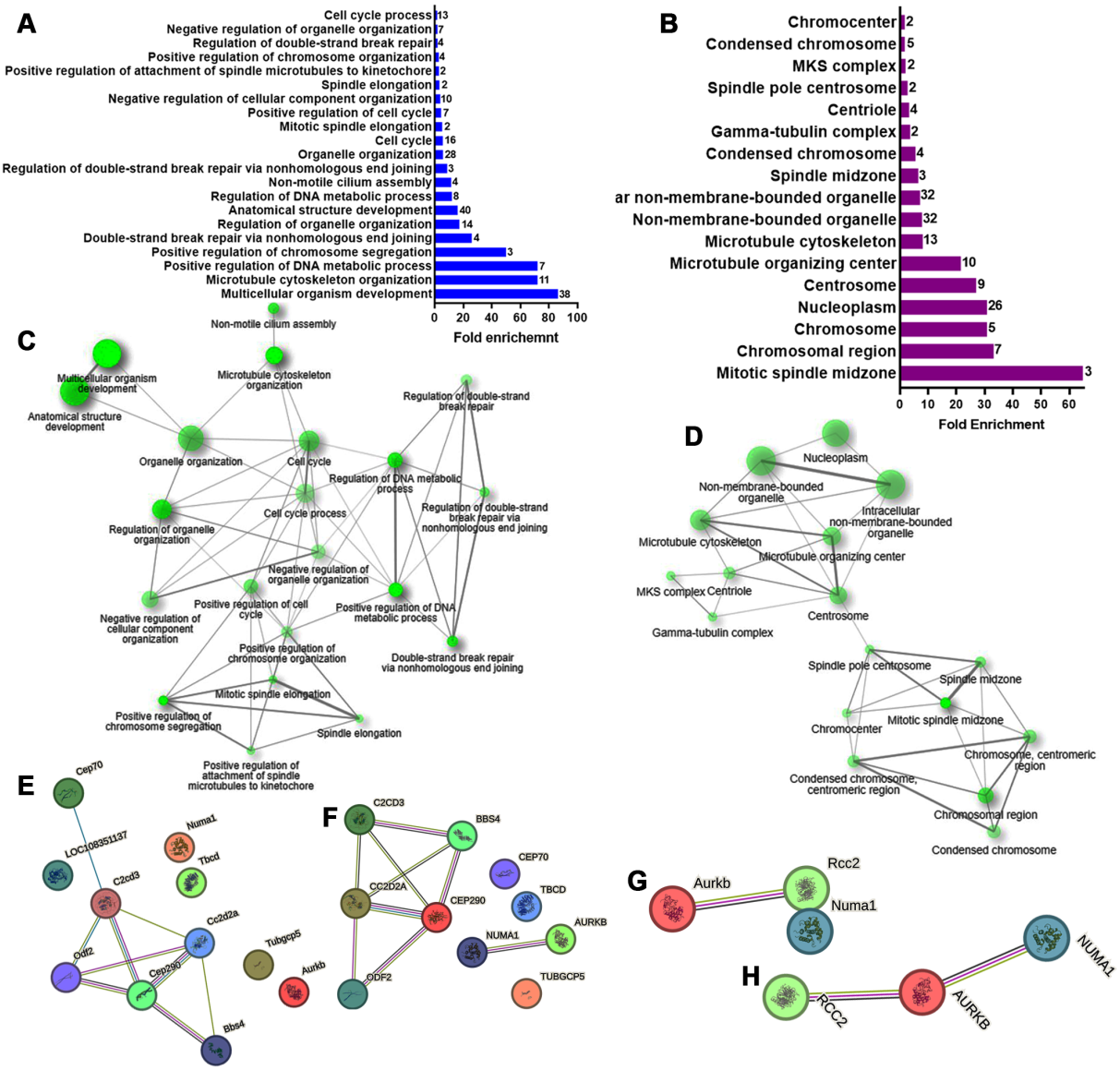

FIGURE 2
Gene ontology (GO) Biological Processes and Cellular Component enrichment analysis of up-regulated genes in E12 dorsal prosencephalon from diabetic dams. **(A, B)** Fold-enrichment graph showing 21 significantly enriched GO biological process terms (blue bars) and 17 cellular components terms (violet bars) in E12 tissue. Number within bars indicate the number of upregulated genes involved in each GO term (cut-off FDR P < 0.05). **(C, D)** Network clustering of GO biological process and cellular components terms. Nodes represent pathways; two nodes are connected if they share 20% or more genes. Darker nodes indicate greater statistical significance, larger nodes represent larger gene sets, and thicker edges indicate a higher gene overlap (overlap coefficient of at least 0.3). **(E, F)** Protein-protein interaction network for the GO term "Microtubule Cytoskeleton Organization" in rat and human, respectively. **(G, H)** Protein-protein interaction network for the GO term "Mitotic spindle midzone" in rat and human, respectively. Circles represent proteins. Interaction types are indicated by colored lines: green (curated databases), pink (experimentally determined), olive green (text mining), and black (co-expression).

Kif24, Camsap1, and Camsap2, which are important for chromosome movement and cilia formation during mitosis (Supplementary Table 5). Network analysis showed that microtubule depolymerization and organelle organization were isolated terms (Figure 3C). STRING analysis in rats revealed a node with Kif2c and Kif18a, proteins with microtubule plus-end depolymerizing activity in mitotic cells (Figure 3E). In humans, an additional node included interactions between Kif24, Camsap1, and Camsap2, which are crucial for anchoring centrosomes and restricting cilia nucleation at centrioles (Figure 3F).

GO analysis of cellular components for down-regulated genes revealed 29 enriched terms (Figure 3B, Supplementary Table 6). The top three were catalytic complex (GO:1902494), nuclear lumen (GO:0031981), and nucleoplasm (GO:0005654). The resultant network linked 24 terms with the protein-containing complex in the center of the network (Figure 3D). STRING analysis revealed three nodes shared between rats (Figure 3G) and humans (Figure 3H). These nodes included: GPI-anchor transamidase complex (GO:0042765) with Pigu and Pigk; ESC/E(Z) complex (GO:0035098) with Ezh1, Phf19, and Jarid2; and cullin-RING

10.3389/fendo.2025.1564441

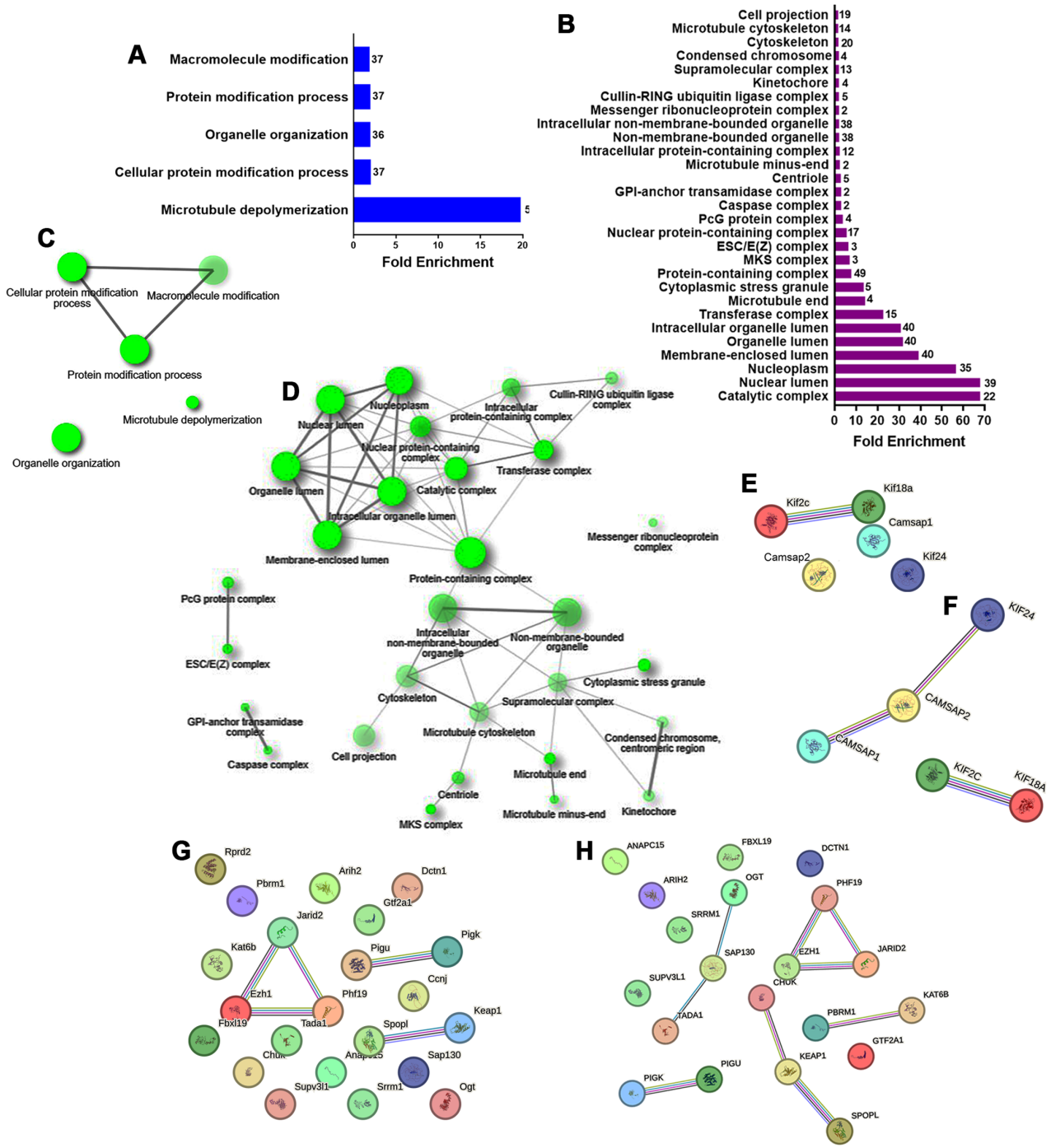

FIGURE 3
GO biological processes and cellular component enrichment analysis of the down-regulated genes in E12 dorsal prosencephalon from diabetic dams. **(A, B)** Fold-enrichment graph showing significantly enriched GO biological process (blue bars) and cellular components (violet bars) terms. Numbers within bars indicates the number of down-regulated genes involved in each term (cut-off FDR P < 0.05). **(C, D)** Network clustering of GO biological process and cellular component terms. Nodes represent pathways; two nodes are connected if they share 20% of genes. Darker nodes indicate greater statistical significance, larger nodes represent larger gene sets, and thicker edges indicate greater gene overlap (overlap coefficient of at least 0.3). **(E, F)** Protein-protein interaction network for down-regulated genes involved in the GO term "Microtubule depolymerization" in rat and human, respectively. **(G, H)** Protein-protein interaction network for down-regulated genes involved in the GO term "Catalytic complex" in rat and human, respectively. Circles represent proteins. Interaction types are indicated by colored lines: pink (experimentally determined), olive green (text mining), cyan (curated database), violet (protein homology), and black (co-expression).

10.3389/fendo.2025.1564441

ubiquitin ligase complex (GO:0031461) with Spopl and Keap1, and in humans CHUK.

3.2 Numa1 and Aurkb expression and spindle morphology

The bioinformatics and the reported increased neurogenic markers in embryos from diabetic rats and mice at E14 and E11.5, respectively (11–13), suggest impaired cell division. Two key genes involved in the planar division, Numa1 and Aurkb, were identified as up-regulated. Since these two genes were involved in more than 50% of the enriched terms significantly affected, emerging as key regulators of mitotic spindle architecture and chromosome segregation. Furthermore, they have been shown that defects in spindle orientation and asymmetric cell division lead to abnormal neurogenesis, which is a hallmark of neurodevelopmental impairments in diabetic conditions (26, 28). qRT-PCR validated their increased expression, showing a 2-fold and a 1.3-fold increase for Numa1 and Aurkb, respectively, in the Db vs the Ctl group (Figure 4A). However, protein levels and AURBT232ph did not showed significant changes (Figures 4B–E).

Immunofluorescence analysis of en-face mounted explants revealed a belt-like distribution of NUMA1 in most cells of both groups, indicative of prometaphase. However, the Db group exhibited a higher number of cells in prometaphase, suggesting an increased entry in mitosis (Figure 5A). In metaphase/anaphase cells, α-TUB staining showed significant spindle abnormalities in the Db group, including monopolar spindles, compared to the typical astral spindles in the Ctl group (Figure 5A).

Similar findings were observed in cultured E12 NSC, where monopolar spindles were prevalent in the Db group (Figure 5B). Analysis of NUMA1 distribution indicated a significant increase in asymmetric cell division in the Db group (1.63-fold vs Ctl), with no significant changes in symmetric divisions (Figure 5C). These results suggest aberrant spindle morphology and premature asymmetric cell division in the cortical neuroepithelium of embryos from diabetic dams.

In prometaphase, AURKBT232ph is typically localized at mid-zone chromosomes, stabilizing spindle elongation and cleavage furrow formation (43). In the Ctl group explants, AURKBT232ph displayed a distinct pattern of four nuclear dots and peripheral staining around chromosomes, with corresponding α-TUB staining at the center. In the Db group, this pattern was disrupted, with irregular dots and reduced

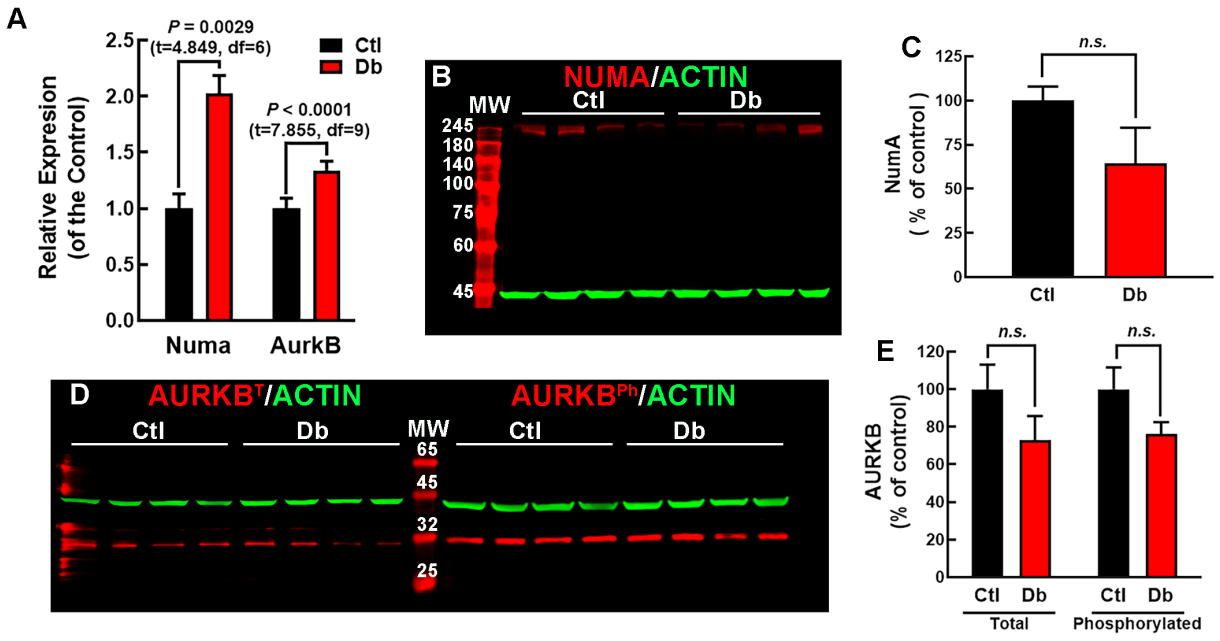

FIGURE 4
Expression analysis of NUMA and AURKB in E12 dorsal prosencephalon from control and diabetic rats. **(A)** Relative expression levels of Numa and Aurkb in control (Ctl, black bars) and diabetic (Db, red bars) groups, determined by qRT-PCR (2-ΔΔCT method). Data are shown as means ± S.E.M. (N = 4). P values were obtained using the Student´s t-test. **(B)** Western blot analysis of NUMA (~238 kDa, red bands) and actin (~42 kDa, green bands) in Ctl and Db groups samples (N = 4). MW = molecular weight marker. **(C)** Quantitative analysis of NUMA/ACTIN fluorescence intensity expressed as a percentage of the Ctl. No significant difference (n.s.) was detected (t- test). **(D)** Western blot analysis of total (AURKBT) and phosphorylated AURKB (AURKBPh ~35 kDa, red bands) with actin (~42 kDa, green bands) in Ctl and Db groups (N = 4). MW = molecular weight marker. **(E)** Quantitative analysis of total and phosphorylated AURKB/ACTIN fluorescence intensity. No significant difference (n.s.) was detected (test).

10.3389/fendo.2025.1564441

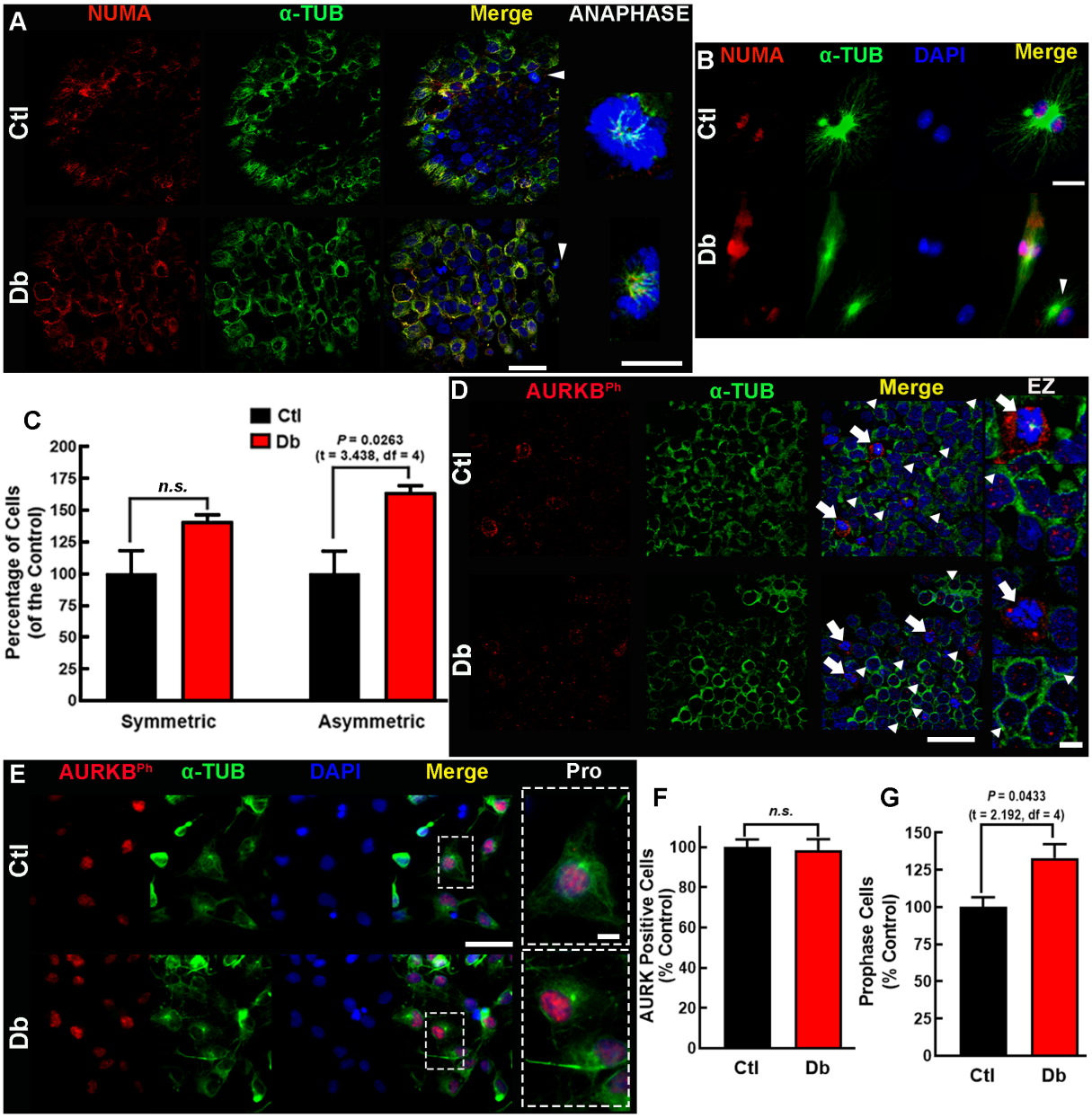

FIGURE 5
In-face view and *in vitro* analysis of NUMA and AURKB expression and distribution. **(A, B)** Representative micrographs (60×) of NUMA (red) and α-tubulin (α-TUB, green) in the ventral zone of E12 dorsal prosencephalon tissue **(A)** and cultured neural stem cell **(B)** from control (Ctl) and diabetic (Db) groups shown in single and merged channels. On the right, zoomed (200×) images of cells in anaphase (white arrowheads). Nuclei are stained with DAPI (blue). **(C)** Quantitative analysis of symmetric and asymmetric NSC divisions, expressed as percentage of Ctl ± SEM (n = 4). P value obtained using the t-Student test. n.s., no significance. **(D, E)** Representative micrographs (40×) of phosphorylated AURKB (AURKBph, red) and α-tubulin (α-TUB, green) immunostaining in E12 dorsal prosencephalon **(D)** and cultured NSC **(E)** presented in single and merged channels. On the right, zooms (EZ; 200×) for cells in anaphase (white arrowheads) and late telophase (arrows). Nuclei stained with DAPI are shown in blue. **(F)** Quantitative analysis of total and **(G)** prophase AURKBPh-positive NSC, expressed as percentage of Ctl ± SEM (n = 4). P value obtained using the Student´s t-test. n.s., no significance. Scale bar = 25 µm and for zoomed images 10 µm.

peripheral staining of AURKBT232ph accompanied by absent α-TUB staining (Figure 5D). Cultured NSC showed no changes in the number of AURKBT232ph-positive cells, but a significant increase in cells undergoing prophase was observed (Figures 5E–G).

Given the enrichment of microtubule depolymerization process in down-regulated genes, we analyze mitotic spindle length using α-TUB staining. The Db group exhibited longer and more robust spindles (Figures 6A–C), supporting the bioinformatic prediction of impaired microtubule depolymerization.

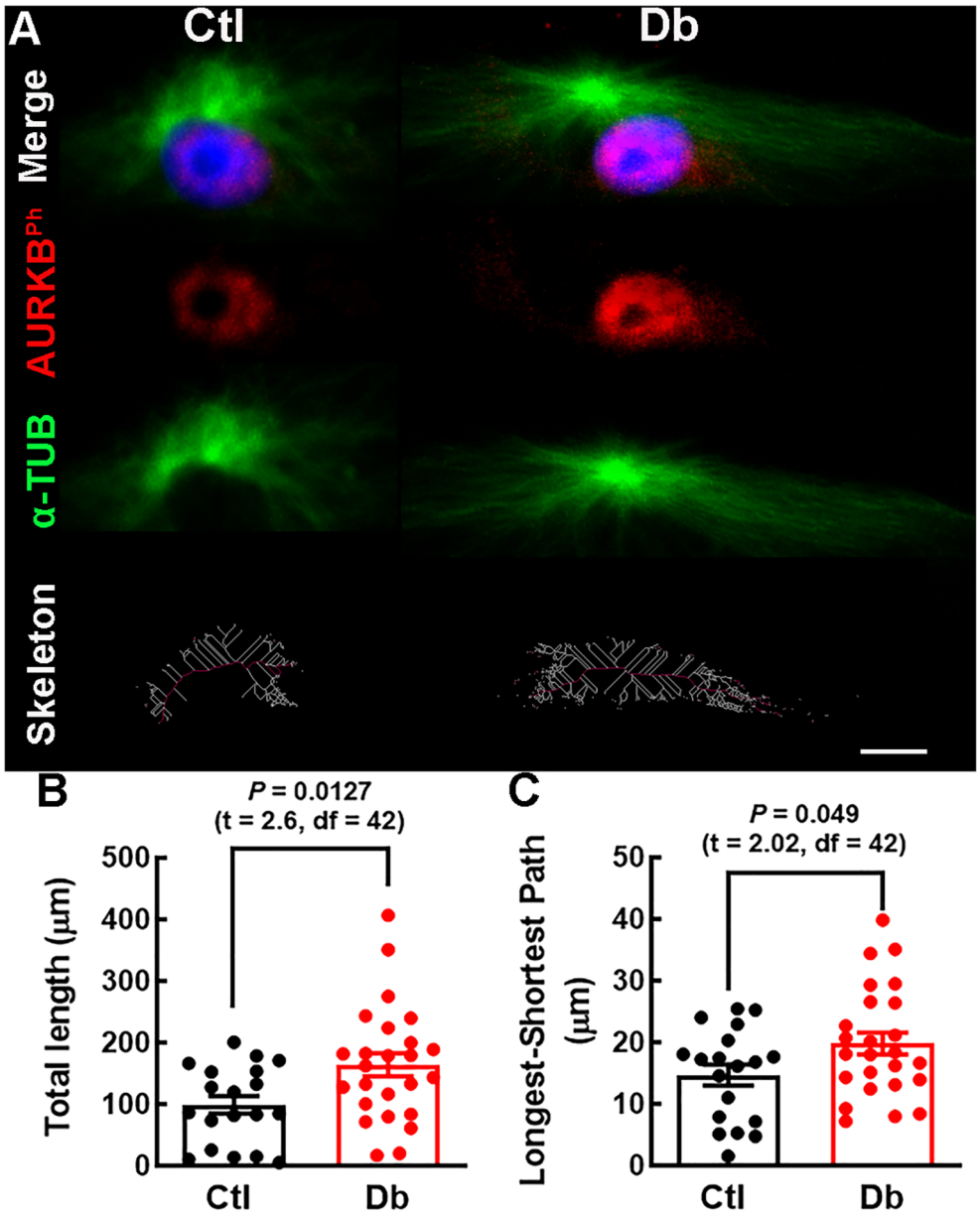

FIGURE 6
Mitotic spindle structure analysis in cultured E12 neural stem cells. **(A)** Representative micrographs (40×) of α-TUBULIN (α-TUB, green) staining of mitotic spindles in cultured E12 NSC. Nuclei are stained with DAPI (blue). Bottom panel; spindle skeleton (white lines) and the longest-shortest path (red line) representing spindle length in late prophase NSC. **(B, C)** Quantitative analysis of total spindle length (White lines) and mitotic spindle size (red line) in control (Ctl, black bars and dots) and diabetic (Db, red bars and dots) groups. Data points represent individual cells from three experiments. P values were obtained using the Student´s t-test. Scale bar = 2 µm.

4 Discussion

This study aimed to understand the molecular disruptions associated with maternal diabetes and their potential impact on early corticogenesis, specifically focusing on cell cycle regulation, spindle dynamics, and neurogenesis.

The bioinformatic analysis of the RNA-seq data from embryonic samples without neural tube defects at E12 provides significant insights into the impact of maternal diabetes on gene expression in the developing dorsal prosencephalon.

Although mating was controlled as carefully as possible, the heterogeneity observed may stem from slight differences in the embryonic stage between litters and stochastic fluctuations in gene expression during early corticogenesis (44, 45). Such variability is expected in developmental studies. Despite sample variability, as highlighted by the PCA and hierarchical clustering analyses, differential gene expression analysis identified 111 up-regulated and 136 down-regulated genes out of 24,170. These findings consistently point to disruptions in cell cycle regulation and spindle dynamics as key consequences of maternal diabetes.

The GO analysis of the up-regulated genes revealed their involvement in key biological processes and cellular components related to cell cycle regulation and mitosis. Enriched terms such as multicellular organism development, microtubule cytoskeleton organization, and positive regulation of DNA metabolic processes suggest that these genes are critical in maintaining proper cell division and genome stability during neurodevelopment. The genes Numa1 and Aurkb emerged as central regulators within these processes. STRING analysis highlighted their inclusion in conserved protein interaction networks in rats and humans, indicating that the underlying molecular mechanisms of cell cycle regulation may be translatable between species.

In contrast, the down-regulation of genes such as Kif18a, Kif2c, and Kif24 are key players in microtubule dynamics, and a decreased expression could disrupt the delicate balance of symmetric and asymmetric cell division necessary for proper neurogenesis and, consequently, neuroblast migration, ultimately affecting corticogenesis. Interestingly, evidence of impaired migration has been previously reported in offspring from diabetic dams (10). The GO-cellular component analysis further supports the hypothesis that maternal diabetes disrupts critical aspects of the mitotic cell cycle, particularly those associated with spindle assembly and chromosome segregation. Disruption in networks such as catalytic complexes, nuclear lumen, and membrane-enclosed lumen components may affect intracellular signaling and gene expression regulation, contributing to neurodevelopmental deficits in offspring.

The identification of similar protein interaction networks in rats and humans involving proteins like KIF2C, KIF18A, PHF19, JARD2, and EZH1 underscores the potential relevance of these findings to human development. Highlighting that the molecular machinery might be affected in both species due to maternal diabetes, supporting the relevance of the results obtained and highlighting the importance of evaluating early corticogenesis in animal models of maternal diabetes.

Microtubules are essential for mitotic spindle architecture, which evolves as neurodevelopment progresses. In early neurogenesis (E12 in rats), astral spindle morphology is typical and associated with symmetric cell division. By the neurogenic peak (E14 in rats), cell division predominantly switches to an asymmetric mode characterized by inner spindle morphology (24). This transition from symmetric to asymmetric division is critical for defining brain cytoarchitecture and size (21, 46, 47).

Our experimental findings show that maternal diabetes affects mitotic spindle morphology and cell division dynamics in the E12 cortical neuroepithelium. At this stage, the dorsal prosencephalon is primarily populated by NSC, and the shift from symmetric to asymmetric division initiates deep-layer neurogenesis (46). The altered expression of Numa1 and Aurkb in the Db group could likely promote an early shift toward asymmetric cell divisions. This premature switch can be associated with increased neurogenic markers previously reported in rodent embryos from diabetic mothers at the neurogenic peak (8, 9). The early commitment of NSCs to neural differentiation could explain the depletion of the NSC pool previously reported (7, 8), which is necessary for later stages of brain development and could also explain the increase in asymmetric cell proliferation observed in this study.

Although Numa1 and Aurkb expression levels were increased in the Db group, this did not correspond to higher protein levels or phosphorylation of AURKBT232, suggesting possible post-transcriptional regulation. However, immunofluorescence analysis supported the presence of mitotic defects. The belt-like distribution of NUMA1 exhibited in Db explants, characteristic of prometaphase cells, indicates potential mitotic delay or dysregulation. Such delays have been linked to abnormal spindle architecture, evidenced by an increased prevalence of monopolar spindles in Db explants and cultured NSCs observed here, contrasting with the typical astral spindle in controls (29, 48).

The spindle assembly checkpoint may be compromised in the Db group, leading to delays in chromosome segregation as cells attempt to correct spindle attachment errors (49). This opens avenues for exploring the interplay between NSC gene expression, protein function, and cell-cycle regulation in maternal diabetes and neurodevelopment.

The observed changes in mitotic spindle morphology may result from impaired microtubule depolymerization, supported by the bioinformatic enrichment of related terms among the down-regulated genes. This aspect must be further studied since it is known that defects in microtubule depolymerization compromise spindle integrity and orientation, which are critical for symmetric and asymmetric cell divisions (24).

Disrupted AURKBT232ph in Db explants suggests potential chromosome segregation issues and cleavage furrow formation (50, 51). In controls, AURKBT232ph displayed a punctuated organized pattern aligned with the chromosomal midzone, facilitating spindle elongation and chromosome separation. This pattern was disrupted in Db samples, indicating potential spindle instability and misalignment, which could interfere with chromosome segregation and cytokinesis. Interestingly, changes in AURKBT232ph have been associated with defective spindle positioning and misorientation during cell division, resulting in premature neurogenesis and differentiation due to early asymmetric cell division processes (49–51).

The chromosomal passenger complex, comprising AURBK, the inner centromere protein, borealin, and survivin, stabilizes microtubules and regulates the spindle assembly checkpoints (52–55). Disrupted AURKBT232ph patterns in the Db embryos may reflect attempts to correct microtubule attachment errors as a mechanism in embryos without neural tube defects to ensure complete development and survival (49, 56). AURKB is considered the central regulator of the error correction process of kinetochore-microtubule attachments through the phospho-regulation of KIF2C, a kinesin-13 family member involved in microtubule depolymerization (57–59), a gene downregulated in the Db group. Thus, in a microtubule low-tension situation, as suggested by longer spindles observed in this study, AURKB may promote microtubule destabilization, promoting error correction. However, further studies are needed to elucidate its precise role during the corticogenesis of embryos exposed to high glucose.

Quantifying mitotic spindle length revealed longer and more robust spindles in the Db group, consistent with impaired microtubule depolymerization. Insufficient depolymerization can lead to aberrant spindle geometry, affecting cell fate decisions and reducing the progenitor pool necessary for cortical expansion (29, 49, 60). The shift toward asymmetric divisions may contribute to long-term neurodevelopmental deficits previously reported in children from diabetic mothers.

The mitotic abnormalities observed in our study are particularly significant because NSCs in the VZ undergo tightly regulated symmetric and asymmetric divisions to maintain balanced neurogenesis and gliogenesis. Normally, symmetric divisions at early neurodevelopmental stages expand the NSC pool, while asymmetric divisions promote time-dependent differentiation into neurons and glia (13). Our findings indicate that maternal diabetes drives this balance toward asymmetric division earlier than expected, which could lead to premature differentiation and an insufficient progenitor pool for later cortical development (21).

This premature neurogenic commitment has been observed in previous studies on diabetic embryopathy. For instance, increased neurogenic markers and reduced neural progenitor proliferation were reported in E14 embryos from diabetic rats (7, 9), suggesting an early exhaustion of progenitor cells. Interestingly, altered mitotic spindles, as observed in our study, are known to affect interkinetic nuclear migration, which is crucial for NSC self-renewal (20). Disruptions in this process may lead to aberrant neuronal positioning and could contribute to the cortical thinning and cytoarchitectural defects reported in the offspring of diabetic mothers (10). Furthermore, the depletion of the NSC pool and premature neurogenesis could have profound consequences for cortical function and behavior. Indeed, reduced cortical progenitor proliferation in diabetic pregnancies has been linked to altered cortical thickness, function, and impaired neuronal connectivity (10, 28). These structural deficits may underlie the cognitive and motor impairments observed in children of diabetic mothers, such as deficiencies in working memory, attention, and executive function (61).

The precise regulation of mitotic spindle orientation and cell cycle progression in NSCs is crucial for maintaining the balance between self-renewal and differentiation. Disruptions in mitotic spindle orientation and cell cycle progression have been linked to neurodevelopmental disorders such as microcephaly and autism spectrum disorders (ASD) (62, 63). Furthermore, aberrant mitotic spindle orientation has been implicated in cortical thinning, misplacement of neurons, and disrupted neuronal connectivity (62). Given that Aurkb and Numa1 play crucial roles in spindle assembly and chromosome segregation (29), their dysregulation under diabetic conditions may contribute to similar neurodevelopmental deficits. Our data suggest that maternal diabetes disrupts self-renewal and differentiation by promoting early asymmetric divisions, possibly depleting the NSC population prematurely, as observed in E14 telencephalons (7). This conclusion is supported by increased expression of Aurkb and Numa1, genes involved in mitotic spindle organization and chromosome segregation, alongside structural abnormalities in spindle morphology.

One mechanism potentially linking maternal diabetes to mitotic dysregulation is oxidative stress, which can impair NSC proliferation and differentiation (27). Hyperglycemia-induced oxidative damage may alter spindle microtubule stability and chromosome segregation, thereby increasing mitotic errors. Additionally, epigenetic modifications such as changes in DNA methylation patterns have been reported in the brains of offspring from diabetic pregnancies, which may influence gene expression programs involved in neurogenesis (26, 64, 65).

Our study has certain limitations, including the use of only one developmental window. However, previous studies by our group and others indicate that, under this same model, findings related to developmental timing and postnatal outcomes collectively offer insights into both prenatal and postnatal cortical development. Moreover, although our transcriptomic and immunofluorescence analyses provide strong evidence of altered mitotic regulation, additional functional assays, such as time-lapse imaging of neural progenitor divisions or *in vivo* lineage tracing, would strengthen our conclusions.

Future studies should explore whether pharmacological or molecular interventions aimed at stabilizing the mitotic spindle or mitigating oxidative stress can offset these effects. Single-cell RNA sequencing could also provide deeper insights into the fate of prematurely differentiated neural progenitors. Moreover, research on microtubule dynamics during mitosis is warranted, given that genes such as Kif18a, Camsap2, Kif24, Camsap1, and Kif2c, which were found to be down-regulated, are involved in microtubule depolymerization together with Numa (65). Employing *in vivo* conditional knockout models or *ex vivo* shRNA approaches would be valuable for dissecting the mechanistic role of these genes in NSC function and corticogenesis.

Clinically, our findings underscore the importance of maternal glycemic control during pregnancy to prevent early neurodevelopmental abnormalities that may predispose offspring to cognitive and behavioral disorders. Understanding the molecular basis of maternal diabetes-induced neurodevelopmental impairments could inform therapeutic strategies. Given that metabolic disorders such as gestational diabetes are increasing in prevalence, identifying early biomarkers of neural dysfunction may aid in developing preventative interventions aimed at improving neurodevelopmental outcomes in affected offspring.

In conclusion, maternal diabetes disrupts the expression of genes critical for microtubule dynamics, spindle formation, and cell division symmetry, thereby impairing early corticogenesis. Aberrant mitotic spindle formation and premature asymmetric cell division may underlie the neurodevelopmental vulnerabilities observed in the offspring of diabetic mothers. The similarities in protein interaction networks between rats and humans highlight the importance of using *in vivo* models to advance our understanding of these mechanisms and their implications for human health. Further research into the molecular pathways affected by maternal diabetes may identify potential therapeutic

targets to prevent neurodevelopmental impairments associated with gestational diabetes.

Data availability statement

The original contributions presented in the study are included in the article/Supplementary Material, further inquiries can be directed to the corresponding author/s.

Ethics statement

The animal study was approved by Instituto Nacional de Perinatología Committee of Research and Animal Care (CICUAL). The study was conducted in accordance with the local legislation and institutional requirements.

Author contributions

RV-B: Formal analysis, Investigation, Methodology, Writing – original draft, Writing – review & editing. DM-G: Formal analysis, Methodology, Writing – original draft. DD-P: Formal analysis, Writing – original draft. ND: Investigation, Methodology, Supervision, Writing – review & editing. DÁ-G: Supervision, Formal analysis, Project administration, Resources, Writing – original draft. AM-H: Conceptualization, Formal analysis, Funding acquisition, Investigation, Methodology, Project administration, Resources, Supervision, Validation, Writing – original draft, Writing – review & editing, Visualization.

Funding

The author(s) declare that financial support was received for the research and publication of this article. Funding to AM-H from Instituto Nacional de Perinatología Isidro Espinosa de los Reyes, federal grant 2018-1-146. All authors have read and agreed with the final version of the manuscript.

Acknowledgments

The authors thank Yuriria Paredes-Vivas and Héctor Herrera-Fernández for laboratory technical support and Talia Estrada-Rojas for animal care.

Conflict of interest

The authors declare that the research was conducted in the absence of any commercial or financial relationships that could be construed as a potential conflict of interest.

Generative AI statement

The author(s) declare that no Generative AI was used in the creation of this manuscript.

Publisher's note

All claims expressed in this article are solely those of the authors and do not necessarily represent those of their affiliated organizations, or those of the publisher, the editors and the reviewers. Any product that may be evaluated in this article, or claim that may be made by its manufacturer, is not guaranteed or endorsed by the publisher.

Supplementary material

The Supplementary Material for this article can be found online at: https://www.frontiersin.org/articles/10.3389/fendo.2025.1564441/full#supplementary-material

References

1. Camprubi Robles M, Campoy C, Garcia Fernandez Lopez-Pedrosa JM, Rueda R, Martin MJ. Maternal diabetes and cognitive performance in the offspring: A systematic review and meta-analysis. *PloS One*. (2015) 10:e0142583. doi: 10.1371/journal.pone.0142583

2. Dionne G, Boivin M, Séguin JR, Pérusse D, Tremblay RE. Gestational diabetes hinders language development in offspring. *Pediatrics*. (2008) 122:e1073–9. doi: 10.1542/peds.2007-3028

3. Bolaños L, Matute E, Ramírez-Dueñas ML, Zarabozo D. Neuropsychological impairment in school-aged children born to mothers with gestational diabetes. *J Child Neurol*. (2015) 30:1616–24. doi: 10.1177/0883073815575574

4. Ornoy A, Reece EA, Pavlinkova G, Kappen C, Miller RK. Effect of maternal diabetes on the embryo, fetus, and children: congenital anomalies, genetic and epigenetic changes and developmental outcomes. *Birth Defects Res C Embryo Today*. (2015) 105:53–72. doi: 10.1002/bdrc.21090

5. Kong L, Norstedt G, Schalling M, Gissler M, Lavebratt C. The risk of offspring psychiatric disorders in the setting of maternal obesity and diabetes. *Pediatrics*. (2018) 142(3):e20180776. doi: 10.1542/peds.2018-0776

6. Friedman NP, Robbins TW. The role of prefrontal cortex in cognitive control and executive function. *Neuropsychopharmacology*. (2022) 47:72–89. doi: 10.1038/s41386-021-01132-0

7. De la Merced-Garcia DS, Sánchez-Barrera S, Hernández-Yonca J, Mancilla I, García-López G, Díaz NF, et al. Increased nuclear FOXP2 is related to reduced neural stem cell number and increased neurogenesis in the dorsal telencephalon of embryos of diabetic rats through histamine H(1) receptors. *Cells*. (2023) 12:4–18. doi: 10.3390/cells12030510

8. Fu J, Tay SSW, Ling EA, Dheen ST. High glucose alters the expression of genes involved in proliferation and cell-fate specification of embryonic neural stem cells. *Diabetologia*. (2006) 49:1027–38. doi: 10.1007/s00125-006-0153-3

9. Solis KH, Méndez LI, García-López G, Díaz NF, Portillo W, De Nova-Ocampo M, et al. The histamine H1 receptor participates in the increased dorsal telencephalic neurogenesis in embryos from diabetic rats. *Front Neurosci*. (2017) 11:676. doi: 10.3389/fnins.2017.00676

10. De la Merced-García DS, Sánchez-Barrera S, Hernández-Yonca J, Mancilla I, García-López G, Díaz NF, et al. Impaired cortical cytoarchitecture and reduced excitability of deep-layer neurons in the offspring of diabetic rats. *Front Cell Dev Biol*. (2020) 8:564561. doi: 10.3389/fcell.2020.564561

11. Tsui D, Vessey JP, Tomita H, Kaplan DR, Miller FD. FoxP2 regulates neurogenesis during embryonic cortical development. *J Neurosci*. (2013) 33:244–58. doi: 10.1523/JNEUROSCI.1665-12.2013

12. Vernes SC, Spiteri E, Nicod Groszer JM, Taylor JM, Davies KE. High-throughput analysis of promoter occupancy reveals direct neural targets of FOXP2, a gene mutated in speech and language disorders. *Am J Hum Genet*. (2007) 81:1232–50. doi: 10.1086/522238

13. Florio M, Huttner WB. Neural progenitors, neurogenesis and the evolution of the neocortex. *Development*. (2014) 141:2182–94. doi: 10.1242/dev.090571

14. Telley L, Agirman G, Prados J, Amberg N, Fièvre S, Oberst P, et al. Temporal patterning of apical progenitors and their daughter neurons in the developing neocortex. *Science*. (2019) 364:1–8. doi: 10.1126/science.aav2522

15. Fietz SA, Huttner WB. Cortical progenitor expansion, self-renewal and neurogenesis-a polarized perspective. *Curr Opin Neurobiol*. (2011) 21:23–35. doi: 10.1016/j.conb.2010.10.002

16. Fernandez V, Llinares-Benadero C, Borrell V. Cerebral cortex expansion and folding: what have we learned? *EMBO J*. (2016) 35:1021–44. doi: 10.15252/embj.201593701

17. Koo B, Lee KH, Ming GL, Yoon JJ, Song H. Setting the clock of neural progenitor cells during mammalian corticogenesis. *Semin Cell Dev Biol*. (2023) 142:43–53. doi: 10.1016/j.semcdb.2022.05.013

18. Molyneaux BJ, Arlotta P, Menezes JRL, Macklis JD. Neuronal subtype specification in the cerebral cortex. *Nat Rev Neurosci*. (2007) 8:427–37. doi: 10.1038/nrn2151

19. Rakic P. Evolution of the neocortex: a perspective from developmental biology. *Nat Rev Neurosci*. (2009) 10:724–35. doi: 10.1038/nrn2719

20. Noctor SC, Martínez-Cerdeño V, Ivic L, Kriegstein AR. Cortical neurons arise in symmetric and asymmetric division zones and migrate through specific phases. *Nat Neurosci*. (2004) 7:136–44. doi: 10.1038/nn1172

21. Gotz M, Huttner WB. The cell biology of neurogenesis. *Nat Rev Mol Cell Biol*. (2005) 6:777–88. doi: 10.1038/nrm1739

22. Matsuzaki F, Shitamukai A. Cell division modes and cleavage planes of neural progenitors during mammalian cortical development. *Cold Spring Harb Perspect Biol*. (2015) 7:a015719. doi: 10.1101/cshperspect.a015719

23. Casas Gimeno G, Paridaen J. The symmetry of neural stem cell and progenitor divisions in the vertebrate brain. *Front Cell Dev Biol*. (2022) 10:885269. doi: 10.3389/fcell.2022.885269

24. Vargas-Hurtado D, Brault JB, Piolot T, Leconte L, Da Silva N, Pennetier C, et al. Differences in mitotic spindle architecture in mammalian neural stem cells influence mitotic accuracy during brain development. *Curr Biol*. (2019) 29:2993–3005. doi: 10.1016/j.cub.2019.07.061

25. Zhao J, Hakvoort TBM, Willemsen AM, Jongejan A, Sokolovic M, Bradley EJ, et al. Effect of hyperglycemia on gene expression during early organogenesis in mice. *PloS One*. (2016) 11:e0158035. doi: 10.1371/journal.pone.0158035

26. Luo SS, Zou KX, Zhu H, Cheng Y, Yan YS, Sheng JZ, et al. Integrated multi-omics analysis reveals the effect of maternal gestational diabetes on fetal mouse hippocampi. *Front Cell Dev Biol*. (2022) 10:748862. doi: 10.3389/fcell.2022.748862

27. Ramya S, Shyamasundar S, Bay BH, Dheen ST. Maternal diabetes alters expression of microRNAs that regulate genes critical for neural tube development. *Front Mol Neurosci*. (2017) 10:237. doi: 10.3389/fnmol.2017.00237

28. Zhao J, Hakvoort TBM, Ruijter JM, Jongejan A, Koster J, Swagemakers SMA, et al. Maternal diabetes causes developmental delay and death in early-somite mouse embryos. *Sci Rep*. (2017) 7:11714. doi: 10.1038/s41598-017-11696-x

29. di Pietro F, Echard A, Morin X. Regulation of mitotic spindle orientation: an integrated view. *EMBO Rep*. (2016) 17:1106–30. doi: 10.15252/embr.201642292

30. Ramkumar N, Patel JV, Anstatt J, Baum J. Aurora B-dependent polarization of the cortical actomyosin network during mitotic exit. *EMBO Rep*. (2021) 22:e52387. doi: 10.15252/embr.202152387

31. Percie du Sert N, Ahluwalia A, Alam S, Avey MT, Baker M, Browne WJ. Reporting animal research: Explanation and elaboration for the ARRIVE guidelines 2.0. *PloS Biol*. (2020) 18:e3000411. doi: 10.1371/journal.pbio.3000411

32. Wingett SW, Andrews S. FastQ Screen: A tool for multi-genome mapping and quality control. *F1000Res*. (2018) 7:1338. doi: 10.12688/f1000research.15931.2

33. Marcel M. Cutadapt removes adapter sequences from high-throughput sequencing reads. *EMBnet. J*. (2011) 17:10–2. doi: 10.14806/ej.17.1.200

34. Langmead B, Salzberg SL. Fast gapped-read alignment with Bowtie 2. *Nat Methods*. (2012) 9:357–9. doi: 10.1038/nmeth.1923

35. Li B, Dewey CN. RSEM: accurate transcript quantification from RNA-Seq data with or without a reference genome. *BMC Bioinf*. (2011) 12:323. doi: 10.1186/1471-2105-12-323

36. Robinson MD, McCarthy DJ, Smyth GK. edgeR: a Bioconductor package for differential expression analysis of digital gene expression data. *Bioinformatics*. (2010) 26:139–40. doi: 10.1093/bioinformatics/btp616

37. Ge SX, Jung D, Yao R. ShinyGO: a graphical gene-set enrichment tool for animals and plants. *Bioinformatics*. (2020) 36:2628–9. doi: 10.1093/bioinformatics/btz931

38. Bradford MM. A rapid and sensitive method for the quantitation of microgram quantities of protein utilizing the principle of protein-dye binding. *Anal Biochem*. (1976) 72:248–54. doi: 10.1006/abio.1976.9999

39. Villanueva MA. Electrotransfer of proteins in an environmentally friendly methanol-free transfer buffer. *Anal Biochem*. (2008) 373:377–9. doi: 10.1016/j.ab.2007.08.007

40. Rujano MA, Basto R, Marthiens V. New insights into centrosome imaging in Drosophila and mouse neuroepithelial tissues. *Methods Cell Biol*. (2015) 129:211–27. doi: 10.1016/bs.mcb.2015.04.005

41. Arganda-Carreras I, Fernández-González R, Muñoz-Barrutia A, Ortiz-De-Solorzano C. 3D reconstruction of histological sections: Application to mammary gland tissue. *Microsc Res Tech*. (2010) 73:1019–29. doi: 10.1002/jemt.20829

42. Polder G, Hovens HLE, Zweers AJ. (2010). Measuring shoot length of submerged aquatic plants using graph analysis, in: *Proceedings of the ImageJ User and Developer Conference*, pp. 172–7. Luxembourg: Centre de Recherche Public Henri Tudor.

43. van der Horst A, Vromans MJM, Bouwman K, van der Waal MS, Hadders MA, Lens SMA. Inter-domain cooperation in INCENP promotes aurora B relocation from centromeres to microtubules. *Cell Rep*. (2015) 12:380–7. doi: 10.1016/j.celrep.2015.06.038

44. Zechner C, Nerli E, Norden C. Stochasticity and determinism in cell fate decisions. *Development*. (2020) 147:dev181495. doi: 10.1242/dev.181495

45. Raj A, van Oudenaarden A. Nature, nurture, or chance: stochastic gene expression and its consequences. *Cell*. (2008) 135:216–26. doi: 10.1016/j.cell.2008.09.050

46. Shen Q, Wang Y, Dimos JT, Fasano CA, Phoenix TN, Lemischka IR. The timing of cortical neurogenesis is encoded within lineages of individual progenitor cells. *Nat Neurosci*. (2006) 9:743–51. doi: 10.1038/nn1694

47. Clancy B, Darlington RB, Finlay BL. Translating developmental time across mammalian species. *Neuroscience*. (2001) 105:7–17. doi: 10.1016/s0306-4522(01)00171-3

48. Silk AD, Holland AJ, Cleveland DW. Requirements for NuMA in maintenance and establishment of mammalian spindle poles. *J Cell Biol*. (2009) 184:677–90. doi: 10.1083/jcb.200810091

49. Ferreira LT, Maiato H. Prometaphase. *Semin Cell Dev Biol*. (2021) 117:52–61. doi: 10.1016/j.semcdb.2021.06.004

50. Munoz-Barrera M, Monje-Casas F. Increased Aurora B activity causes continuous disruption of kinetochore-microtubule attachments and spindle instability. *Proc Natl Acad Sci U S A*. (2014) 111:E3996–4005. doi: 10.1073/pnas.1408017111

51. Zeitlin SG, Shelby RD, Sullivan KF. CENP-A is phosphorylated by Aurora B kinase and plays an unexpected role in completion of cytokinesis. *J Cell Biol*. (2001) 155:1147–57. doi: 10.1083/jcb.200108125

52. Maresca TJ, Groen AC, Gatlin JC, Ohi R, Mitchison TJ, Salmon ED. Spindle assembly in the absence of a RanGTP gradient requires localized CPC activity. *Curr Biol*. (2009) 19:1210–5. doi: 10.1016/j.cub.2009.05.061

53. Sampath SC, Ohi R, Leismann O, Salic A, Pozniakovski A, Funabiki H. The chromosomal passenger complex is required for chromatin-induced microtubule stabilization and spindle assembly. *Cell*. (2004) 118:1–16. doi: 10.1016/j.cell.2004.06.026

54. Klein UR, Nigg EA, Gruneberg U. Centromere targeting of the chromosomal passenger complex requires a ternary subcomplex of Borealin, Survivin, and the N-terminal domain of INCENP. *Mol Biol Cell*. (2006) 17:2547–58. doi: 10.1091/mbc.e05-12-1133

55. Santaguida S, Vernieri C, Villa F, Ciliberto A, Musacchio A. Evidence that Aurora B is implicated in spindle checkpoint signalling independently of error correction. *EMBO J*. (2011) 30:1508–19. doi: 10.1038/emboj.2011.70

56. Hauf S, Cole RW, LaTerra S, Zimmer C, Schnapp G, Walter R, et al. The small molecule Hesperadin reveals a role for Aurora B in correcting kinetochore-microtubule attachment and in maintaining the spindle assembly checkpoint. *J Cell Biol*. (2003) 161:281–94. doi: 10.1083/jcb.200208092

57. Andrews PD, Ovechkina Y, Morrice N, Wagenbach M, Duncan K, Wordeman L, et al. Aurora B regulates MCAK at the mitotic centromere. *Dev Cell*. (2004) 6:253–68. doi: 10.1016/s1534-5807(04)00025-5

58. DeLuca JG, Gall WE, Ciferri C, Cimini D, Musacchio ASalmon ED. Kinetochore microtubule dynamics and attachment stability are regulated by Hec1. *Cell*. (2006) 127:969–82. doi: 10.1016/j.cell.2006.09.047

59. Ohi R, Sapra T, Howard J, Mitchison TJ. Differentiation of cytoplasmic and meiotic spindle assembly MCAK functions by Aurora B-dependent phosphorylation. *Mol Biol Cell*. (2004) 15:2895–906. doi: 10.1091/mbc.e04-02-0082

60. Jin M, Pomp O, Shinoda T, Toba S, Torisawa T, Furuta K. Katanin p80, NuMA and cytoplasmic dynein cooperate to control microtubule dynamics. *Sci Rep*. (2017) 7:39902. doi: 10.1038/srep39902

61. Rodolaki K, Pergialiotis V, Iakovidou N, Boutsikou T, Iliodromiti Z, Kanaka-Gantenbein C. The impact of maternal diabetes on the future health and neurodevelopment of the offspring: a review of the evidence. *Front Endocrinol (Lausanne)*. (2023) 14:1125628. doi: 10.3389/fendo.2023.1125628

62. Lancaster MA, Renner M, Martin CA, Wenzel D, Bicknell LS, Hurles ME. Cerebral organoids model human brain development and microcephaly. *Nature*. (2013) 501:373–9. doi: 10.1038/nature12517

63. Marchetto MC, Belinson H, Tian Y, Freitas BC, Fu C, Vadodaria KC. Altered proliferation and networks in neural cells derived from idiopathic autistic individuals. *Mol Psychiatry*. (2017) 22:820–35. doi: 10.1038/mp.2016.95

64. Parween S, Alawathugoda TT, Prabakaran AD, Dheen ST, Morse RH, Emerald BS, et al. Nutrient sensitive protein O-GlcNAcylation modulates the transcriptome through epigenetic mechanisms during embryonic neurogenesis. *Life Sci Alliance*. (2022) 5. doi: 10.26508/lsa.202201385

65. Sun M, Jia M, Ren H, Yang B, Chi W, Xin G, et al. NuMA regulates mitotic spindle assembly, structural dynamics and function via phase separation. *Nat Commun*. (2021) 12:7157. doi: 10.1038/s41467-021-27528-6

frontiers | Frontiers in Immunology

TYPE Original Research
PUBLISHED 09 June 2025
DOI 10.3389/fimmu.2025.1595222

OPEN ACCESS

EDITED BY
Sruthi Alahari,
University of Toronto, Canada

REVIEWED BY
Iane Oliveira Pires Porto,
University of Rio Verde, Brazil
Yongbo Zhao,
Shanghai First Maternity and Infant Hospital, China

*CORRESPONDENCE
Mengjia Peng
pemeji@wmu.edu.cn
Ying Hua
wzfeyhy1015@126.com

RECEIVED 17 March 2025
ACCEPTED 22 May 2025
PUBLISHED 09 June 2025

CITATION
Chen J, Zhang D, Zhu C, Lin L, Ye K, Hua Y and Peng M (2025) Explainable machine learning reveals ribosome biogenesis biomarkers in preeclampsia risk prediction. *Front. Immunol.* 16:1595222. doi: 10.3389/fimmu.2025.1595222

Explainable machine learning reveals ribosome biogenesis biomarkers in preeclampsia risk prediction

Jingjing Chen[1], Dan Zhang[1], Chengxiu Zhu[1], Lin Lin[1], Kejun Ye[1], Ying Hua[2*] and Mengjia Peng[1*]

[1]Department of Gynecology and Obstetrics, The Third Affiliated Hospital of Wenzhou Medical University, Rui'an, China, [2]Department of Gynecology and Obstetrics, The Second Affiliated Hospital of Wenzhou Medical University, Wenzhou, China

Background: Preeclampsia, a hypertensive disorder during pregnancy affecting 2-8% of pregnancies globally, remains a leading cause of maternal and fetal morbidity. Current diagnostic reliance on late-onset clinical features and suboptimal biomarkers underscores the need for early molecular predictors. Ribosome biogenesis, critical for cellular homeostasis, is hypothesized to drive placental dysfunction in PE, though its role remains underexplored.

Methods: We integrated placental transcriptomic data from two datasets (GSE75010, GSE10588) to systematically investigate ribosome biogenesis dysregulation in preeclampsia. Functional enrichment analyses delineated the dysregulation of pathways, while weighted gene co-expression network analysis identified hub genes within ribosome biogenesis-associated modules. A multi-algorithm machine learning framework was employed to optimize predictive performance, with model interpretability achieved through SHapley Additive exPlanations and diagnostic accuracy validated by receiver operating characteristic curves. Immune microenvironment profiling and regulatory network analyses elucidated mechanistic links. Finally, qRT-PCR confirmed the differential expression of key genes in clinical samples.

Results: We identified 25 ribosome biogenesis-related differentially expressed genes, which were significantly enriched in RNA degradation and rRNA processing. Weighted gene co-expression network analysis prioritized seven hub genes. A random forest model incorporating six key feature genes (*GLUL*, *DDX28*, *NCL*, *RIOK1*, *SUV39H1*, *RRS1*) demonstrated robust diagnostic performance, achieving an AUC of 0.972 in the training dataset and 0.917 in the validation dataset. SHapley Additive exPlanations interpretability analysis revealed *SUV39H1* as the dominant risk contributor, while *GLUL* exhibited a protective effect. Regulatory network reconstruction identified 32 transcription factors, 24 RNA-binding proteins, and 62 miRNAs as putative upstream regulators of key genes. Immune Microenvironment Profiling linked key genes to altered placental immune cell populations. qRT-PCR confirmed that *GLUL* and *NCL* expression decreased and *DDX28* and *RIOK1* expression increased in clinical placental samples of preeclampsia group.

Conclusion: This study identifies ribosome biogenesis as one of the pivotal molecular mechanisms to PE pathogenesis, leveraging SHAP-interpretable machine learning to pinpoint six biomarkers. Future research is requisite for the validation of CRISPR and the integration of multi-omics to translate the findings into clinical diagnosis and targeted therapy.

KEYWORDS

preeclampsia, ribosome biogenesis dysregulation, multi-algorithm machine learning, risk model, biomarker validation

1 Introduction

Preeclampsia (PE), a multisystem hypertensive disorder of pregnancy affecting approximately 2-8% of global pregnancies, remains a leading cause of maternal and perinatal morbidity and mortality, accounting for over 70,000 maternal deaths annually with disproportionate impacts in low-resource settings due to limited prenatal care access (1, 2). PE arises from multifactorial interactions between maternal, fetal, and placental components. Central to its pathophysiology is impaired trophoblast function, specifically defective invasion leading to inadequate uterine spiral artery remodeling, which results in shallow placental implantation (3, 4). These placental aberrations induce malperfusion-induced ischemia, endothelial dysfunction, and systemic inflammatory activation, clinically manifesting as gestational hypertension with multiorgan complications. Without timely intervention, progressive disease may culminate in critical maternal complications such as eclampsia and hemolysis, elevated liver enzymes, and low platelet count (HELLP) syndrome (3, 4). Current diagnostic approaches predominantly depend on late-onset clinical features (e.g., proteinuria, hypertension) and suboptimal biomarkers such as soluble fms-like tyrosine kinase-1 to placental growth factor (sFlt-1/PlGF) ratio, which significantly constrains timely clinical intervention. This limitation underscores the critical need for predictive models based on early-stage biomarkers (5, 6).

Ribosome biogenesis is a dynamic, multi-step process involving RNA polymerase I (Pol I)-driven transcription of 47S pre-rRNA, ribosomal protein (RP) assembly, and nucleolar maturation. This fundamental process serves as a pivotal regulator of cellular proteostasis and plays a crucial role in mediating adaptive responses to metabolic and oxidative stress (7). During placental development, ribosome biogenesis is tightly regulated by nutrient-sensing pathways, including MYC-mediated transcriptional activation and mTOR-dependent ribosomal protein synthesis, which collectively coordinate trophoblast proliferation, differentiation, and invasive capacity (7, 44). Dysregulation of ribosome biogenesis disrupts nucleolar architecture, triggering nucleolar stress characterized by impaired rRNA processing, defective ribosomal RNA (rRNA) surveillance, and p53-dependent cell cycle arrest. These molecular perturbations directly contribute to PE's characteristic pathological features of inadequate placental implantation and vascular dysfunction (8, 44). Moreover, defects in mitochondrial ribosome biogenesis further exacerbate oxidative injury by impairing electron transport chain (ETC) complex assembly, leading to reactive oxygen species (ROS) overproduction and trophoblast apoptosis, as evidenced by downregulated mitochondrial RP expression in PE placentas (8, 45). Concurrently, ribosomopathies reduce translational precision, causing dysregulation of key epithelial-mesenchymal transition (EMT) mediators such as E-cadherin and Snail, thereby suppressing trophoblast migration and spiral artery remodeling (9). These pathological cascades are amplified by epigenetic dysregulation, which represses Pol I activity and exacerbates nucleolar stress (46). The resultant proteostatic imbalance activates compensatory mechanisms such as ribophagy and unfolded protein response (UPR), further depleting functional ribosomes and creating a feedforward loop of placental ischemia and sterile inflammation (47, 48). While these pathophysiological parallels underscore ribosome biogenesis as a critical node in PE pathogenesis, the key feature genes which could predict the PE risk and associated mechanisms remain underexplored, necessitating systematic investigations to translate these insights into biomarkers and treatment targets.

In this study, we hypothesized that dysregulated ribosome biogenesis represents a key molecular driver of PE progression and may serve as a predictive biomarker for PE risk. To address this, we explored the ribosome biogenesis-related differentially expressed genes (RiboRDEGs) in PE and developed a ribosome biogenesis-centric framework for PE risk prediction. Our multi-cohort transcriptomic analysis identified 25 RiboDEGs significantly associated with PE pathogenesis. Functional characterization of these genes revealed their critical roles in PE development. Using weighted gene co-expression network analysis (WGCNA) coupled with ensemble machine learning approaches, we identified six core predictive biomarkers (*GLUL*, *DDX28*, *NCL*, *RIOK1*, *SUV39H1*, and *RRS1*) with high diagnostic potential. SHapley Additive exPlanations (SHAP) analysis elucidated the synergistic contributions of these feature genes to PE risk, while integrated

regulatory network analysis uncovered their coordinated transcriptional and post-transcriptional control mechanisms. Importantly, immune microenvironment profiling demonstrated significant associations between key RiboDEGs and altered placental immune cell compositions. These findings provide novel insights into the role of ribosome biogenesis dysregulation in PE pathogenesis. Furthermore, we present a clinically applicable prediction model that bridges molecular mechanisms with early risk assessment, representing a significant advancement toward personalized obstetric care.

2 Materials and methods

2.1 Data acquisition and preprocessing

Gene expression profiles of PE were retrieved from the National Center for Biotechnology Information (NCBI) Gene Expression Omnibus (GEO) database (7). Three placental tissue-derived Homo sapiens datasets were analyzed: GSE75010 (GPL6244 platform; 80 PE cases and 77 controls) (8–13), GSE10588 (GPL2986 platform; 17 PE cases and 26 controls) (14), and GSE54618 (GPL10558 platform; 12 PE cases and 12 controls) (15) (Table 1). Probe annotation was performed for GSE75010 and GSE10588 using platform-specific annotation files, followed by dataset merging and batch effect correction via the sva R package (v3.52.0) (16). The combined dataset (97 PE cases and 103 controls) underwent normalization using the R package limma (v3.60.4) (17), with principal component analysis (PCA) (18) confirming effective batch effect removal. The GSE54618 dataset served as an independent validation cohort, processed identically with probe annotation and normalization.

2.2 Acquisition of ribosome biogenesis-related genes

RiboRGs were systematically acquired through a dual-source approach. Firstly, the GeneCards database (19) was queried using the keyword "ribosome biogenesis," retaining protein-coding genes with a relevance score >5, which yielded 59 candidate genes. Secondly, 331 RiboRGs were retrieved from the published literature using the same keyword on the PubMed website (20). After merging these two gene lists and removing duplicates, a final set of 344 nonrepetitive RiboRGs was generated for subsequent analysis (Supplementary Table S1).

2.3 Identification of RiboRDEGs in PE

Differentially expressed genes (DEGs) between PE and control groups were identified using the R package limma with thresholds of |log2 fold change (log2FC)| > 0.1 and adjusted p-value (P.adj) < 0.05 (Benjamini-Hochberg correction). Upregulated and downregulated DEGs were defined as log2FC > 0.1 and log2FC < -0.1, respectively, with statistical significance (P.adj < 0.05). Volcano plots were generated using R package ggplot2 (v3.5.1) to visualize differential expression patterns. RiboRDEGs were subsequently identified by intersecting the DEG list with the precompiled 344 RiboRGs, with results visualized through a Venn diagram. Heatmaps generated by R package ComplexHeatmap (v2.20.0) (21) employed Z-score-normalized counts, hierarchical clustering (Euclidean distance, complete linkage), and three-dimensional PCA maps generated by R package rgl (v1.3.1) demonstrated clear separation of PE and controls.

2.4 Functional enrichment analysis

Gene set enrichment analysis (GSEA) (22) was performed on the combined dataset using the R package clusterProfiler (v4.12.6) (23) with the Kyoto Encyclopedia of Genes and Genomes (KEGG) database (24), employing gene set size thresholds of 10–500 genes and significance criteria of P.adj < 0.05 (Benjamini-Hochberg method) and false discovery rate (FDR) < 0.05. To elucidate the biological functions of RiboRDEGs, Gene Ontology (GO) (25), which encompasses biological process (BP), cellular component (CC), and molecular function (MF), and KEGG pathway analysis were performed using clusterProfiler, with the same statistical thresholds. Pathway interaction networks were reconstructed using the R package CBNplot (v1.4.0) (26), where Bayesian networks were inferred through the bnpathplot function by modeling biological pathways as nodes weighted by pathway activity scores derived from RiboRDEG expression profiles.

2.5 Weighted gene co-expression network construction and hub gene identification

WGCNA was implemented using the R package WGCNA (v1.73) (27) to identify hub genes among RiboRDEGs. A scale-free topology model was constructed by selecting an optimal soft-thresholding power (β) to maximize network connectivity while minimizing spurious correlations. The adjacency matrix was

TABLE 1 GEO microarray chip information.

Series	Platform	Species	Tissue	PE Samples	Control Samples	Cohort
GSE75010	GPL6244	Homo sapiens	Placenta	80	77	Training
GSE10588	GPL2986	Homo sapiens	Placenta	17	26	Training
GSE54618	GPL10558	Homo sapiens	Placenta	12	12	Validation

GEO, Gene Expression Omnibus; PE, Preeclampsia.

transformed into a topological overlap matrix (TOM) to quantify gene co-expression similarity, followed by dynamic tree cutting to define gene modules. Module-trait relationships were assessed by calculating Pearson correlation coefficients between module eigengenes (MEs) and PE status, with the most significantly associated module ($p < 0.05$) selected for downstream analysis. Hub genes were identified as the intersection of RiboRDEGs and genes within the PE-correlated module, visualized via Venn diagrams. Pairwise Spearman correlations among hub genes were computed and displayed using the corrplot R package (v0.94).

2.6 Predictive model construction and feature gene identification via integrated machine learning

A comprehensive machine learning framework comprising (28) 113 prediction models was developed using the combined dataset to identify key feature genes associated with PE risk. Twelve distinct algorithms spanning linear models (Stepglm, Lasso, Ridge, Enet), ensemble methods (XGBoost, RandomForest, GBM), Bayesian approaches (NaiveBayes), hybrid dimensionality reduction & regularization (plsRglm) and supervised learning techniques (SVM, glmBoost, LDA) were implemented through their respective R packages (glmnet, xgboost, randomForest, etc.), with algorithm combinations detailed in Supplementary Table S2. Model performance was evaluated via 10-fold cross-validation, receiver operating characteristic (ROC) curve analysis, and decision curve analysis (DCA), with diagnostic efficacy quantified by mean area under curve (AUC) values across training and validation cohorts (GSE54618). Models demonstrating AUC >0.9 were prioritized as high-diagnostic-value candidates. Final feature gene selection was guided by consensus across top-performing models, validated through calibration curves and confusion matrices to ensure robustness.

2.7 Interpretability analysis of optimal predictive model

Model interpretability was assessed using SHAP (29) to delineate the contribution of key feature genes to PE risk prediction. SHAP values were computed via the R package kernelshap (v0.7.0), with positive/negative values indicating directional effects on risk (increase/decrease). Global feature importance rankings were derived from mean absolute SHAP values using shapviz (v0.9.5), visualized through bar plots (overall importance) and beeswarm plots (feature value-SHAP value distributions). SHAP interaction values quantified pairwise feature interdependencies, visualized via scatterplots, while waterfall plots generated for representative cases provided localized interpretability of model decisions. This comprehensive SHAP-based interpretability framework quantifies the importance of key feature genes in predictive model decisions in PE.

2.8 ROC curve analysis and protein-protein interaction network analysis of key genes

Key genes were assessed for differential expression between PE and control groups using Mann-Whitney U tests, with results visualized through violin plots. Diagnostic performance was evaluated via ROC curve analysis using the R package pROC (v1.18.5) (30), calculating AUC values to quantify predictive capacity. PPI networks were reconstructed via the GeneMANIA database (31), integrating key genes with functionally associated partners to infer biological modules relevant to PE pathogenesis.

2.9 Regulatory network reconstruction

Transcriptional and post-transcriptional regulatory networks were systematically reconstructed to elucidate molecular interactions involving key genes. Transcription factor (TF)-gene interactions were identified using the ChIPBase database (32), retaining TF-gene pairs with combined upstream/downstream supporting samples ≥8. RNA binding protein (RBP) and microRNA (miRNA) interactors were predicted via the ENCORI database (33), applying evidence-based thresholds of clipExpNum ≥10 for RBPs and ≥7 for miRNAs. All interaction networks (TF-gene, RBP-gene, miRNA-gene) were integrated and visualized using Cytoscape (v3.10.2).

2.10 Immune microenvironment characterization

Placental immune cell infiltration profiles were quantified via single-sample gene set enrichment analysis (ssGSEA) using the R package GSVA (v1.52.3), with 28 immune cell-specific gene sets derived from established markers (34). Enrichment scores representing relative immune cell abundance were compared between PE and control groups, identifying differentially infiltrated cell types. Spearman correlation matrices generated via the R package linkET (v0.0.7.4) revealed intercellular immune interactions and key gene-immune cell associations ($|r| > 0.3$), visualized through network diagrams. Significant correlations ($|r| > 0.3$) were further validated using scatterplots to delineate linear relationships.

2.11 Clinical sample collection and processing

Placental tissue samples were collected from 20 singleton pregnancies (10 PE cases, 10 gestational age-matched controls, each group included five term pregnancy and five preterm pregnancies) undergoing cesarean delivery at the Third Affiliated Hospital of Wenzhou Medical University. PE diagnosis followed ISSHP criteria: sustained hypertension (≥140/90 mmHg) with proteinuria (≥0.3 g/24h) emerging after 20 gestational weeks. Inclusion criteria

required maternal age 20–40 years, uncomplicated antenatal course prior to PE onset, and absence of fetal anomalies. Exclusion criteria encompassed pre-existing comorbidities (chronic hypertension, diabetes), acute infections (including COVID-19), gestational diabetes, fetal congenital disorders, and exposure to confounding medications. Full-thickness placental biopsies were obtained from the central region within 15 minutes of delivery, snap-frozen in liquid nitrogen, and stored at −80°C. Ethical approval was granted by the Research Ethics Committee of Ruian People's Hospital (Approval No. YJ2024178), with written informed consent obtained from all participants.

2.12 RNA isolation and quantitative real-time PCR validation

Total RNA was isolated from placental tissues using the Tissue Total RNA Isolation Kit V2 (Vazyme Biotech, RC112-01), with purity and concentration assessed via NanoDrop spectrophotometry (Thermo Fisher Scientific; A260/A280 ratios: 1.8–2.0). Reverse transcription was performed with 1 μg RNA using HiScript III All-in-One RT SuperMix (Vazyme Biotech, R333-01) under optimized conditions: 25°C for 5 min, 50°C for 15 min, and 85°C for 5 min. qRT-PCR assays were conducted on a CFX Connect system (Bio-Rad) with Taq Pro Universal SYBR Master Mix (Vazyme Biotech, Q712-02) in 10 μL reactions (40 cycles: 95°C/10 s denaturation, 60°C/30 s annealing/extension). Melt curve analysis confirmed amplification specificity, and relative gene expression was normalized to GAPDH using the 2−ΔΔCt method. All reactions included triplicate technical replicates, with fold-change calculations relative to control samples.

2.13 Statistical analysis

All analyses were conducted within the R statistical environment (v4.4.0). Normality assumptions were verified through Shapiro-Wilk testing, with parametric comparisons (Student's t-test) applied to normally distributed continuous variables and non-parametric alternatives (Mann-Whitney U test) for skewed distributions. Spearman's rank correlation coefficient (ρ) quantified associations between molecular features. Unless otherwise stated, all reported p-values were two-tailed, with statistical significance defined as $p < 0.05$. Multiple testing correction was implemented via the Benjamini-Hochberg method for high-throughput datasets to control false discovery rate (FDR < 0.05).

3 Results

3.1 Analytical flow diagram

Figure 1 displays the technical approach of the study, providing a concise overview of the analytical processes used in this study. The analytical flow commenced with merging transcriptomic datasets GSE75010 and GSE10588, followed by identification of DEGs. RiboRGs were intersected with DEGs to derive RiboRDEGs. Subsequent multi-modal enrichment analyses included GSEA, GO, KEGG pathway mapping, and Bayesian network inference to elucidate functional associations. WGCNA identified PE-correlated modules and key genes, while machine learning algorithms refined core diagnostic biomarkers. Model interpretability was enhanced through SHAP, with ROC curve analysis validating diagnostic efficacy using external dataset GSE10588. Immune infiltration profiling via ssGSEA revealed microenvironmental interactions of key genes. Regulatory networks encompassing mRNA-TF, mRNA-miRNA, and mRNA-RBP interactions were reconstructed to delineate molecular mechanisms. Final clinical validation confirmed differential expression patterns of candidate genes in PE cohorts.

3.2 Identification of ribosome biogenesis-related differentially expressed genes

The GSE75010 and GSE10588 datasets were merged into a combined cohort (n=200) and subjected to batch effect correction using the R package sva, followed by normalization via the R package limma. Pre-correction boxplots (Supplementary Figure S1A) revealed pronounced inter-batch variability in expression distributions, which resolved post-correction (Supplementary Figure S1B). PCA demonstrated distinct separation between original datasets along PC1 and PC2 prior to adjustment (Supplementary Figure S1C), whereas post-correction PCA (Supplementary Figure S1D) showed overlapping clusters with reduced variance contributions (PC1: 2.97%, PC2: 2.19%), confirming effective batch effect mitigation. Based on this combined cohort, we conducted differential expression analysis using the R package limma and identified 2,783 DEGs (|log2FC| > 0.1, P.adj < 0.05) between PE and control groups, comprising 1,304 upregulated and 1,479 downregulated genes (Figure 2A). Intersection of these DEGs with the precompiled ribosome biogenesis-related gene set (344 RiboRGs) yielded 25 RiboRDEGs, including *C1QBP*, *DDX28*, *DDX51*, *DHX30*, *EXOSC2*, *GLUL*, *LSM6*, *MPHOSPH6*, *MRPL36*, *NCL*, *NOL6*, *PAK1IP1*, *POLR1B*, *PRKDC*, *RAN*, *RIOK1*, *RNASEL*, *RPP25*, *RPS27L*, *RRS1*, *SUV39H1*, *TBL3*, *TFB1M*, *WDR12* and *XRCC5* (Figure 2B). The heatmap reveals the stratified clustering and expression disparity of 25 RiboRDEGs between the PE group and the control group (Figure 2C), which is corroborated by 3D PCA demonstrating significant intergroup separation (Figure 2D).

3.3 Functional enrichment profiling

For exploring significantly dysregulated pathways in PE, we conducted GSEA analysis on the combined dataset. Results showed that top enriched terms in PE including HIF-1 signaling, AMPK signaling, and proteasome activity (Figure 3A). Subsequent GO and

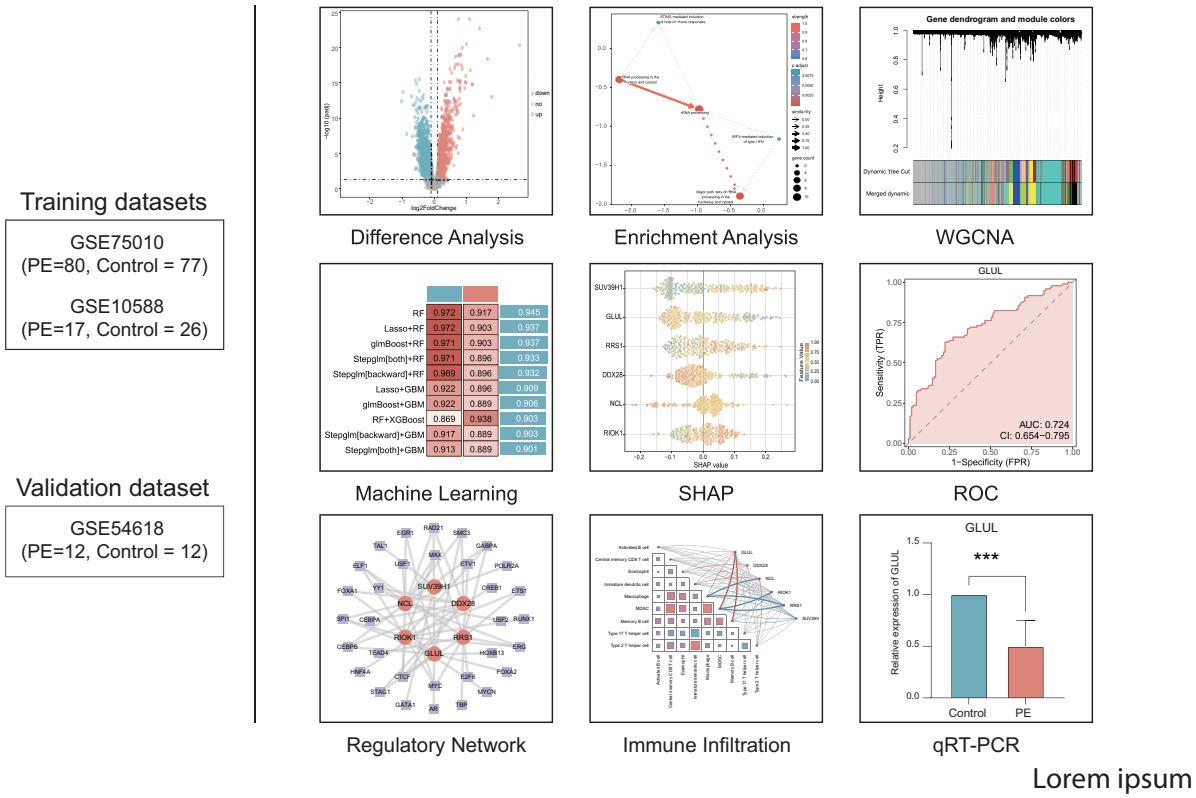

FIGURE 1
Technology roadmap.

KEGG analyses of the 25 RiboRDEGs demonstrated their predominant involvement in rRNA metabolic processes (BP: ncRNA processing, ribosome biogenesis), nucleolar complexes (CC: 90S preribosome, small-subunit processome), and RNA helicase activities (MF: U3 snoRNA binding) (Figure 3B). KEGG pathway enrichment further implicated these genes in ribosome biogenesis and RNA degradation. Bayesian network analysis identified rRNA processing as a central hub (Figures 3C, D), exhibiting robust connectivity with immune response pathways (STING-mediated host immunity, IRF3-dependent IFN induction) and subcellular rRNA maturation processes.

3.4 Weighted gene co-expression network analysis and hub gene prioritization

A scale-free co-expression network was constructed using WGCNA (power = 10, scale-free fit $R^2 = 0.9$; Figure 4A). Dynamic module detection identified 9 gene clusters (Figures 4B, C), with low inter-module correlations confirmed by a heatmap analysis (Figure 4D). The MEblue module exhibited the strongest positive correlation with PE (cor = 0.66, $p = 3\times10^{-26}$; Figure 4E). Intersection of MEblue module genes (n=955) with RiboRDEGs revealed seven hub genes (*GLUL*, *LSM6*, *DDX28*, *NCL*, *RIOK1*, *RRS1*, *SUV39H1*; Figure 4F). Spearman correlation analysis demonstrated strong co-expression patterns among hub genes (Figure 4G), suggesting functional synergy in PE pathogenesis.

3.5 Machine learning-based predictive model construction and validation

A multi-algorithm framework comprising 113 model combinations was implemented to identify optimal predictors of PE risk using seven hub genes (Figure 5A). Random Forest (RF) demonstrated superior diagnostic performance, achieving AUCs of 0.972 (95% CI: 0.953–0.988) in the training cohort and 0.917 (95% CI: 0.757–1.000) in the validation cohort (Figure 5B). The final RF model incorporated six feature genes (*GLUL*, *DDX28*, *NCL*, *RIOK1*, *SUV39H1*, *RRS1*; Table 2). DCA shows that this model can provide substantial clinical net benefits for clinical decision making (Figure 5C), while calibration curves showed strong concordance between predicted and observed PE probabilities (Figure 5D). Confusion matrices further validated the model's diagnostic accuracy, achieving sensitivity >90% and specificity >85% in both training and validation cohorts (Figure 5E).

To elucidate the potential impact of the six feature genes on the risks associated with PE, we conducted SHAP analysis. This analysis revealed *SUV39H1* as the most influential feature in the RF model (mean |SHAP| = 0.0944), followed by *GLUL* (|SHAP| = 0.0843),

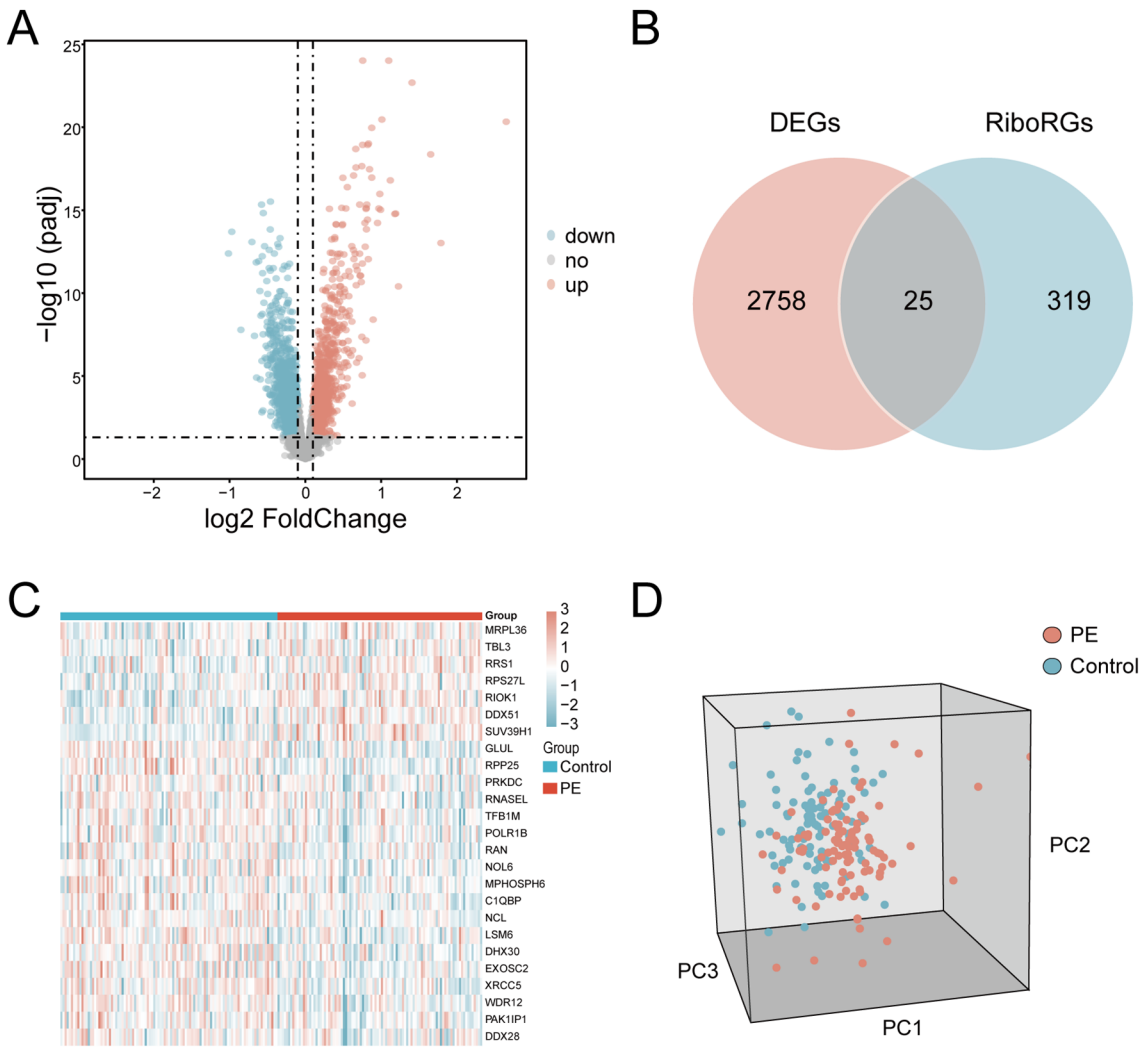

FIGURE 2
Identification of RiboRDEGs. **(A)** Volcano plot of DEGs (|log2FC| > 0.1, P.adj < 0.05), red indicates upregulated genes and blue indicates downregulated genes **(B)** Venn diagram intersecting DEGs and RiboRGs,red indicates DEGs and blue indicates RiboRGs. **(C)** Heatmap of RiboRDEG expression across samples, red indicates high expression and blue indicates low expression. **(D)** 3D PCA plot demonstrating group segregation based on RiboRDEG profiles, red indicates PE samples, blue indicates normal samples.

RRS1 (mean |SHAP| = 0.0649), *DDX28* (mean |SHAP| = 0.0606), *NCL* (mean |SHAP| = 0.0534) and *RIOK1* (mean |SHAP| = 0.0495) (Figure 6A). The expression levels of these genes have different directional effects on PE risk. Elevated *SUV39H1*, *RRS1* and *RIOK1* expression correlated with increased PE probability, whereas higher *GLUL*, *DDX28* and *NCL* levels exhibited protective effects (Figure 6B). Interaction analysis identified synergistic risk amplification between *SUV39H1* and *RRS1* (Figure 6C), while *GLUL-NCL* co-expression showed concerted risk reduction (Figure 6D). A negative interaction between *RRS1* and *NCL* (Figure 6E) suggested compensatory regulatory dynamics. Waterfall plots for representative PE (predicted probability = 0.864) and control (probability = 0.131) cases demonstrated model interpretability, with *SUV39H1* contributing most substantially to risk prediction (Figures 6F, G).

3.6 ROC curve analysis and protein interaction network of key genes

Differential expression analysis confirmed significant downregulation of *GLUL*, *DDX28*, and *NCL* ($p < 0.01$; Figures 7A–C) alongside upregulation of *RIOK1*, *SUV39H1*, and *RRS1* ($p < 0.001$; Figures 7D–F) in PE placentas. ROC analysis revealed moderate diagnostic utility for *GLUL* (AUC = 0.724), *RIOK1* (AUC = 0.707), and *SUV39H1* (AUC = 0.745) in the training cohort, with weaker performance for *DDX28* (AUC = 0.613), *NCL* (AUC = 0.634), and *RRS1* (AUC = 0.663) (Figures 7G–L). External validation in GSE54618 maintained moderate diagnostic accuracy for *DDX28* (AUC = 0.847), *RIOK1* (AUC = 0.771), *SUV39H1* (AUC = 0.840), and *RRS1* (AUC = 0.764), while *GLUL* (AUC = 0.604) and *NCL* (AUC = 0.688) showed

10.3389/fimmu.2025.1595222

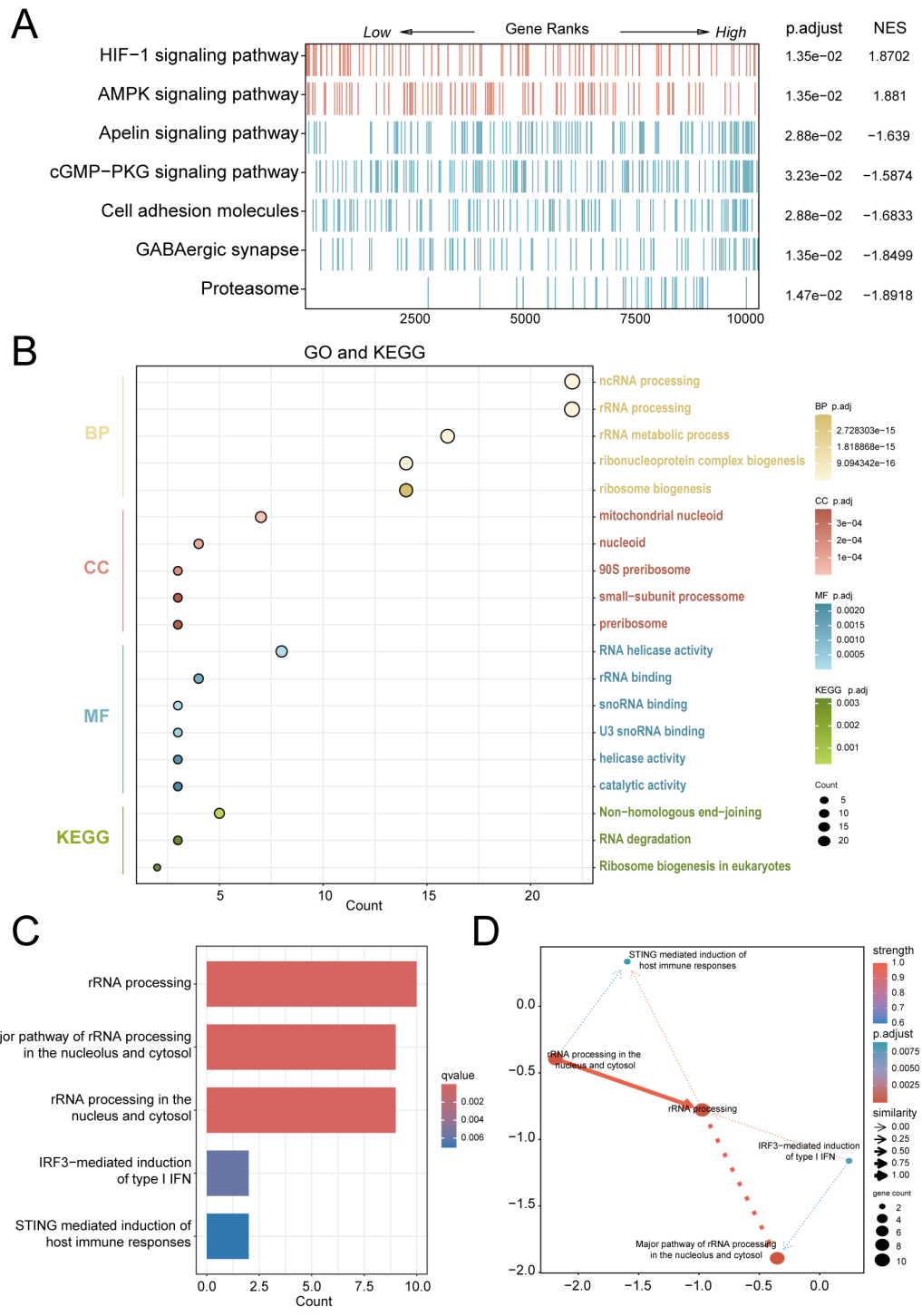

FIGURE 3
Multi-modal enrichment analysis of PE-associated molecular pathways. **(A)** GSEA heatmap of combined dataset pathways (red: leading-edge enrichment; blue: trailing-edge enrichment). **(B)** Bubble plot of RiboRDEG-enriched GO terms (BP, CC, MF) and KEGG pathways, with term counts on the x-axis. **(C)** Bayesian pathway enrichment bar plot. **(D)** Bayesian network illustrating pathway interactions, with node size reflecting functional centrality and edge properties indicating interaction strength (thickness) and directionality (arrows). Solid/dashed lines distinguish established vs. hypothesized regulatory relationships.

limited discriminative power (Figures 7M–R). Protein-protein interaction (PPI) network analysis via GeneMANIA identified 20 functionally associated partners (Figure 7S), with co-expression (47.61%) and physical interactions (51.88%) as predominant interaction modes, suggesting that these key genes may collaboratively regulate ribosome biogenesis and RNA processing through transcriptional coordination and direct molecular binding, thereby contributing to placental dysfunction in PE pathogenesis.

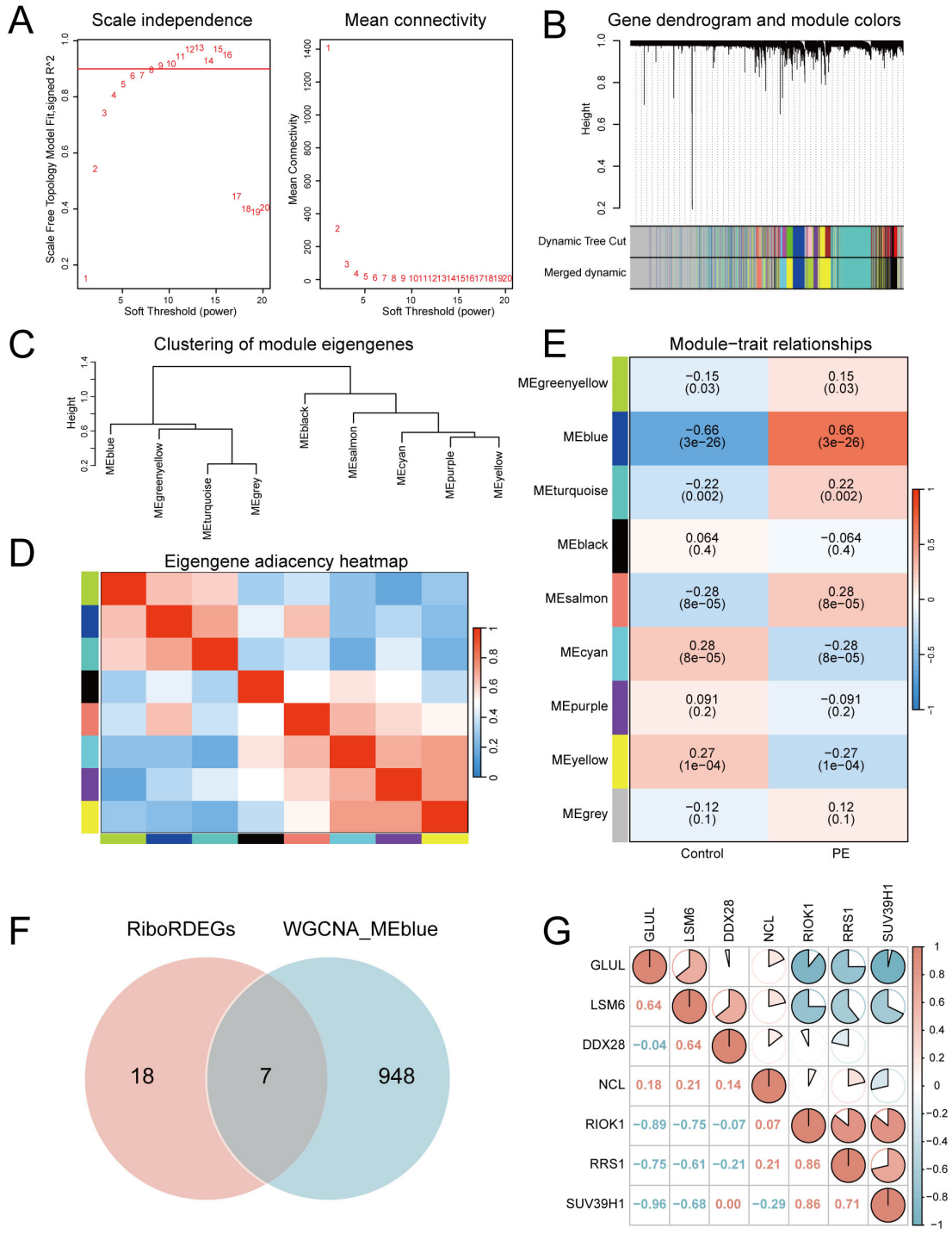

FIGURE 4
Co-expression network construction and hub gene identification. **(A)** Soft-threshold selection for scale-free topology (left: fit index; right: mean connectivity). **(B)** Hierarchical clustering dendrogram with merged modules. **(C)** Module eigengene clustering tree. **(D)** Inter-module correlation heatmap. **(E)** Module-trait correlation heatmap highlighting MEblue-PE association. (upper: correlation coefficients; lower: p-values) **(F)** Venn diagram intersecting MEblue genes and RiboRDEGs. **(G)** Correlation heatmap of seven hub genes. In the heatmap, red indicates a positive correlation and blue indicates a negative correlation. $|r|>0.95$: significant correlation; $|r|\geq 0.8$: highly correlated; $0.5\leq|r|<0.8$: moderately correlated; $0.3\leq|r|<0.5$: weakly correlated; $|r|<0.3$: not correlated.

10.3389/fimmu.2025.1595222

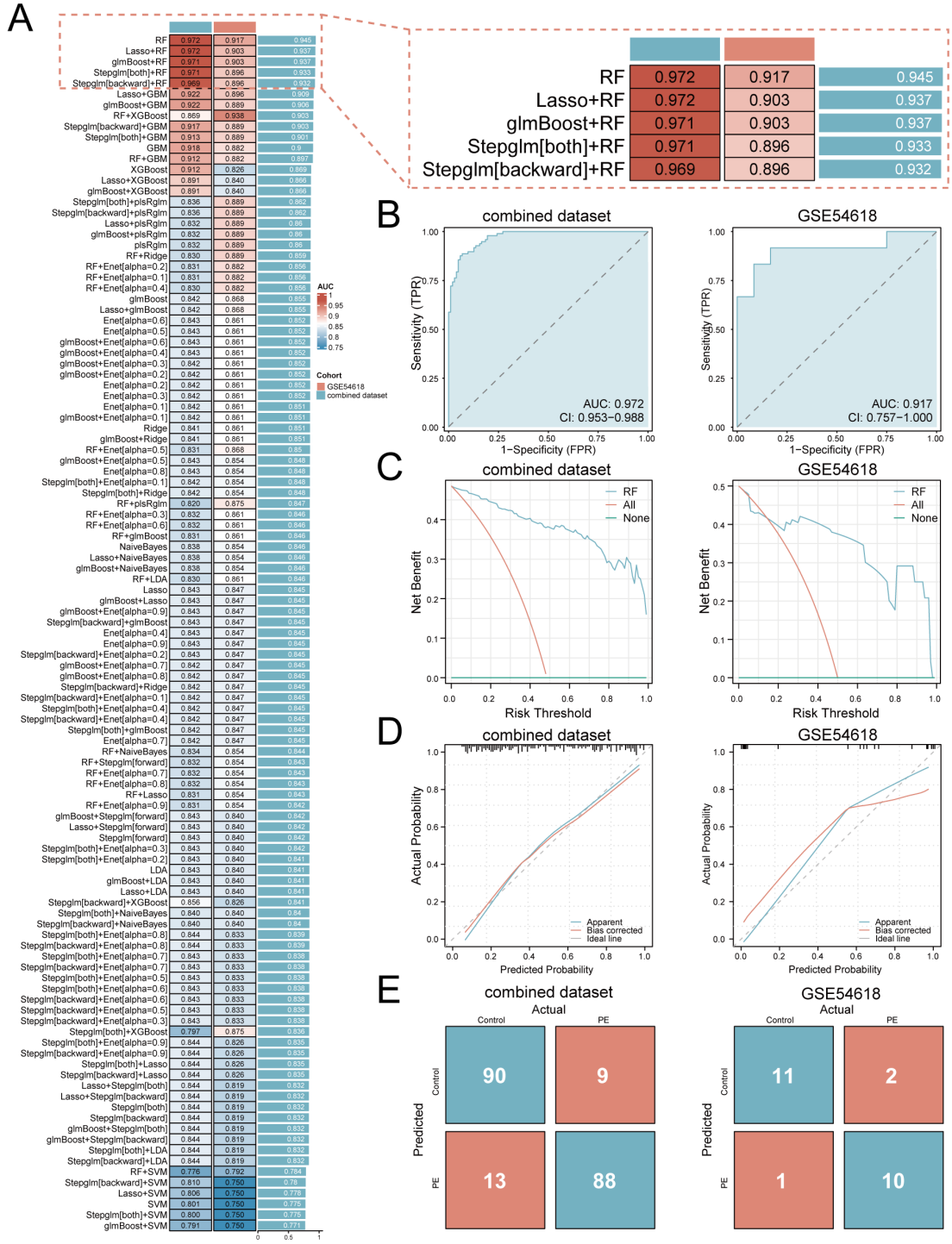

FIGURE 5
Development and validation of the machine learning-based predictive model. **(A)** Bar plot comparing mean AUCs of 113 algorithm combinations across training and validation cohorts. **(B)** ROC curves of the RF model (TPR, true positive rate; FPR, false positive rate; AUC>0.9 indicates high diagnostic value). **(C)** Decision curve analysis evaluating clinical utility. **(D)** Calibration curves assessing prediction accuracy. **(E)** Confusion matrices quantifying classification performance.

3.7 Reconstruction of regulatory networks

To explore the systematic regulatory network of ribosome biogenesis in preeclampsia, the reconstruction of regulatory networks was conducted. Transcriptional and post-transcriptional regulatory networks were systematically mapped to elucidate molecular interactions involving key genes. The TF network, constructed using ChIPBase with a stringent filtering criterion (combined upstream/downstream supporting samples ≥8), comprised 6 key genes (*GLUL*, *DDX28*, *NCL*, *RIOK1*, *SUV39H1*,

TABLE 2 Description of RiboRDEGs.

ID	Description	log2FC	AveExpr	t	adj.P.Val	B
GLUL	*Glutamate-Ammonia Ligase*	-0.37296	11.51056	-5.9997	3.05E-07	9.640216
DDX28	*DEAD-Box Helicase 28*	-0.10067	8.489916	-2.97947	0.014957	-2.47268
NCL	*Nucleolin*	-0.13118	11.62773	-3.11307	0.010559	-2.08675
RIOK1	*RIO Kinase 1*	0.173268	9.869928	5.106692	1.42E-05	5.379976
SUV39H1	*SUV39H1 Histone Lysine Methyltransferase*	0.293488	8.689993	6.640665	1.39E-08	12.98921
RRS1	*Ribosome Biogenesis Regulator 1 Homolog*	0.144664	9.323376	3.859158	0.001257	0.344918

RiboRDEGs, ribosome biogenesis-related differentially expressed genes.

RRS1) interacting with 32 TFs through 59 regulatory pairs (Supplementary Figure S2A, Supplementary Table S3). RBP interactions predicted via ENCORI (clipExpNum ≥10) revealed 45 functional associations between 6 key genes (*GLUL*, *DDX28*, *NCL*, *RIOK1*, *SUV39H1*, *RRS1*) and 24 RBPs (Supplementary Figure S2B, Supplementary Table S4). miRNA-mediated regulation analysis identified 63 mRNA-miRNA pairs involving *GLUL*, *SUV39H1*, and *NCL* with 62 miRNAs (clipExpNum ≥7; Supplementary Figure S2C, Supplementary Table S5), highlighting transcriptional and post-transcriptional modulation of ribosome biogenesis pathways in PE.

3.8 Immune microenvironment profiling via ssGSEA

To explore the role of Ribosome biogenesis in the immune microenvironment of PE, we conducted an ssGSEA analysis on the combined dataset. ssGSEA revealed significant dysregulation of nine immune cell types in PE placentas compared to controls ($p < 0.05$; Figure 8A). Activated B cells and Th17 cells were enriched in PE, while central memory CD8+ T cells, eosinophils, immature dendritic cells, macrophages, MDSCs, memory B cells, and Th2 cells exhibited reduced infiltration. Correlation network analysis demonstrated interconnected immune cell dynamics in PE, with key genes showing cell-type-specific associations (Figure 8B). Notably, *GLUL* expression positively correlated with MDSC ($r = 0.352$, $p < 0.001$; Figure 8C) and memory B cell abundance ($r = 0.333$, $p < 0.001$; Figure 8D). Conversely, *RRS1* displayed negative correlations with macrophages ($r = -0.372$, $p < 0.001$; Figure 8E) and MDSCs ($r = -0.337$, $p < 0.001$; Figure 8F), while *NCL* and *RIOK1* inversely associated with macrophage ($r = -0.334$, $p < 0.001$; Figure 8G) and MDSC infiltration ($r = -0.301$, $p = 0.003$; Figure 8H), respectively.

3.9 Experimental validation of key genes in PE

qRT-PCR validation in placental tissues from 10 PE patients and 10 gestational age-matched controls (primers listed in Table 3) confirmed significant dysregulation of ribosome biogenesis-associated genes. *DDX28* ($p < 0.01$) and *RIOK1* ($p < 0.001$) expression was markedly elevated in PE placentas, while *GLUL* ($p < 0.001$) and *NCL* ($p < 0.001$) showed significant downregulation (Figures 9A–D). *SUV39H1* and *RRS1* exhibited non-significant expression trends (Figures 9E, F). Clinical assessment revealed significantly elevated systolic blood pressure in PE cases compared to gestational age-matched controls (155.1 ± 24.27 vs. 122.6 ± 7.91 mmHg, $p < 0.001$), with diastolic pressures similarly increased (92.9 ± 9.73 vs. 74.4 ± 3.69 mmHg, $p < 0.001$). No significant differences were observed in maternal age (30.4 ± 5.21 vs. 29.7 ± 4.60 years, $p = 0.754$), neonatal birth weight (2,724 ± 500.16 vs. 3,014 ± 503.42 g, $p = 0.213$), or Apgar scores at 1 min (9: 10% vs. 0%, $p = 0.305$) and 5 min (9: 10% vs. 0%, $p = 0.305$) (Table 4).

4 Discussion

Conventional PE biomarkers, including PlGF and sFlt-1, exhibit limited predictive accuracy during early gestation due to insufficient sensitivity and specificity (6). These markers fail to resolve molecular heterogeneity across clinical PE subtypes and primarily reflect angiogenic imbalance while neglecting synergistic pathogenic mechanisms such as inflammatory and metabolic dysregulation (35). Emerging evidence indicates that ribosome biogenesis dysregulation is closely associated with the core PE pathological features, such as placental malperfusion and aberrant vascular remodeling, by disrupting nucleolar structural integrity, inducing oxidative stress, and impairing trophoblast function (36, 37). These evidences collectively suggest that the disruption of ribosome homeostasis may represent a pivotal molecular hub in the early PE pathogenesis.

Our analysis reveals that RiboRDEGs are significantly enriched in rRNA metabolic processes (including ncRNA processing and 90S preribosome assembly) and show strong Bayesian network connectivity to immune pathways (STING/IRF3-mediated interferon responses). These findings suggest that ribosome biogenesis defects in PE may drive placental dysfunction through dual mechanisms: (1) impaired ribosomal stress adaptation via disrupted rRNA maturation (38), and (2) immune activation triggered by nucleolar-derived damage-associated molecular patterns (DAMPs) (39, 40). The co-enrichment of HIF-1 and AMPK signaling pathways aligns with placental hypoxia-

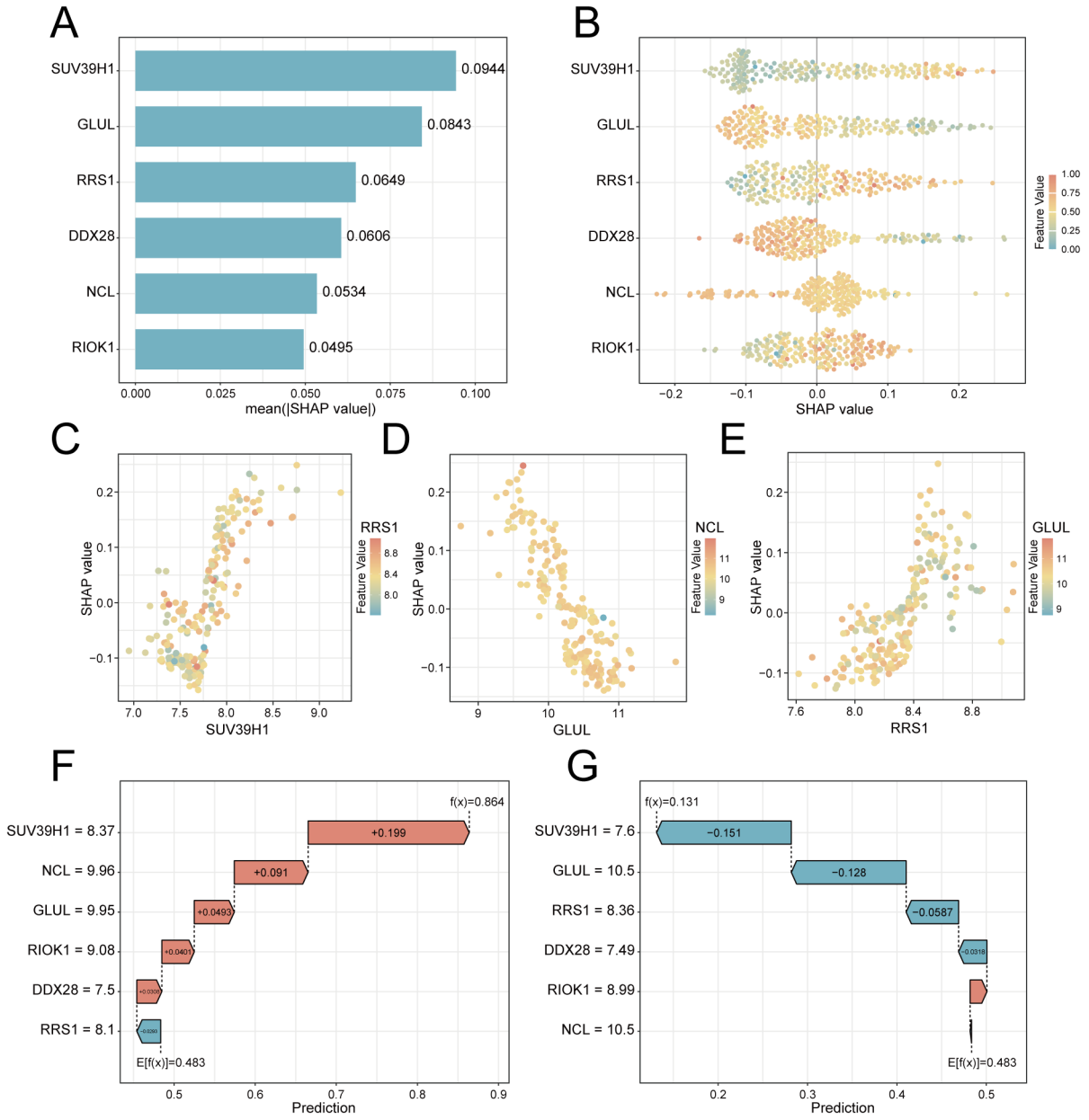

FIGURE 6
SHAP-based interpretation of key feature genes in the RF predictive model. **(A)** Feature importance bar plot ranked by mean absolute SHAP values. **(B)** Beeswarm plot showing SHAP value directionality (x-axis) versus gene expression (color scale: red = high, blue = low). **(C–E)**. Interaction scatterplots: x-axis = gene expression, y-axis = SHAP value, color = interacting gene expression. **(F)** Waterfall plot for a PE case (predicted risk = 0.864). **(G)** Control case waterfall plot (risk = 0.131). Arrows indicate SHAP contributions (red: risk increase; blue: decrease).

reperfusion injury in PE, where hypoxia-inducible factors may suppress rRNA transcription while energy stress activates AMPK-mediated ribophagy to eliminate defective ribosomes (41, 42). Additionally, KEGG pathway analysis demonstrates concurrent proteasome activation, likely representing a compensatory mechanism to remove misfolded ribosomal proteins generated during biogenesis stress, a process previously linked to PE-associated oxidative injury (40, 43). These findings collectively position ribosome biogenesis as a nexus integrating metabolic stress, proteostatic imbalance, and sterile inflammation in PE pathogenesis. The identified RiboDEGs emerge as key molecular mediators linking nucleolar dysfunction to clinical disease manifestations.

Analysis of the combined dataset revealed distinct immune dysregulation in PE placentas, characterized by Th17 polarization, MDSC depletion, and impaired macrophage infiltration, which is consistent with the Th17/Th2 imbalance feature of PE (44). These immunological alterations might represent secondary outcome of ribosome biogenesis stress and the release of DAMPs due to nuclear instability. These DAMPs engage cytoplasmic sensors (e.g., RIG-I,

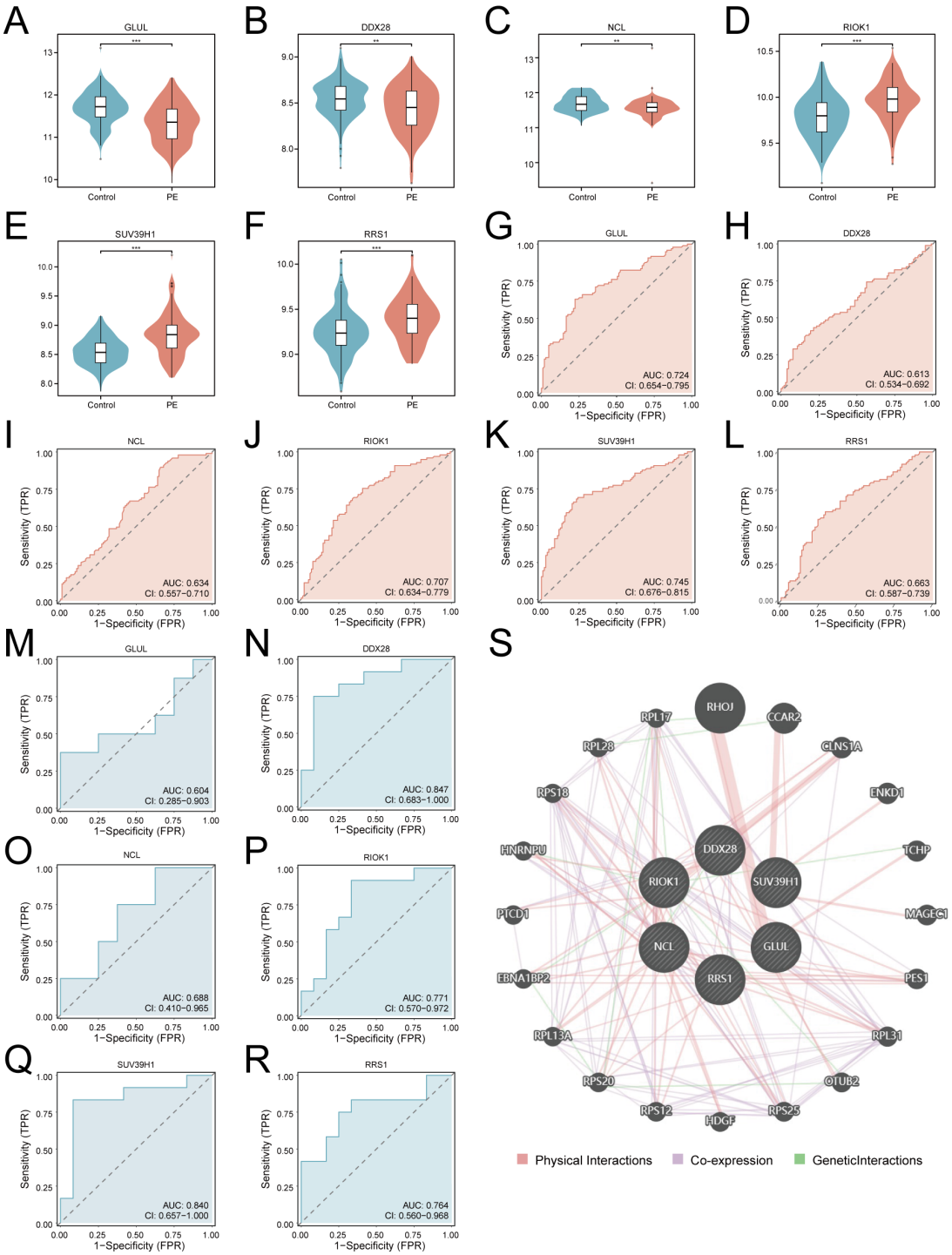

FIGURE 7
Diagnostic validation and functional interaction networks of key genes. **(A–F)**. Violin plots of key gene expression in PE (red) vs. controls (blue): *GLUL* **(A)**, *DDX28* **(B)**, *NCL* **(C)**, *RIOK1* **(D)**, *SUV39H1* **(E)**, *RRS1* **(F)**. G-L. ROC curves for training cohort: *GLUL* **(G)**, *DDX28* **(H)**, *NCL* **(I)**, *RIOK1* **(J)**, *SUV39H1* **(K)**, *RRS1* **(L)**. **(M–R)**. Validation cohort ROC curves: *GLUL* **(M)**, *DDX28* **(N)**, *NCL* **(O)**, *RIOK1* **(P)**, *SUV39H1* **(Q)**, *RRS1* **(R)**. An AUC of 0.5–0.7 indicates low diagnostic utility, while an AUC of 0.7–0.9 suggests moderate diagnostic value. **(S)** PPI network (nodes: key genes and functionally associated partners; edges: physical interactions (red), co-expression (purple), geneticInteractions (green); thickness: interaction confidence). ***$p < 0.001$; **$p < 0.01$.

MDA5) and toll-like receptors (TLRs) on placental immune cells, driving NF-κb-dependent pro-inflammatory cytokines (IL-6, IL-17), while suppressing anti-inflammatory mediators (IL-10, TGF-β). This imbalance establishes a self-sustaining inert inflammatory cycle and activates the toll-like receptor (TLR)-mediated inflammatory cascade reaction (39, 44). Notably, *GLUL* expression positively correlated with MDSC and memory B cell abundance, suggesting glutamine synthetase activity may modulate

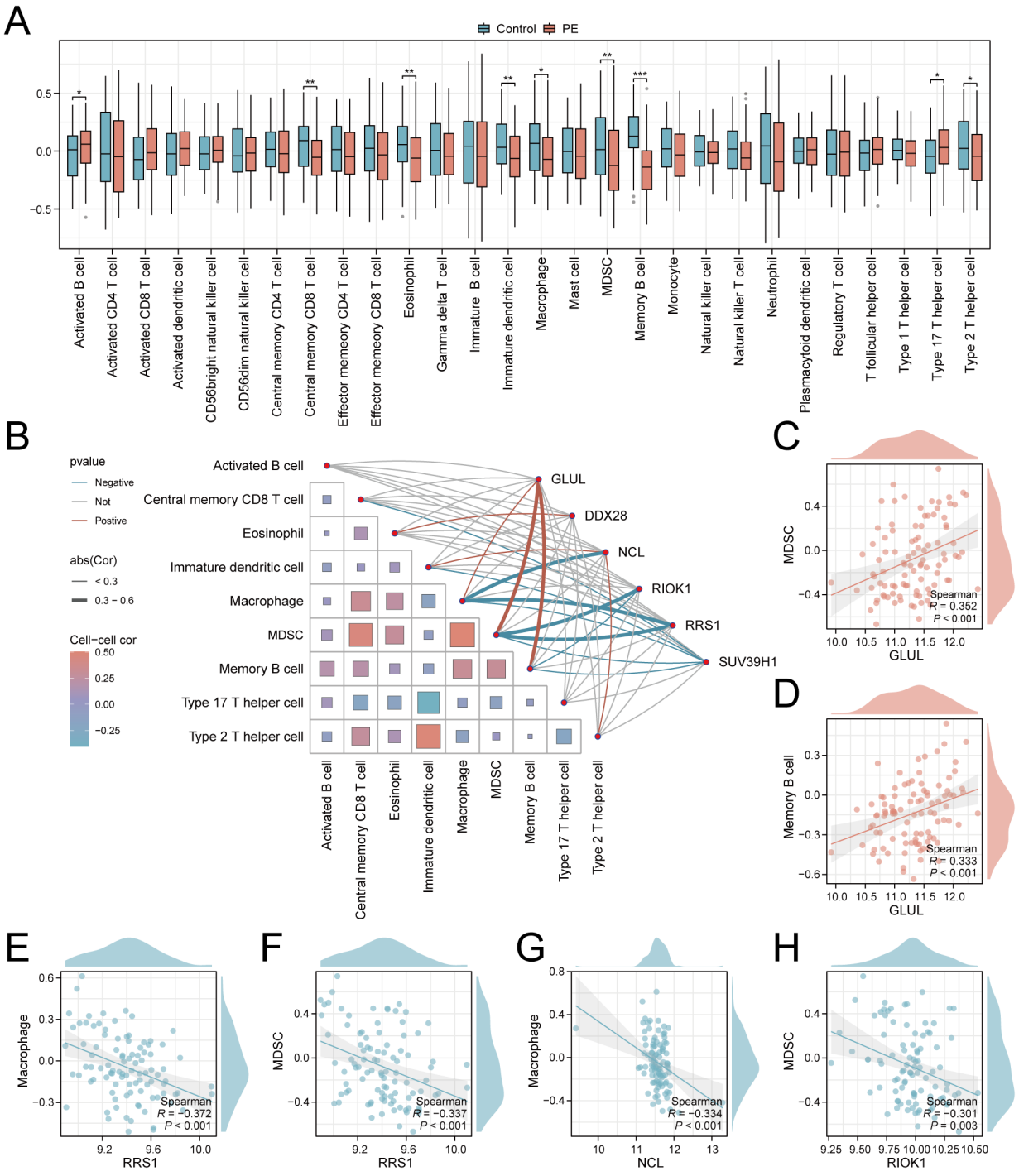

FIGURE 8
Immune infiltration landscape and key gene correlations in PE. **(A)** Boxplots comparing immune cell enrichment scores between PE (red) and controls (blue). **(B)** Correlation network of immune cells and key genes. **(C–H)**. Scatterplots of key gene-immune cell correlations: *GLUL*-MDSC **(C)**, *GLUL*-Memory B cell **(D)**, *RRS1*-Macrophage **(E)**, *RRS1*-MDSC **(F)**, *NCL*-Macrophage **(G)**, *RIOK1*-MDSC **(H)**. *$p < 0.05$; **$p < 0.01$; ***$p < 0.001$. red indicates a positive correlation and blue indicates a negative correlation. $0.3 \leq |r| < 0.5$: weakly correlated.

immunosuppressive niches, potentially through mTORC1-dependent metabolic reprogramming of myeloid cells (45). Conversely, *RRS1* and *NCL* showed negative associations with macrophages and MDSCs, implicating their roles in restraining pro-inflammatory polarization, possibly via ER stress pathways that regulate phagocytic clearance of ribosomal debris (40). The coordinated depletion of tolerogenic MDSCs and macrophages further exacerbates vascular dysfunction, creating a feedforward loop between ribosomal stress, oxidative injury, and immune-mediated endothelial damage (46).

TABLE 3 Primer sequences for qRT-PCR.

Gene	Primer sequences (5′-3′)
GLUL	AAGAGTTGCCTGAGTGGAATTTC (forward) AGCTTGTTAGGGTCCTTACGG (reverse)
DDX28	TGCGAAAGCTCTCGTCTAAGG (forward) CCTCCTGTAGTGCGTGCAG (reverse)
NCL	GCACCTGGAAAACGAAAGAAGG (forward) GAAAGCCGTAGTCGGTTCTGT (reverse)
RIOK1	GGCTCGGGAGTTGTACCTG (forward) CCACGGACTGAGACACGTC (reverse)
SUV39H1	CCTGCCCTCGGTATCTCTAAG (forward) ATATCCACGCCATTTCACCAG (reverse)
RRS1	GTTACCTCCCGTTTCCCACTT (forward) CATCACCGATTGGTCATCTCTTG (reverse)
GAPDH	TGTGGGCATCAATGGATTTGG (forward) ACACCATGTATTCCGGGTCAAT (reverse)

qRT–PCR, quantitative real–time PCR.

To elucidate the predictive potential of RiboRDEGs in PE risk, we pioneered an explainable machine learning (XML) approach that integrates ribosome biogenesis biology with advanced computational modeling to address the critical need for mechanistically interpretable biomarkers in PE risk prediction. By implementing a multi-algorithm framework encompassing 113 model combinations, we developed a RF model that achieves exceptional diagnostic accuracy while maintaining biological interpretability, representing a significant advance over conventional 'black-box' approaches (47). The SHAP interpretability analysis revealed *SUV39H1* as the dominant risk contributor (mean |SHAP|=0.0944), with *GLUL* and *RRS1* exhibiting counteractive protective/risk effects, demonstrating how XML disentangles complex gene interactions that collectively drive PE pathogenesis (48). This approach successfully identified six ribosome biogenesis-related biomarkers (*GLUL*, *DDX28*, *NCL*, *RIOK1*, *SUV39H1* and *RRS1*) and mapped their nonlinear synergies, such as the risk-amplifying *SUV39H1-RRS1* interaction and protective *GLUL-NCL* axis. This findings provide unprecedented

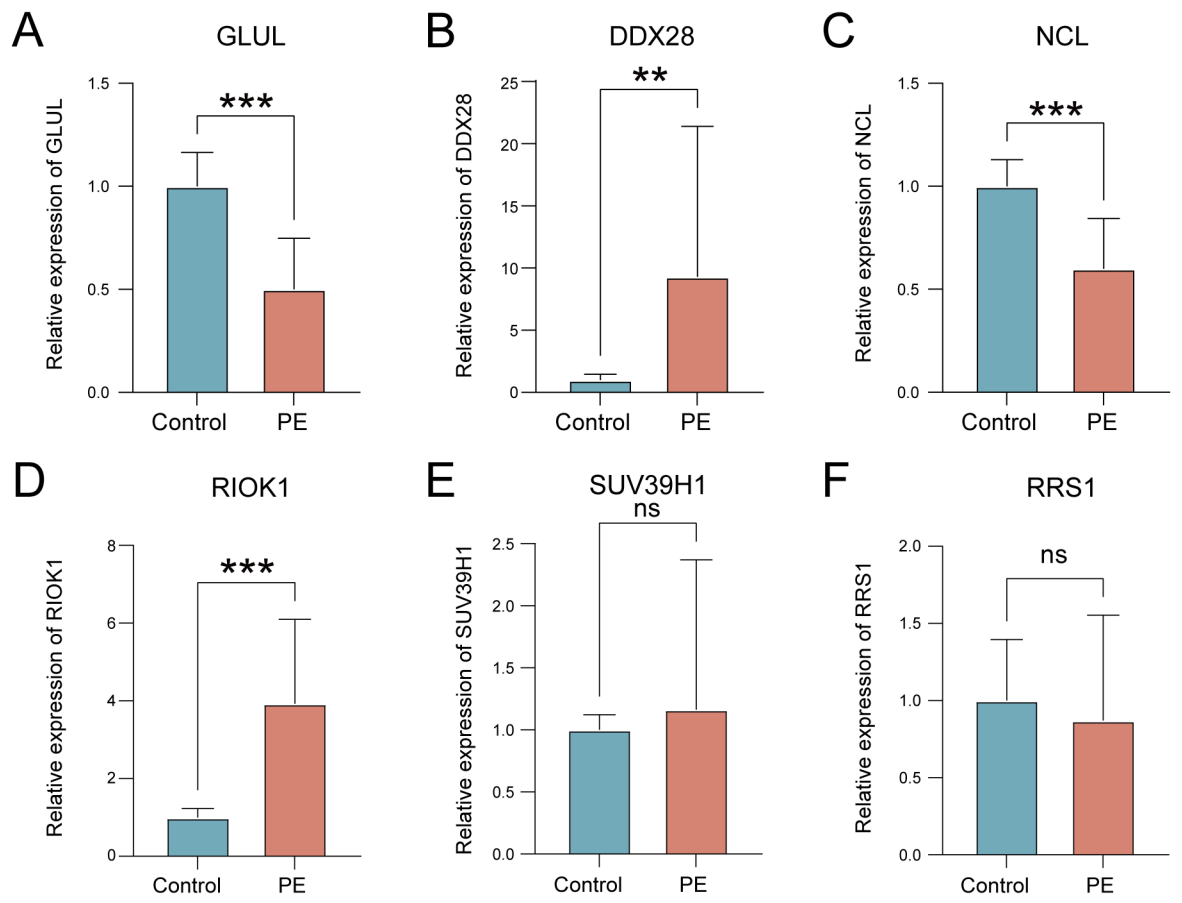

FIGURE 9
Validation of key gene expression in PE placental tissues. **(A–F)** mRNA expression levels of *GLUL* **(A)**, *DDX28* **(B)**, *NCL* **(C)**, *RIOK1* **(D)**, *SUV39H1* **(E)**, and *RRS1* **(F)** in control (blue) versus PE (red) groups. ns, not significant; $^{**}p < 0.01$; $^{***}p < 0.001$.

TABLE 4 Clinical information of the patients.

Category	PE (n = 10)	Control (n = 10)	*p*-value
Gestational age at delivery (weeks)	36.1 ± 1.66	36.1 ± 1.66	1.000
Age (years)	30.4 ± 5.21	29.7 ± 4.60	0.754
Systolic blood pressure (mmHg)	155.1 ± 24.27	122.6 ± 7.91	< 0.001
Diastolic blood pressure (mmHg)	92.9 ± 9.73	74.4 ± 3.69	< 0.001
Neonatal birth weight (g)	2724 ± 500.16	3014 ± 503.42	0.213
1 min Apgar (score)			0.305
10	9 (90%)	10 (100%)	
9	1 (10%)	0 (0%)	
5 min Apgar (score)			0.305
10	9 (90%)	10 (100%)	
9	1 (10%)	0 (0%)	

insights into how ribosomal stress pathways coalesce to induce placental dysfunction.

The clinical validity of our model was comprehensively demonstrated through two complementary approaches: decision curve analysis confirmed substantial net benefit across clinically relevant risk thresholds, and protein-protein interaction networks revealed these biomarkers functionally coordinate ribosome biogenesis through both physical binding and co-expression relationships. While individual genes showed moderate diagnostic power, their ensemble performance underscores the necessity of multi-gene panels for capturing PE's molecular heterogeneity — an optimization of current single-biomarker approaches such as the sFlt-1/PlGF ratio (6). Our XML-driven strategy bridges the critical gap between computational prediction and biological mechanism, offering both a clinically deployable risk assessment tool and a systems-level understanding of ribosomal dysregulation in PE pathogenesis (49).

While our explainable machine learning framework provides novel insights into ribosome biogenesis biomarkers for PE risk prediction, several limitations warrant consideration. First, the retrospective design and reliance on public placental transcriptomic datasets may introduce selection bias, as these lack detailed clinical subtyping (e.g., early- vs. late-onset PE) and longitudinal samples to track biomarker dynamics across gestation. Second, the modest clinical validation cohort limits statistical power to detect subtle expression differences, potentially explaining non-significant qRT-PCR trends for *SUV39H1* and *RRS1*. Third, while the model shows promising cross-cohort performance, its generalizability requires testing in multi-ethnic populations and early-pregnancy blood samples, given the inaccessibility of placental biopsies for prenatal screening. Additionally, the exclusive focus on transcriptional regulation overlooks post-translational modifications (e.g., phosphorylation) and epigenetic mechanisms modulating ribosome biogenesis. Furthermore, SHAP-derived gene interactions remain hypothetical without experimental confirmation through CRISPR-based functional validation in trophoblast models. To address these gaps, future studies need to further validate the mechanistic contribution of key biomarkers through functional experiments (such as CRISPR gene editing and ribosome dynamic analysis) and build a multi-omics integration framework — using single-cell transcriptomes to analyze the specific regulatory network of placental trophoblast/immune cell subsets and combining spatial transcriptomes to map the spatial distribution of ribosomal stress signals in the microenvironment. The effect of post-translational modifications (such as phosphorylation) on ribosome assembly was quantitatively analyzed by the proteome, and the synergistic regulatory pattern of DNA methylation/histone modification was characterized by the epigenome. Multi-dimensional data (metabolome, cell free RNA) of prenatal longitudinal blood samples were further integrated to establish a dynamic risk prediction model based on machine learning. This systematic biological strategy from molecular mechanism to clinical phenotype will reveal the cross-scale regulation of PE development driven by the imbalance of ribosome quality control and then promote the transformation process of biomarkers into clinical diagnostic tools.

5 Conclusion

This study establishes dysregulation of ribosome biogenesis as one of the pivotal molecular mechanisms underlying the pathogenesis of PE and leveraging XML to identify clinically actionable biomarkers. Through multi-cohort transcriptomic integration, we identified 25 RiboRDEGs, with six hub genes (*GLUL*, *DDX28*, *NCL*, *RIOK1*, *SUV39H1*, *RRS1*) forming the core of a high-performance predictive model (AUC >0.9). SHAP interpretability analysis revealed *SUV39H1* as the dominant risk contributor, while *GLUL* and *NCL* exhibited protective effects, highlighting bidirectional regulatory dynamics in placental stress adaptation. Functional enrichment and Bayesian network analyses linked these genes to rRNA processing, nucleolar stress, and immune dysregulation, with immune microenvironment profiling demonstrating significant correlations between RiboRDEGs and altered placental immune cell populations (e.g., MDSCs, macrophages). Experimental validation confirmed dysregulation of key genes. Despite these advances, our study has limitations including retrospective design, potential selection bias in public datasets, and modest validation cohort size. Future work requires CRISPR-based functional validation of key biomarkers and multi-omics integration (single-cell/spatial transcriptomics, proteomics, epigenomics) to map the mechanism of ribosome biogenesis. Development of blood-based machine learning models incorporating longitudinal metabolomic/cfRNA data could enable dynamic risk prediction. Elucidating post-translational modifications (e.g., phosphorylation) and epigenetic regulation of ribosome biogenesis will clarify cross-scale mechanisms underlying

PE pathogenesis. These efforts will bridge ribosome biogenesis insights to clinical translation, advancing early diagnosis and targeted therapies for PE.

Data availability statement

Publicly available datasets were analyzed in this study. This data can be found here: https://www.ncbi.nlm.nih.gov/geo/.

Ethics statement

The studies involving humans were approved by The Research Ethics Committee of Ruian People's Hospital. The studies were conducted in accordance with the local legislation and institutional requirements. The participants provided their written informed consent to participate in this study.

Author contributions

JC: Data curation, Formal analysis, Writing – original draft. DZ: Writing – review & editing, Validation. CZ: Writing – review & editing, Investigation. LL: Visualization, Writing – review & editing. KY: Writing – review & editing. YH: Writing – review & editing, Validation. MP: Conceptualization, Project administration, Writing – review & editing, Methodology.

Funding

The author(s) declare that financial support was received for the research and/or publication of this article. This study was supported by the Wenzhou Medical Health Research Project (No: 2024056) and the Wenzhou Basic Research Project (No: Y20240606).

Acknowledgments

We extend our heartfelt thanks to the patients who generously provided placental samples, making this research possible.

Conflict of interest

The authors declare that the research was conducted in the absence of any commercial or financial relationships that could be construed as a potential conflict of interest.

Generative AI statement

The author(s) declare that Generative AI was used in the creation of this manuscript.

We would like to acknowledge the use of DeepSeek R1 for language refinement and grammar checking in the preparation of this manuscript. DeepSeek-R1, developed by Deepseek Limited, assisted in enhancing the clarity and coherence of the text.

Publisher's note

Supplementary material

The Supplementary Material for this article can be found online at: https://www.frontiersin.org/articles/10.3389/fimmu.2025.1595222/full#supplementary-material

References

1. Rana S, Lemoine E, Granger JP, Karumanchi SA. Preeclampsia: pathophysiology, challenges, and perspectives. *Circ Res*. (2019) 124:1094–112. doi: 10.1161/CIRCRESAHA.118.313276

2. Mol BWJ, Roberts CT, Thangaratinam S, Magee LA, de Groot CJM, Hofmeyr GJ. Pre-eclampsia. *Lancet*. (2016) 387:999–1011. doi: 10.1016/S0140-6736(15)00070-7

3. Hypertension in pregnancy. Report of the American college of obstetricians and gynecologists' Task force on hypertension in pregnancy. *Obstet Gynecol*. (2013) 122:1122–31. doi: 10.1097/01.AOG.0000437382.03963.88

4. Steegers EA, von Dadelszen P, Duvekot JJ, Pijnenborg R. Pre-eclampsia. *Lancet*. (2010) 376:631–44. doi: 10.1016/S0140-6736(10)60279-6

5. Rana S, Powe CE, Salahuddin S, Verlohren S, Perschel FH, Levine RJ, et al. Angiogenic factors and the risk of adverse outcomes in women with suspected preeclampsia. *Circulation*. (2012) 125:911–9. doi: 10.1161/CIRCULATIONAHA.111.054361

6. Zeisler H, Llurba E, Chantraine F, Vatish M, Staff AC, Sennstrom M, et al. Predictive value of the sFlt-1:PlGF ratio in women with suspected preeclampsia. *N Engl J Med*. (2016) 374:13–22. doi: 10.1056/NEJMoa1414838

7. Barrett T, Wilhite SE, Ledoux P, Evangelista C, Kim IF, Tomashevsky M, et al. NCBI GEO: archive for functional genomics data sets–update. *Nucleic Acids Res*. (2013) 41:D991–5. doi: 10.1093/nar/gks1193

8. Leavey K, Benton SJ, Grynspan D, Kingdom JC, Bainbridge SA, Cox BJ. Unsupervised placental gene expression profiling identifies clinically relevant subclasses of human preeclampsia. *Hypertension*. (2016) 68:137–47. doi: 10.1161/HYPERTENSIONAHA.116.07293

9. Leavey K, Benton SJ, Grynspan D, Bainbridge SA, Morgen EK, Cox BJ. Gene markers of normal villous maturation and their expression in placentas with maturational pathology. *Placenta*. (2017) 58:52–9. doi: 10.1016/j.placenta.2017.08.005

10. Christians JK, Leavey K, Cox BJ. Associations between imprinted gene expression in the placenta, human fetal growth and preeclampsia. *Biol Lett*. (2017) 13. doi: 10.1098/rsbl.2017.0643

11. Leavey K, Wilson SL, Bainbridge SA, Robinson WP, Cox BJ. Epigenetic regulation of placental gene expression in transcriptional subtypes of preeclampsia. *Clin Epigenetics*. (2018) 10:28. doi: 10.1186/s13148-018-0463-6

12. Benton SJ, Leavey K, Grynspan D, Cox BJ, Bainbridge SA. The clinical heterogeneity of preeclampsia is related to both placental gene expression and placental histopathology. *Am J Obstet Gynecol*. (2018) 219:604 e1–604. doi: 10.1016/j.ajog.2018.09.036

13. Gibbs I, Leavey K, Benton SJ, Grynspan D, Bainbridge SA, Cox BJ. Placental transcriptional and histologic subtypes of normotensive fetal growth restriction are comparable to preeclampsia. *Am J Obstet Gynecol*. (2019) 220:110.e1–110. doi: 10.1016/j.ajog.2018.10.003

14. Sitras V, Paulssen RH, Gronaas H, Leirvik J, Hanssen TA, Vartun A, et al. Differential placental gene expression in severe preeclampsia. *Placenta*. (2009) 30:424–33. doi: 10.1016/j.placenta.2009.01.012

15. Jebbink JM, Boot RG, Keijser R, Moerland PD, Aten J, Veenboer GJ, et al. Increased glucocerebrosidase expression and activity in preeclamptic placenta. *Placenta*. (2015) 36:160–9. doi: 10.1016/j.placenta.2014.12.001

16. Leek JT, Johnson WE, Parker HS, Jaffe AE, Storey JD. The sva package for removing batch effects and other unwanted variation in high-throughput experiments. *Bioinformatics*. (2012) 28:882–3. doi: 10.1093/bioinformatics/bts034

17. Ritchie ME, Phipson B, Wu D, Hu Y, Law CW, Shi W, et al. limma powers differential expression analyses for RNA-sequencing and microarray studies. *Nucleic Acids Res*. (2015) 43:e47. doi: 10.1093/nar/gkv007

18. Yeung KY, Ruzzo WL. Principal component analysis for clustering gene expression data. *Bioinformatics*. (2001) 17:763–74. doi: 10.1093/bioinformatics/17.9.763

19. Stelzer G, Rosen N, Plaschkes I, Zimmerman S, Twik M, Fishilevich S, et al. The geneCards suite: from gene data mining to disease genome sequence analyses. *Curr Protoc Bioinf*. (2016) 54:1.30.1–1.30.33. doi: 10.1002/cpbi.5

20. Zang Y, Ran X, Yuan J, Wu H, Wang Y, Li H, et al. Genomic hallmarks and therapeutic targets of ribosome biogenesis in cancer. *Brief Bioinform*. (2024) 25. doi: 10.1093/bib/bbae023

21. Gu Z, Eils R, Schlesner M. Complex heatmaps reveal patterns and correlations in multidimensional genomic data. *Bioinformatics*. (2016) 32:2847–9. doi: 10.1093/bioinformatics/btw313

22. Subramanian A, Tamayo P, Mootha VK, Mukherjee S, Ebert BL, Gillette MA, et al. Gene set enrichment analysis: a knowledge-based approach for interpreting genome-wide expression profiles. *Proc Natl Acad Sci U S A*. (2005) 102:15545–50. doi: 10.1073/pnas.0506580102

23. Yu G, Wang LG, Han Y, He QY. clusterProfiler: an R package for comparing biological themes among gene clusters. *OMICS*. (2012) 16:284–7. doi: 10.1089/omi.2011.0118

24. Kanehisa M, Goto S. KEGG: kyoto encyclopedia of genes and genomes. *Nucleic Acids Res*. (2000) 28:27–30. doi: 10.1093/nar/28.1.27

25. Mi H, Muruganujan A, Ebert D, Huang X, Thomas PD. PANTHER version 14: more genomes, a new PANTHER GO-slim and improvements in enrichment analysis tools. *Nucleic Acids Res*. (2019) 47:D419–26. doi: 10.1093/nar/gky1038

26. Sato N, Tamada Y, Yu G, Okuno Y. CBNplot: Bayesian network plots for enrichment analysis. *Bioinformatics*. (2022) 38:2959–60. doi: 10.1093/bioinformatics/btac175

27. Langfelder P, Horvath S. WGCNA: an R package for weighted correlation network analysis. *BMC Bioinf*. (2008) 9:559. doi: 10.1186/1471-2105-9-559

28. Dietterich TG. Ensemble methods in machine learning. In: *International workshop on multiple classifier systems*. Berlin, Heidelberg: Springer Berlin Heidelberg (2000). p. 1–15.

29. Aas K, Jullum M, Løland AJAI. *Explaining individual predictions when features are dependent: More accurate approximations to Shapley values*. Artificial Intelligence (2021) 298:103502.

30. Robin X, Turck N, Hainard A, Tiberti N, Lisacek F, Sanchez JC, et al. pROC: an open-source package for R and S+ to analyze and compare ROC curves. *BMC Bioinf*. (2011) 12:77. doi: 10.1186/1471-2105-12-77

31. Franz M, Rodriguez H, Lopes C, Zuberi K, Montojo J, Bader GD, et al. GeneMANIA update 2018. *Nucleic Acids Res*. (2018) 46:W60–4. doi: 10.1093/nar/gky311

32. Zhou KR, Liu S, Sun WJ, Zheng LL, Zhou H, Yang JH, et al. ChIPBase v2.0: decoding transcriptional regulatory networks of non-coding RNAs and protein-coding genes from ChIP-seq data. *Nucleic Acids Res*. (2017) 45, D43–50 doi: 10.1093/nar/gkw965

33. Li JH, Liu S, Zhou H, Qu LH, Yang JH. starBase v2.0: decoding miRNA-ceRNA, miRNA-ncRNA and protein-RNA interaction networks from large-scale CLIP-Seq data. *Nucleic Acids Res*. (2014) 42:D92–7. doi: 10.1093/nar/gkt1248

34. Xiao B, Liu L, Li A, Xiang C, Wang P, Li H, et al. Identification and verification of immune-related gene prognostic signature based on ssGSEA for osteosarcoma. *Front Oncol*. (2020) 10:607622. doi: 10.3389/fonc.2020.607622

35. Hahn S, Lapaire O, Than NG. Biomarker development for presymptomatic molecular diagnosis of preeclampsia: feasible, useful or even unnecessary? *Expert Rev Mol Diagn*. (2015) 15:617–29. doi: 10.1586/14737159.2015.1025757

36. Hong Y, Lin Q, Zhang Y, Liu J, Zheng Z. Research progress of ribosomal proteins in reproductive development. *Int J Mol Sci*. (2024) 25. doi: 10.3390/ijms252313151

37. Jiao L, Liu Y, Yu XY, Pan X, Zhang Y, Tu J, et al. Ribosome biogenesis in disease: new players and therapeutic targets. *Signal Transduct Target Ther*. (2023) 8:15. doi: 10.1038/s41392-022-01285-4

38. Boulon S, Westman BJ, Hutten S, Boisvert FM, Lamond AI. The nucleolus under stress. *Mol Cell*. (2010) 40:216–27. doi: 10.1016/j.molcel.2010.09.024

39. Ma M, Jiang W, Zhou R. DAMPs and DAMP-sensing receptors in inflammation and diseases. *Immunity*. (2024) 57:752–71. doi: 10.1016/j.immuni.2024.03.002

40. Banerjee S, Huang Z, Wang Z, Nakashima A, Saito S, Sharma S, et al. Etiological value of sterile inflammation in preeclampsia: is it a non-infectious pregnancy complication? *Front Cell Infect Microbiol*. (2021) 11:694298. doi: 10.3389/fcimb.2021.694298

41. Liu L, Simon MC. Regulation of transcription and translation by hypoxia. *Cancer Biol Ther*. (2004) 3:492–7. doi: 10.4161/cbt.3.6.1010

42. Ni C, Buszczak M. The homeostatic regulation of ribosome biogenesis. *Semin Cell Dev Biol*. (2023) 136:13–26. doi: 10.1016/j.semcdb.2022.03.043

43. Hetz C. The unfolded protein response: controlling cell fate decisions under ER stress and beyond. *Nat Rev Mol Cell Biol*. (2012) 13:89–102. doi: 10.1038/nrm3270

44. Peng X, Chinwe Oluchi-Amaka I, Kwak-Kim J, Yang X. A comprehensive review of the roles of T-cell immunity in preeclampsia. *Front Immunol*. (2025) 16:1476123. doi: 10.3389/fimmu.2025.1476123

45. Dai W, Shen J, Yan J, Bott AJ, Maimouni S, Daguplo HQ, et al. Glutamine synthetase limits beta-catenin-mutated liver cancer growth by maintaining nitrogen homeostasis and suppressing mTORC1. *J Clin Invest*. (2022) 132. doi: 10.1172/JCI161408

46. Burton GJ, Jauniaux E. Placental oxidative stress: from miscarriage to preeclampsia. *J Soc Gynecol Investig*. (2004) 11:342–52. doi: 10.1016/j.jsgi.2004.03.003

47. Lundberg SM, Lee S-I. A unified approach to interpreting model predictions. *Neural computing and applications* (2017) 30:.

48. Vellido A. The importance of interpretability and visualization in machine learning for applications in medicine and health care. (2020) 32:18069–83. doi: 10.1007/s00521-019-04051-w

49. Libbrecht MW, Noble WS. Machine learning applications in genetics and genomics. *Nat Rev Genet*. (2015) 16:321–32. doi: 10.1038/nrg3920

frontiers | Frontiers in Pediatrics

TYPE Original Research
PUBLISHED 26 August 2025
DOI 10.3389/fped.2025.1622610

OPEN ACCESS

EDITED BY
Leonardo Ermini,
University of Siena, Italy

REVIEWED BY
Cristina Loddo,
Azienda Ospedaliero-Universitaria Cagliari, Italy
Andrea Balduit,
Institute for Maternal and Child Health Burlo Garofolo (IRCCS), Italy
Jana Semberova,
Coombe Women & Infants University Hospital, Ireland

*CORRESPONDENCE
Tingting Zhu
✉ zttclxxyq@126.com
Yuan Ai
✉ 33310251@qq.com

RECEIVED 04 May 2025
ACCEPTED 29 July 2025
PUBLISHED 26 August 2025

CITATION
Huang H, Zhao J, Huang J, Ai Y and Zhu T (2025) Effects of pre-eclampsia/eclampsia on platelet parameters in small for gestational age preterm infants.
Front. Pediatr. 13:1622610.
doi: 10.3389/fped.2025.1622610

Effects of pre-eclampsia/eclampsia on platelet parameters in small for gestational age preterm infants

Huiling Huang[1,2], Jing Zhao[1,3], Jichong Huang[1,3], Yuan Ai[1,3]* and Tingting Zhu[1,3]*

[1]Department of Pediatrics, West China Second University Hospital, Sichuan University, Chengdu, Sichuan, China, [2]Medical College Shantou University, Shantou, Guangdong, China, [3]Key Laboratory of Obstetric & Gynecologic and Pediatric Diseases and Birth Defects of Ministry of Education, Sichuan University, Chengdu, Sichuan, China

Objectives: To investigate whether pre-eclampsia/eclampsia (PE/E) alters platelet parameters, including platelet count (PLT), mean platelet volume (MPV), and platelet distribution width (PDW), in small for gestational age (SGA) infants.
Methods: We enrolled 245 SGA preterm infants between 2020 and 2023. They were grouped according to their mother's PE/E status. We assessed the PLT, MPV, PDW, and prevelence of thrombocytopenia during the first 30 days after birth. Groups were compared using either $\chi 2$ test or Fisher's exact test.
Results: SGA neonates born to mothers with PE/E had a lower PLT on Day 7 than those born to mothers without PE/E ($P = 0.0211$). PDW and MPV values gradually increased for the first several days, and eventually stabilized around the first week. There was no statistical difference in MPV, PDW, or thrombocytopenia prevalence between SGA neonates between born to mothers with PE/E and those born to mothers without PE/E.
Conclusions: Evidence to support an association between PE/E and platelets parameter in neonates is limited. SGA may be the real reason for alterations in platelet parameters in neonates.

KEYWORDS
pre-eclampsia, eclampsia, platelet, thrombocytopenia, small for gestational age

Introduction

Small for gestational age (SGA) infants are those whose birth weight (BW) is below the 10th percentile for gestational age (GA) and sex compared to a given reference population (1). Global estimates for 2020 suggest that 13.4 million live births were preterm, with rates over the past decade remaining static, and 23.4 million were SGA (2). There is a a higher proportion of SGA infants among term and preterm infant in low-income countries compared to high income countries (3, 4). The prevalence of preterm SGA infants in Africa increased up to 12.3% (4). Children born SGA have higher perinatal morbidity and mortality compared to appropriate-for-gestational-age (AGA) infants, and represent a major challenge in perinatal management.

Previous studies have reported that SGA infants have low peripheral white blood cell, absolute neutrophil, and platelet counts (PLTs) in the first few days after birth (5–7). Takeshita et al. (7) reported that PLTs were significantly lower in the SGA group than in the non-SGA group at the time of the lowest PLT within 72 h of birth.

Approximately 30% of SGA neonates develop thrombocytopenia during the first week after birth (6), which is associated with high mortality (7). However, the cause of these alterations in the blood cell counts of SGA infants remains unknown.

Preeclampsia/eclampsia (PE/E) is among the most common complications of pregnancy and the leading cause of premature delivery and SGA in infants. Preeclampsia is characterized by new-onset hypertension and is often accompanied by proteinuria (8). Eclampsia represents a severe progression of preeclampsia and is defined by the occurrence of seizures in a patient who has preeclampsia (8). The increasing prevalence of hypertension poses challenges for both mothers and neonates. Up to 15% of mothers have hypertensive disorders during pregnancy (9). In China's National Maternal Near-Miss Surveillance System, 2.27% of pregnant women had superimposed preeclampsia, and 50.17% had pre-eclampsia or eclampsia from 2012 to 2020 (10). PE/E is closely related to neonatal death and hypothesized to induce a lower PLT in the offspring (11).

Therefore, in this retrospectively study, we investigated the effect of PE/E on platelet parameters in SGA infants. We aimed to investigate (1) platelet parameters, alterations in SGA infants during the first 30 days after birth; (2) whether PE/E influenced their platelet parameters; and (3) whether it increased their risk of thrombocytopenia in SGA infants.

Methods

The level III neonatal intensive care unit (NICU) of West China Second University Hospital of Sichuan University is the largest neonatal medical unit in Western China. The demographic, clinical, and laboratory data of neonates and their mothers were retrieved from its electronic medical record system. All preterm neonates (GA <37 weeks) with SGA admitted to the NICU within 24 h after birth between November 1st, 2020 and January 1st, 2023 were retrospectively enrolled. Informed written consent was obtained from the parents after the nature of the study was fully explained to them. This study was approved by the Ethics Committee of Sichuan University. All research processes were conducted according to the relevant guidelines and regulations.

SGA was diagnosed based on normative values (12). PE/E was classified based on the criteria of the American College of Obstetricians & Gynecologists (13). Preterm SGA neonates were excluded due to lack of complete blood count (CBC), death within 24 h after admission to the NICU, and the presence of other diseases associated with platelet reduction such as congenital malformation, perinatal asphyxia (Apgar score at 1 min less than 4), early-onset sepsis (defined as isolation of a pathogenic organism from blood and/or CSF culture obtained within 3 days after infant birth), disseminated intravascular coagulation, and immune-mediated thrombocytopenia.

Neonates were grouped according to their mother's PE/E status. We collected characteristic data including maternal age, antenatal steroid usage, sex, BW, GA, Apgar score, mode of delivery, and clinical conditions. Neonatal outcome included mortality, duration of mechanical ventilation, length of hospitalization, hemodynamically significant patent ductus arteriosus, necrotizing enterocolitis (Bell's stage ≥II), bronchopulmonary dysplasia (BPD, defined as the use of O2 at 36 wk postmenstrual age), severe intracranial hemorrhage (IVH, ≥grade 3) and retinopathy of premature infants (ROP, ≥grade 3). Platelets parameters of venous blood samples were measured using automated analyzers at the Clinical Laboratory of West China Second University Hospital. We extracted each neonate's CBC from the laboratory database, if more than one CBC was conducted on the same day, the lowest PLT value was selected. We calculated the mean platelet volume (MPV) and platelet distribution width (PDW). We tried to demonstrate the value changes of PLT, PDW and MPV in preterm SGA after birth. We calculated the mean and various percentile values of PLT, PDW and MPV during first week and different time interval after first week.

The data were compared between the PE/E group and non-PE/E groups. Continuous variables were expressed as the mean ± SD (standard deviation) or median with the interquartile range, based on the data distribution, and were compared using the Student's *t*-test or Mann–Whitney *U* test, respectively. We described the categorical variables using numbers and percentages (%), and compared them with either χ^2 test or Fisher's exact test. All statistical analyses were performed using IBM SPSS Statistics (Windows, version 25.0.).

Results

During the study period, 277 preterm SGA neonates were admitted to our NICUs; 32 were excluded because of congenital malformations, early-onset sepsis, severe neonatal asphyxia, death, or discharge 24 h after birth. Therefore, a total of 245 SGA neonates were included in the analysis (Figure 1).

The baseline characteristics of mothers and neonates, including BW, GA, sex, cesarean delivery rate, antenatal steroid use, maternal diabetes and intrahepatic cholestasis of pregnancy are shown in Table 1. The mean GA and BW in the PE/E group were 33.2 weeks and 1,449.8 gram. The mean GA and BW in the non-PE/E group were 34.1 weeks and 1,593.4 gram. The proportion of infants with a BW <1,500 g was significantly higher in the PE/E group. More infants in the PE/E group were administered antenatal steroids. The mean PLT, MPV, and PDW on the first day did not significantly differ between the two groups.

Table 2 shows the neonatal outcomes of the study population. Our results showed that SGA infants born to women with non-PE/E had longer hospital stay. This could be due to neonatal necrotizing enterocolitis (NEC), and patients with BPD in the PE/E group had more severe diseases and required longer treatment time. There were no significant differences in any of the other neonatal outcomes, including NEC, BPP, severe ROP, severe IVH, blood transfusion, and mortality between the two groups.

The PDW and MPV values of the two groups are shown in Figure 2. The ranges for PDW and MPV in the neonates during their first month (5th to 95th percentile limits) were shown in

10.3389/fped.2025.1622610

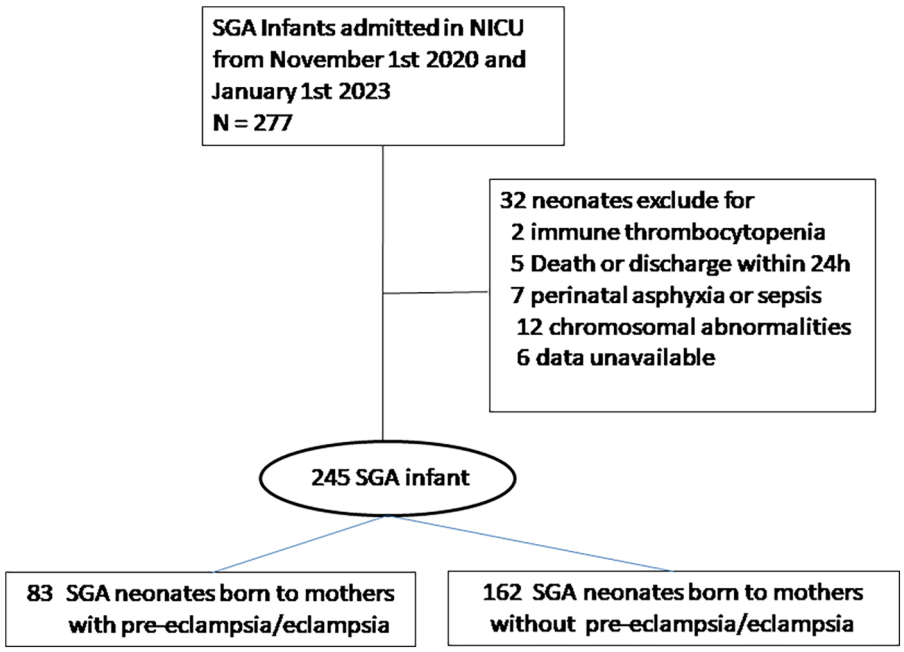

FIGURE 1
Study flowchart showing numbers of neonates enrolled.

TABLE 1 Maternal and infant clinical data of SGA preterm infants.

Characteristics	PE/E (*n* = 83)	no PE/E (*n* = 162)	*p* value
GA (weeks), mean (SD)	33.2 (1.9)	34.1 (2.0)	0.0009
GA group (%)			
<32 w	16 (19.3)	15 (9.3)	0.0406
32 ≤ 34 w	26 (31.3)	31 (19.1)	0.0383
34 ≤ 37 w	41 (49.4)	116 (71.6)	0.0007
BW (gm), mean (SD)	1,449.8 (326.0)	1,593.4 (351.3)	0.0023
BW group (%)			
<1,500 g	44 (53.0)	60 (37.0)	0.0203
1,500–2,000 g	37 (44.6)	89 (54.9)	0.1386
>2,000 g	2 (2.4)	13 (8.1)	0.0969
Male (%)	36 (43.4)	78 (48.1)	0.5012
Singleton pregnancy (%)	54 (65.1)	61 (37.7)	<0.0001
Cesarean delivery (yes, %)	2 (2.4)	13 (8.0)	0.0969
Antenatal steroid use (yes, %)	67 (80.7)	93 (57.4)	0.0004
Surfactant use (yes, %)	13 (15.7)	14 (8.6)	0.1300
Invasive ventilation (yes, %)	13 (15.7)	19 (11.7)	0.4253
Maternal ICP (yes, %)	8 (9.6)	18 (11.1)	0.8285
Maternal diabetes (yes, %)	14 (16.9)	40 (24.7)	0.1937
Platelet count in first day (10^9/L), mean (SD)	211.1 (77.7)	210.3 (64.0)	0.8609
MPV in first day (fL), mean (SD)	10.2 (0.9)	10.2 (0.8)	0.8961
PDW in first day (fL), mean (SD)	11.5 (1.9)	11.5 (2.2)	0.8002

PE/E, preeclampsia/eclampsia; SGA, small for gestational age infants; GA, gestational age; BW, birth weight; w, weeks; gm, grammage; ICP, intrahepatic cholestasis of pregnancy; SD, standard deviation; PLT, platelet count; MPV, mean platelet volume; PDW, platelet distribution width.

Supplementary File 1. The PDW and MPV values did not differ between PE/E and non-PE/E group ($P > 0.05$); they both gradually increased during the first week. The PDW values will eventually stabilized on days 6–7, and those of MPV on day 5–7.

Lower PLTs were observed in the first week (See Supplementary File 2). On Day 7, SGA neonates in the PE/E group had lower PLTs (mean 133×10^9/L) than those in the non- PE/E ($P = 0.0211$).

There were no significant differences in the prevalence of thrombocytopenia (<150×10^9/L) in SGA neonates during the first month between the two groups ($P < 0.05$). The prevalence in both groups was >20% during the first week, then peaked at 58%

10.3389/fped.2025.1622610

TABLE 2 Comparison of neonatal outcome between the groups of maternal preeclampsia/eclampsia in preterm SGA.

Outcome	PE/E (n = 83)	no PE/E (n = 162)	p value
Length of hospital (day, mean, SD)	26.8 (11.9)	35.5 (20.6)	0.0276
Length of invasive ventilation (day, mean, SD)	0.7 (2.1)	0.7 (2.8)	0.9904
Length of non-invasive ventilation (day, mean, SD)	6.1 (9.4)	3.3 (8.0)	0.0193
Transfusion (yes, %)	12 (14.4)	17 (10.5)	0.4043
NEC (yes, %)	5 (6.0)	11 (6.8)	1.0000
BPD (yes, %)	3 (3.6)	7 (4.3)	1.0000
Severe ROP (yes, %)	3 (3.6)	7 (4.3)	1.0000
Severe IVH (yes, %)	1 (1.2)	0 (0)	0.3388
hs PDA (yes, %)	4 (4.8)	4 (2.5)	0.4490
Mortality (yes, %)	1 (1.2)	1 (0.6)	1.0000

PE/E, preeclampsia/eclampsia; SGA, small for gestational age infants; SD, standard deviation; BPD, bronchopulmonary dysplasia; IVH, intraventricular hemorrhage; ROP, retinopathy of prematurity; NEC, necrotizing enterocolitis; hs PDA, hemodynamically significant patent ductus arteriosus.

and 64% over the next 3 weeks in non-PE/Eand PE/E group, respectively (Figure 3).

Discussion

Our study showed that the PLT, MPV, and PDW decreased in SGA infants in both the PE/E and non-PE/E groups, throughout the first week after birth. PE/E did not influence the infant's first PLT or increase the prevalence of thrombocytopenia and did not affect PDW and MPV.

Studies on PDW and MPV in SGA neonates are scarce. Wasiluk et al. (14) used blood samples collected from the umbilical artery to compare 61 full-term SGA newborns with 71 full-term AGA newborns. MPV was higher in SGA newborns (8.25 fl) as compared with AGA newborns (7.84 fl; $P = 0.008$), and while the PDW was nearly identical between groups. Go et al. (15) explored the relationship between perinatal factors and platelet parameters on the first day of life. PDW and MPV did not differ between the SGA and non-SGA groups in late preterm or term neonates. However, the PDW and MPV results in these studies were only compared at a single time point. Despite our small sample size, our study revealed the changes in PDW and MPV in preterm SGA neonates during the 30 days after birth. PDW and MPV values in the early days after birth were lower than those at 1 week after birth ($P < 0.05$ day 7 vs. day 1), they then stabilized with only slight variations over the next 3 weeks. To the best of our knowledge, no study has investigated the effects of PE/E on MPV or PDW in SGA neonates. One study conducted by Elgari et al. (16) reported that MPV in umbilical cord blood of newborns was not associated with PE (cord blood of mothers with PE vs. control group, mean = 9.8 ± 0.98 vs. mean = 9.8 ± 1.0). Participants in this study include full-term and preterm babies, and their mean GA of the PE group was 37.4 ± 2.4 weeks. In the present study, we selected only preterm SGA neonates, and compared the results of PDW and MPV for different days after birth. PE/E did not influence PDW or MPV in preterm SGA neonates during the first month. However, more cohort studies with lager sample size are needed to confirm these findings.

Thrombocytopenia is common among SGA neonates; however, the correlation between PLT in neonates and PE/E remains unknown. A study by Delaney et al. focused on thrombocytopenia among extremely premature infants exposed to maternal hypertension (17). Exposed premature infants had a lower absolute PLT and a higher prevalence of PLT $<150 \times 10^9$/L and $<100 \times 10^9$/L, at their first CBC. PLTs remained low in infants exposed to maternal hypertension at 2, 32 and 36 weeks post-menstrual age, and at discharge. However, mixed effect linear model demonstrated no association between maternal hypertension and the trend of PLTs after adjusting for SGA status ($\beta = -9 \times 10^9$/L, $P = .70$). Similarly, Joslyn et al. (18) reported that for infants in the subgroup of hypertension and SGA, the presence of either PE with severe features was not associated with a lower first PLT or an increased risk of a first PLT $<150 \times 10^9$/L in the first 24 h of life. In our study, the proportion of thrombocytopenia cases during the first month after birth was not significantly different between the PE/E and control groups. The mean PLT in the PE/E group was lower than that in the control group at most time points; however, the difference was not statistically significant ($P > 0.05$). We only observed that on day 7, the PLT in SGA infants born to women with PE/E was lower than non-PE/E group (133.5/59.4 vs. 193.0/99.1, $P = 0.0211$). This cannot rule out the potential effect of PE/E on the PLT in neonates.

The proposed mechanisms by which SGA or PE/E affected platelet parameters lack sufficient evidence. It has been previously postulated that the cause of reduced in platelets in SGA was insufficient thrombopoietin (TPO) production, which impairs megakaryopoietic activity (7, 19–20). Takeshita et al. demonstrated that a decrease in TPO production due to hepatic dysmaturation resulted in thrombocytopenia in SGA model rats (19). In agreement with the results, SGA infants with thrombocytopenia had lower immatureplatelet fraction and serum TPO levels than non-SGA infants with thrombocytopenia (7). Cremer et al. (20) hypothesized that moderate and severe thrombocytopenia in SGA neonates might be due to megakaryopoiesis suppression. This is because, they found a trend toward lower immature fractions, which reflects reduced platelet production, in SGA neonates with thrombocytopenia compared with non-SGA neonates with thrombocytopenia who had an infection. Hypertension during pregnancy results in abnormal trophoblast invasion of the spiral arteries during implantation, resulting in placental perfusion deficiency, causing chronic placental insufficiency and subsequent fetal hypoxia (21). The defective trophoblastic invasion characteristic of this condition can also trigger widespread endothelial damage, leading to alterations in the coagulation process between platelets and endothelial cells (22).

Our study had certain limitations. The main GA of the SGA neonates ranged between 34 and 37 weeks. Notably, smaller GA and lower BW are important indicators of thrombocytopenia. Our study did not examine the effect of PE on platelet parameters in extremely preterm infants. We grouped neonates based on the presence or absence of PE/E in their mothers. We did not assess

10.3389/fped.2025.1622610

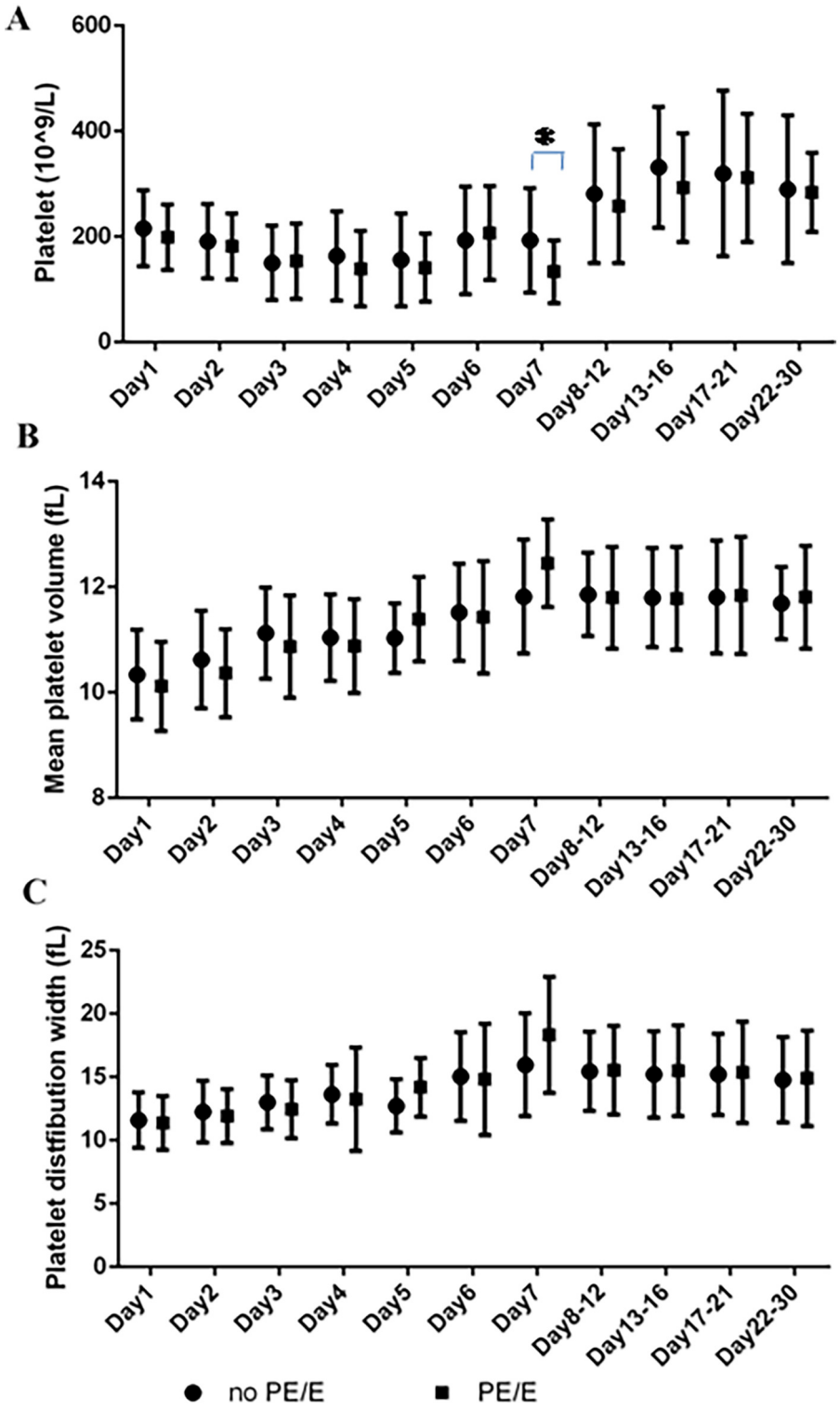

FIGURE 2
Platelets parameters at the various time points in maternal PE/E group and control group during their first 30 days. **(A)** Platelet count; **(B)** mean platelet volume; **(C)** platelet distribution width. (*$P = 0.0211$; On Day 7, SGA neonates born to mothers with PE/E had lower PLTs than those born to mothers without PE/E).

the effects of different forms of maternal hypertension, such as gestational and chronic hypertension, on neonatal platelet parameters. Whether the differentiation of the hypertensive disorders of pregnancy into its subtypes is crucial for platelet parameters remains unknown. Finally, none of the neonates with thrombocytopenia required platelet transfusion. However, the

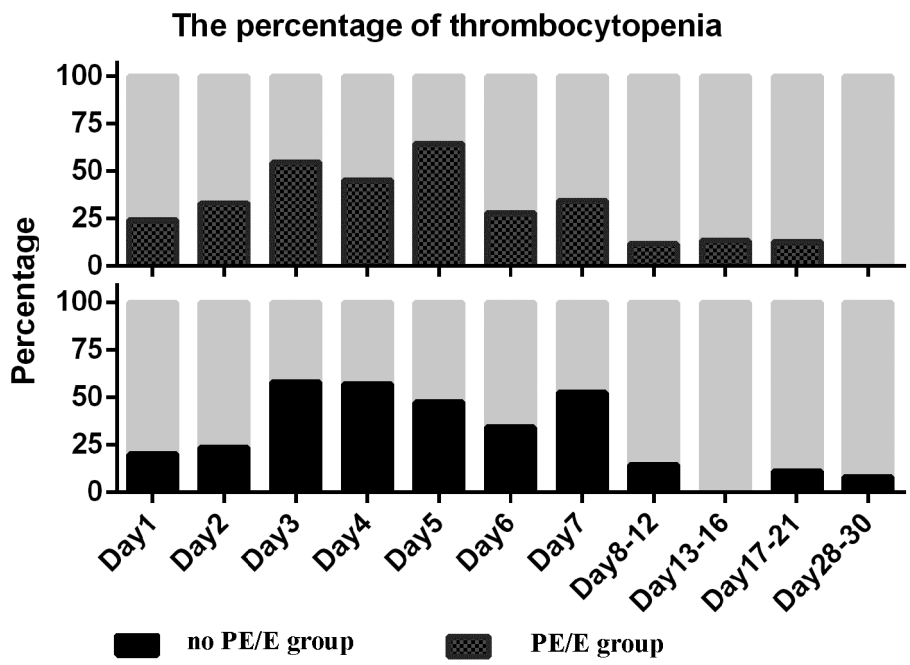

FIGURE 3
Percentage of thrombocytopenia in small for gestational age infants with or without maternal preeclampsia/eclampsia during the study period. Thrombocytopenia defined as PLT less than 150×10^9/L; PE/E, maternal preeclampsia/eclampsia group; no PE/E, no maternal preeclampsia/eclampsia group.

patient clinical manifestations may be relatively mild; therefore, the impact of PE on platelets could have been masked

Despite these limitations, to our best knowledge, this is the first study to explore the impact of PE/E on platelet parameters in preterm neonates with SGA during the first month after birth. Further studies are needed to investigate whether PE/E affects platelet parameters in neonates or whether SGA is an independent risk factor.

Data availability statement

The raw data supporting the conclusions of this article will be made available by the authors, without undue reservation.

Ethics statement

The studies involving human participants were reviewed and approved by the Ethics Committee of Sichuan University. Written informed consent to participate in this study was provided by the patients' legal guardians.

Author contributions

HH: Methodology, Conceptualization, Formal analysis, Writing – original draft. JZ: Formal analysis, Writing – original draft, Data curation, Investigation. JH: Writing – original draft, Formal analysis, Data curation. YA: Writing – original draft, Formal analysis, Data curation, Methodology. TZ: Writing – original draft, Supervision, Writing – review & editing, Conceptualization, Methodology.

Funding

The author(s) declare that financial support was received for the research and/or publication of this article. The search was founded by the Medical Research Project of Sichuan Medical Association (S23008).

Conflict of interest

The authors declare that the research was conducted in the absence of any commercial or financial relationships that could be construed as a potential conflict of interest.

Generative AI statement

The author(s) declare that no Generative AI was used in the creation of this manuscript.

Any alternative text (alt text) provided alongside figures in this article has been generated by Frontiers with the support of artificial

intelligence and reasonable efforts have been made to ensure accuracy, including review by the authors wherever possible. If you identify any issues, please contact us.

Publisher's note

All claims expressed in this article are solely those of the authors and do not necessarily represent those of their affiliated organizations, or those of the publisher, the editors and the reviewers. Any product that may be evaluated in this article, or claim that may be made by its manufacturer, is not guaranteed or endorsed by the publisher.

Supplementary material

The Supplementary Material for this article can be found online at: https://www.frontiersin.org/articles/10.3389/fped.2025.1622610/full#supplementary-material

References

1. Villar J, Ismail LC, Victora CG, Ohuma EO, Bertino E, Altman DG, et al. International standards for newborn weight, length, and head circumference by gestational age and sex: the newborn cross-sectional study of the INTERGROWTH-21st project. *Lancet*. (2014) 384(9946):857–68. doi: 10.1016/S0140-6736(14)60932-6

2. Lawn JE, Ohuma EO, Bradley E, Idueta LS, Hazel E, Okwaraji YB, et al. Small babies, big risks: global estimates of prevalence and mortality for vulnerable newborns to accelerate change and improve counting. *Lancet*. (2023) 401(10389):1707–19. doi: 10.1016/S0140-6736(23)00522-6

3. Katz J, Lee AC, Kozuki N, Lawn JE, Cousens S, Blencowe H, et al. Mortality risk in preterm and small-for-gestational-age infants in low-income and middle-income countries: a pooled country analysis. *Lancet*. (2013) 382:417–25. doi: 10.1016/S0140-6736(13)60993-9

4. Lee ACC, Katz J, Blencowe H, Cousens S, Kozuki N, Vogel JP, et al. National and regional estimates of term and preterm babies born small for gestational age in 138 low-income and middle-income countries in 2010. *Lancet Glob Health*. (2013) 1: e26–36. doi: 10.1016/S2214-109X(13)70006-8

5. Ozyürek E, Cetintaş S, Ceylan T, Oğüş E, Haberal A, Gürakan B, et al. Complete blood count parameters for healthy, small-for-gestational-age, full-term newborns. *Clin Lab Haematol*. (2006) 28(2):97–104. doi: 10.1111/j.1365-2257.2006.00767.x

6. Christensen RD, Baer VL, Henry RE, Snow GL, Butler A, Sola-Visner MC. Thrombocytopenia in small for gestational age infants. *Pediatrics*. (2015) 136(2): e361–70. doi: 10.1542/peds.2014-4182

7. Takeshita S, Kakita H, Asai S, Asai T, Mori M, Ueda H, et al. Thrombocytopenia and insufficient thrombopoietin production in human small-for-gestational-age infants. *Pediatr Res*. (2023) 93(3):619–24. doi: 10.1038/s41390-022-02107-7

8. ACOG Practice Bulletin No. 202: gestational hypertension and preeclampsia. *Obstet Gynecol*. (2019) 133(1):e1–25. doi: 10.1097/AOG.0000000000003018

9. Medjedovic E, Kurjak A, Stanojevic M, Salihagic-Kadic A, Begic E. Preeclampsia: still a disease of theories. *Donald Sch J Ultrasound Obstet Gynecol*. (2022) 16:138–47. doi: 10.5005/jp-journals-10009-1922

10. Yang Y, Xie Y, Li M, Yi M, Peiran C, Liu Z, et al. Characteristics and fetal outcomes of pregnant women with hypertensive disorders in China: a 9-year national hospital-based cohort study. *BMC Pregnancy Childbirth*. (2022) 22(1):924. doi: 10.1186/s12884-022-05260-3

11. Rolim ACB, Lambert MA, Borges JPG, Abbas SA, Bordin JO, Junior DML. Blood cells profile in umbilical cord of late preterm and term newborns. *Rev Paul Pediatr*. (2019) 37(3):264–74. doi: 10.1590/1984-0462/;2019;37;3;00008

12. Zhu L, Zhang R, Zhang S, Shi W, Yan W, Wang X, et al. Chinese Neonatal birth weight curve for different gestational age. *Zhonghua Er Ke Za Zhi*. (2015) 53:97–103.

13. Hypertension G. Gestational hypertension and preeclampsia: aCOG practice bulletin summary, number 222. *Obstet Gynecol*. (2020) 135:1492–5. doi: 10.1097/AOG.0000000000003892

14. Wasiluk A, Dabrowska M, Osada J, Jasinska E, Laudanski T, Redzko S. Platelet indices in SGA newborns. *Adv Med Sci*. (2011) 56(2):361–5. doi: 10.2478/v10039-011-0030-2

15. Go H, Ohto H, Nollet KE, Kashiwabara N, Chishiki M, Hoshino M, et al. Perinatal factors affecting platelet parameters in late preterm and term neonates. *PLoS One*. (2020) 15(11):e0242539. doi: 10.1371/journal.pone.0242539

16. Elgari MM, Khabour OF, Alhag SM. Correlations between changes in hematological indices of mothers with preeclampsia and umbilical cord blood of newborns. *Clin Exp Hypertens*. (2019) 41(1):58–61. doi: 10.1080/10641963.2018.1441861

17. Delaney J, Nunes GDC, Simoneau J, Beltempo M, Malhamé I, Goudie C, et al. Thrombocytopenia and neonatal outcomes among extremely premature infants exposed to maternal hypertension. *Pediatr Blood Cancer*. (2023) 70(2):e30131. doi: 10.1002/pbc.30131

18. Joslyn P, Rosenbaum C, Chapple AG, Heard A, Velez M, Barkemeyer B. The effects of maternal hypertension on the early neonatal platelet count. *J Perinatol*. (2022) 42(6):796–802. doi: 10.1038/s41372-021-01278-1

19. Takeshita S, Kakita H, Toriuchi K, Aoki H, Ueda H, Wakatsuki A, et al. Insufficient thrombopoietin due to hepatic dysmature results in thrombocytopenia in small-for-gestational-age rats. *Br. J. Haematol*. (2021) 192:e105–8. doi: 10.1111/bjh.17294

20. Cremer M, Weimann A, Schmalisch G, Hammer H, Bührer C, Dame C. Immature platelet values indicate impaired megakaryopoietic activity in neonatal early-onset thrombocytopenia. *Thromb Haemost*. (2010) 103:1016–21. doi: 10.1160/TH09-03-0148

21. Backes CH, Markham K, Moorehead P, Cordero L, Nankervis CA, Giannone PJ. Maternal preeclampsia and neonatal outcomes. *J Pregnancy*. (2011) 2011::214365. doi: 10.1155/2011/214365

22. Yang SW, Cho SH, Kwon HS, Sohn IS, Hwang HS. Significance of the platelet distribution width as a severity marker for the development of preeclampsia. *Eur J Obstet Gynecol Reprod Biol*. (2014) 175:107–11. doi: 10.1016/j.ejogrb.2013.12.036

frontiers | Frontiers in Endocrinology

TYPE Original Research
PUBLISHED 09 September 2025
DOI 10.3389/fendo.2025.1611257

OPEN ACCESS

EDITED BY
Leonardo Ermini,
University of Siena, Italy

REVIEWED BY
Luiz Vinicius De Alcantara Sousa,
Faculdade de Medicina do ABC, Brazil
Alaa Ismail,
Women's Health Hospital;Ass, Egypt

*CORRESPONDENCE
Fang Wang
ery_fwang@lzu.edu.cn

RECEIVED 14 April 2025
ACCEPTED 19 August 2025
PUBLISHED 09 September 2025

CITATION
Wei Y, Xin X, Mu F and Wang F (2025) Progesterone decline threshold in predicting early pregnancy loss: a retrospective study. *Front. Endocrinol.* 16:1611257. doi: 10.3389/fendo.2025.1611257

Progesterone decline threshold in predicting early pregnancy loss: a retrospective study

Yanling Wei, Xiaoyu Xin, Fangxiang Mu and Fang Wang*

Department of Reproductive Medicine, Lanzhou University Second Hospital, Lanzhou, China

Objective: The single measurement of serum progesterone is considered a predictor for non-viable pregnancies. However, the dynamic change in progesterone during early pregnancy loss (EPL) remains uninvestigated. This study evaluated the association between serum progesterone decline thresholds (PDT) and EPL.

Methods: This retrospective study included 664 pregnant women who visited a single medical center from January 2023 to December 2024. Based on pregnancy outcomes within the first trimester, participants were classified into the ongoing pregnancy group (n=388) and the EPL group (n=286). PDT was defined as a decline of ≥ 1/5 standard deviation (SD), 1/3 SD, 1/2 SD, 7/10 SD, or 1 SD compared with the last measurement of serum progesterone levels. SD was calculated based on the baseline serum progesterone levels. Multivariate logistic regression was applied to explore the association between PDT and EPL. Receiver operating characteristic (ROC) curve analysis was conducted to assess the diagnostic value of PDT. Subgroup analyses were performed to evaluate the robustness of the results.

Results: Compared with the ongoing pregnancy group, the EPL group had significantly lower baseline serum progesterone levels ($P < 0.05$). PDT ≥ 1/5 SD, 1/3 SD, and 1/2 SD were all significantly associated with EPL (OR [95%CI]=2.74 [1.76, 4.27], $P < 0.001$; OR [95%CI]=1.74 [1.18, 2.56], P=0.005; and OR [95%CI] =1.63 [1.07, 2.49], P=0.024, respectively). The corresponding AUC values were 0.502, 0.512, and 0.503. Additionally, a linear positive correlation was observed between the number of occurrences of PDT ≥ 1/3 SD and EPL. For each additional occurrence of PDT ≥ 1/3 SD, the risk of EPL increased by 36% (OR [95%CI]=1.36 [1.09, 1.70], P=0.006). Subgroup analyses supported the robustness of these results.

Conclusion: PDT ≥ 1/5 SD, 1/3 SD, and 1/2 SD are significantly associated with an increased risk of EPL. This suggests that these thresholds hold potential predictive value in EPL diagnosis and may help identify pregnant women at higher risk for early intervention.

KEYWORDS

pregnancy, progesterone, early pregnancy loss, progesterone decline threshold, risk assessment

1 Introduction

Pregnancy loss affects 15%–25% of clinically recognized pregnancies (1). Approximately 80% of pregnancy losses occur during the first trimester (up to 12 weeks and 6/7 days), termed early pregnancy loss (EPL) (2). Common symptoms of EPL include vaginal bleeding and uterine cramping (3); however, these symptoms are also observed in normal and ectopic pregnancies, which makes the diagnosis and management of EPL challenging.

Transvaginal ultrasonographic (TVS) diagnosis is the primary method for confirming EPL by detecting fetal cardiac activity. However, due to incomplete embryonic development in early pregnancy, a single TVS examination may not provide a definitive diagnosis, often requiring follow-up scans within 7–14 days (4–6). Consequently, researchers have focused on identifying highly sensitive and specific biomarkers for early EPL diagnosis (7–9).

Progesterone is secreted by the corpus luteum, which ensures normal embryonic development by establishing maternal-fetal immune tolerance, inhibiting uterine contractions, and improving uteroplacental circulation (10). Its levels remain relatively stable before 9 weeks of gestation and gradually increase after 10–12 weeks as the placenta takes over secretion (11). Studies have consistently confirmed that serum progesterone levels are significantly lower in women experiencing pregnancy loss compared to those with ongoing pregnancies (12, 13), and baseline progesterone levels in early pregnancy have been shown to aid in discriminating between viable and non-viable pregnancies (14–16). However, progesterone levels fluctuate significantly within individuals due to pulsatile secretion patterns, hormone distribution, and dietary influences (17–19), particularly when gestational age is not consistently recorded in studies. Furthermore, studies have suggested that the progesterone level partially overlaps between normal and abnormal pregnancies (20, 21), which complicates their clinical application.

Therefore, we hypothesize that the dynamic monitoring of serum progesterone decline might address the limitations of single measurements because it captures changes in progesterone levels between measurements. In this study, we aimed to evaluate the association between progesterone decline threshold (PDT) and EPL, which may provide predictive value for EPL diagnosis.

2 Methods

2.1 Participants

This retrospective analysis was conducted on 1,865 pregnant women who visited the Department of Reproductive Medicine, Lanzhou University Second Hospital between January 2023 and December 2024. The study was approved by the Ethics Committee of Lanzhou University Second Hospital (Approval No. 2019A-231), and all participants provided written informed consent.

The inclusion criteria were as follows (1): Age between 18 and 45 years (2); Natural conception (3); Availability of early pregnancy outcome (4); At least two progesterone measurements completed between 3 and 12 weeks of pregnancy.

Participants were excluded if they had (1): Parental or embryonic chromosomal abnormalities (2); Congenital uterine anomalies (e.g., septate uterus, unicornuate uterus, bicornuate uterus, or uterus didelphys) without surgical correction during the current pregnancy (3); Multiple pregnancies (4); Infertility (5); Ectopic pregnancy (6); Missing progesterone data or fewer than two measurements. The participants' demographics were also recorded, including maternal age, body mass index (BMI), age at menarche, and menstrual regularity.

2.2 Progesterone measurement

Progesterone (ng/mL) was the exposure variable in this study. Peripheral venous blood was collected from all patients during their visits, and serum was separated after centrifugation. Progesterone levels were measured using an automated chemiluminescence immunoassay analyzer (Immulite 1000, Siemens Healthineers). The timing of subsequent measurements was determined based on pregnancy status.

2.3 Definition of PDT

In this study, any progesterone level lower than the last measurement was considered a decline. To explore the association between PDT and EPL, PDT was defined as a decline of ≥ 1/5 standard deviation (SD), 1/3 SD, 1/2 SD, 7/10 SD, and 1 SD compared to the last measurement of serum progesterone levels. SD was calculated from the baseline serum progesterone levels of the eligible participants.

2.4 Study outcomes

The study outcomes were pregnancy loss (including biochemical pregnancy) and ongoing pregnancy within 12 weeks of gestation. Embryonic viability was assessed using TVS. Ongoing pregnancy was defined as the presence of embryonic cardiac activity, while EPL was defined as the absence of cardiac activity, confirmed by repeated TVS after 7–14 days.

2.5 Statistical analysis

Categorical variables were presented as numbers and percentages (%), and group comparisons were performed using the Chi-square test. Continuous variables, if normally distributed, were described as mean ± SD; otherwise, they were presented as median (interquartile range). Group differences for continuous variables were compared using the Student's t-test or the Kruskal-Wallis H test. Missing data were handled using multiple imputation.

The association between PDT and EPL was investigated using multivariate logistic regression analysis. To control for confounding factors, three adjusted models were constructed: Model 1 adjusted

for age; Model 2 adjusted for age and baseline serum progesterone; Model 3 adjusted for age, baseline serum progesterone, and number of progesterone measurements. Receiver operator characteristic (ROC) curve analysis was conducted to assess the diagnostic value of PDT, and the area under the ROC curve (AUC) was calculated using the DeLong test. Restricted cubic spline analysis was utilized to explore potential non-linear relationships between the number of PDT occurrences and EPL. Furthermore, subgroup analyses were performed by dividing participants into two groups based on whether their progesterone levels fell below baseline, to assess the robustness of the association between PDT and EPL.

All statistical analyses were conducted using R version 4.3.1 (http://www.R-project.org, The R Foundation) and EmpowerStats version 4.2 (https://www.empowerstats.net/en/; X&Y solutions, Inc.). All statistical tests were two-tailed, with $P < 0.05$ considered statistically significant.

3 Results

3.1 Baseline characteristics of the participants

This study included 664 women who met the inclusion criteria (Figure 1), with 276 cases of EPL and 388 cases of ongoing pregnancy. Table 1 summarizes the characteristics of the participants. The EPL group had significantly higher age (31.56 ± 3.98 vs. 30.62 ± 3.70 years, P=0.004) and body mass index (22.04 ± 2.95 vs. 21.52 ± 2.92 kg/m^2, P=0.018), as well as significantly lower number of progesterone measurements (5.84 ± 3.42 vs. 8.78 ± 3.78, $P < 0.001$) and baseline serum progesterone levels (30.73 ± 24.74 vs. 35.62 ± 25.47 ng/mL, $P < 0.001$) compared to the ongoing pregnancy group (all $P < 0.05$). Other characteristics were comparable between the two groups.

3.2 Association between PDT and EPL

In Models 1 and 2, PDT was not significantly associated with EPL ($P > 0.05$). In Model 3, however, PDT ≥ 1/5 SD, 1/3 SD, and 1/2 SD were positively associated with EPL, with risks of 2.74-fold (95%CI: 1.76, 4.27, $P < 0.001$), 1.74-fold (95%CI: 1.18, 2.56, P=0.005), and 1.63-fold (95%CI: 1.07, 2.49, P=0.024) for those experiencing a decline compared to those without a decline, respectively (Table 2, Figure 2).

3.3 Diagnostic value of PDT

The ROC analysis showed that when PDT ≥ 1/5 SD, 1/3 SD, and 1/2 SD, the AUC values were 0.502, 0.512, and 0.503, respectively (Table 3). The DeLong test results were not significant ($P > 0.05$), indicating no significant differences in diagnostic performance for EPL across these decline magnitudes.

3.4 Association between the number of occurrences of PDT ≥ 1/3 SD and EPL

The logistic regression results presented in Table 4 indicated that, in Model 3, the number of occurrences of PDT ≥ 1/3 SD was significantly positively associated with EPL. Each additional occurrence of this decline increased the risk of EPL by 36% (OR=1.36, 95%CI: 1.09, 1.70, P=0.006). Similarly, restricted cubic spline analysis also demonstrated a linear association between the number of occurrences

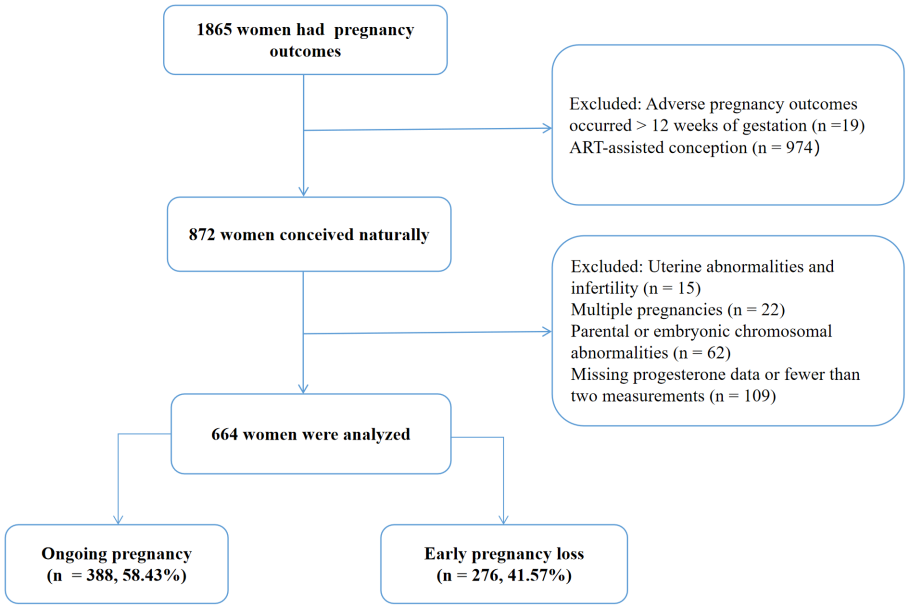

FIGURE 1
Participant selection flow diagram.

10.3389/fendo.2025.1611257

TABLE 1 Baseline characteristics of participants.

Characteristics	Total (n=664)	Ongoing pregnancy (n=388)	EPL (n=276)	P value
Age, years, mean ± SD	31.01 ± 3.85	30.62 ± 3.70	31.56 ± 3.98	0.004
BMI, kg/m^2, mean ± SD	21.73 ± 2.94	21.52 ± 2.92	22.04 ± 2.95	0.018
Age at menarche, years, mean ± SD	13.00 ± 1.33	12.98 ± 1.22	13.02 ± 1.47	0.747
Baseline serum progesterone, ng/mL, mean ± SD	33.59 ± 25.27	35.62 ± 25.47	30.73 ± 24.74	<0.001
Number of progesterone measurements, mean ± SD	7.56 ± 3.91	8.78 ± 3.78	5.84 ± 3.42	<0.001
Regularity of menstruation, n (%)				0.690
No	147 (22.14%)	88 (22.68%)	59 (21.38%)	
Yes	517 (77.86%)	300 (77.32%)	217 (78.62%)	
Serum progesterone below baseline, n (%)				0.615
No	98 (14.76%)	55 (14.18%)	43 (15.58%)	
Yes	566 (85.24%)	333 (85.82%)	233 (84.42%)	
Serum progesterone declined, n (%)				0.056
No	31 (4.67%)	13 (3.35%)	18 (6.52%)	
Yes	633 (95.33%)	375 (96.65%)	258 (93.48%)	
PDT ≥ 1/5 SD, n (%)				0.905
No	170 (25.60%)	100 (25.77%)	70 (25.36%)	
Yes	494 (74.40%)	288 (74.23%)	206 (74.64%)	
PDT ≥ 1/3 SD, n (%)				0.556
No	311 (46.84%)	178 (45.88%)	133 (48.19%)	
Yes	353 (53.16%)	210 (54.12%)	143 (51.81%)	
PDT ≥ 1/2 SD, n (%)				0.849
No	455 (68.52%)	267 (68.81%)	188 (68.12%)	
Yes	209 (31.48%)	121 (31.19%)	88 (31.88%)	
PDT ≥ 7/10 SD, n (%)				0.870
No	520 (78.31%)	303 (78.09%)	217 (78.62%)	
Yes	144 (21.69%)	85 (21.91%)	59 (21.38%)	
PDT ≥ 1 SD, n (%)				0.095
No	551 (82.98%)	314 (80.93%)	237 (85.87%)	
Yes	113 (17.02%)	74 (19.07%)	39 (14.13%)	

EPL, early pregnancy loss; SD, standard deviation; BMI, body mass index; PDT, progesterone decline threshold.

of PDT ≥ 1/3 SD and EPL ($P < 0.05$), with an increasing risk of EPL as the occurrences of declines increased (Figure 3).

3.5 Subgroup analysis

When PDT ≥ 1/5 SD and 1/3 SD, along with the serum progesterone levels below baseline levels, they were significantly positively associated with EPL risk (OR=2.76, 95%CI: 1.66, 4.60, $P < 0.001$ for 1/5SD; OR=1.54, 95%CI: 1.01, 2.34, P=0.043 for 1/3 SD) (Table 5). However, no significant associations with EPL were observed in the other subgroups. Additionally, all P for interaction values across subgroups were not significant, suggesting that the significant associations between PDT ≥ 1/5 SD, 1/3 SD, 1/2 SD, and EPL were robust regardless of whether the serum progesterone levels after decline were below baseline.

10.3389/fendo.2025.1611257

TABLE 2 The association between PDT and EPL.

Exposure	Model 1 OR (95%CI)	P value	Model 2 OR (95%CI)	P value	Model 3 OR (95%CI)	P value
Serum progesterone declined						
No	Reference	—	Reference	—	Reference	—
Yes	0.55 (0.26, 1.15)	0.113	0.61 (0.29, 1.29)	0.195	2.13 (0.96, 4.71)	0.063
PDT ≥ 1/5 SD						
No	Reference	—	Reference	—	Reference	—
Yes	0.98 (0.69, 1.40)	0.919	1.14 (0.78, 1.65)	0.498	2.74 (1.76, 4.27)	<0.001
PDT ≥ 1/3 SD						
No	Reference	—	Reference	—	Reference	—
Yes	0.89 (0.65, 1.22)	0.470	1.08 (0.77, 1.52)	0.664	1.74 (1.18, 2.56)	0.005
PDT ≥ 1/2 SD						
No	Reference	—	Reference	—	Reference	—
Yes	0.98 (0.70, 1.38)	0.929	1.33 (0.90, 1.96)	0.149	1.63 (1.07, 2.49)	0.024
PDT ≥ 7/10 SD						
No	Reference	—	Reference	—	Reference	—
Yes	0.91 (0.63, 1.34)	0.642	1.34 (0.85, 2.11)	0.210	1.55 (0.94, 2.53)	0.083
PDT ≥ 1 SD						
No	Reference	—	Reference	—	Reference	—
Yes	0.65 (0.43, 1.01)	0.053	0.88 (0.53, 1.47)	0.625	1.03 (0.59, 1.80)	0.910

OR, odds ratio; CI, confidence interval; PDT, progesterone decline threshold; SD, standard deviation.
Model 1: adjusted for age.
Model 2: adjusted for age and baseline serum progesterone.
Model 3: adjusted for age, baseline serum progesterone, and number of progesterone measurements.

4 Discussion

Developing useful and reliable clinical prediction models based on serum biomarkers is crucial for identifying at-risk populations to improve their pregnancy outcomes. To our knowledge, this study is the first to investigate the predictive value of varying decline thresholds of progesterone levels for EPL. The results indicate that changes in progesterone levels can effectively predict pregnancy outcomes. Specifically, when PDT ≥ 1/5 SD, 1/3 SD, and 1/2 SD, the risk of EPL increased by 2.74 times, 1.76 times, and 1.63 times, respectively. Furthermore, each additional occurrence of PDT ≥ 1/3 SD increased the risk of EPL by 36%. These findings remained robust even when serum progesterone levels, after a decline, were below baseline levels. This study supports that PDT ≥ 1/5 SD, 1/3 SD, and 1/2 SD holds potential predictive value in EPL diagnosis, which may aid clinicians in developing more targeted interventions.

Progesterone levels fluctuate and rise during pregnancy, playing a critical role in maintaining gestation. A decrease in progesterone levels in early pregnancy may reflect inadequate luteal function or abnormal placental development, leading to compromised pregnancy maintenance (22, 23). The lower the serum progesterone levels, the lower the likelihood of pregnancy viability (24). Therefore, previous studies have sought to identify a progesterone cut-off value for predicting pregnancy outcome. Hanita et al., (25) Li et al., (26) and Puget etal., (27) reported cut-off values of 32.7, 19.4, and 6.2 ng/mL ng/mL, respectively, for predicting non-viable pregnancies. However, Sakar reported that a 10.7 ng/mL cut-off value more accurately identified viable pregnancies but poorly diagnosed non-viable ones (28). Additionally, some studies noted that the diagnostic cut-off value for non-viable pregnancies might be influenced by gestational age and symptoms (e.g., bleeding or pain) (29, 30). Collectively, inter-study heterogeneity complicates the selection of a reliable cut-off value. In contrast, this study introduces dynamic monitoring of serum progesterone changes and suggests that PDT ≥ 1/5 SD, 1/3 SD, and 1/2 SD has predictive value for diagnosing EPL. This approach minimizes bias from assay variability and population differences, allows earlier prediction of EPL, and may improve clinical decision-making and management.

Dynamic monitoring of early pregnancy hormones is clinically valuable for assessing gestational outcomes. Whittaker et al. performed serial measurements of progesterone, estradiol, and human chorionic gonadotropin (hCG) from gestational days 21 to 91 in asymptomatic women who later experienced early pregnancy failure. They observed that, around day 50, hormone levels continued to rise in normal pregnancies but declined in the early-failure group, indicating that dynamic monitoring can identify high-risk, asymptomatic women earlier (7). Similarly, Li et al. showed that

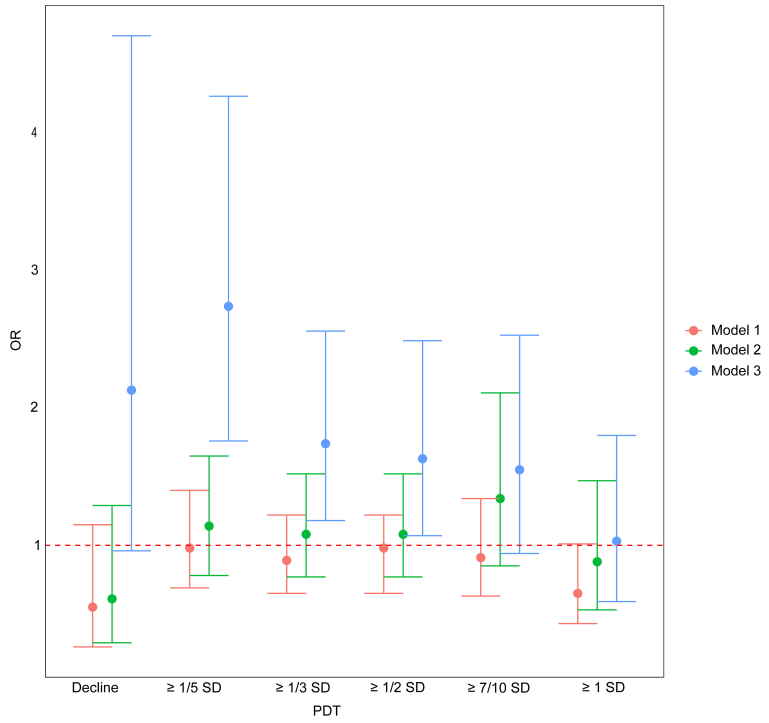

FIGURE 2
The association between PDT and EPL. OR, odds ratio; PDT, progesterone decline threshold; SD, standard deviation. Model 1: adjusted for age; Model 2: adjusted for age and baseline serum progesterone; Model 3: adjusted for age, baseline serum progesterone, and number of progesterone measurements.

TABLE 3 ROC analysis of the predictive value of PDT in predicting EPL.

Exposure	Area of ROC	95%CI	Z	P value
PDT ≥ 1/5 SD	0.502	0.468, 0.536	-0.286	0.775[a]
PDT ≥ 1/3 SD	0.512	0.473, 0.550	0.234	0.815[b]
PDT ≥ 1/2 SD	0.503	0.468, 0.539	-0.074	0.941[c]

ROC, Receiver operating characteristic; PDT, progesterone decline threshold; EPL, early pregnancy loss; SD, standard deviation. AUC, Area under curve.
[a]PDT ≥1/5 SD vs PDT ≥1/3 SD;
[b]PDT ≥1/3SD vs PDT ≥ 1/2 SD;
[c]PDT ≥1/5 SD vs PDT ≥ 1/2 SD.

TABLE 4 The association between the number of occurrences of PDT ≥ 1/3 SD and EPL.

Exposure	Model 1 OR (95%CI)	P value	Model 2 OR (95%CI)	P value	Model 3 OR (95%CI)	P value
Number of occurrences	0.84 (0.71,0.98)	0.034	0.92 (0.76,1.11)	0.376	1.36 (1.09,1.70)	0.006

PDT, progesterone decline threshold; EPL, early pregnancy loss; SD, standard deviation; OR, odds ratio; CI, confidence interval.
Model 1: adjusted for age.
Model 2: adjusted for age and baseline serum progesterone.
Model 3: adjusted for age, baseline serum progesterone, and number of progesterone measurements.

tracking changes in estradiol and hCG over time enabled earlier detection of bad pregnancy outcomes (31). Additionally, Mu et al. reported that the average estradiol decreased times correlated positively with EPL risk (32). Su et al. further examined the absolute rate of progesterone change (Δprogesterone) between weeks 6 and 10, finding it predictive of outcome—though not as strongly as ΔhCG or Δestradiol (33). Our findings also support the significance of dynamic monitoring for pregnancy progress. We define PDT to stratify declines between consecutive measurements and suggest its significant predictive value for EPL.

Although our findings have positive clinical implications for managing pregnant women, they should be interpreted with caution. We observed that as PDT increased, the associated risk of EPL weakened, and PDT ≥ 7/10 SD and 1 SD did not show

10.3389/fendo.2025.1611257

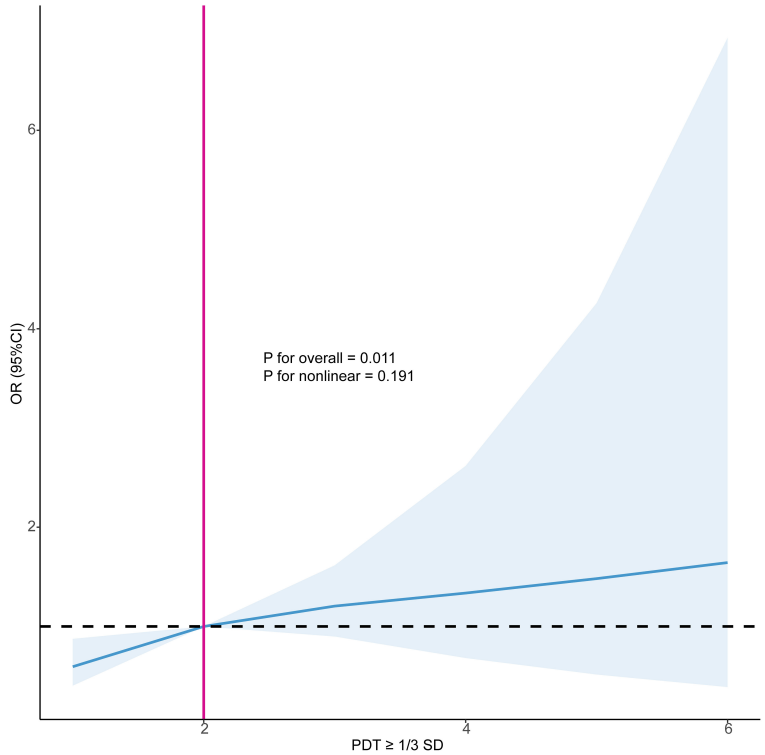

FIGURE 3
Restricted cubic splines examined the association between the number of occurrences of PDT ≥ 1/3 SD and EPL. PDT, progesterone decline threshold; SD, standard deviation; OR, odds ratio; CI, confidence interval.

TABLE 5 Subgroup analyses of the effect of PDT on EPL.

Subgroups	PDT	n	OR (95%CI)	P value	P for interaction
Serum progesterone below baseline	PDT ≥ 1/5 SD				0.441
No	No	54	Reference	—	
	Yes	44	2.08 (0.72,5.98)	0.174	
Yes	No	116	Reference	—	
	Yes	450	2.76 (1.66,4.60)	<0.001	
	PDT ≥ 1/3 SD				0.386
No	No	70	Reference	—	
	Yes	28	2.87 (0.96,8.64)	0.060	
Yes	No	241	Reference	—	
	Yes	325	1.54 (1.01,2.34)	0.043	
	PDT ≥ 1/2 SD				0.340
No	No	83	Reference	—	
	Yes	15	3.19 (0.89,11.49)	0.076	
Yes	No	372	Reference	—	
	Yes	194	1.47 (0.93,2.33)	0.102	

PDT, progesterone decline threshold; EPL, early pregnancy loss; SD, standard deviation; OR, odds ratio; CI, confidence interval.

significance. This may be due to the reduced sample size of participants with progesterone decline participants as PDT increased, leading to lower statistical power. Future studies should aim to expand sample sizes and adopt prospective designs to more accurately assess the relationship between PDT and the risk of EPL. Additionally, our model's AUC values were relatively low (0.502, 0.503, and 0.512), indicating limited predictive ability on their own. This may reflect progesterone's intrinsic pulsatile secretion, in which a single decline may indicate physiological fluctuations rather than a pathological state; furthermore, our study did not control the intervals between measurements, inherently introducing risks of information bias. As a result, in clinical practice, these PDT indicators should serve as supplementary or adjunctive diagnostic tools. For example, combining other available indicators, such as new ultrasonographic parameters, hCG, estradiol, and PAPP-A (31, 34), to conduct multivariate analysis could enhance the diagnostic performance of the predictive models. Moreover, this study was retrospective and relied on historical case data, excluding patients with incomplete progesterone testing records, which inherently introduced risks of selection bias and potential information bias. In addition, we did not obtain medication information for these participants, making it impossible to exclude the use of progesterone supplements, which affects the accuracy of the results. Finally, as these results lack external validation, we plan to confirm their reliability in larger, independent, multicenter cohorts.

In conclusion, our study suggests that PDT ≥ 1/5 SD, 1/3 SD, and 1/2 SD may provide useful information for identifying high-risk EPL populations, thereby assisting clinical decision-making. Currently, EPL diagnosis primarily relies on TVS examinations, which have limited utility in early pregnancy due to incomplete embryonic development. Our findings offer a potential complementary tool for this diagnostic process. By incorporating dynamic assessments of progesterone levels, particularly cases where serum progesterone decline exceeds 1/5 SD, 1/3 SD, and 1/2 SD, clinicians may identify high-risk EPL populations earlier. This could enable more frequent pregnancy monitoring or early interventions, providing scientifically based decision support for early screening and management of EPL.

5 Conclusion

PDT ≥ 1/5 SD, 1/3 SD, and 1/2 SD significantly increased the risk of EPL. These results may aid in EPL diagnosis and help clinicians optimize pregnancy management strategies. Future large-scale studies are needed to further validate the application value of these findings.

Data availability statement

The raw data supporting the conclusions of this article will be made available by the authors, without undue reservation.

Ethics statement

The studies involving humans were approved by Ethics Committee of Lanzhou University Second Hospital (Approval No. 2019A-231). The studies were conducted in accordance with the local legislation and institutional requirements. The participants provided their written informed consent to participate in this study.

Author contributions

YW: Conceptualization, Data curation, Writing – original draft. XX: Data curation, Formal analysis, Writing – original draft. FM: Validation, Visualization, Writing – original draft. FW: Conceptualization, Writing – review & editing.

Funding

The author(s) declare financial support was received for the research and/or publication of this article. This study was supported by the Science Foundation of Lanzhou University (Grant No. 071100132).

Conflict of interest

The authors declare that the research was conducted in the absence of any commercial or financial relationships that could be construed as a potential conflict of interest.

Generative AI statement

The author(s) declare that no Generative AI was used in the creation of this manuscript.

Any alternative text (alt text) provided alongside figures in this article has been generated by Frontiers with the support of artificial intelligence and reasonable efforts have been made to ensure accuracy, including review by the authors wherever possible. If you identify any issues, please contact us.

Publisher's note

References

1. Practice Committee of the American Society for Reproductive Medicine. Evaluation and treatment of recurrent pregnancy loss: a committee opinion. *Fertility sterility*. (2012) 98:1103–11. doi: 10.1016/j.fertnstert.2012.06.048

2. American College of Obstetricians and Gynecologists' Committee on Practice Bulletins—Gynecology. ACOG practice bulletin no. 200: early pregnancy loss. *Obstet Gynecol*. (2018) 132:e197–207. doi: 10.1097/AOG.0000000000002899

3. Sapra KJ, Joseph KS, Galea S, Bates LM, Louis GM, Ananth CV. Signs and symptoms of early pregnancy loss. *Reprod Sci (Thousand Oaks Calif)*. (2017) 24:502–13. doi: 10.1177/1933719116654994

4. Preisler J, Kopeika J, Ismail L, Vathanan V, Farren J, Abdallah Y, et al. Defining safe criteria to diagnose miscarriage: prospective observational multicenter study. *BMJ (Clinical Res ed)*. (2015) 351:h4579. doi: 10.1136/bmj.h4579

5. Huchon C, Deffieux X, Beucher G, Capmas P, Carcopino X, Costedoat-Chalumeau N, et al. Pregnancy loss: French clinical practice guidelines. *Eur J obstetrics gynecology Reprod Biol*. (2016) 201:18–26. doi: 10.1016/j.ejogrb.2016.02.015

6. Doubilet PM, Benson CB, Bourne T, Blaivas M, Barnhart KT, Benacerraf BR, et al. Diagnostic criteria for nonviable pregnancy early in the first trimester. *New Engl J Med*. (2013) 369:1443–51. doi: 10.1056/NEJMra1302417

7. Whittaker PG, Schreiber CA, Sammel MD. Gestational hormone trajectories and early pregnancy failure: a reassessment. *Reprod Biol endocrinology: RB&E*. (2018) 16:95. doi: 10.1186/s12958-018-0415-1

8. Huang J, Lv P, Lian Y, Zhang M, Ge X, Li S, et al. Construction of machine learning tools to predict threatened miscarriage in the first trimester based on AEA, progesterone and β-hCG in China: a multicenter, observational, case-control study. *BMC Pregnancy Childbirth*. (2022) 22:697. doi: 10.1186/s12884-022-05025-y

9. Pillai RN, Konje JC, Tincello DG, Potdar N. Role of serum biomarkers in the prediction of outcome in women with threatened miscarriage: a systematic review and diagnostic accuracy meta-analysis. *Hum Reprod update*. (2016) 22:228–39. doi: 10.1093/humupd/dmv054

10. Di Renzo GC, Giardina I, Clerici G, Brillo E, Gerli S. Progesterone in normal and pathological pregnancy. *Hormone Mol Biol Clin Invest*. (2016) 27:35–48. doi: 10.1515/hmbci-2016-0038

11. Taraborrelli S. Physiology, production and action of progesterone. *Acta obstetricia gynecologica Scandinavica*. (2015) 94 Suppl 161:8–16. doi: 10.1111/aogs.12771

12. Duan L, Yan D, Zeng W, Yang X, Wei Q. Predictive power progesterone combined with beta human chorionic gonadotropin measurements in the outcome of threatened miscarriage. *Arch gynecology obstetrics*. (2011) 283:431–5. doi: 10.1007/s00404-010-1367-7

13. Lek SM, Ku CW, Allen JC Jr., Malhotra R, Tan NS, Østbye T, et al. Validation of serum progesterone <35nmol/L as a predictor of miscarriage among women with threatened miscarriage. *BMC Pregnancy Childbirth*. (2017) 17:78. doi: 10.1186/s12884-017-1261-4

14. Yalçin I, Taşkin S, Pabuçcu EG, Söylemez F. The value of placental protein 13, β-human chorionic gonadotropin and progesterone in the prediction of miscarriages in threatened miscarriage patients. *J obstetrics gynecology*. (2015) 35:283–6. doi: 10.3109/01443615.2014.948822

15. Ucyigit A, Fuller JL, Poon LC, Johns J, Ross JA. The significance of low first trimester serum progesterone in ongoing early pregnancies presenting as pregnancies of unknown location. *Eur J obstetrics gynecology Reprod Biol*. (2021) 258:294–8. doi: 10.1016/j.ejogrb.2021.01.013

16. He S, Allen JC Jr., Malhotra R, Østbye T, Tan TC. Association of maternal serum progesterone in early pregnancy with low birth weight and other adverse pregnancy outcomes. *J maternal-fetal neonatal Med*. (2016) 29:1999–2004. doi: 10.3109/14767058.2015.1072159

17. Filicori M, Butler JP, Crowley WF Jr. Neuroendocrine regulation of the corpus luteum in the human. Evidence for pulsatile progesterone secretion. *J Clin Invest*. (1984) 73:1638–47. doi: 10.1172/JCI111370

18. Schliep KC, Mumford SL, Hammoud AO, Stanford JB, Kissell KA, Sjaarda LA, et al. Luteal phase deficiency in regularly menstruating women: prevalence and overlap in identification based on clinical and biochemical diagnostic criteria. *J Clin Endocrinol Metab*. (2014) 99:E1007–14. doi: 10.1210/jc.2013-3534

19. Nakajima ST, McAuliffe T, Gibson M. The 24-hour pattern of the levels of serum progesterone and immunoreactive human chorionic gonadotropin in normal early pregnancy. *J Clin Endocrinol Metab*. (1990) 71:345–53. doi: 10.1210/jcem-71-2-345

20. Radwanska E, Frankenberg J, Allen EI. Plasma progesterone levels in normal and abnormal early human pregnancy. *Fertility sterility*. (1978) 30:398–402. doi: 10.1016/S0015-0282(16)43571-5

21. Ku CW, Allen JC Jr., Lek SM, Chia ML, Tan NS, Tan TC. Serum progesterone distribution in normal pregnancies compared to pregnancies complicated by threatened miscarriage from 5 to 13 weeks gestation: a prospective cohort study. *BMC Pregnancy Childbirth*. (2018) 18:360. doi: 10.1186/s12884-018-2002-z

22. Shah D, Nagarajan N. Luteal insufficiency in first trimester. *Indian J Endocrinol Metab*. (2013) 17:44–9. doi: 10.4103/2230-8210.107834

23. Tuckey RC. Progesterone synthesis by the human placenta. *Placenta*. (2005) 26:273–81. doi: 10.1016/j.placenta.2004.06.012

24. Bobdiwala S, Kyriacou C, Christodoulou E, Farren J, Mitchell-Jones N, Al-Memar M, et al. Evaluating cut-off levels for progesterone, β human chorionic gonadotropin and β human chorionic gonadotropin ratio to exclude pregnancy viability in women with a pregnancy of unknown location: A prospective multicenter cohort study. *Acta obstetricia gynecologica Scandinavica*. (2022) 101:46–55. doi: 10.1111/aogs.14295

25. Hanita O, Hanisah AH. Potential use of single measurement of serum progesterone in detecting early pregnancy failure. *Malaysian J pathology*. (2012) 34:41–6. doi: 10.1002/jcla.23559

26. Li H, Qin S, Xiao F, Li Y, Gao Y, Zhang J, et al. Predicting first-trimester outcome of embryos with cardiac activity in women with recurrent spontaneous abortion. *J Int Med Res*. (2020) 48:300060520911829. doi: 10.1177/0300060520911829

27. Puget C, Joueidi Y, Bauville E, Laviolle B, Bendavid C, Lavoué V, et al. Serial hCG and progesterone levels to predict early pregnancy outcomes in pregnancies of uncertain viability: A prospective study. *Eur J obstetrics gynecology Reprod Biol*. (2018) 220:100–5. doi: 10.1016/j.ejogrb.2017.11.020

28. Sakar MN, Balsak D, Demir SS, Budak MŞ, Tahaoglu AE, Gungor SE, et al. The ability of a single serum progesterone measurement to predict the prognosis of first trimester pregnancy. *Gynecology Obstetrics Reprod Med*. (2020) 26:1–5. doi: 10.21613/GORM.2019.942

29. Deng W, Sun R, Du J, Wu X, Ma L, Wang M, et al. Prediction of miscarriage in first trimester by serum estradiol, progesterone and β-human chorionic gonadotropin within 9 weeks of gestation. *BMC Pregnancy Childbirth*. (2022) 22:112. doi: 10.1186/s12884-021-04158-w

30. Verhaegen J, Gallos ID, van Mello NM, Abdel-Aziz M, Takwoingi Y, Harb H, et al. Accuracy of single progesterone test to predict early pregnancy outcome in women with pain or bleeding: meta-analysis of cohort studies. *BMJ (Clinical Res ed)*. (2012) 345:e6077. doi: 10.1136/bmj.e6077

31. Li Y, Zhang J, Zhang K, Wang E, Shu J. Significance of dynamically monitoring serum estrogen and β-human chorionic gonadotropin in early pregnancy assessment. *J Clin Lab analysis*. (2021) 35:e23559. doi: 10.1002/jcla.23559

32. Mu F, Wang C, Li X, Wang F. The relationship between the average decreased times of estradiol and early miscarriage: an observational study. *Reprod Sci (Thousand Oaks Calif)*. (2025) 32:358–65. doi: 10.1186/s12884-021-04158-w

33. Su R, Wang Y, Lu Y, Lin B, An J. Weekly changes in serum β-human chorionic gonadotropin, estradiol, and progesterone levels for pregnancy assessment in women with unexplained recurrent miscarriage. *J Int Med Res*. (2025) 53:3000605251327478. doi: 10.1177/03000605251327478

34. Bucuri CE, Ciortea R, Malutan AM, Berceanu C, Rada MP, Mihu D. Progesterone's serum level and a new ultrasonographic parameter in the first trimester pregnancy - prognostic factors for embryonic demise. *Rev Bras ginecologia e obstetricia: Rev da Federacao Bras das Sociedades Ginecologia e Obstetricia*. (2019) 41:525–30. doi: 10.1515/hmbci-2015-0030

frontiers | Frontiers in Endocrinology

TYPE Original Research
PUBLISHED 11 September 2025
DOI 10.3389/fendo.2025.1576240

OPEN ACCESS

EDITED BY
Leonardo Ermini,
University of Siena, Italy

REVIEWED BY
Etienne Marbaix,
Université Catholique de Louvain, Belgium
Sofia Passaponti,
University of Siena, Italy

*CORRESPONDENCE
Soraya Mezouar
soraya.mezouar@univ-amu.fr

†These authors have contributed equally to this work and share first authorship

‡These authors have contributed equally to this work and share last authorship

RECEIVED 13 February 2025
ACCEPTED 23 July 2025
PUBLISHED 11 September 2025

CITATION
Andrieu J, Donet A, Cocallemen J-F, Charbonnier G, Resseguier N, Paganini J, Mège J-L, Mezouar S and Bretelle F (2025) Dual specificity phosphatase 1 as a non-invasive circulating biomarker candidate in preeclampsia.
Front. Endocrinol. 16:1576240.
doi: 10.3389/fendo.2025.1576240

Dual specificity phosphatase 1 as a non-invasive circulating biomarker candidate in preeclampsia

Jonatane Andrieu[1†], Agathe Donet[2,3†], Jean-François Cocallemen[3], Guillaume Charbonnier[4], Noémie Resseguier[5], Julien Paganini[4], Jean-Louis Mège[1,6†], Soraya Mezouar[1,7*‡] and Florence Bretelle[2,3‡]

[1]Aix-Marseille Univ, Centre National de la Recherche Scientifique, Établissement Français du Sang, Anthropologie bio-culturelle, Droit, Éthique et Santé, Marseille, France, [2]Aix-Marseille Univ, Institut Recherche Développement, Assistance Publique – Hôpitaux de Marseille, Microbe, Evolution, Phylogeny Infection, Marseille, France, [3]Department of Gynecology-Obstetric, La Conception Hospital, Marseille, France, [4]Department of Bioinformatics and Biostatistics, Xegen, Gemenos, France, [5]Aix-Marseille Univ, Assistance Publique – Hôpitaux de Marseille, La Timone Hospital, Department of Epidemiology and Health Economics, Clinical Research Unit, Direction of Health Research, Marseille, France, [6]Department of Immunology, La Conception Hospital, Marseille, France, [7]Faculty of Medical and Paramedical Sciences, Aix-Marseille University, Health Improvement Through Physical Exercise (HIPE) Human Lab, Marseille, France

Introduction: Preeclampsia (PE) is a multisystem pregnancy complication. Factors pointing to a placental origin are the development of the pathology only during pregnancy, and its disappearance in the post-partum period.

Methods: Here, we aim to identify early predictive biomarkers. Whole blood and serum samples were collected at the time of the first event of PE (V1) and same samples after remote delivery (30-60 postpartum days, V2). These two samples enabled investigation of PE markers found in V1 but absent in V2. To confirm that these candidates are associated with PE, an investigation of associated placental biopsy was also realized (J0).

Results: Our study identified a specific signature of PE including five Gene Ontology clusters including "angiogenesis and differentiation", "cell-cycle", "cell-adhesion", "inflammatory response" and "cellular metabolism". DUSP1 (Dual Specificity Phosphatase 1) gene was found specifically modulated in PE. PE women have a higher concentration of DUSP1 in serum compared to healthy donors. Interesting, at a distance from childbirth (V2), DUSP1 finds a rate like control group showing its predictive interest as a promising predictive biomarker of PE.

Discussion: The investigation of DUSP1 in a prospective study with a larger cohort, including the severity aspect of the disease, is necessary to confirm its value as a predictive biomarker in PE.

KEYWORDS

preeclampsia, placenta, hypertension, DUSP1, RNA-seq

Introduction

Preeclampsia (PE) is a progressive, multisystem pregnancy complication that affects 3%–5% of pregnancies, making it one of the major causes of maternal and fetal morbidity and mortality (1). PE is responsible for hematological complications and severe organ failure, particularly affecting the placenta, nervous system, liver, lungs, kidneys, and cardiovascular system (2, 3). Fetal complications include life-threatening complications such as intrauterine growth retardation, malformations, and induced prematurity (4). PE is a complex pathological process that originates at the maternal–fetal interface (5, 6). It is widely accepted that PE is a disease of maternal endothelium with placental origins. Supporting this theory is the observation that the pathology develops only during pregnancy and resolves in the postpartum period.

Several early prognostic clinical indicators (e.g., mean arterial pressure) and ultrasonography markers (e.g., uterine artery pulsatility index) have been combined to diagnose PE. At the biological level, placental growth factor (PlGF) and pregnancy-associated plasma protein A (PAPP-A) have been proposed to predict the risk of preterm PE. With a positive predictive value of approximately 85%–90%, the Fetal Medicine Foundation (FMF) test was developed to assess the risk of early PE. This means that 10%–15% of FMF tests may yield a high-risk result but will not result in premature PE (1). Other studies have focused on trophoblastic cells, as placental cells, by examining their processes of migration and invasion (7). Markers such as programmed death-ligand 1 (PD-L1) (8) and angiopoïetine like 4 (ANGPTL4) (9) have been shown to significantly increase trophoblast invasion and migration in PE, and have also implicated the yes-associated protein (YAP)–Hippo trophoblast differentiation pathway (10). However, these factors only contribute to a better understanding of PE physiopathology.

There has been growing interest in early predictive biomarkers for PE. Effective predictive tests would facilitate early diagnosis, targeted monitoring, and prompt management, using biomarkers capable of identifying risk early in pregnancy (before 16 weeks) in women at high risk of clinical complications (11). The anti-angiogenic factor soluble fms-like tyrosine kinase 1 (sFlt-1), found in the placenta and measured in plasma and serum, has been proposed as a specific biomarker for the onset and severity of PE (12). Evaluation of the ratio of sFlt-1 to the pro-angiogenic factor PlGF was found to have a high negative predictive value (13) and can be used to predict the short-term absence of PE in women for whom the disease was previously suspected clinically. Unfortunately, its predictive value is strongly linked to the prevalence of the disease. Ongoing studies are focused on the selection of women for early intervention to prevent PE onset, particularly through acetylsalicylic acid prescription (14). The ASPRE trial showed that identification of at-risk women using a score that includes mean arterial pressure, uterine artery pulsatility index, and maternal serum PAPP-A and PlGF can reduce early PE (15, 16). However, the overall rate was not decreased, which encourages further studies on the identification of new tools or factors.

The aim of this study was to identify new early biomarkers of PE based on a transcriptional signature present at the time of the event, using both maternal peripheral blood and placental biopsy samples. The secondary objective was to evaluate the evolution of this signature's expression during the progression of pregnancy, particularly at the time of delivery, using samples from maternal blood and placental tissue.

Materials and methods

Ethics statement

This single-center, prospective, longitudinal study was conducted in accordance with the Declaration of Helsinki and French laws on research involving humans. The study protocol was approved by an independent national ethics review board, "CPP Sud Mediterranean 1" (approval no. 2010-A00633-36). All pregnant women provided written informed consent. Participants were recruited at the gynecology–obstetrics departments of Hôpital de la Conception and Hôpital Nord (Marseille, France) between February 2019 and July 2020.

Study participants and sample collection

The study included 10 pregnant women as controls and 10 pregnant women diagnosed with PE between 20 and 37 weeks of gestation (Table 1). Pregnant women with PE presented with arterial hypertension (systolic blood pressure greater than or equal to 140 mmHg and/or diastolic blood pressure greater than or equal to 90 mmHg) associated with proteinuria (positive urine dipstick or proteinuria greater than 0.3 g protein per 24 h). PE and control groups were matched for maternal age and gestational age at inclusion.

Clinical parameters recorded included maternal age, geographic origin, body mass index (kg/m^2), and obstetrical characteristics (gestational age, parity, spontaneous or induced pregnancy, and any pregnancy-related complications). Detailed fetal outcomes were monitored, including ultrasound findings, fetal heart rate analysis, and neonatal data.

Total blood samples (PAXgene tubes, PreAnalytiX) were collected at the time of PE diagnosis (and at matched gestational age for controls) and again 4–6 weeks postpartum (Supplementary Figure S1). PAXgene tubes were stored at 4°C for 24 h, then frozen at −20°C for 24 h before permanent storage at −80°C. A placental biopsy was also performed at the time of delivery for all participants. Each biopsy consisted of a macroscopically selected placental area of 2x2 cm including both chorionic and basal membranes. Biopsies were preserved in RNA*later* (Thermo Fisher Scientific) for 24 h at 4°C, then frozen for 24 h at −20°C, and finally stored at −80°C.

RNA extraction

Total RNA from whole blood samples was extracted using the PAXgene Blood RNA Kit (Qiagen) according to the manufacturer's

10.3389/fendo.2025.1576240

TABLE 1 Initial characteristics of the population at the time of inclusion.

Characteristics	Control (n=10) n (%)	Preeclampsia (n=10) n (%)	*p-value*
Pregnant women			
Age (years)	29.50 ± 4.45	31.20 ± 7.43	*0.54*
Geographical origin • Caucasian • African • Asian	 7 (70) 3 (30) 0	 9 (90) 1 (10) 0	*0.58*
BMI (Kg/m^2)	23.70 ± 4.27	24.50 ± 3.98	*0.68*
Smoking status • Absence • Active (>10 cig/day)	 9 (90) 1 (10)	 10 (100) 0 (0)	–
Obstetrical characteristics			
Gestational age at diagnosis (weeks)	31.4 ± 4.30	29.5 ± 3.13	*0.29*
Conception type • Spontaneous pregnancy • Induced IVF pregnancy	 10 (100) 0 (0)	 8 (80) 2 (20)	*0.47*
Delivery route • Vaginal delivery • Caesarean section	 8 (80) 2 (20)	 0 (0) 10 (100)	*0.0007*
Maternal complications • Absence • Presence - Uncontrolled hypertension - Proteinuria >6g/day - Acute renal failure - HELLP syndrome	 10 (100) 0 (0) 0 (0) 0 (0) 0 (0) 0 (0)	 6 (60) 4 (40) 3 (30) 2 (20) 1 (10) 2 (20)	*0.0867*
Fetal outcome			
Gestational age at birth (weeks)	39.5 ± 1.13	30.1 ± 3.1	*<0.001*
Days between inclusion and delivery	61.6 ± 31.25	3.3 ± 3.05	*<0.001*
Fetal growth • Eutrophic fetus • Intrauterine growth retardation	 10 (100) 0 (0)	 7 (70) 3 (30)	*0.21*
Fetal Doppler • Normal fetal Doppler • Doppler anomalies	 10 (100) 0 (0)	 7 (70) 3 (30)	*0.21*
Neonatal complications • Absence • Presence - Fetal growth restriction - Respiratory distress - Neonatal death	 8 (80) 2 (20) 0 (0) 2 (20) 0 (0)	 2 (20) 8 (80) 4 (40) 3 (30) 1 (10)	*0.02*
Birth weight (g)	3174.4 ± 281	1203.5 ± 611.1	*<0.001*

BMI, body mass index; HELLP syndrome, syndrome of hemolysis, elevated liver enzymes, and low platelet count.

instructions. Briefly, total blood was lysed using proteinase K, and nucleic acids were precipitated by ethanol. DNA was digested with RNase-free DNase I for 15 min at room temperature. Total RNA was eluted and incubated at 65°C for 5 min before being stored at -80°C.

Total RNA from placental biopsies was extracted using the RNeasy Mini Kit according to the procedure recommended by the manufacturer (Qiagen). After dissolution of placental tissue in RLT buffer with (RLT)-β-mercapto-ethanol, nucleic acids were precipitated with ethanol. DNA digestion was performed with RNase-free DNase I for 15 min at room temperature. Total RNA was eluted and stored at −80°C.

The quality and quantity of extracted RNA were evaluated using the Bioanalyzer 2100 (Agilent Technologies) and a NanoDrop Spectrophotometer (Nanodrop Technologies).

RNA-sequencing and data processing

Reads were aligned and quantified using STAR (https://doi.org/10.1093/bioinformatics/bts635) on the hg19 genome assembly with GENCODE v19 annotations. The raw gene count table was variance-stabilized and reduced into principal components and uniform manifold approximation and projection (UMAP) for quality control. The raw count table was also used to perform differential expression analysis (DEA) using the Deseq2 framework (17), with apeglm shrinkage applied to the $\log_2$ fold change (18). Individual DEA results were compiled into integration plots, retaining genes that were significant in at least one design based on a Benjamini–Hochberg adjusted p-value <0.05 in at least one design. Data from RNASeq data analysis were submitted on the GEO data collection (GSE262147). Gene expression changes (up- or downregulation) were evaluated relative to control samples.

Quantitative reverse transcription-polymerase chain reaction

Reverse transcription of isolated RNA was performed using the Moloney murine leukemia virus reverse transcriptase kit (Life Technologies) and oligo(dT) primers. Gene expression was evaluated using real-time qPCR with the Smart SYBR Green Fast Master Kit (Roche Diagnostics) and specific primers (Supplementary Table S1). qPCRs reactions were performed using a CFX Touch Real-Time PCR Detection System (Bio-Rad). Results were normalized to the expression of the *ACTB* housekeeping gene and are expressed as relative quantity (RQ) using the $2^{-\Delta Ct}$ with $\Delta Ct = Ct_{Target} - Ct_{ACTB}$ as previously described (19).

Immunoassays

FLT1 (fms related receptor tyrosine kinase 1) and DUSP1 (Dual Specificity Phosphatase 1) levels were quantified in serum from study population with appropriate ELISA (enzyme-linked immunosorbent assay) according to the manufacturer's instructions (Antibodies). The sensitivity was 6.99 pg/ml for FLT1 and 9.4 pg/ml for DUSP1.

Protein interactome

The protein interactome between DUSP1 and FLT1 was generated using the STRING functional association networks protein software.

Statistical analysis

Descriptive statistics of the initial characteristics of the population were carried out using R software version 3.6.1. Quantitative variables were described using the mean and standard error of the mean (SEM). Qualitative variables were described using percentages and p-values. Categorical variables were compared using the Chi-square test or Fisher's exact test, as appropriate. The alpha risk was defined at 5%. Statistical analysis of gene signatures was performed using GraphPad Prism 6 (Graphpad Software Inc.). Gene expression was analyzed using the one-way ANOVA (analysis of variance) test and Tukey's multiple comparisons test. Values represent the mean ± SEM. The limit of significance was set at $p<0.05$.

Results

Study design

We conducted a prospective, longitudinal study to investigate novel biomarkers for PE diagnosis. Ten patients with PE were included during the study period at a university medical center. Ten pregnant women with normal pregnancies and no significant medical history were matched as controls to the PE patients based on maternal age and gestational age at the time of PE diagnosis.

The study design is shown in Supplementary Figure S1. Whole blood and serum samples were collected at the time of the first PE event (V1), and the same types of samples were collected after remote delivery (30 to 60 postpartum days, V2). These two samples enabled the investigation of PE markers found in V1 but absent in V2. To confirm that these biomarkers were associated with PE, placental biopsies collected after delivery were also analyzed (J0).

We first focused on the study population at the time of inclusion. As illustrated in Table 1, maternal age (years) at diagnosis was comparable between cases and controls, 31 ± 7.43 and 29.5 ± 4.45, respectively ($p=0.54$). Gestational age (weeks) at diagnosis showed no significant difference between the two groups: 29.54 ± 3.13 in PE and 31.38 ± 4.30 in controls ($p=0.29$). No significant differences were observed for body mass index and smoking.

Considering pregnancy outcomes in the two groups (Table 1), as expected, gestational age at delivery was significantly earlier in the PE group (30.07 ± 3.12) than in the control group (39.52 ± 1.13) ($p<0.001$). The time between inclusion and delivery (days) was significantly shorter in the PE group (3.3 ± 3.05) than in the control group (61.6 ± 31.25) ($p<0.001$). Patients with PE delivered by cesarean section in 100% of cases, compared to 20% in the control group ($p = 0.0007$). Serious maternal complications were observed in the PE group, such as uncontrolled hypertension (30%), heavy proteinuria (20%), acute renal failure (10%), and HELLP syndrome (20%). However, no significant differences were observed between the two groups ($p = 0.0867$).

Similarly, there were also significant differences in neonatal outcomes. Neonatal weight (g) was significantly lower in the PE group (1,203.5 ± 611.1) than in the control group (3,174.4 ± 28) ($p<0.001$). Neonatal complications were significantly increased in the PE group (80% vs. 20%, $p=0.02$). In our cohort, they mainly consisted of severe sepsis (40%) and respiratory distress (30%), as well as one case of neonatal death.

Preeclampsia RNA profile

After raw data normalization, differences between samples from pregnant women with PE and healthy donors were visualized in Figure 1. The hierarchical clustering heatmap showed that placental samples clustered separately from whole blood samples (Figure 1A). RNA-seq analysis revealed 23,919 differentially expressed genes (fold change >2 and false discovery rate (FDR) < 0.05) with sufficient variance for statistical analysis using DESeq2, as illustrated in the volcano plot (Figure 1B). Principal component analysis demonstrated contrasts among the two investigated groups regarding the sample type (Figure 1C) but not by study group (PE vs. control) (Figure 1D). When the sample type variable was excluded, no clear grouping emerged by study group among individuals (Figures 1E, F).

We next investigated gene modulation between PE and control groups at each of the three time points: V1, BP, and V2. Differential expression analysis was adjusted for time as a covariate. After filtering for variance and significance ($p<0.05$), 300 genes were identified as significantly modulated based on Benjamini–Hochberg adjusted p-value <0.05 in at least one comparison. When focusing on the model adjusted for time, 27% of these genes (81) were upregulated and 20% (61) were downregulated (Figure 2A). Notably, at the time of first inclusion (V1), corresponding to the initial PE event, 108 genes were found to be upregulated in whole blood samples from the PE group compared to controls (Figure 2B). A similarly high number of upregulated genes was observed in the transcriptional signature of placental biopsies (Figure 2D). In contrast, at V2—corresponding to the postpartum sample—upregulated and downregulated gene counts were more balanced. The aim of this study was to determine relevant biomarkers that might reflect the pathophysiological mechanisms underlying PE. We therefore focused on genes that were up- or down-regulated in whole blood at V1, absent at V2, and concurrently expressed in placenta samples from PE patients but not controls. Under these conditions, 25 genes were identified as a specific PE signature, as shown in the hierarchical clustering (Figure 3A) and volcano plot (Figure 3B).

Gene Ontology (GO) analysis of "Biological Process" terms revealed five GO clusters. In decreasing order, 30.8% of genes were associated with "angiogenesis and differentiation," 26.9% with "cell cycle," 19.2% with "cell adhesion," 15.4% with "cellular metabolism," and 7.7% with "inflammatory response" (Figure 3C and Supplementary Table S2).

Identification of a specific signature for preeclampsia

Genes identified were next evaluated using quantitative reverse transcription–polymerase chain reaction (qRT-PCR) (Figure 4). Among the genes associated with "cellular metabolism," only *A2M* showed a significant difference between V1 and V2 in the PE group ($p = 0.0236$) (Figure 4A). No significant differences were observed for *TCN2, SPAG6*, and *ADAMTS2*.

Within the "inflammatory response" cluster, only *TNFRSF21* was significantly increased at V1 in the PE group compared to the control group ($p<0.0001$), and a significant decrease was observed in the PE group between V1 and V2 ($p<0.0001$) (Figure 4B). No differences were found for *CD163*.

Among the four genes associated with the "cell adhesion" cluster (*ITGA2B*, *THBS1*, *EPCAM*, *SDK1*), two (*THBS1* and *SDK1*) were differentially modulated between the PE and control groups (Figure 4C). *THBS1* was significantly increased in the PE group at the placental level ($p=0.0073$), although no statistical difference was observed at the blood level. *SDK1* was significantly increased at V1 in PE compared to the control group ($p=0.0099$), and showed a significant decrease between V1 and V2 in the PE group ($p=0.0267$) (Figure 4C).

Among the seven genes associated with the "cell cycle" cluster (*BIN2*, *PER1*, *MIR25*, *IRS2*, *ESRG*, *STAG3*, *GPER1*), three were differentially modulated between the PE and control groups (Figure 4D). In whole blood, *MIR25* was significantly increased at V1 in PE compared to the control group ($p = 0.0012$) and for the PE group, a significant decrease was observed between V1 and V2 ($p=0.044$) (Figure 4D). At the placental level, *ESRG* and *GPER1* were significantly increased in the PE group compared to the control ($p<0.0001$ and $p=0.0017$, respectively).

Finally, we identified eight modulated genes associated with the "angiogenesis and differentiation" cluster (*GRB10, FN1, FLT1, DUSP1, NRP1, ANG, ARMC12, FSTL1*) (Figure 4E). Among them, six genes were found differentially modulated between the investigated groups (*FN1, FLT1, ANG, GRB10, FSTL1, DUSP1*). *FN1* and *ANG* were significantly increased in placental biopsies from PE patients compared to controls ($p=0.0007$ and $p<0.0001$, respectively). *FSLT1* and *GRB10* were significantly increased at V1 in PE compared to the control group ($p=0.0007$ and $p<0.0001$, respectively), and both showed significant decreases between V1 and V2 in the PE group ($p<0.0001$ and $p=0.007$, respectively). Interestingly, *FLT1*, a well-established biomarker in PE (13), also showed consistent modulation in our study. *FLT1* was significantly increased at V1 in the PE group compared to the control group ($p<0.0001$) and significantly decreased at V2 in the PE group compared to V1 ($p<0.0001$). At the placental level, FLT1 was also significantly overexpressed in PE patients compared to controls ($p<0.0001$), further confirming its relevance in PE pathophysiology (13, 20–22)Among all the investigated genes, *DUSP1* showed the same state of significant expression modulation as *FLT1*: (1) significantly increased at V1 in PE compared to controls ($p=0.0185$); (2) significantly decreased at V2 in PE compared to V1 ($p=0.0011$); and (3) significantly increased at the placental level in PE compared to controls ($p = 0.0006$). Taken together, our findings highlight *DUSP1* as a promising gene of interest in PE.

DUSP1 modulation in preeclampsia

We next evaluated levels of DUSP1 in serum samples using immunoassays. As illustrated in Figure 5A, DUSP1 was barely

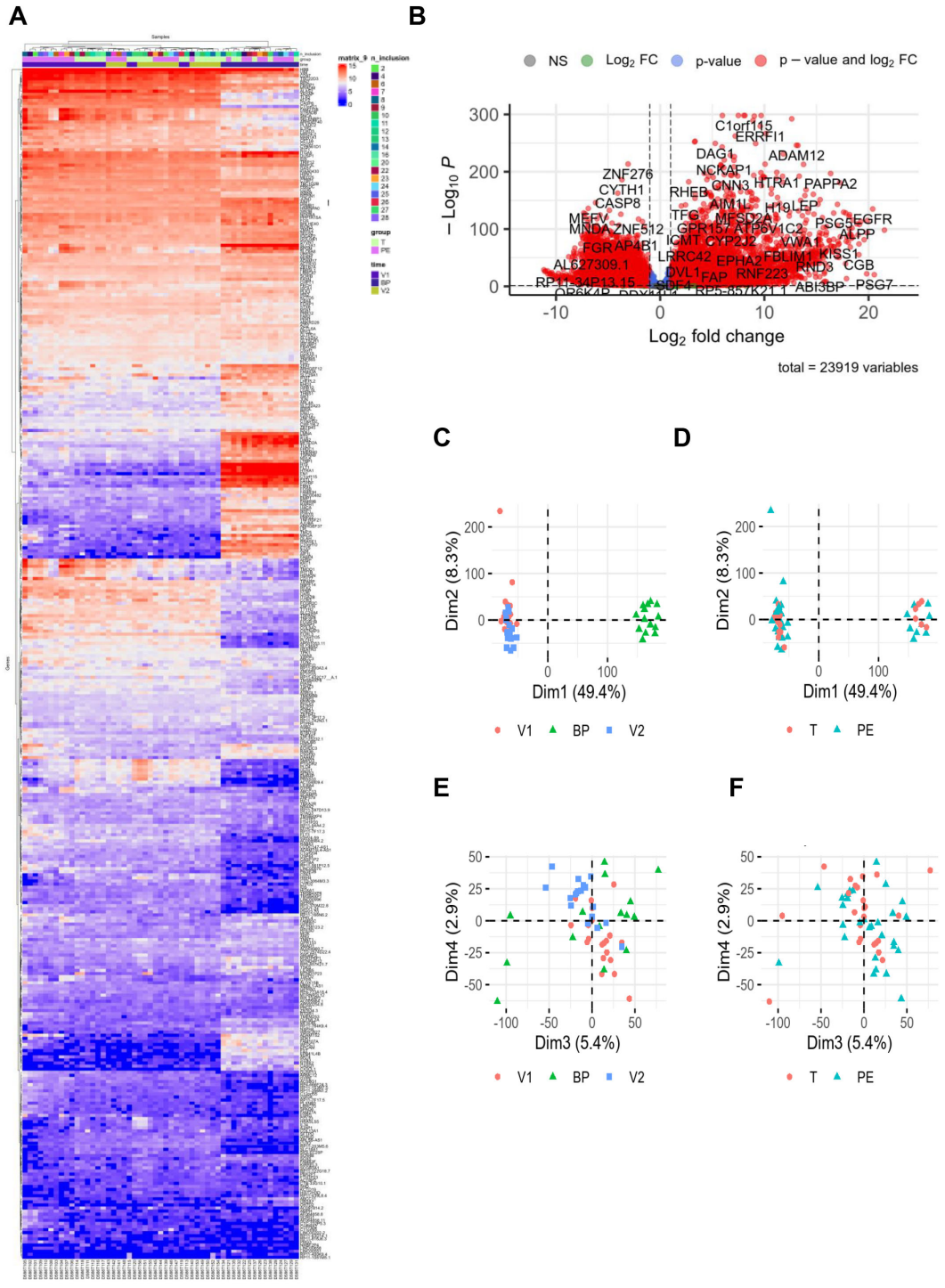

FIGURE 1
RNAseq data. RNA sequencing was performed with 24 healthy controls (C, 10V1, 8V2, 6BP) and 29 preeclamptic women (PE, 10V1, 10V2, 9BP). **(A)** Hierarchical clustering and **(B)** volcano plot highlighted modulated genes from RNA-seq data analysis, revealing 23,919 differentially expressed genes (fold change >2 and false discovery rate [FDR] <0.05). For the hierarchical clustering, "n_inclusions" corresponds to the number assigned to included patients in the cohort. The groups are T = control (light green square) and PE = preeclampsia (pink square). "Time" corresponds to the three types of sampling: V1 = first blood sampling (purple square), BP = placental biopsy performed on the day of delivery (dark blue square), and V2 = *post-partum* blood sampling (green square). **(C–F)** Principal component analysis illustrated the distribution of the investigated groups (V1, BP, and V2). BP, biopsy from placenta; FC, fold change; T, control group.

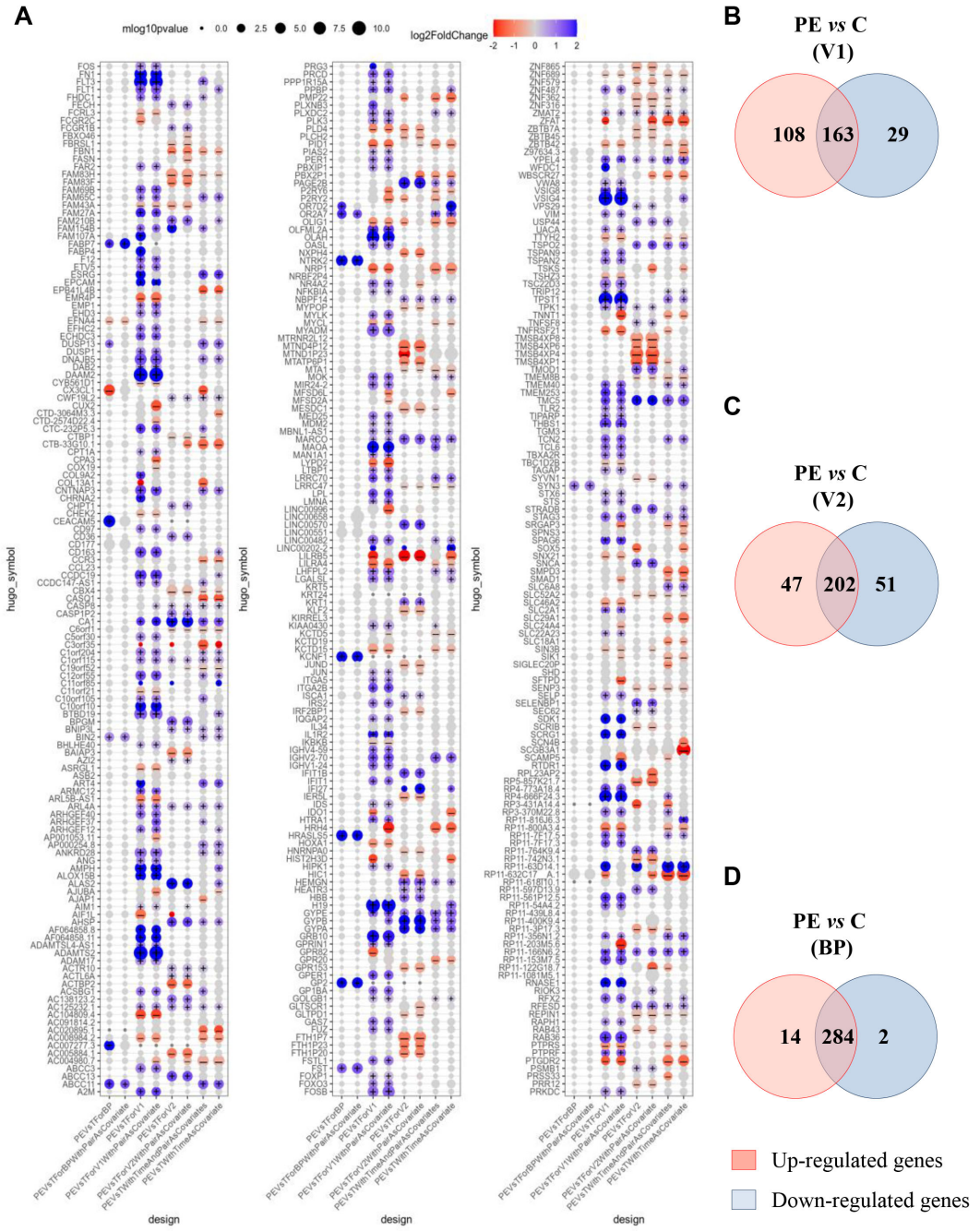

FIGURE 2
Modulated genes associated with preeclampsia. **(A)** Clusters show 300 modulated genes obtained after adjustment and selection based on variance and p<0.05, according to the Benjamini–Hochberg method. **(B–D)** Venn diagrams illustrated up- and down-modulated genes in preeclampsia (PE) *versus* control group for **(B)** V1, **(C)** V2 and **(D)**. BP, biopsy from placenta. Each intersection shows the number of genes that are neither up- nor down-regulated. (+) and (–) indicate p-value <0.05 and absolute value of log2FoldChange > 0.1.

detected in healthy donor serum during pregnancy (V1) or postpartum (V2). Interestingly, pregnant women with PE showed significantly higher concentrations of DUSP1 at V1 compared to controls (*p<0.0001*), suggesting that DUSP1 could be an interesting biomarker. Focusing on the PE group, we found that DUSP1 levels decreased after childbirth; at V2, levels were similar to those observed in the control group (*p<0.0001*). A similar modulation pattern was observed for FLT1 concentrations, which were significantly elevated in PE donors compared to healthy donors at V1, then decreased at V2 (p<0.0001) for all comparisons.

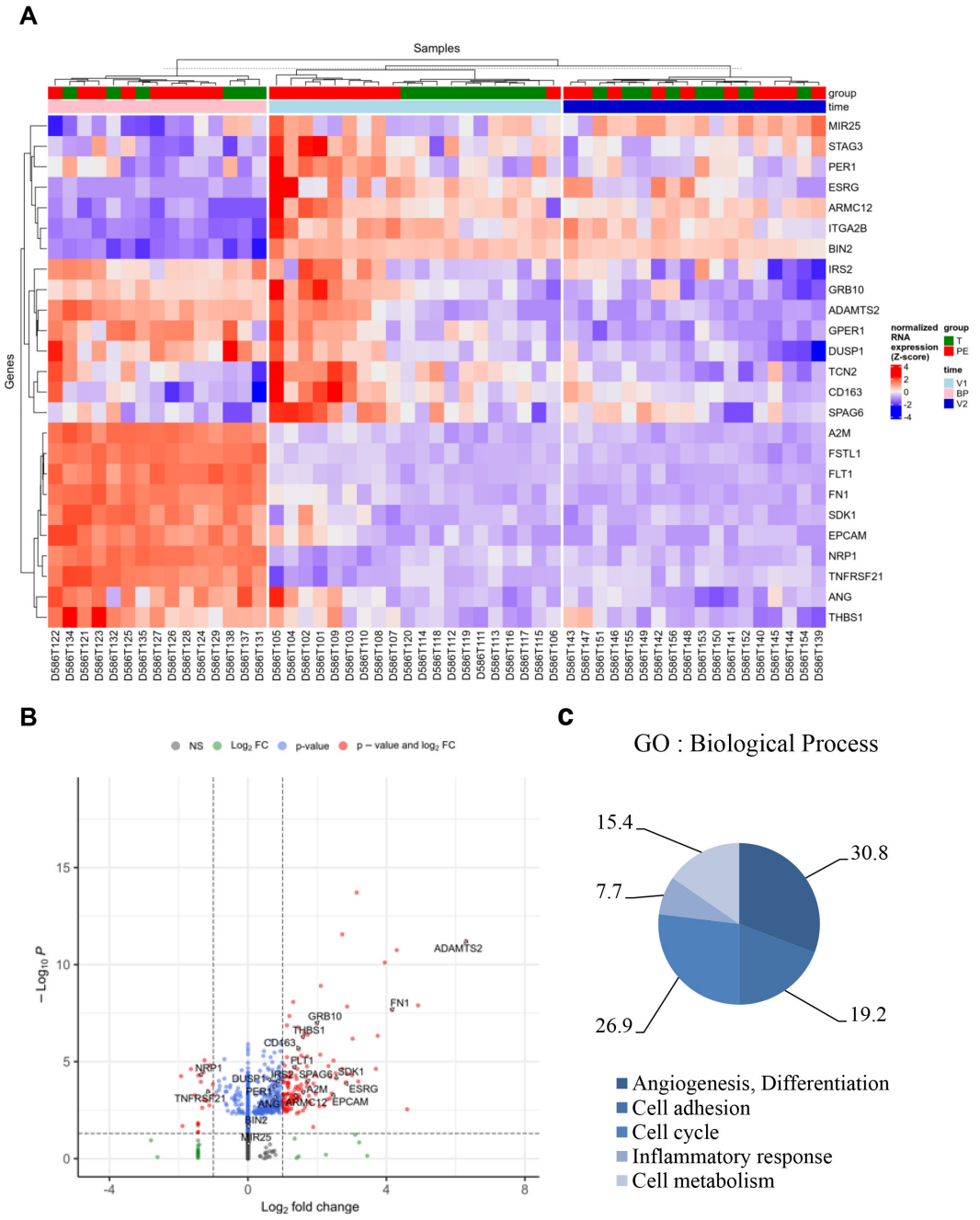

FIGURE 3
Specific genes associated with preeclampsia. Based on the selection of 300 genes modulated in V1, absent in V2, and present in the placental biopsy (BP) for the PE group compared to the control (T) group, 25 genes were identified as a specific signature of PE. **(A)** Hierarchical clustering and **(B)** volcano plot illustrated the 25 modulated genes. **(C)** Graph illustrating the Gene Ontology (GO) analysis based on "Biological Process," including the percentage of genes associated with "angiogenesis and differentiation," "cell cycle," "cell adhesion," "inflammatory response," and "cellular metabolism." FC, fold change.

To further investigate molecular signature changes involving *DUSP1* and their potential role in PE pathophysiology, we performed a protein pathway analysis (Figure 5B). This analysis identified 12 proteins associated with DUSP1. Among them, FLT1 was found, suggesting shared signaling pathways that may explain their similar expression profiles. There were also proteins associated with VEGF (vascular endothelial growth factor) and PGF (placental growth factor), which have previously been described as associated

10.3389/fendo.2025.1576240

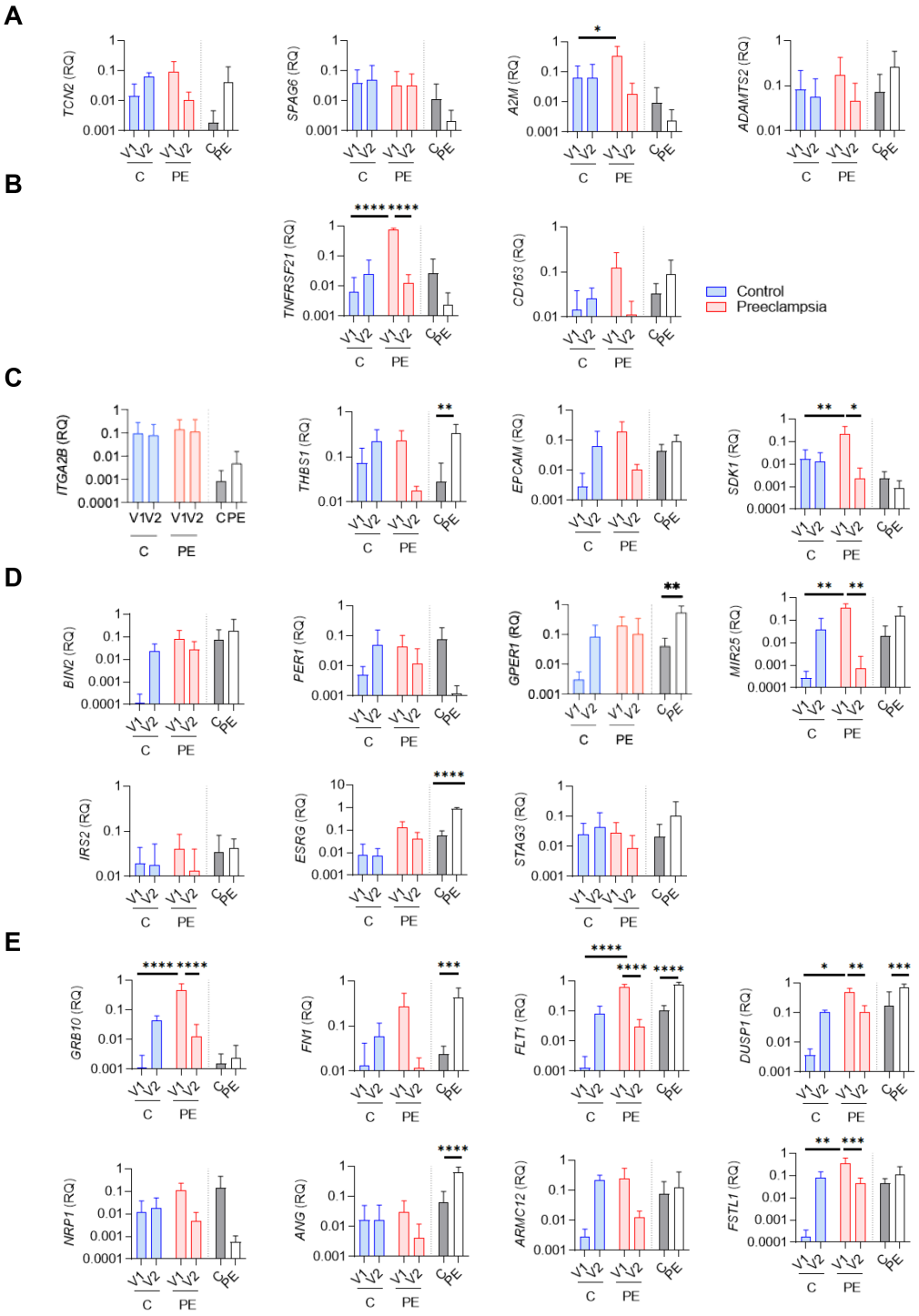

FIGURE 4
qRTPCR evaluation of specific genes associated with preeclampsia. Relative quantity evaluation of genes involved in **(A)** "cellular metabolism," **(B)** "inflammatory response," **(C)** "cell adhesion," **(D)** "cell cycle," and **(E)** "angiogenesis and differentiation" pathways. Modulated genes were obtained after qRTPCR experiments using whole blood (V1, V2) and biopsy from placenta (BP) from six healthy controls **(C)** and six preeclamptic women (PE), shown with gray and white bars, respectively. Data values represent the mean ± standard error of the mean (SEM); experiments were carried out in triplicate. Statistical analysis was performed with one-way ANOVA (analysis of variance) and Tukey's multiple comparison test. *$p \leq 0.05$, **$p \leq 0.01$, ***$p \leq 0.001$ and ****$p \leq 0.0001$.

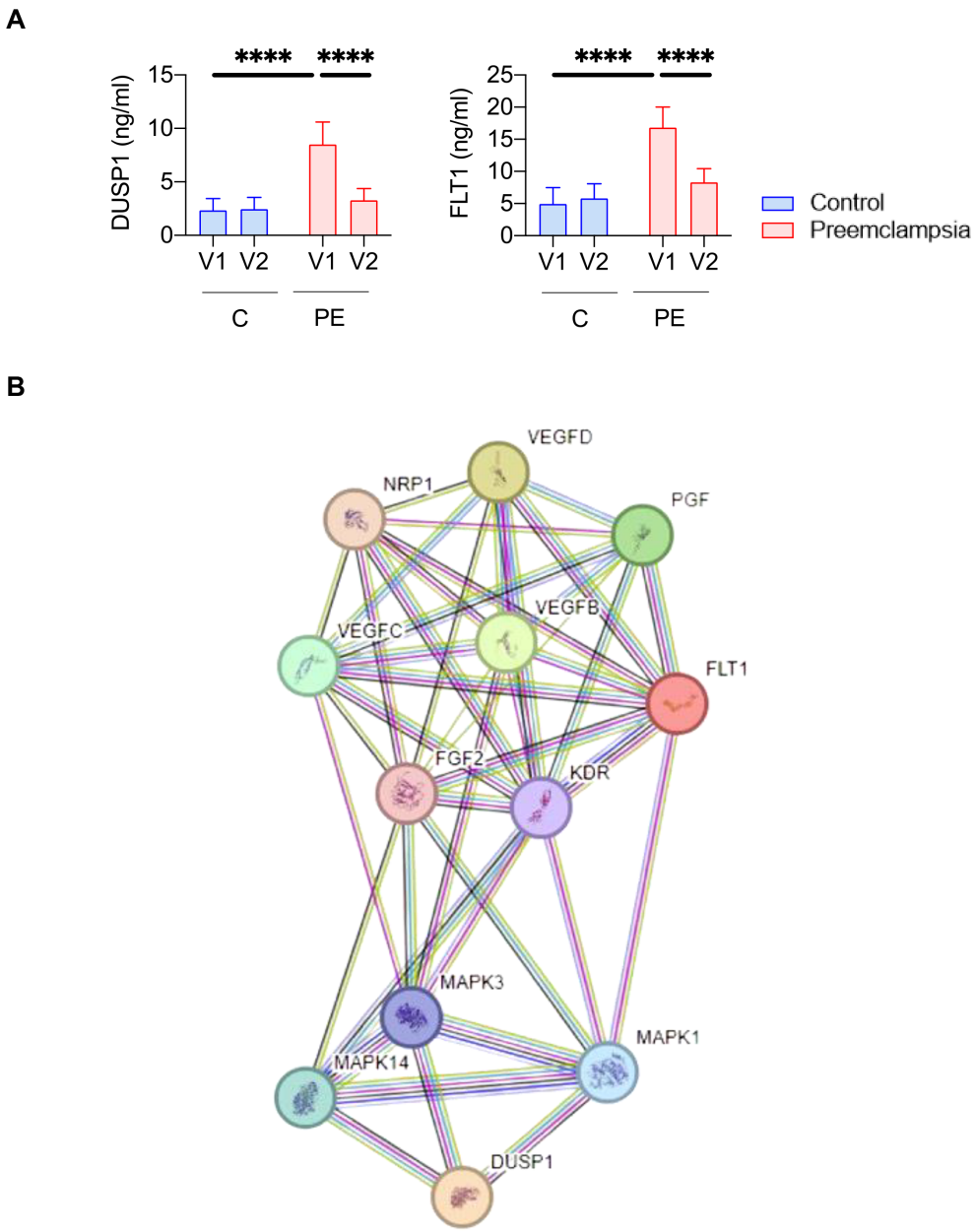

FIGURE 5
DUSP1 represents a biomarker candidate of preeclampsia. **(A)** Quantification of DUSP1 and FLT1 protein levels by immunoassay in serum samples (V1 and V2) from nine controls (C) and nine preeclamptic women (PE). Statistical analysis was performed using one-way ANOVA (analysis of variance) and Tukey's multiple comparisons test. ****$p \leq 0.0001$.. **(B)** Protein pathways linked to DUSP1.

with PE pathophysiology (13)Taken together, these results highlight DUSP1 as a promising blood-based biomarker candidate for the diagnosis of PE in pregnant women.

Discussion

The clinical diagnosis of PE remains challenging and is often delayed due to the lack of reliable early biomarkers. Although studies have used large biobanks and cohorts, the identification of efficient biomarkers for early PE diagnosis is still warranted. In this study, we adopted a specific study design strategy to investigate new candidate biomarkers by evaluating gene expression at both the blood and placental levels in women with PE—specifically focusing on genes not expressed postpartum, at a distance from delivery. Our study highlights DUSP1 as a promising non-invasive blood biomarker candidate for PE.

Current screening tools are essentially in the form of diagnostic trees combining several risk factors for PE to predict its occurrence in the short term. They combine several early markers: clinical (mean blood pressure), ultrasound (pulsatility index of uterine arteries) and biological (PAPP-A and PlGF), allowing to predict

the risk of PE before term—with a false-positive rate of approximately 10%–15% (23, 24). Recent data from literature has opened new avenues through molecular approaches, particularly by exploring gene expression in this pathology (25–27). However, many studies focus on the investigation of genes on samples, at the blood or placenta level, only at the time of diagnosis. The strength of our study was primarily its prospective design, which contributed to its robustness. Controls were rigorously matched to patients with PE based on two major confounding factors: maternal age and gestational age at diagnosis. The two groups (PE and control) were comparable across all baseline characteristics, thereby addressing potential confounding bias. Another strength of our study is its transversality, as patients in each group were followed from the first clinical manifestations of PE through to the postnatal period. Each patient was evaluated at the three major stages of the disease: diagnosis (first symptoms), childbirth (signs of severity requiring fetal delivery and/or maternal intervention), and postpartum (remission). This transversality is a major asset, allowing us to follow the evolution of the PE transcriptional signature in parallel with the progression of the disease.

Our study highlighted a specific gene signature of PE. Among the modulated genes, the associated biological processes have previously been described in the pathophysiology of PE (28, 29). Interestingly, we also identified the *FLT1* gene, whose role as a biomarker in PE is well documented (12, 30). The presence of this gene indicates that the cohort choice and design strategy of the study is similar to previous studies. We showed that *FLT1* has the same significant expression modulation profile as *DUSP1*, with both genes returning to a physiological baseline after pregnancy. We also found that *FLT1* is part of the *DUSP1* pathway. Additional studies based on other cohorts should be carried out to define the relevance of DUSP1 and FLT1 in PE, either as individual biomarker candidates or as part of a combined signature.

Our study identified DUSP1 as a biomarker candidate for PE. DUSP1 belongs to a large superfamily of 30 types of DUSP involved in signal transduction pathways that inactivate mitogen-activated protein (MAP) kinases. Specifically, DUSP1 modulation affects several pathways, including MAP kinase phosphatase activity, tyrosine kinase receptor activity, angiogenesis, and cell–cell signaling (31). Its role in tumor biology is well documented (32).

Interestingly, several studies have also highlighted the relationship between DUSP1 and hypoxia, a major contributor to the placental abnormalities observed in women with PE. Hypoxic conditions lead to *DUSP1* overexpression and increased interaction with hypoxia-inducible factor 1-alpha (HIF-1α), a molecule (33) involved in PE pathogenesis (34, 35). DUSP1 has also been identified as a contributing gene in cases of recurrent miscarriage (36, 37). DUSP1 expression abnormalities in primary human decidual stromal cells or decidua tissue have been linked to the pathophysiology of recurrent miscarriages. Further studies are needed to highlight the mechanism of action of DUSP1 in PE.

Previous studies have investigated DUSP1 as a potential biomarker for the identification of PE (38). The authors investigated *DUSP1* expression in placental tissue and umbilical cord blood. The authors reported conflicting data regarding DUSP1 expression in placental tissue: DUSP1 mRNA expression in the PE group was significantly lower than in the healthy group, whereas protein levels assessed by immunohistochemistry were similar between PE and control groups. Considering DUSP1 as a biomarker, the authors investigated DUSP1 protein levels in umbilical cord blood and found significantly lower DUSP1 expression in PE women compared to healthy donors. Moreover, the authors used a limited cohort (400 controls *versus* 5 PE samples) and did not investigate the gestational age at diagnosis that constitutes a major confounding factor associated with potential confusion bias. In contrast, Yonghong Wang et al. reported an indirect role for DUSP1 in the occurrence of PE (39). The authors reported that miR-141-5p reduced DUSP1 expression *in vitro*, thereby affecting the MAPK/ERK pathway and promoting PE features. Although further studies are needed to identify the role of DUSP1 in PE, this study demonstrated DUSP1 expression in immortalized JEG-3 trophoblastic cells (39), whose role in pregnancy and involvement in PE pathogenesis still need to be defined.

In our prospective study, healthy donors were matched with PE patients based on the two main factors: maternal age and gestational age at diagnosis. To prevent any potential bias, both groups were comparable in all baseline characteristics. From the earliest clinical signs of PE through the postpartum period, patients in each group were monitored. As a result, each patient contributed samples at the three major stages of the disease: diagnosis (first symptoms), delivery (severe signs indicating the need for fetal birth and/or maternal rescue), and postpartum (remission). This transversality is a key advantage for tracking the evolution of the PE transcriptional signature in relation to disease progression.

Our study is limited by the size of the cohort. Validation of DUSP1 as a biomarker candidate for PE should be conducted in larger, multicenter cohorts.

In conclusion, based on an original study design, we report a set of genes associated with PE, some of which have been previously linked to the pathophysiology of the disease. Further investigation of DUSP1 in a larger cohort—both before and after the onset of PE, and including assessments of disease severity—is necessary to confirm its value as a biomarker. The RANSPre study, a French multicenter cohort, may provide an alternative strategy to evaluate this candidate further.

Data availability statement

The datasets presented in this study can be found in online repositories. The names of the repository/repositories and accession number(s) can be found in the article/Supplementary Material.

Ethics statement

The studies involving humans were approved by CPP Sud Mediterranean 1" n° 2010-A00633-36. The studies were conducted in accordance with the local legislation and institutional requirements. The participants provided their written informed consent to participate in this study.

Author contributions

JA: Investigation, Methodology, Visualization, Writing – review & editing. AD: Data curation, Investigation, Methodology, Validation, Visualization, Writing – original draft. J-FC: Conceptualization, Investigation, Validation, Visualization, Writing – review & editing. GC: Methodology, Software, Validation, Visualization, Writing – review & editing. NR: Methodology, Validation, Visualization, Writing – review & editing. JP: Validation, Visualization, Writing – review & editing. J-LM: Supervision, Validation, Visualization, Writing – review & editing. SM: Investigation, Methodology, Project administration, Supervision, Validation, Visualization, Writing – original draft, Writing – review & editing. FB: Conceptualization, Funding acquisition, Validation, Visualization, Writing – review & editing.

Funding

The author(s) declare financial support was received for the research and/or publication of this article. This work was supported by the French government under the Investissements d'avenir (Investments for the Future) program managed by the Agence Nationale de la Recherche (reference number 10-IAHU-03). This work was supported by the "Comité" 10–28 project managed by the "Assistance Publique Hopitaux de Marseille" (reference ID RCB 2012-A00633-36).

Conflict of interest

The authors declare that the research was conducted in the absence of any commercial or financial relationships that could be construed as a potential conflict of interest.

Generative AI statement

The author(s) declare that no Generative AI was used in the creation of this manuscript.

Any alternative text (alt text) provided alongside figures in this article has been generated by Frontiers with the support of artificial intelligence and reasonable efforts have been made to ensure accuracy, including review by the authors wherever possible. If you identify any issues, please contact us.

Publisher's note

Supplementary material

The Supplementary Material for this article can be found online at: https://www.frontiersin.org/articles/10.3389/fendo.2025.1576240/full#supplementary-material

SUPPLEMENTARY FIGURE 1
Study design. Samples from included patients were taken at three major time points: at the diagnosis of preeclampsia (PE) (V1, first symptoms), at childbirth (biopsy from placenta (BP), signs of severity indicating fetal birth and/or maternal rescue), and postpartum (V2, remission). V1 and V2 correspond to whole blood and serum samples; BP corresponds to placental biopsy samples. Total RNA was isolated and analyzed using RNA sequencing(10 samples from PE and control groups). qRTPCR (6 samples from PE and control (C) groups) and ELISA (9 samples from PE and control groups) were performed on isolated RNA and serum samples, respectively. Abbreviations: RNAseq, RNA sequencing; qRT-PCR, quantitative reverse transcription-polymerase chain reaction; ELISA, enzyme-linked immunosorbent assay.

SUPPLEMENTARY TABLE 1
List of primers used for qRTPCR.

SUPPLEMENTARY TABLE 2
List of genes associated with the preeclampsia signature.

References

1. Dimitriadis E, Rolnik DL, Zhou W, Estrada-Gutierrez G, Koga K, Francisco RPV, et al. Pre-eclampsia. *Nat Rev Dis Primer*. (2023) 9:1–22. doi: 10.1038/s41572-023-00417-6

2. Chappell LC, Cluver CA, Kingdom J, Tong S. Pre-eclampsia. *Lancet*. (2021) 398:341–54. doi: 10.1016/S0140-6736(20)32335-7

3. Ives CW, Sinkey R, Rajapreyar I, Tita ATN, Oparil S. Preeclampsia—Pathophysiology and clinical presentations: JACC state-of-the-art review. *J Am Coll Cardiol*. (2020) 76:1690–702. doi: 10.1016/j.jacc.2020.08.014

4. Tita AT, Szychowski JM, Boggess K, Dugoff L, Sibai B, Lawrence K, et al. & Chronic hypertension and pregnancy (CHAP) trial consortium. Treatment for mild chronic hypertension during pregnancy. *N Engl J Med*. (2022) 386:1781–92. doi: 10.1056/NEJMoa2201295

5. Chappell LC, Brocklehurst P, Green ME, Hunter R, Hardy P, Juszczak E, et al. Planned early delivery or expectant management for late preterm pre-eclampsia (PHOENIX): a randomised controlled trial. *Lancet Lond Engl*. (2019) 394:1181–90. doi: 10.1016/S0140-6736(19)31963-4

6. Say L, Chou D, Gemmill A, Tunçalp Ö, Moller A-B, Daniels J, et al. Global causes of maternal death: a WHO systematic analysis. *Lancet Glob Health*. (2014) 2:e323–33. doi: 10.1016/S2214-109X(14)70227-X

7. Redman CWG, Staff AC, Roberts JM. Syncytiotrophoblast stress in preeclampsia: the convergence point for multiple pathways. *Am J Obstet Gynecol*. (2022) 226:S907–27. doi: 10.1016/j.ajog.2020.09.047

8. Zhang R, Jia L, Meng L, Peng H, Zhang D, He Q, et al. PD-L1 enhances migration and invasion of trophoblasts by upregulating ARHGDIB via transcription factor PU.1. *Cell Death Discov*. (2022) 8:1–10. doi: 10.1038/s41420-022-01171-6

9. Yin W, Romeo S, Chang S, Grishin NV, Hobbs HH, Cohen JC. Genetic variation in ANGPTL4 provides insights into protein processing and function *. *J Biol Chem*. (2009) 284:13213–22. doi: 10.1074/jbc.M900553200

10. Meinhardt G, Haider S, Kunihs V, Saleh L, Pollheimer J, Fiala C, et al. Pivotal role of the transcriptional co-activator YAP in trophoblast stemness of the developing human placenta. *Proc Natl Acad Sci*. (2020) 117:13562–70. doi: 10.1073/pnas.2002630117

11. MacDonald TM, Walker SP, Hannan NJ, Tong S, Kaitu'u-Lino TJ. Clinical tools and biomarkers to predict preeclampsia. *EBioMedicine*. (2021) 75:103780. doi: 10.1016/j.ebiom.2021.103780

12. Verlohren S, Brennecke SP, Galindo A, Karumanchi SA, Mirkovic LB, Schlembach D, et al. Clinical interpretation and implementation of the sFlt-1/PlGF ratio in the prediction, diagnosis and management of preeclampsia. *Pregnancy Hypertens*. (2022) 27:42–50. doi: 10.1016/j.preghy.2021.12.003

13. Zeisler H, Llurba E, Chantraine F, Vatish M, Staff AC, Sennström M, et al. Predictive value of the sFlt-1:PlGF ratio in women with suspected preeclampsia. *N Engl J Med*. (2016) 374:13–22. doi: 10.1056/NEJMoa1414838

14. Jain V, Bujold E. Screening for preeclampsia risk and prophylaxis with acetylsalicylic acid. *CMAJ Can Med Assoc J J Assoc Medicale Can*. (2023) 195:E1557–8. doi: 10.1503/cmaj.230620

15. Rolnik DL, Wright D, Poon LCY, Syngelaki A, O'Gorman N, De Paco Matallana C, et al. ASPRE trial: performance of screening for preterm pre-eclampsia. *Ultrasound Obstet Gynecol*. (2017) 50:492–5. doi: 10.1002/uog.18816

16. Rolnik DL, Wright D, Poon LC, O'Gorman N, Syngelaki A, de Paco Matallana C, et al. Aspirin versus Placebo in Pregnancies at High Risk for Preterm Preeclampsia. *N Engl J Med*. (2017) 377:613–22. doi: 10.1056/NEJMoa1704559

17. Love MI, Huber W, Anders S. Moderated estimation of fold change and dispersion for RNA-seq data with DESeq2. *Genome Biol*. (2014) 15:550. doi: 10.1186/s13059-014-0550-8

18. Zhu A, Ibrahim JG, Love MI. Heavy-tailed prior distributions for sequence count data: removing the noise and preserving large differences. *Bioinformatics*. (2019) 35:2084–92. doi: 10.1093/bioinformatics/bty895

19. Mezouar S, Benammar I, Boumaza A, Diallo AB, Chartier C, Buffat C, et al. Full-term human placental macrophages eliminate *Coxiella burnetii* through an IFN-γ autocrine loop. *Front Microbiol*. (2019) 10:2434. doi: 10.3389/fmicb.2019.02434

20. Luttun A, Carmeliet P. Soluble VEGF receptor Flt1: the elusive preeclampsia factor discovered? *J Clin Invest*. (2003) 111:600–2. doi: 10.1172/JCI18015

21. Austdal M, Silva GB, Bowe S, Thomsen LCV, Tangerås LH, Bjørge L, et al. Metabolomics identifies placental dysfunction and confirms flt-1 (FMS-like tyrosine kinase receptor 1) biomarker specificity. *Hypertension*. (2019) 74:1136–43. doi: 10.1161/HYPERTENSIONAHA.119.13184

22. Maynard SE, Min J-Y, Merchan J, Lim K-H, Li J, Mondal S, et al. Excess placental soluble fms-like tyrosine kinase 1 (sFlt1) may contribute to endothelial dysfunction, hypertension, and proteinuria in preeclampsia. *J Clin Invest*. (2003) 111:649–58. doi: 10.1172/JCI17189

23. O'Gorman N, Wright D, Syngelaki A, Akolekar R, Wright A, Poon LC, et al. Competing risks model in screening for preeclampsia by maternal factors and biomarkers at 11–13 weeks gestation. *Am J Obstet Gynecol*. (2016) 214:103.e1–103.e12. doi: 10.1016/j.ajog.2015.08.034

24. Chappell LC, Duckworth S, Seed PT, Griffin M, Myers J, Mackillop L, et al. Diagnostic accuracy of placental growth factor in women with suspected preeclampsia: a prospective multicenter study. *Circulation*. (2013) 128:2121–31. doi: 10.1161/CIRCULATIONAHA.113.003215

25. Enquobahrie DA, Meller M, Rice K, Psaty BM, Siscovick DS, Williams MA. Differential placental gene expression in preeclampsia. *Am J Obstet Gynecol*. (2008) 199:566.e1–11. doi: 10.1016/j.ajog.2008.04.020

26. Okazaki S, Sekizawa A, Purwosunu Y, Farina A, Wibowo N, Okai T. Placenta-derived, cellular messenger RNA expression in the maternal blood of preeclamptic women. *Obstet Gynecol*. (2007) 110:1130–6. doi: 10.1097/01.AOG.0000286761.11436.67

27. Textoris J, Ivorra D, Ben Amara A, Sabatier F, Ménard J-P, Heckenroth H, et al. Evaluation of current and new biomarkers in severe preeclampsia: A microarray approach reveals the VSIG4 gene as a potential blood biomarker. *PloS One*. (2013) 8:e82638. doi: 10.1371/journal.pone.0082638

28. Kondoh K, Akahori H, Muto Y, Terada T. Identification of key genes and pathways associated with preeclampsia by a WGCNA and an evolutionary approach. *Genes*. (2022) 13:2134. doi: 10.3390/genes13112134

29. Mohamad MA, Mohd Manzor NF, Zulkifli NF, Zainal N, Hayati AR. & Ahmad asnawi, A. W. A review of candidate genes and pathways in preeclampsia-an integrated bioinformatical analysis. *Biology*. (2020) 9:62. doi: 10.3390/biology9040062

30. Stepan H, Hund M, Andraczek T. Combining biomarkers to predict pregnancy complications and redefine preeclampsia: the angiogenic-placental syndrome. *Hypertens Dallas Tex*. (2020) 1979:75, 918–926. doi: 10.1161/HYPERTENSIONAHA.119.13763

31. Huang C-Y, Tan T-H. DUSPs, to MAP kinases and beyond. *Cell Biosci*. (2012) 2:24. doi: 10.1186/2045-3701-2-24

32. Shen J, Zhou S, Shi L, Liu X, Lin H, Yu H, et al. DUSP1 inhibits cell proliferation, metastasis and invasion and angiogenesis in gallbladder cancer. *Oncotarget*. (2017) 8:12133–44. doi: 10.18632/oncotarget.14815

33. Liu C, Shi Y, Du Y, Ning X, Liu N, Huang D, et al. Dual-specificity phosphatase DUSP1 protects overactivation of hypoxia-inducible factor 1 through inactivating ERK MAPK. *Exp Cell Res*. (2005) 309:410–8. doi: 10.1016/j.yexcr.2005.06.022

34. Tal R. The role of hypoxia and hypoxia-inducible factor-1alpha in preeclampsia pathogenesis. *Biol Reprod*. (2012) 87:134. doi: 10.1095/biolreprod.112.102723

35. Luo S, Cao N, Tang Y, Gu W. Identification of key microRNAs and genes in preeclampsia by bioinformatics analysis. *PloS One*. (2017) 12:e0178549. doi: 10.1371/journal.pone.0178549

36. Xu C, Zhao W, Huang X, Jiang Z, Liu L, Cui L, et al. TORC2/3-mediated DUSP1 upregulation is essential for human decidualization. *Reproduction*. (2021) 161:573–80. doi: 10.1530/REP-21-0036

37. Yang Y, Zhao A, Wang T, Tang Q, Qi S, Shi X, et al. Identification of driving genes of recurrent miscarriage based on transcriptome sequencing and immunoinfiltration analysis. *Int Immunopharmacol*. (2024) 143:113095. doi: 10.1016/j.intimp.2024.113095

38. Wang J, Zhou J-Y, Kho D, Reiners JJ, Wu GS. Role for DUSP1 (dual-specificity protein phosphatase 1) in the regulation of autophagy. *Autophagy*. (2016) 12:1791–803. doi: 10.1080/15548627.2016.1203483

39. Wang Y, Cheng K, Zhou W, Liu H, Yang T, Hou P, et al. miR-141-5p regulate ATF2 via effecting MAPK1/ERK2 signaling to promote preeclampsia. *Biomed Pharmacother*. (2019) 115:108953. doi: 10.1016/j.biopha.2019.108953

frontiers | Frontiers in Endocrinology

TYPE Original Research
PUBLISHED 02 October 2025
DOI 10.3389/fendo.2025.1674540

OPEN ACCESS

EDITED BY
Leonardo Ermini,
University of Siena, Italy

REVIEWED BY
Yunzhen Ye,
Fudan University, China
Haoyi Cui,
University of Southern California, United States

*CORRESPONDENCE
Jie Li
jie1967@126.com
Ya-Li Hu
yalihu@nju.edu.cn

†These authors have contributed equally to this work and share first authorship

RECEIVED 28 July 2025
ACCEPTED 22 September 2025
PUBLISHED 02 October 2025

CITATION
Li T-S, Wang Y, Wang Y, Tang H-R, Duan H-L, Zhao G-F, Li J and Hu Y-L (2025) Association of Placental Growth Factor with the risk of adverse pregnancy outcomes: a prospective cohort study in Chinese pregnant women. *Front. Endocrinol.* 16:1674540. doi: 10.3389/fendo.2025.1674540

Association of Placental Growth Factor with the risk of adverse pregnancy outcomes: a prospective cohort study in Chinese pregnant women

Tai-Shun Li[1,2†], Yuan Wang[1†], Ya Wang[1], Hui-Rong Tang[1], Hong-Lei Duan[1], Guang-Feng Zhao[1], Jie Li[1*] and Ya-Li Hu[1*]

[1]Department of Obstetrics and Gynecology, Nanjing Drum Tower Hospital, The Affiliated Hospital of Nanjing University Medical School, Nanjing, China, [2]Medical Statistics and Analysis Center, Nanjing Drum Tower Hospital, The Affiliated Hospital of Nanjing University Medical School, Nanjing, China

Background: Adverse pregnancy outcomes, such as preterm birth, preeclampsia (PE), small for gestational age (SGA), pose significant risks to maternal and neonatal health and contribute to healthcare burdens. Placental Growth Factor (PlGF), a key pro-angiogenic biomarker involved in placental development, has been implicated in the pathophysiology of these complications. This study aimed to investigate the association between maternal serum PlGF levels and adverse pregnancy outcomes in a prospective cohort.

Methods: We conducted a cohort study involving 5,870 women with singleton pregnancies enrolled at Nanjing Drum Tower Hospital from January 2017 to September 2020. Participants were followed from early pregnancy (≤14 gestational weeks) through delivery. Logistic regression models were used to evaluate the associations between serum PlGF levels (measured at 11–14 gestational weeks) and adverse pregnancy outcomes, reported as adjusted odds ratios (ORs) with 95% confidence intervals (CIs). Dose–response relationships were assessed using restricted cubic spline analysis.

Results: Serum PlGF concentrations in early pregnancy were inversely associated with PE (OR = 0.97, 95% CI:0.96 – 0.98), preterm PE (OR = 0.96, 0.94 – 0.98), SGA <10th percentile (OR = 0.99, 0.98 – 0.99) and SGA <3rd percentile (OR = 0.98, 0.97 – 0.99). Expressed as multiples of the median (MoM), PlGF showed stronger associations with these outcomes, including PE (OR = 0.32, 0.21 – 0.48), preterm PE (OR = 0.23, 0.09 – 0.56), SGA <10th percentile (OR = 0.67, 0.54 – 0.83) and SGA <3rd percentile (OR = 0.43, 0.29 – 0.64), compared with its absolute concentrations. Notably, PlGF demonstrated a consistent inverse association with PE across different modes of conception, including spontaneous pregnancies (OR = 0.97, 0.96 – 0.98) and those conceived via ovulation induction or *in vitro* fertilization (OR = 0.95, 0.92 – 0.97). The highest predictive performance for PE was observed between 28–34 gestational weeks, with an area under the curve (AUC) of 0.79 (95% CI: 0.77 – 0.81). Additionally, dose–response analysis revealed nonlinear associations between PlGF levels and risks of SGA <10th and SGA <3rd.

10.3389/fendo.2025.1674540

Conclusion: This cohort study reinforces the inverse association between maternal PIGF levels and the risks of PE and SGA. The findings highlight the potential clinical utility of PIGF as a gestational age–specific biomarker in prenatal risk stratification.

KEYWORDS

preeclampsia, small for gestational age, placental growth factor, cohort, adverse pregnancy outcomes

1 Introduction

Adverse pregnancy outcomes such as preeclampsia (PE), preterm birth, and small for gestational age (SGA) pose significant threats to maternal and neonatal health, and contribute to increased perinatal morbidity and mortality worldwide (1–4). Numerous maternal risk factors have been implicated, including advanced maternal age, elevated pre-pregnancy body mass index, chronic hypertension, renal dysfunction, and autoimmune diseases (5–8). However, identifying early biomarkers to predict and manage these complications remains a major clinical priority.

Placental Growth Factor (PIGF), a pro-angiogenic protein secreted by the placenta, plays a central role in placental vascular development and has garnered attention as a potential biomarker for pregnancy complications (9). Several studies have shown that low maternal serum PIGF levels are associated with an increased risk of PE (10–12), low birth weight, and fetal growth restriction (FGR) (13). In contrast, elevated PIGF concentrations have been linked to a reduced risk of spontaneous preterm birth (14). Nevertheless, the predictive performance of PIGF remains variable across studies, potentially due to differences in population characteristics, gestational timing of sampling, and methodological heterogeneity (15–17).

Importantly, limited evidence exists regarding the performance of PIGF across different modes of conception—such as spontaneous pregnancy, ovulation induction (OI), and *in vitro* fertilization (IVF)—and whether its predictive utility varies according to gestational age at measurement. Moreover, few studies have systematically characterized the dose–response relationships between PIGF and pregnancy outcomes, or assessed gestational age–specific predictive performance using standardized multiples of the median (MoM) values.

To address these gaps, we utilized data from our large prospective cohort study to investigate the association between maternal serum PIGF levels and a spectrum of adverse pregnancy outcomes. We examined dose–response patterns, assessed predictive performance across gestational age windows, and performed subgroup analyses stratified by mode of conceptions. Our findings aim to generate evidence that may inform future applications of PIGF in individualized risk assessment and screening strategies during early and mid-pregnancy.

Abbreviations: AUC, area under the curve; BMI, body mass index; CI, confidence interval; FGR, fetal growth restriction; GW, gestational weeks; IVF, *in vitro* fertilization; MAP, mean arterial pressure; MoM, multiple of the median; LBW, low birth weight; LGA, large for gestational age; OI, ovulation induction; OR, odds ratio; PE, preeclampsia; PIGF, placental growth factor; RCS, restricted cubic splines; SGA, small for gestational age.

2 Materials and methods

2.1 Study design and participants

This prospective, longitudinal cohort study included 5,870 singleton pregnant women who were admitted to Nanjing Drum Tower Hospital between January 2017 and September 2020. Participants were followed from early pregnancy (within 14 gestational weeks (GW), defined by a crown–rump length of 45–84 mm) through delivery. The study aimed to identify predictive factors for PE and collected comprehensive data on baseline characteristics, biochemical and biophysical markers, as well as maternal and fetal outcomes. Ethical approval was obtained from the Research Ethics Committee of Nanjing Drum Tower Hospital (Approval No. 2016-113-01).

The inclusion criteria for this study were defined as follows (1): maternal age ≥18 years (2); singleton pregnancy; (3) confirmed fetal viability at 11–13 GW; and (4) provision of written informed consent. The exclusion criteria were: (1) multiple pregnancy; (2) presence of major fetal structural abnormalities detected at 11–13 GW; (3) planned termination of pregnancy; and (4) cognitive impairment or inability to provide informed consent.

2.2 The measurement of Placental Growth Factor levels in serum

Blood samples were collected from all participants on the day of enrollment, between the 11–14 GW. In addition, for the first 1,800 participants, additional blood samples were also obtained at three subsequent time points: 18–24 GW, 28–34 GW, and after 35 GW. Serum separation was performed according to a standardized operating procedure (18). PIGF concentrations were quantified

using the Cobas e602 analyzer (Roche Diagnostics, Germany). Quality control procedures adhered to both institutional and manufacturer guidelines. Specifically, the coefficient of variation for quality control materials at different concentrations within each batch was required to remain below 5%. Furthermore, quality control measurement values for each assay were required to fall within ±2 standard deviations of the established target values.

2.3 Adverse pregnancy outcomes

Adverse pregnancy outcomes assessed in this cohort included gestational diabetes mellitus (GDM), gestational hypertension, PE, ectopic pregnancy, placental abruption, premature rupture of membranes (PROM), spontaneous abortion, placenta praevia, single live birth, large for gestational age (LGA), SGA, and preterm birth. The definitions and diagnostic criteria for each outcome are provided in Supplementary Material 1. Specifically, the definitions of LGA and SGA were based on gestational age-specific growth curves constructed from our own Chinese cohort, ensuring that the cutoff values were tailored to the study population (19).

2.4 Covariates

Maternal covariates included maternal age (years), pre-pregnancy body mass index (BMI, kg/m^2), mean arterial pressure (MAP, mmHg) measured at 11–14 GW, gestational age at the time of PIGF testing, parity (0, 1, 2, or 3), smoking status (no/yes), and medical history including diabetes (no/yes), hypertension (no/yes), renal disease (no/yes), and systemic lupus erythematosus (no/yes).

2.5 Statistical analysis

All statistical analyses were conducted using R software (version 4.2.2). For continuous data, descriptive statistics were expressed as mean and standard deviation. Comparisons between groups were performed using independent-sample t-tests or non-parametric tests, as appropriate. Categorical data were presented using frequency and percentage, and comparisons between groups were made using Chi-square tests or Fisher's exact test. A two-sided $P < 0.05$ was considered statistically significant. Logistic regression models were applied to assess the relationship between PIGF levels and adverse pregnancy outcomes. In the multivariable models, key covariates such as maternal age, pre-pregnancy BMI, and MAP were adjusted. Additional covariates, including parity, smoking status, and medical history of diabetes, hypertension, renal disease, and systemic lupus erythematosus, were included in sensitivity analyses. PIGF concentrations were converted to MoM, calculated by dividing the observed value by the expected median value for the corresponding gestational age. The methodology for MoM calculation was based on the approach described by H N Madsen (20)., and PIGF MoM values were obtained using calculators provided by the Fetal Medicine Foundation (https://fetalmedicine.org/). To assess potential non-linear dose–response relationships between PIGF levels and maternal-fetal outcomes, restricted cubic splines (RCS) were fitted using the R package 'rcssci'.

3 Results

3.1 General characteristics of cohort participants

The flow diagram of the cohort study is shown in Figure 1. A total of 5,870 eligible pregnant women were initially enrolled. Among them, 560 participants (9.5%) were excluded, including 525 who discontinued participation without providing follow-up outcomes and 35 who selected to terminate the pregnancy before 28 GW. The final analytical cohort included 5,310 women: 4,664 (87.8%) in the spontaneous conception group, 79 (1.5%) in the OI group, and 567 (10.7%) in the IVF group. Follow-up results revealed that 515 participants (9.7%) developed gestational diabetes, and 278 (5.27%) were diagnosed with PE, including 64 cases (1.22%) of preterm PE. There were 5,268 singleton live births (99.23%), of which 246 (4.67%) were preterm births. A total of 655 neonates (12.43%) were SGA below the 10th percentile (SGA <10th), among them 238 cases (4.52%) classified as SGA <3rd percentile.

Baseline characteristics of participants are summarized in Table 1. Women in the IVF group were older and had higher pre-pregnancy body weight and MAP compared with those in the spontaneous and OI groups ($P < 0.05$), and higher incidence of gestational diabetes, PE, placental abruption, placenta praevia, and ectopic pregnancy ($P < 0.05$). Fetal outcomes were generally comparable across the groups, with no statistically significant differences observed.

3.2 Association between PIGF levels and adverse maternal-fetal outcomes

Table 2 summarizes the associations between serum PIGF levels in 11–14 GW and adverse pregnancy outcomes. In adjusted logistic regression models, higher PIGF concentrations were inversely associated with PE (odds ratio [OR] = 0.97, 95% confidence interval [CI]: 0.96 – 0.98), preterm PE (OR = 0.96, 95% CI: 0.94 – 0.98), SGA <10th percentile (OR = 0.99, 95% CI: 0.98 – 0.99), and SGA <3rd percentile (OR = 0.98, 95% CI: 0.97 – 0.99). When using PIGF MoM values, the inverse associations were stronger for PE (OR = 0.32, 95% CI: 0.21 – 0.48), preterm PE (OR = 0.23, 95% CI: 0.09 – 0.56), SGA <10th percentile (OR = 0.67, 95% CI: 0.54 – 0.83), and SGA <3rd percentile (OR = 0.43, 95% CI: 0.29 – 0.64). These associations remained robust in sensitivity analyses further adjusting for parity, smoking, history of diabetes, history of hypertension, history of renal disease, and systemic lupus erythematosus (Supplementary Table S1).

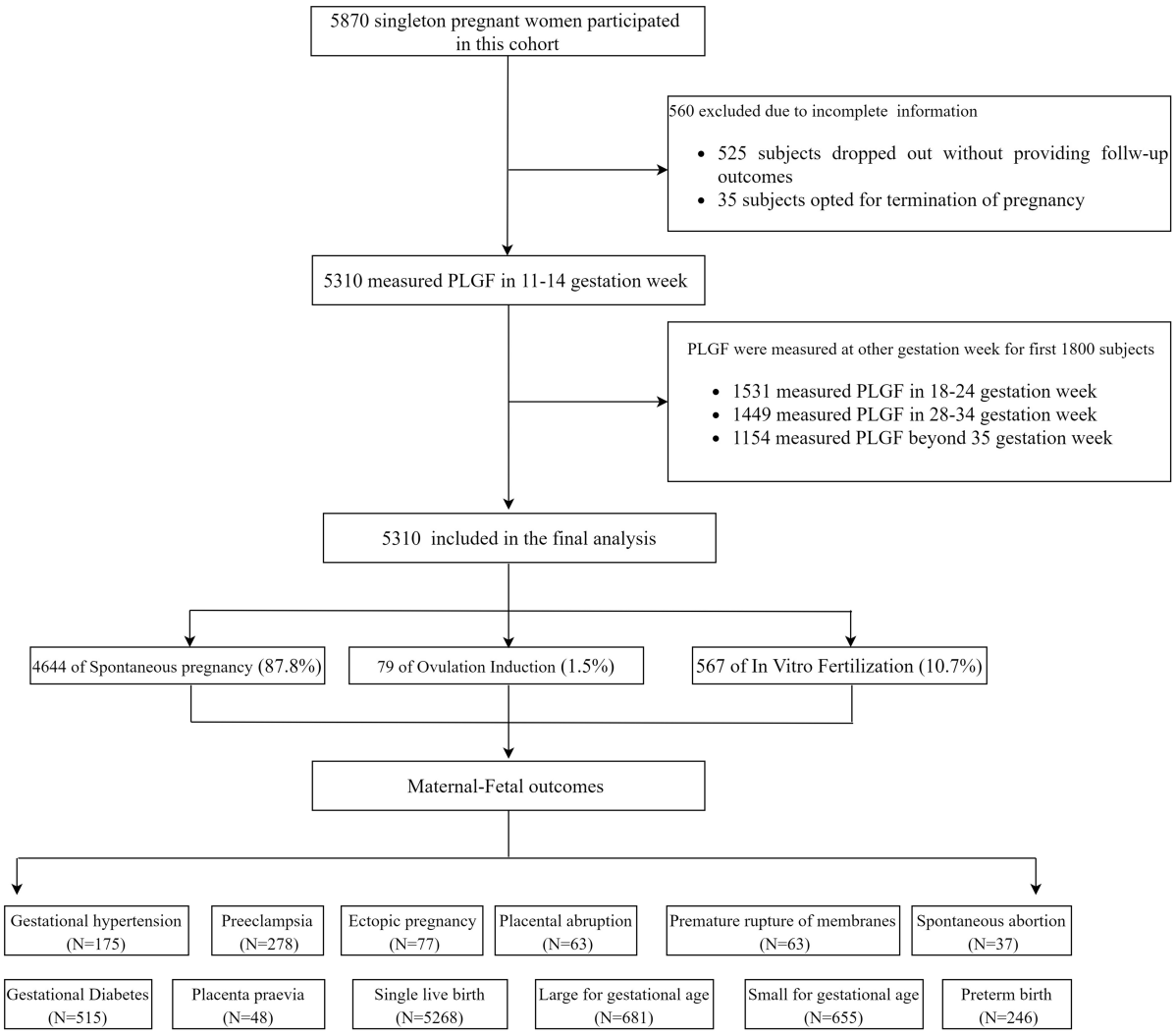

FIGURE 1
The flow diagram of the cohort study.

3.3 Subgroup analysis

Subgroup analysis stratified by mode of conception are presented in Table 3. In the spontaneous conception group, serum PIGF concentrations were inversely related to PE (OR = 0.97, 95% CI: 0.96 – 0.98), preterm PE (OR = 0.96, 95% CI: 0.94 – 0.99), SGA <10th percentile (OR = 0.99, 95% CI: 0.98 – 0.99), and SGA <3rd percentile (OR = 0.98, 95% CI: 0.97 – 0.99). Similarly, inverse associations between PIGF levels and PE were observed in both the IVF and OI subgroups. In these groups, the ORs for PE were 0.95 (95% CI: 0.92 – 0.97) for raw PIGF levels and 0.14 (95% CI: 0.05 – 0.37) for PIGF MoM values, respectively. However, no significant associations were found between PIGF levels (both raw and MoM values) and the risks of preterm PE, SGA <10th percentile, or SGA <3rd percentile in the IVF and OI subgroups. Interaction analysis with GDM (Supplementary Table S2) showed that the associations between PIGF levels and PE were evident only in the non-GDM group, whereas no significant associations were observed in the GDM group. By contrast, PIGF was significantly inversely associated with SGA in both the GDM and non-GDM groups. The inverse association of PIGF MoM values with SGA <3rd percentile was stronger in the GDM group (OR = 0.24, 95% CI: 0.06 – 0.86), while it also remained significant in the non-GDM group (OR = 0.46, 95% CI: 0.30 – 0.69).

3.4 Evaluation of predictive performance

The predictive performance of PIGF levels in the 11–14 GW for identifying adverse pregnancy outcomes is detailed in Table 4. Generally, PIGF levels during early pregnancy showed an area under the curve (AUC) of 0.61 for predicting PE, 0.64 for preterm PE, 0.57 for SGA < 10th percentile, and 0.59 for SGA < 3rd percentile. Similar trends were observed in the spontaneous

TABLE 1 Study population characteristics.

Characteristic	Spontaneous (N = 4664)	OI (79)	IVF (567)	All (N=5310)	*P*
Maternal characteristic					
Maternal age, year*	29.90 ± 3.69	29.81 ± 3.03	32.45 ± 3.85	30.17 ± 3.78	<.001
Height, cm*	162.10 ± 4.70	160.62 ± 5.21	160.89 ± 5.13	161.95 ± 4.78	<.001
Pre-pregnancy weight, kg*	57.31 ± 8.77	57.72 ± 7.87	58.74 ± 9.17	57.47 ± 8.81	0.001
Pre-pregnancy Body Mass Index, kg/m2*	21.79 ± 3.06	22.39 ± 2.94	22.66 ± 3.20	21.89 ± 3.08	<.001
Early pregnancy mean arterial pressure, mmHg*	83.07 ± 7.90	83.52 ± 7.11	86.08 ± 8.51	83.39 ± 8.01	<.001
Placental growth factor, pg/mL*	32.51 ± 46.69	37.35 ± 50.67	30.61 ± 16.48	32.38 ± 44.52	0.382
Gestational week at Delivery, week*	38.95 ± 2.14	38.82 ± 2.44	38.60 ± 2.35	38.91 ± 2.17	<.001
Maternal outcome					
Gestational Diabetes, n (%)	405(8.68)	7(8.86)	103(18.17)	515(9.70)	<.001
Gestational hypertension, n (%)	145(3.11)	2(2.53)	28(4.94)	175(3.30)	0.065
Preeclampsia, n (%)	215(4.64)	6(7.69)	57(10.16)	278(5.27)	<.001
Preterm Preeclampsia, n (%)	53(1.14)	1(1.28)	10(1.79)	64(1.22)	0.425
Ectopic pregnancy, n (%)	38(0.81)	2(2.53)	37(6.53)	77(1.45)	<.001
Placental Abruption, n (%)	49(1.05)	0(0.00)	14(2.47)	63(1.19)	0.020
Premature rupture of membranes, n(%)	996(21.36)	16(20.25)	104(18.34)	1116(21.02)	0.247
Spontaneous abortion, n (%)	30(0.64)	1(1.27)	6(1.06)	37(0.70)	0.225
Placenta praevia, n (%)	31(0.66)	1(1.27)	16(2.82)	48(0.90)	<.001
Fetal outcome					
Single live birth, n (%)	4630(99.29)	78(98.73)	560(98.77)	5268(99.23)	0.256
NICU > 24h, n (%)	9(0.19)	0(0.00)	0(0.00)	9(0.17)	0.659
Neonatal asphyxia, n (%)	3(0.06)	0(0.00)	0(0.00)	3(0.05)	1.000
Large for gestational age, n (%)	591(12.73)	83(14.77)	7(8.97)	681(12.73)	0.230
SGA < 10th, n(%)	577(12.46)	7(8.97)	71(12.66)	655(12.43)	0.642
SGA < 3rd, n (%)	202(4.36)	3(3.85)	33(5.88)	238(4.52)	0.251
Preterm birth (< 37w), n (%)	209(4.51)	3(3.85)	34(6.07)	246(4.67)	0.241

*Data are presented as mean ± standard deviation. Spontaneous, Spontaneous pregnancy; OI, Ovulation Induction; IVF, *In Vitro* Fertilization; SGA < 10th, birth weight below the 10th percentile for gestational age; SGA < 3rd, birth weight below the 3rd percentile for gestational age.

conception subgroup (N = 4635). In contrast, within the IVF and OI subgroup (N = 639), no statistically significant associations were identified between PIGF levels and the risks of preterm PE, SGA <10th percentile, or SGA <3rd percentile. Nonetheless, for PE in the IVF and OI subgroup, the AUC reached 0.65, with a sensitivity of 0.78 and a specificity of 0.49. The MoM values of PIGF displayed similar predictive performance to that of raw PIGF levels.

To place our findings in context, we further summarized recent studies published in the past five years that evaluated PIGF for risk stratification across different pregnancy complications (Supplementary Table S3). These studies covered diverse clinical indications including preterm birth, PE, discordant fetal growth, and ectopic pregnancy, with reported PIGF thresholds ranging from 15.5 pg/ml to 290 pg/ml. The predictive performance varied by outcome and study design (with AUCs ranging from 0.72 to 0.90), but consistently supported the potential clinical utility of PIGF as a biomarker for early risk stratification in pregnancy.

3.5 Dose-response relationship analysis

The dose–response relationships between serum PIGF concentrations measured during 11–14 GW and adverse pregnancy outcomes were examined using RCS models (Figure 2). A linear inverse association was observed for both PE (Figure 2A) and preterm PE (Figure 2B). In contrast, non-linear associations were found for SGA <10th percentile and SGA <3rd percentile (Figures 2C, D, respectively). The optimal PIGF cut-off value for minimizing the risk of SGA <10th percentile was 27.27 pg/mL, while that for SGA <3rd percentile was 26.92 pg/mL (Table 5).

10.3389/fendo.2025.1674540

TABLE 2 Multivariable logistic regression analysis on the association between PIGF and adverse pregnancy outcomes.

Outcome	PIGF			Mom value of PIGF		
	OR*	95%CI	*P*	OR *	95%CI	*P*
Maternal outcome						
Gestational Diabetes	1.00	0.99-1.01	0.908	1.01	0.92-1.21	0.436
Gestational hypertension	0.99	0.98-1.00	0.883	0.94	0.70-1.26	0.683
Preeclampsia	0.97	0.96-0.98	<0.001	0.32	0.21-0.48	<0.001
Preterm Preeclampsia	0.96	0.94-0.98	0.001	0.23	0.09-0.56	0.001
Ectopic pregnancy	0.99	0.98-1.01	0.654	1.00	0.69-1.46	0.985
Placental Abruption	0.99	0.98-1.01	0.501	0.83	0.46-1.47	0.513
Premature rupture of membranes	1.00	0.98-1.00	0.355	0.95	0.85-1.06	0.372
Spontaneous abortion	1.00	0.98-1.02	0.824	0.92	0.48-1.77	0.805
Placenta praevia	0.98	0.96-1.01	0.144	0.62	0.28-1.38	0.246
Fetal outcome						
Single live birth	1.00	0.98-1.02	0.660	1.18	0.58-2.39	0.648
Large for gestational age	1.00	0.99-1.01	0.839	1.08	0.96-1.21	0.220
SGA < 10th	0.99	0.98-0.99	<0.001	0.67	0.54-0.83	<0.001
SGA < 3rd	0.98	0.97-0.99	<0.001	0.43	0.29-0.64	<0.001
Preterm birth	1.00	0.99-1.01	0.805	1.01	0.82-1.25	0.928

OR, odds ratio; CI, confidence interval. SGA < 10th, birth weight below the 10th percentile for gestational age; SGA < 3rd, birth weight below the 3rd percentile for gestational age.
*adjusted model: adjusted for maternal age, BMI, mean arterial pressure, gestational week for PIGF testing.

Two-piecewise logistic regression models were further used to evaluate the threshold effects of PIGF on SGA outcomes, as shown in Table 4. After adjusting for potential confounders, a significant inverse association was observed below the inflection points: for SGA <10th percentile (OR = 0.96, 95% CI: 0.94 – 0.98) and SGA <3rd percentile (OR = 0.95, 95% CI: 0.92 – 0.98). No significant associations were found to the above the thresholds ($P > 0.05$).

3.6 Comparative analysis of the association between PIGF levels and adverse maternal-fetal outcomes across gestational stages

The results of a logistic regression analysis evaluating the association between PIGF levels and adverse maternal-fetal outcomes at different stages of pregnancy are presented in

TABLE 3 Subgroup analysis on the association between PIGF level and adverse pregnancy outcomes.

Outcome	Spontaneous			IVF and OI		
	OR*	95%CI	*P*	OR*	95%CI	*P*
PIGF						
Preeclampsia	0.97	0.96-0.98	<0.001	0.95	0.92-0.97	0.001
Preterm Preeclampsia	0.96	0.94-0.99	0.003	0.96	0.91-1.02	0.220
SGA<10th	0.99	0.98-0.99	0.001	0.99	0.97-1.01	0.177
SGA<3rd	0.98	0.97-0.99	<0.001	0.99	0.97-1.02	0.596
MoM value of PIGF level						
Preeclampsia	0.36	0.23-0.58	<0.001	0.13	0.05-0.37	<0.001
Preterm Preeclampsia	0.24	0.09-0.62	0.003	0.27	0.03-2.60	0.256
SGA<10th	0.67	0.54-0.84	<0.001	0.63	0.33-1.22	0.170
SGA<3rd	0.37	0.24-0.58	<0.001	0.82	0.37-1.83	0.631

Spontaneous, Spontaneous pregnancy; OI, Ovulation Induction; IVF, *In Vitro* Fertilization; OR, odds ratio; CI, confidence interval. SGA<10th, birth weight below the 10th percentile for gestational age; SGA<3rd, birth weight below the 3rd percentile for gestational age. *adjusted model: adjusted for maternal age, BMI, mean arterial pressure, gestational week for PIGF testing.

TABLE 4 Predictive performance of the PIGF levels at 11–14 gestational week for the detection of adverse pregnancy outcomes.

Group	Outcome	PIGF			Mom value of PIGF		
		AUC (95%CI)	Se (95%CI)	Sp (95%CI)	AUC (95%CI)	Se (95%CI)	Sp (95%CI)
All (N = 5310)	PE	0.61 (0.60-0.63)	0.70 (0.64 – 0.76)	0.47 (0.45 – 0.48)	0.61 (0.59-0.62)	0.60 (0.54 – 0.66)	0.57 (0.56 – 0.59)
	Preterm PE	0.64 (0.63-0.65)	0.55 (0.42 – 0.67)	0.68 (0.67 – 0.70)	0.63 (0.62-0.65)	0.53 (0.40 – 0.66)	0.70 (0.69 – 0.71)
	SGA<10th	0.57 (0.56-0.58)	0.48 (0.45 – 0.52)	0.64 (0.62 – 0.65)	0.57 (0.56-0.59)	0.47 (0.43 – 0.51)	0.65 (0.64 – 0.67)
	SGA<3rd	0.59 (0.58-0.61)	0.53 (0.46 – 0.59)	0.62 (0.61 – 0.64)	0.60 (0.59-0.62)	0.53 (0.46 – 0.59)	0.65 (0.63 – 0.66)
Spontaneous Pregnancy (N = 4635)	PE	0.60 (0.59-0.62)	0.87 (0.82 – 0.92)	0.27 (0.26 – 0.29)	0.61 (0.60-0.63)	0.70 (0.64 – 0.76)	0.47 (0.45 – 0.48)
	Preterm PE	0.64 (0.62-0.65)	0.53 (0.39 – 0.67)	0.69 (0.68 – 0.70)	0.62 (0.61-0.64)	0.45 (0.32 – 0.59)	0.76 (0.75 – 0.77)
	SGA<10th	0.57 (0.56-0.58)	0.48 (0.44 – 0.53)	0.64 (0.63 – 0.66)	0.57 (0.56-0.59)	0.44 (0.40 – 0.48)	0.69 (0.67 – 0.70)
	SGA<3rd	0.60 (0.59-0.62)	0.54 (0.46 – 0.61)	0.63 (0.61 – 0.64)	0.61 (0.60-0.63)	0.42 (0.35 – 0.49)	0.76 (0.75 – 0.78)
IVF and OI* (N = 639)	PE	0.65 (0.61-0.68)	0.78 (0.66 – 0.87)	0.49 (0.45 – 0.54)	0.66 (0.63-0.70)	0.67 (0.54 – 0.78)	0.63 (0.59 – 0.69)

AU, Area Under the Curve; Se, Sensitivity; Sp, Specificity; PE, Preeclampsia; SGA,C Small for gestational age; CI, Confidence Interval; Spontaneous, Spontaneous pregnancy; OI, Ovulation Induction; IVF, *In Vitro* Fertilization. *In the IVF and OI subgroup, no significant statistical association was identified between PIGF levels and the outcomes of preterm PE, SGA<10th and SGA<3rd. hence no predictive performance analysis is performed here.

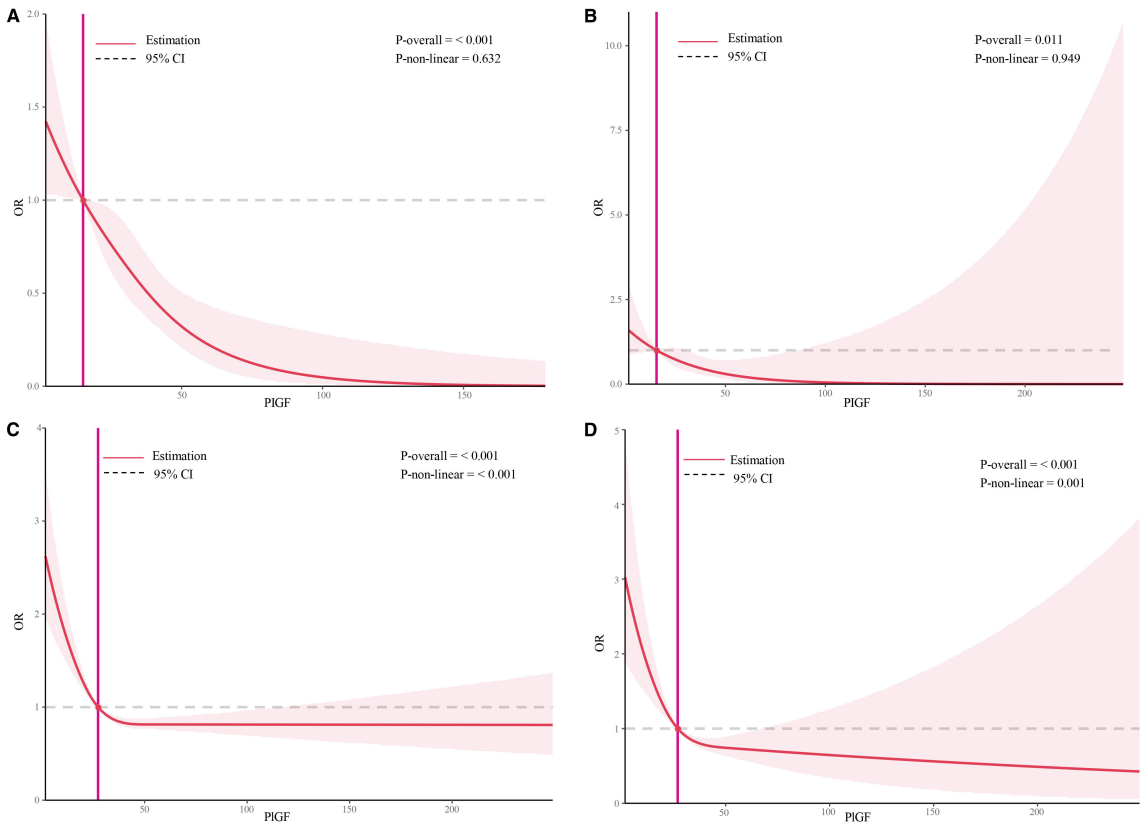

FIGURE 2
Restricted cubic spline plots of the association between serum placental growth factor level and adverse pregnancy outcomes. **(A)** Restricted cubic spline analysis of PLGF in relation to PE outcomes, with a simplified plot using an odds ratio of 1 as the cutoff point; **(B)** Restricted cubic spline analysis of PLGF in relation to preterm PE outcomes, with a simplified plot using an odds ratio of 1 as the cutoff point; **(C)** Restricted cubic spline analysis of PLGF in relation to SGA<10th, with a simplified plot using an odds ratio of 1 as the cutoff point; **(D)** Restricted cubic spline analysis of PLGF in relation to SGA<3rd, with a simplified plot using an odds ratio of 1 as the cutoff point.

TABLE 5 Threshold effect analysis of PIGF level on both SGA<10th and SGA<3rd by the two-piecewise logistic regression.

Inflection point	Unadjusted model			Adjusted model*		
	OR	95%CI	*P*	OR	95%CI	*P*
SGA<10th						
PIGF ≤ 27.267	0.96	0.94-0.98	<0.001	0.96	0.94-0.98	<0.001
PIGF > 27.267	1.00	0.99-1.01	0.846	1.00	0.99-1.01	0.828
MoM values of PIGF ≤ 0.716	0.22	0.11-0.45	<0.001	0.22	0.11-0.45	<0.001
MoM values of PIGF > 0.716	0.98	0.82-1.17	0.826	0.98	0.81-1.17	0.795
SGA<3rd						
PIGF ≤ 26.919	0.95	0.92-0.98	<0.001	0.95	0.92-0.98	0.001
PIGF > 26.919	0.99	0.98-1.01	0.465	0.99	0.98-1.01	0.378
MoM values of PIGF ≤ 0.713	0.15	0.05-0.42	<0.001	0.16	0.05-0.45	<0.001
MoM values of PIGF > 0.713	0.77	0.47-1.29	0.333	0.76	0.45-1.30	0.322

SGA, Small for gestational age; OR, odds ratio; CI, confidence interval. *adjusted model: adjusted for maternal age, BMI, mean arterial pressure, gestational week for PIGF testing.

Supplementary Table S4. Overall, PIGF MoM values were consistently inversely associated with PE, SGA <10th percentile, and SGA <3rd percentile across all gestational stages. Specifically, for PE, the ORs were 0.27 (95% CI: 0.14 – 0.55) at 18–24 GW, 0.11 (95% CI: 0.04 – 0.27) at 28–34 GW, and 0.18 (95% CI: 0.06 – 0.49) after 35 GW. Additionally, PIGF MoM values during 28–34 GW were inversely associated with preterm birth (OR = 0.62, 95% CI: 0.41 – 0.93) and positively associated with LGA (OR = 1.39, 95% CI: 1.21 – 1.61). Detailed characteristics of the study population across different gestational stages are provided in Supplementary Table S5.

The predictive performance of PIGF levels for adverse pregnancy outcomes at different gestational stages is summarized in Table 6. The highest predictive performance for both PE and preterm PE was observed during 28–34 GW, with AUCs of 0.79 (95% CI: 0.77 – 0.81) and 0.86 (95% CI: 0.85 – 0.88), respectively. Similarly, the best performance for SGA <10th

TABLE 6 The predictive performance of PIGF values for adverse pregnancy outcomes at different stages of pregnancy.

GW	Outcome	PIGF			MOM of PIGF		
		AUC (95%CI)	Se (95%CI)	Sp (95%CI)	AUC (95%CI)	Se (95%CI)	Sp (95%CI)
11–14 GW (N = 5310)	PE	0.61 (0.60-0.63)	0.70 (0.64-0.76)	0.47 (0.45-0.48)	0.61 (0.59-0.62)	0.60 (0.54-0.66)	0.58 (0.56-0.59)
	Preterm PE	0.64 (0.63-0.65)	0.55 (0.42-0.67)	0.69 (0.67-0.70)	0.63 (0.62-0.64)	0.53 (0.40-0.66)	0.70 (0.69-0.71)
	SGA < 10th	0.57 (0.56-0.58)	0.48 (0.45-0.52)	0.64 (0.62-0.65)	0.57 (0.56-0.59)	0.47 (0.43-0.51)	0.65 (0.64-0.67)
	SGA < 3rd	0.59 (0.58-0.61)	0.53 (0.46-0.59)	0.62 (0.61-0.64)	0.60 (0.59-0.62)	0.53 (0.46-0.59)	0.65 (0.63-0.66)
18–24 GW (N = 1531)	PE	0.70 (0.68-0.73)	0.54 (0.41-0.67)	0.79 (0.77-0.81)	0.66 (0.63-0.68)	0.68 (0.54-0.79)	0.62 (0.59-0.65)
	Preterm PE	0.73 (0.71-0.75)	0.67 (0.43-0.85)	0.72 (0.70-0.74)	0.66 (0.63-0.68)	0.57 (0.34-78.2)	0.73 (0.71-0.75)
	SGA < 10th	0.61 (0.58-0.63)	0.43 (0.36-0.50)	0.74 (0.72-0.77)	0.61 (0.58-0.63)	0.47 (0.40-0.55)	0.71 (0.68-0.73)
	SGA < 3rd	0.65 (0.62-0.67)	0.51 (0.39-0.64)	0.74 (0.72-0.76)	0.66 (0.64-0.68)	0.73 (0.60-0.82)	0.55 (0.52-0.57)
28–34 GW (N = 1449)	PE	0.79 (0.77-0.81)	0.64 (0.50-0.77)	0.82 (0.80-0.84)	0.78 (0.76-0.80)	0.69 (0.53-0.80)	0.78 (0.76-0.80)
	Preterm PE	0.86 (0.85-0.88)	0.87 (0.62-0.98)	0.81 (0.79-0.83)	0.85 (0.83-0.87)	0.87 (0.62-0.98)	0.81 (0.80-0.84)
	SGA < 10th	0.63 (0.57-0.66)	0.57 (0.49-0.65)	0.63 (0.60-0.66)	0.65 (0.62-0.67)	0.61 (0.53-0.68)	0.61 (0.58-0.63)
	SGA < 3rd	0.67 (0.65-0.70)	0.64 (0.51-0.76)	0.62 (0.60-0.65)	0.69 (0.67-0.72)	0.69 (0.56-0.80)	0.60 (0.57-0.62)
>35 GW (N = 1154)	PE	0.74 (0.71-0.77)	0.73 (0.54-0.88)	0.65 (0.62-0.68)	0.72 (0.70-0.75)	0.83 (0.65-0.94)	0.53(0.50-0.56)
	Preterm PE*	–	–	–	–	–	–
	SGA < 10th	0.61 (0.58-0.64)	0.64 (0.55-0.72)	0.57 (0.54-0.60)	0.61 (0.58-0.64)	0.67 (0.58-0.75)	0.54(0.51-0.57)
	SGA < 3rd	0.69 (0.67-0.72)	0.55 (0.40-0.69)	0.76 (0.74-0.79)	0.69 (0.66-0.72)	0.53 (0.38-0.67)	0.77 (0.74-0.79)

PIGF, Placental Growth Factor; AUC, Area Under the Curve; Se, Sensitivity; Sp, Specificity; CI, Confidence Interval; GW, Gestational Weeks; PE, Preeclampsia; SGA < 10th, birth weight below the 10th percentile for gestational age; SGA < 3rd, birth weight below the 3rd percentile for gestational age.
*Preterm PE is defined as occurring before 37 GW. Consequently, in cases extending beyond 35 GW, preterm PE would have manifested and been addressed, resulting in the absence of data for this group.

percentile was also noted during 28–34 GW, with an AUC of 0.63 (95% CI: 0.57 – 0.66). In contrast, the optimal predictive performance for SGA <3rd percentile was observed after 35 GW, with an AUC of 0.69 (95% CI: 0.66 – 0.72). Moreover, PIGF levels during 28–34 GW demonstrated predictive value for LGA (AUC = 0.58, 95% CI: 0.56 – 0.61) and preterm birth (AUC = 0.65, 95% CI: 0.62 – 0.67), as shown in Supplementary Table S6.

4 Discussion

In this prospective cohort study, we investigated the associations between maternal serum PIGF concentrations measured at 11–14 GW and a range of adverse maternal and fetal outcomes. Both raw PIGF values and MoM values showed inverse associations with PE, preterm PE, and SGA below the 10th and 3rd percentiles. These associations were consistent across different modes of conception, with PIGF showing predictive value for PE regardless of whether the pregnancy was spontaneous, achieved through OI or IVF. The highest predictive performance for PE was observed during the 28–34 GW. Moreover, dose-response analysis suggested a linear inverse association between PIGF and PE outcomes, whereas the associations with SGA <10th and <3rd percentiles were non-linear, indicating a possible threshold effect.

PIGF, an angiogenic factor, has been reported to be associated with pregnancy complications, particularly PE and SGA. However, existing literature reports inconsistent findings regarding its predictive performance for PE (15). Some researchers showed that PIGF had relatively high predictive accuracy for PE at 11–14 GW, with AUCs above 0.7 and sensitivities above 60% (21, 22), and others showed its limited predictive performance, with AUCs below 0.6 and sensitivities below 25% (23, 24). These discrepancies may stem from differences in study populations, cutoff thresholds, or analytical platforms used. In our cohort, the predictive performance of PIGF for PE at 11–14 GW was moderate (AUC = 0.61; sensitivity = 70%), suggesting that although PIGF contributes to risk stratification, it may not serve as a standalone predictor, and PIGF with maternal demographic characteristics, MAP, uterine artery pulsatility index, and pregnancy-associated plasma protein A could significantly improve predictive performance for PE at 11–14 GW (25). Consistently, the Fetal Medicine Foundation (FMF) Bayes-based competing risk model and other studies have also recommended integrating PIGF with maternal characteristics and additional biomarkers in the first trimester to optimize PE prediction (26–29). Similarly, the predictive performance for SGA <10th and <3rd percentiles was limited when using PIGF alone, reinforcing the need to integrate PIGF with other clinical and ultrasonography markers to enhance screening accuracy. In addition, our findings revealed that PIGF MoM values showed stronger associations with PE and SGA than absolute concentrations, which underscores the importance of standardizing for gestational age of and maternal characteristics (30, 31).

Previous studies have provided limited data regarding the influence of conception method on PIGF levels. A study reported no significant difference in serum PIGF concentrations between IVF and spontaneous pregnancies at 10 weeks' gestation (32), a finding consistent with our results. In the present analysis, the predictive performance of PIGF for PE was slightly higher in the IVF and OI subgroups than in the spontaneous conception group. However, no significant associations were found between PIGF levels and preterm PE or SGA outcomes in the IVF and OI subgroups. These findings suggest that while PIGF retains its association with PE across conception methods, its role in predicting other outcomes may be more variable. This highlights the potential need for tailored screening strategies when evaluating pregnancy risks in assisted reproductive technology (ART) populations. Notably, in our interaction analysis with GDM, the inverse association between maternal PIGF levels and the risk of SGA was more pronounced in the GDM group than in the non-GDM group, although the underlying mechanisms and potential explanations remain to be elucidated.

This study also explored the dose-response relationship between early pregnancy PIGF levels and adverse outcomes, with a particular focus on non-linear associations. RCS analyses demonstrated linear associations between PIGF and both PE and preterm PE. In contrast, the relationships between PIGF and SGA <10th or <3rd percentile were nonlinear. The strongest associations for SGA were observed below the identified inflection points (27.3 pg/mL for SGA <10th and 26.9 pg/mL for SGA <3rd), while associations diminished beyond these thresholds. These findings are consistent with prior reports (33), which also reported a nonlinear association between mid-pregnancy PIGF and SGA. RCS modeling, with its ability to flexibly capture inflection points, provides valuable insight for determining clinically meaningful thresholds that may optimize screening and intervention strategies.

This study has several notable strengths. First, it utilized a large, prospective cohort with detailed clinical data and well-defined pregnancy outcomes, allowing for comprehensive and reliable analyses. Second, the inclusion of participants with different modes of conception—spontaneous, OI, and IVF—enabled stratified subgroup analyses that are rarely explored in prior research. Third, we assessed the predictive performance of PIGF across different gestational windows, identifying that its predictive ability for PE peaked at 28–34 GW, which may inform the optimal timing for clinical screening.

However, several limitations should be acknowledged. Although the prospective design strengthens the temporal relationship between exposure and outcome, the observational nature of the study does not permit causal inferences. Despite adjustment for a range of maternal characteristics and clinical factors, residual confounding from unmeasured variables may still exist. Additionally, subgroup analyses in the IVF and OI populations were limited by smaller sample sizes, potentially reducing statistical power to detect associations with outcomes such as preterm PE or SGA. Finally, the cohort was drawn from a single regional center, which may limit the generalizability of our findings to broader populations or healthcare systems. Despite these limitations, this study adds important evidence on the association between early pregnancy PIGF levels and adverse outcomes, including nuanced subgroup differences by conception mode and

non-linear dose-response patterns with SGA. Future studies should aim to track dynamic changes in PIGF throughout gestation and evaluate whether incorporating PIGF into multi-marker screening algorithms can improve early risk stratification and guide targeted interventions.

In conclusion, our study demonstrates that maternal serum PIGF levels, particularly MoM-standardized values, are significantly associated with the risk of PE and SGA, especially when measured between 28–34 GW. The predictive value of PIGF varies by gestational age and conception mode, with the strongest performance observed in spontaneous pregnancies during mid-to-late gestation. Moreover, a non-linear dose–response relationship was observed between PIGF and SGA risk, suggesting a threshold effect. These findings underscore the potential of gestational age–tailored PIGF screening for pregnancy risk stratification, and highlight the need for further validation in multi-center studies with diverse populations.

Data availability statement

The raw data supporting the conclusions of this article will be made available by the authors, without undue reservation.

Ethics statement

The studies involving humans were approved by the Research Ethics Committee of Nanjing Drum Tower Hospital. The studies were conducted in accordance with the local legislation and institutional requirements. The participants provided their written informed consent to participate in this study.

Author contributions

T-SL: Formal Analysis, Writing – original draft. YuW: Formal Analysis, Writing – original draft. YaW: Investigation, Writing – original draft. H-RT: Data curation, Writing – original draft. H-LD: Data curation, Writing – original draft. G-FZ: Formal Analysis, Software, Writing – original draft. JL: Conceptualization, Writing – review & editing. Y-LH: Conceptualization, Writing – review & editing.

Funding

The author(s) declare financial support was received for the research and/or publication of this article. This study was funded by grants from the National Key R&D Program of China (The grant number: 2021YFC2701603).

Conflict of interest

The authors declare that the research was conducted in the absence of any commercial or financial relationships that could be construed as a potential conflict of interest.

Generative AI statement

The author(s) declare that no Generative AI was used in the creation of this manuscript.

Any alternative text (alt text) provided alongside figures in this article has been generated by Frontiers with the support of artificial intelligence and reasonable efforts have been made to ensure accuracy, including review by the authors wherever possible. If you identify any issues, please contact us.

Publisher's note

Supplementary material

The Supplementary Material for this article can be found online at: https://www.frontiersin.org/articles/10.3389/fendo.2025.1674540/full#supplementary-material

SUPPLEMENTARY MATERIAL 1
The diagnostic criteria and definitions of study outcome.

References

1. Crump C, Sundquist J, Sundquist K. Adverse pregnancy outcomes and long-term risk of chronic kidney disease in women: national cohort and co-sibling study. *Am J obstetrics gynecology*. (2023) 230:563.e1-563.e20. doi: 10.1016/j.ajog.2023.10.008

2. Crump C, Sundquist J, McLaughlin MA, Dolan SM, Govindarajulu U, Sieh W, et al. Adverse pregnancy outcomes and long term risk of ischemic heart disease in mothers: national cohort and co-sibling study. *BMJ*. (2023) 380:e072112. doi: 10.1136/bmj-2022-072112

3. Khan SS, Petito LC, Huang X, Harrington K, McNeil RB, Bello NA, et al. Body mass index, adverse pregnancy outcomes, and cardiovascular disease risk. *Circ Res*. (2023) 133:725–35. doi: 10.1161/CIRCRESAHA.123.322762

4. Patro Golab B, Santos S, Voerman E, Lawlor DA, Jaddoe VWV, Gaillard R, et al. Influence of maternal obesity on the association between common pregnancy complications and risk of childhood obesity: an individual participant data meta-analysis. *Lancet Child Adolesc Health*. (2018) 2:812–21. doi: 10.1016/S2352-4642(18)30273-6

5. Singh M, Wambua S, Lee SI, Okoth K, Wang Z, Fazla F, et al. Autoimmune diseases and adverse pregnancy outcomes: an umbrella review. *Lancet*. (2023) 402 Suppl 1:S84. doi: 10.1016/S0140-6736(23)02128-1

6. Xiong Y, Wang J, Huang S, Liu C, Liu Y, Qi Y, et al. Association between maternal prepregnancy body mass index and pregnancy outcomes following assisted

reproductive technology: A systematic review and dose-response meta-analysis. *Obes Rev*. (2021) 22:e13219. doi: 10.1111/obr.13219

7. McLennan AS, Gyamfi-Bannerman C, Ananth CV, Wright JD, Siddiq Z, D'Alton ME, et al. The role of maternal age in twin pregnancy outcomes. *Am J obstetrics gynecology*. (2017) 217:80 e1– e8. doi: 10.1016/j.ajog.2017.03.002

8. Bramham K, Parnell B, Nelson-Piercy C, Seed PT, Poston L, Chappell LC. Chronic hypertension and pregnancy outcomes: systematic review and meta-analysis. *BMJ*. (2014) 348:g2301. doi: 10.1136/bmj.g2301

9. De Falco S. The discovery of placenta growth factor and its biological activity. *Exp Mol Med*. (2012) 44:1–9. doi: 10.3858/emm.2012.44.1.025

10. Levine RJ, Maynard SE, Qian C, Lim KH, England LJ, Yu KF, et al. Circulating angiogenic factors and the risk of preeclampsia. *New Engl J Med*. (2004) 350:672–83. doi: 10.1056/NEJMoa031884

11. Balyan K, Humtso BY, Meena B, Sapna S, Rana A, Kumar M. Materno-fetal outcome with plgf above or below cutoff during second half of pregnancy in high-risk women. *Int J gynaecology obstetrics: Off Organ Int Fed Gynaecology Obstetrics*. (2023) 165:211–9. doi: 10.1002/ijgo.15143

12. Duhig KE, Myers J, Seed PT, Sparkes J, Lowe J, Hunter RM, et al. Placental growth factor testing to assess women with suspected pre-eclampsia: A multicentre, pragmatic, stepped-wedge cluster-randomised controlled trial. *Lancet*. (2019) 393:1807–18. doi: 10.1016/S0140-6736(18)33212-4

13. Benton SJ, McCowan LM, Heazell AE, Grynspan D, Hutcheon JA, Senger C, et al. Placental growth factor as a marker of fetal growth restriction caused by placental dysfunction. *Placenta*. (2016) 42:1–8. doi: 10.1016/j.placenta.2016.03.010

14. Sovio U, Gaccioli F, Cook E, Charnock-Jones DS, Smith GCS. Maternal serum levels of soluble fms-like tyrosine kinase-1 and placental growth factor at 20 and 28 weeks of gestational age and the risk of spontaneous preterm birth. *Am J obstetrics gynecology*. (2023) 229:164 e1– e18. doi: 10.1016/j.ajog.2023.02.001

15. Agrawal S, Shinar S, Cerdeira AS, Redman C, Vatish M. Predictive performance of plgf (Placental growth factor) for screening preeclampsia in asymptomatic women: A systematic review and meta-analysis. *Hypertension (Dallas Tex: 1979)*. (2019) 74:1124–35. doi: 10.1161/HYPERTENSIONAHA.119.13360

16. Zhang L, Li W, Chi X, Sun Q, Li Y, Xing W, et al. Predictive performance of sflt-1, plgf and the sflt-1/plgf ratio for preeclampsia: A systematic review and meta-analysis. *J Gynecol Obstet Hum Reprod*. (2025) 54:102925. doi: 10.1016/j.jogoh.2025.102925

17. Chen W, Wei Q, Liang Q, Song S, Li J. Diagnostic capacity of sflt-1/plgf ratio in fetal growth restriction: A systematic review and meta-analysis. *Placenta*. (2022) 127:37–42. doi: 10.1016/j.placenta.2022.07.020

18. Zeisler H, Llurba E, Chantraine F, Vatish M, Staff AC, Sennstrom M, et al. Predictive value of the sflt-1:Plgf ratio in women with suspected preeclampsia. *New Engl J Med*. (2016) 374:13–22. doi: 10.1056/NEJMoa1414838

19. Wang Y, Wang Y, Tang HR, Zhang Y, Dai CY, Li J, et al. Establishment method and significance of birthweight curve and reference in single center. *Chin J Obstetrics Gynecology*. (2023) 58:334–42. doi: 10.3760/cma.j.issn.0529-567x.2014.07.001

20. Madsen HN, Ball S, Wright D, Torring N, Petersen OB, Nicolaides KH, et al. A reassessment of biochemical marker distributions in trisomy 21-affected and unaffected twin pregnancies in the first trimester. *Ultrasound obstetrics gynecology: Off J Int Soc Ultrasound Obstetrics Gynecology*. (2011) 37:38–47. doi: 10.1002/uog.8845

21. Foidart JM, Munaut C, Chantraine F, Akolekar R, Nicolaides KH. Maternal plasma soluble endoglin at 11–13 weeks' Gestation in pre-eclampsia. *Ultrasound obstetrics gynecology: Off J Int Soc Ultrasound Obstetrics Gynecology*. (2010) 35:680–7. doi: 10.1002/uog.7621

22. Youssef A, Righetti F, Morano D, Rizzo N, Farina A. Uterine artery doppler and biochemical markers (Papp-a, pigf, sflt-1, P-selectin, ngal) at 11 + 0 to 13 + 6 weeks in the prediction of late (> 34 weeks) pre-eclampsia. *Prenatal diagnosis*. (2011) 31:1141–6. doi: 10.1002/pd.2848

23. Schneuer FJ, Nassar N, Guilbert C, Tasevski V, Ashton AW, Morris JM, et al. First trimester screening of serum soluble fms-like tyrosine kinase-1 and placental growth factor predicting hypertensive disorders of pregnancy. *Pregnancy hypertension*. (2013) 3:215–21. doi: 10.1016/j.preghy.2013.04.119

24. Skrastad RB, Hov GG, Blaas HG, Romundstad PR, Salvesen KA. A prospective study of screening for hypertensive disorders of pregnancy at 11–13 weeks in a scandinavian population. . *Acta Obstet Gynecol Scand*. (2014) 93:1238–47. doi: 10.1111/aogs.12479

25. Li T, Xu M, Wang Y, Wang Y, Tang H, Duan H, et al. Prediction model of preeclampsia using machine learning based methods: A population based cohort study in China. *Front Endocrinol (Lausanne)*. (2024) 15:1345573. doi: 10.3389/fendo.2024.1345573

26. O'Gorman N, Wright D, Poon LC, Rolnik DL, Syngelaki A, Wright A, et al. Accuracy of competing-risks model in screening for pre-eclampsia by maternal factors and biomarkers at 11–13 weeks' Gestation. *Ultrasound obstetrics gynecology: Off J Int Soc Ultrasound Obstetrics Gynecology*. (2017) 49:751–5. doi: 10.1002/uog.17399

27. Ansbacher-Feldman Z, Syngelaki A, Meiri H, Cirkin R, Nicolaides KH, Louzoun Y. Machine-learning-based prediction of pre-eclampsia using first-trimester maternal characteristics and biomarkers. *Ultrasound obstetrics gynecology: Off J Int Soc Ultrasound Obstetrics Gynecology*. (2022) 60:739–45. doi: 10.1002/uog.26105

28. Tiruneh SA, Rolnik DL, Selvaratnam R, da Silva Costa F, McLennan A, Hyett J, et al. External validation of the fetal medicine foundation model for preterm pre-eclampsia prediction at 11–14 weeks in an Australian population. *Acta Obstet Gynecol Scand*. (2025) 104:1774–82. doi: 10.1111/aogs.70002

29. Zhao Q, Li J, Diao Z, Zhang X, Feng S, Hou G, et al. Early prediction of preeclampsia from clinical, multi-omics and laboratory data using random forest model. *BMC Pregnancy Childbirth*. (2025) 25:531. doi: 10.1186/s12884-025-07582-4

30. Ekelund CK, Rode L, Tabor A, Hyett J, McLennan A. Placental growth factor and adverse obstetric outcomes in a mixed-risk cohort of women screened for preeclampsia in the first trimester of pregnancy. *Fetal diagnosis Ther*. (2021) 48:304–12. doi: 10.1159/000514201

31. O'Gorman N, Wright D, Syngelaki A, Akolekar R, Wright A, Poon LC, et al. Competing risks model in screening for preeclampsia by maternal factors and biomarkers at 11–13 weeks gestation. *Am J obstetrics gynecology*. (2016) 214:103.e1–.e12. doi: 10.1016/j.ajog.2015.08.034

32. Lee MS, Cantonwine D, Little SE, McElrath TF, Parry SI, Lim KH, et al. Angiogenic markers in pregnancies conceived through *in vitro* fertilization. *Am J obstetrics gynecology*. (2015) 213:212 e1–8. doi: 10.1016/j.ajog.2015.03.032

33. Darling AM, McDonald CR, Conroy AL, Hayford KT, Liles WC, Wang M, et al. Angiogenic and inflammatory biomarkers in midpregnancy and small-for-gestational-age outcomes in Tanzania. *Am J obstetrics gynecology*. (2014) 211:509 e1–8. doi: 10.1016/j.ajog.2014.05.032

frontiers | Frontiers in Endocrinology

TYPE Original Research
PUBLISHED 29 October 2025
DOI 10.3389/fendo.2025.1640635

OPEN ACCESS

EDITED BY
Leonardo Ermini,
University of Siena, Italy

REVIEWED BY
Mahita Kadmiel,
Allegheny College, United States
Diallo Aissatou Bailo,
IHU Mediterranee Infection, France

*CORRESPONDENCE
Francisco J. Valenzuela-Melgarejo
fvalenzuela@ubiobio.cl

RECEIVED 04 June 2025
ACCEPTED 14 October 2025
PUBLISHED 29 October 2025

CITATION
Venegas C, Jara-Medina K, Cueto N, Cabello-Guzmán G, Lagunas C, Lillo L and Valenzuela-Melgarejo FJ (2025) Melatonin modulates the gene expression of WEE1 kinase and clock genes: a crosstalk between the molecular clocks of the placenta?. *Front. Endocrinol.* 16:1640635. doi: 10.3389/fendo.2025.1640635

Melatonin modulates the gene expression of WEE1 kinase and clock genes: a crosstalk between the molecular clocks of the placenta?

Carlos Venegas[1], Kevins Jara-Medina[1], Nicole Cueto[1], Gerardo Cabello-Guzmán[2], Constanza Lagunas[1], Luis Lillo[1] and Francisco J. Valenzuela-Melgarejo[1]*

[1]Laboratory of Molecular Cell Biology, Department of Basic Sciences, Universidad del Bío-Bío, Chillán, Chile, [2]Department of Basic Sciences, Universidad del Bío-Bío, Chillán, Chile

Background: The circadian system organizes during 24 hours the temporal variations in biological processes such as the cell cycle, metabolism, and hormone production. This occurs by a transcriptional/translational feedback loop of core clock genes, namely, *BMAL1*, *PER1-3*, and *CRY1-2*. The CLOCK–BMAL1 complex regulates clock-controlled genes like WEE1 kinase, a key modulator of mitotic entry and placental cell proliferation.
Objective: We aimed to identify temporally regulated gene expression patterns in the human placenta using bioinformatics analysis of available microarrays in Gene Expression Omnibus (GEO) datasets and to validate selected findings in cultured placental explants.
Methods: Temporal microarray data from the GEO were analyzed to identify circadian and cell cycle-related genes. Selected targets were validated *in vitro* using explant cultures of human placenta sampled every 4 hours for 36 hours, with or without 10 nM melatonin.
Results: We observed rhythmic expression of *BMAL1*, *PER1*, *PER2*, and *WEE1* in human placental explants, consistent with the temporal patterns detected *in silico*. Melatonin treatment suppressed the circadian oscillation of *BMAL1*, *PER2*, and *WEE1*. Interestingly, the placenta produced melatonin steadily over 36 hours, and exogenous melatonin did not alter this production.

KEYWORDS

melatonin, placenta, clock gene, cell cycle, pregnancy

1 Introduction

The coordinated function of the circadian system and the cell cycle is critical for cell development, homeostasis (1–3), and tissue regeneration (1, 4–7). The disruption of circadian rhythms elevates the cancer risk (8) due to the impaired expression of the target genes from the cell cycle, i.e., cyclins, proto-oncogenes, and tumor suppressor genes (7, 9–15).

The central clock of the circadian system resides in the suprachiasmatic nucleus (SCN) (16–21), which synchronizes the peripheral oscillators through neural and humoral pathways. The primary humoral signal used by the body is the pineal hormone melatonin, a hormone synthesized during dark hours and playing a central role as a systemic timekeeping (22–30).

At the molecular level, circadian oscillations depend on a transcriptional/translational feedback loop involving a group of clock genes, namely, *BMAL1* (also known as *ARNTL*), *CLOCK*, *PER1-3*, and *CRY1-2* (31, 32). The CLOCK/BMAL1 heterodimeric complex initiates the circadian transcription by binding to conserved promoter sequences, namely, E-box (CACGTG) from clock genes *PER1–3* and *CRY1-2* (31), thereby giving the circadian output signals to clock-controlled genes. One such target is the kinase WEE1, which can inhibit Cdc2-cyclin B complexes, delaying G2/M transition and modulating cell proliferation in a time-dependent manner (1, 7).

Like the circadian system, the cell cycle is a finely timed and temporal process capable of generating a coordinated series of cell divisions, regulated by cyclin-dependent protein kinases (Cdk) essential for the stage transition (33–35). *WEE1* is of particular interest because its promoter contains E-box motifs responsive to CLOCK/BMAL1, positioning it at the interface between circadian clock and cell cycle regulation (1, 7, 36–39).

The placenta is an endocrine tissue with a circadian production of hormones essential for pregnancy maintenance (40–43). The disruption of these temporal events has been linked to altered trophoblast proliferation, differentiation, and invasion (44, 45). All those temporal events are hallmarks of placental pathologies during pregnancy (31) and placental tumors (46–49).

Studies in trophoblast cells, previously stimulated by serum shock, have shown the circadian expression of the clock gene *PER2* (50, 51) and the *ex vivo* expression of *CLOCK*, *BMAL1*, and *PER1-2* (52–55). Moreover, maternal melatonin can cross the placental barrier, exhibiting a diurnal rhythm during pregnancy, suggesting that it can give a chronobiotic signal to the placenta (31, 56–60). Interestingly, shift work modifies the temporal production of melatonin, which increases cancer incidence, suggesting an association between melatonin secretion, oncogenesis, and cell proliferation (61–66).

Recent transcriptomic datasets available in the Gene Expression Omnibus (GEO) provide the opportunity to explore temporal data of differentially expressed genes (DEGs) in the placenta, showing potential targets critical for placental physiology. DEG analysis can provide insight into the crosstalk between the circadian system and the cell cycle. We found common pathways modified by time hours and further investigated using placental culture and quantitative PCR. In this context, we speculated that the human placenta clocks can be modified by melatonin supplementation. These can determine the circadian output of critical signals to clock-controlled genes like the cell cycle regulator WEE1.

The placenta expresses melatonin-synthesizing enzymes such as AANAT and ASMT, as well as melatonin receptors, and maternal melatonin can cross the placental barrier (57, 67, 68). These findings provide a biological rationale for testing the effects of exogenous melatonin on placental circadian gene expression.

2 Materials and methods

2.1 Data source and bioinformatics analysis

The bioinformatics analysis was designed to identify time-dependent placental DEGs enriched for circadian and cell cycle pathways across independent GEO datasets. We analyzed datasets from the Gene Expression Omnibus (http://www.ncbi.nlm.nih.gov/geo) similar to what was reported previously (69, 70) for the terms “placenta and clock”, “placenta and circadian”, and “trophoblast and culture” (n = 139). We excluded platform data without temporal samples or incomplete incoming data. “GSE86171”, “GSE60433”, and “GSE40182” include temporal samples between 0 and 48 hours that were visualized using GEO Profiles graphics and the parameter Benjamin and Hochberg false discovery rate methodology with significance thresholds set at log2 fold change (logFC) ≥1 and adjusted p-value <0.05. We utilized the Kyoto Encyclopedia of Genes and Genomes (KEGG) for the functional analysis of cell cycle and circadian rhythms. In the present study, we collected, combined, and identified the gene expression profile using a Venn diagram. $p < 0.05$ was considered a significant difference by employing DAVID Bioinformatics 6.8, released Oct. 2016. The GO terms were “circadian rhythms”, “circadian regulation of gene expression”, “regulation of circadian rhythm”, “entrainment of the circadian clock by photoperiod”, and “cell cycle”.

2.2 Human placental tissue collection and culture

Term placentas from uncomplicated vaginal deliveries were obtained at approximately 07:00 hours at Herminda Martín Hospital (Chillán, Chile) after written informed consent was provided. The Ethics Committee approved the protocols of the Hospital and the University of the Bío Bío. Placentas were maintained at 4°C and processed at 07:00 hours. The tissue was washed three times with ice-cold phosphate-buffered saline (PBS) to eliminate red blood cells and trimmed to obtain a fetal portion of the placenta (chorion). Fifty-four explants of approximately 2 mm (L) × 2 mm (W) × 2 mm (H) and a mass of 45 ± 0.841 mg (wet mass) were used, according to the protocol of Cemerikic et al. (71).

Explants were cultured individually following previously described protocols (71–73). They were preincubated in M-199 medium (pH 7.2) and maintained in a humidified environment at 37°C and 5% CO_2 for 4 hours. Then, they were transferred to fresh

medium either alone (control) or supplemented with 10 nM melatonin (treatment group). The concentration of 10 nM melatonin was selected as a physiologically relevant dose, within the range used in previous studies on peripheral tissues (e.g., 10–100 nM) (74–79). This lower concentration was chosen to avoid potential pharmacological effects while maintaining biological activity. A sampling of three explants and the supernatant was conducted every 4 hours. All explants were weighed and stored with 1 mL TRIzol reagent (Invitrogen, Invitrogen Corporation, Carlsbad, California, USA). Explants and supernatant were stored frozen at −20°C.

2.3 Extraction of total RNA and reverse transcription (RT-PCR)

Explants of the human placenta were extracted in two stages: i) by the TRIzol method modified following the manufacturer's instructions (80) (phase separation, precipitation, and washing RNA) to the ethanol phase and later and ii) extraction using Kit SV Total RNA Isolation System modified following the instructions of the manufacturer (Promega Corporation, Madison, Wisconsin, USA) (purification of RNA). The absorbance was measured at 260 and 280 nm using a spectrophotometer to determine the concentration of RNA. Reverse transcription of 20 ng of extracted RNA was performed using the Improm Kit II Reverse Transcription System (Promega, Promega Corporation, Madison, Wisconsin, USA) in a final volume of 20 µL. The reverse transcription was at 70 °C for 5 minutes, 4°C for 5 minutes, 25°C for 5 minutes, 42°C for 60 minutes, and 70°C for 15 minutes.

2.4 Quantitative real-time PCR

The relative expression of the mRNAs of clock genes *BMAL1*, *PER1-2*, and *WEE1* was measured in samples of total cDNA. The PCR was performed in a final volume of 10 µL containing 0.33 µL of primers, forward and reverse primers of the genes studied, 3.8 µL of nuclease-free H_2O, and 5.5 µL of Master Mix II SYBR Brilliant Green (Agilent Technologies, Santa Clara, California, USA). The following primers were used: *BMAL1*, forward, 5′-CTGCATCCTAAAGATATTGCCAAAG-3′, and reverse, 5′-GTCGTGCTCCAGAACATAATCG-3′; *PER1*, forward, 5′-GGGCAAGGACTCAGAAAGAA-3′, and reverse, 5′-AGGCTCCATTGCTGGTAGAA-3′; *PER2*, forward, 5′-TGGATGAAAGGGCGGTCCCT-3′, and reverse, 5′-ACTGCAGGATCTTTTTGTGGA-3′; *WEE1*, forward, 5′-CGCGATGAGCTTCCTGAGCCG-3′, and reverse, 5′-CAGCGCACCGGCGAGAAAGAG-3′; cyclophilin, forward, CTCCTTTGAGCTGTTTGCAG-3′, and reverse, 5′-CACCACATGCTTGCCATCC-3′. For expression from quantitative real-time PCR (qPCR) data, all expression was normalized with cyclophilin for calculating relative gene expression by double delta Ct (ΔΔCt) and transformed to $2^{-\Delta\Delta Ct}$.

2.5 Melatonin measurement

The supernatant was cleaned with activated charcoal and measured by spectroscopic imaging using Fourier transform infrared (FTIR) spectroscopy associated with Attenuated Total Reflectance (ATR) (ATR–FTIR). Spectral measurements of the melatonin standard curve at 0.3–3,000 nM (Sigma-Aldrich, St. Louis, Missouri, USA.) were conducted, and supernatant samples were measured in triplicate using ATR–FTIR. The sample spectrum of 10 µL was recorded at room temperature in the region 1,000–4,000 cm^{-1} directly on a JASCO FT/IR-4100 Fourier transform infrared spectrophotometer with a 4.0 cm^{-1} resolution. A linear relationship was found for melatonin measurement at 1,492 cm^{-1}. The melatonin content was calculated following the methodology described by Filali et al. (81). The inter-assay and intra-assay coefficients of variation were less than 18%. Endogenous melatonin was quantified in explants maintained without supplementation. Exogenous melatonin levels were evaluated in explants supplemented with 10 nM melatonin. Paired untreated controls and the standard curve were used to differentiate between the hormone secreted by the tissue and the exogenous melatonin added to the medium.

2.6 Statistical data analysis

Data were expressed as mean ± SEM and analyzed using repeated-measures ANOVA, followed by Newman–Keuls *post-hoc* test, or Student's t-test as appropriate. Rhythmicity in gene expression was evaluated using non-linear regression of the sine-wave function expressed as Y = Baseline + Amplitude * Sine (Frequency X + Phase shift). All data were normalized between 0 and 1; the data were analyzed using the GraphPad Prism 5 software, and $p < 0.05$ was considered statistically significant.

3 Results

3.1 Identification and functional classification of differentially expressed genes

To explore whether circadian and cell cycle pathways were consistently represented in placental gene expression, we first analyzed publicly available transcriptomic datasets (GEO). We first asked whether time of day-dependent transcriptional changes in placental tissue preferentially involve circadian and cell cycle pathways across independent datasets. The expression profiling dataset of mRNA (GEO database) gives the tools for bioinformatics analysis of molecular pathways modified by time hours in the placenta. We performed the identification of DEGs via GO term enrichment and functional classification using DAVID. We selected the GO

classification related to the circadian system and cell cycle. We used terms such as "cell cycle", "circadian rhythms", "circadian regulation of gene expression", "regulation of circadian rhythm", and "entrainment of the circadian clock by photoperiod". We detected three complete microarray experiments for analysis: "GSE86171", "GSE60433", and "GSE40182". The periods studied in the microarrays were 0, 3, 12, 24, and 48 hours.

Functional annotation using DAVID identified 391 common DEGs (60.9%) during all time hours studied. Functional enrichment analysis (DAVID/KEGG) of the 391 common DEGs revealed significant overrepresentation of the "circadian rhythm" and "cell cycle" pathways (adjusted $p < 0.05$). Additional enriched terms included apoptosis and DNA repair, consistent with the central role of circadian regulation in cell proliferation and survival. Figure 1 shows the Venn diagram demonstrating the intersections of genes at different times of the day. Approximately 643, 283, and 1,179 common genes changed their expression level over all the time hours studied. Volcano plots for each dataset (Figures 2A–C) display the distribution of DEGs over time, and the pattern is visualized at every time studied in "GSE86171", "GSE60433", and "GSE40182". Similarly, the data of clock genes and regulators of the cell cycle for log2(fold change) and −log10(p-value) are shown in Table 1 for every time hour. The relative expression values suggest the time variation of clock gene expression in the placenta for at least 24 hours, with a peak for *PER2* and *CRY1* during the first half of the day. *BMAL1* shows a peak early in the morning, and the cell cycle genes *TP53*, *CIPC*, and *WEE1* show a peak during the interval between early in the morning and noon, suggesting a temporal variation of genes of circadian and cell cycle clocks.

3.2 *In vitro* expression of clock gene and the WEE1 gene in human placental explants

We next examined whether placental explants maintained circadian oscillations of core clock genes and the cell cycle regulator *WEE1* in culture. To validate the *in silico* observations associated with temporal variations observed in the microarray of the placenta, we cultured human placental explants and measured gene expression every 4 hours for 36 hours. We observed that the *BMAL1*, *PER1*, *PER2*, and *WEE1* genes maintain their mRNA expression in the culture of the human placenta for at least 36 hours (Figure 3).

As shown in Figure 3A, clock gene *BMAL1* expression increases during daylight hours, showing a rise between 03:00 and 11:00 hours. Also, *BMAL1* showed a local peak at 11:00 hours (range 03:00–11:00 hours is different from 15:00–23:00 hours of the second day of culture; $p < 0.05$, one-way ANOVA and Newman–Keuls post-test), whereas this expression showed a local minimum at 23:00 hours. The relative mRNA expression of *PER1* showed no significant changes during the hours studied but exhibited a trend toward higher expression in the evening (Figure 3B).

PER2 expression changed during the hours of culture, showing a peak expression at 19:00 hours on the first day ($p < 0.05$ ANOVA and Newman–Keuls) and low expression levels in the following hours studied (Figure 3C). Wee1 expression showed no significant differences but trended upward during nighttime hours (Figure 3D).

The temporal data suggest an endogenous oscillation in *BMAL1* and *PER2* occurring in antiphase with a ~12-hour interval, indicative of a functional circadian clock in placental tissue.

3.3 Melatonin inhibits the expression of clock genes and the WEE1 gene

Given that the placenta expresses the capacity to synthesize melatonin and receptors, we tested whether exogenous melatonin modulates the oscillations of *BMAL1*, *PER2*, and *WEE1*. The exposure of placental explants to 10 nM melatonin suppressed the rhythmic peaks of *BMAL1* and *PER2* expression observed in untreated cultures. Although *PER1* and *WEE1* did not show statistically significant changes, *BMAL1* expression was reduced between 07:00 and 19:00 hours under melatonin treatment

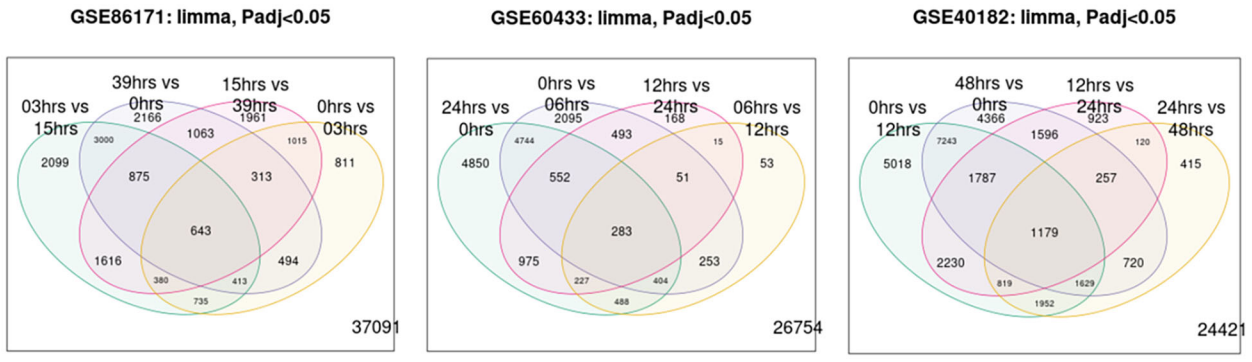

FIGURE 1
A Venn diagram of genes between Gene Expression Omnibus (GEO) and the time of day.

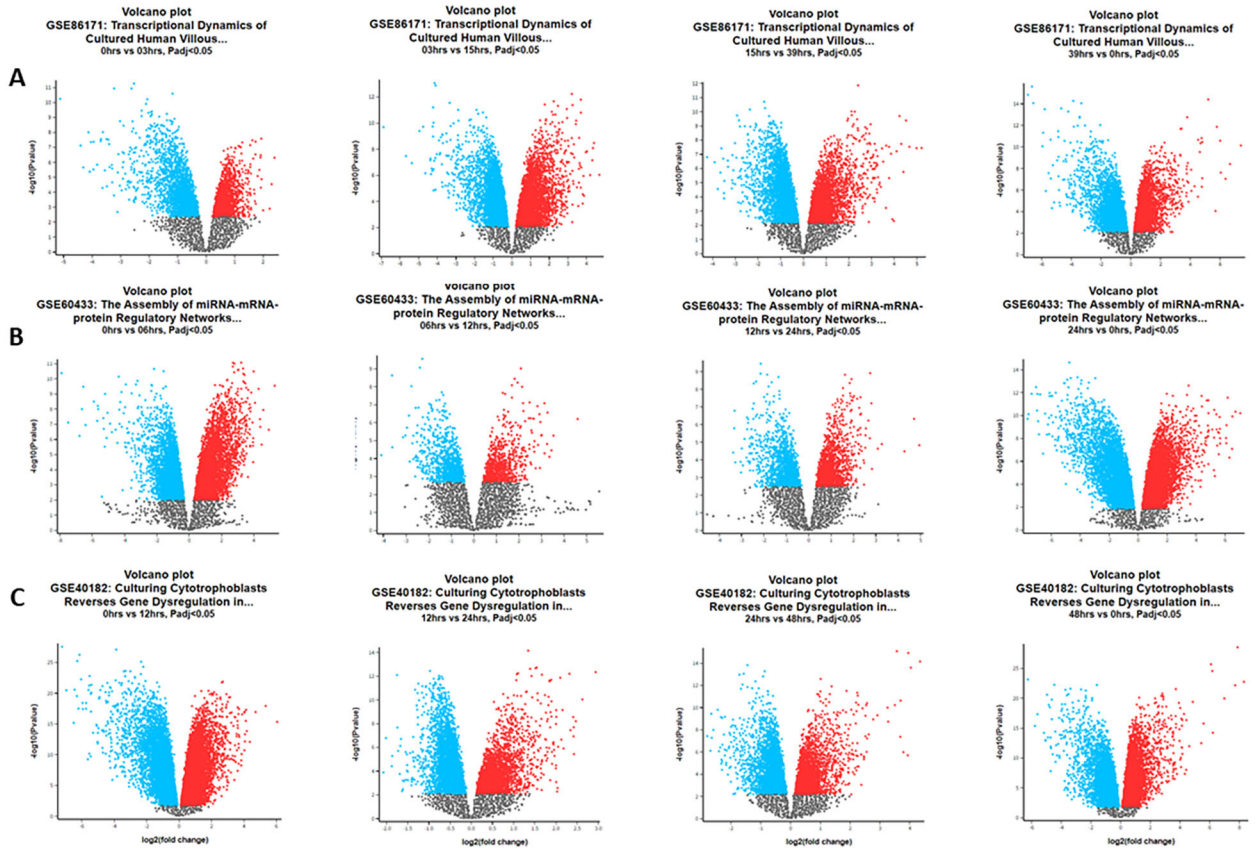

FIGURE 2
Volcano plots of differentially expressed genes in the Gene Expression Omnibus (GEO) datasets during the hour of the day. **(A)** Data GSE86171: at 0 vs. 3 hours, we detected 2,381 upregulated and 2,418 downregulated genes. At 3 vs. 15 hours, we detected 4,583 upregulated and 5,162 downregulated genes. At 15 vs. 39 hours, we detected 3,385 upregulated and 4,474 downregulated genes. At 39 vs. 0 hours, we detected 4,701 upregulated and 4,250 downregulated genes. **(B)** Data GSE60433: at 0 vs. 6 hours, we detected 4,523 upregulated and 4,344 downregulated genes. At 6 vs. 12 hours, we detected 824 upregulated and 949 downregulated genes. At 12 vs. 24 hours, we detected 1,407 upregulated and 1,356 downregulated genes. At 24 vs. 0 hours, we detected 6,286 upregulated and 6,224 downregulated genes. **(C)** Data GSE40182: at 0 vs. 12 hours, we detected 10,932 upregulated and 10,019 downregulated genes. At 12 vs. 24 hours, we detected 3,426 upregulated and 5,483 downregulated genes. At 24 vs. 48 hours, we detected 3,215 upregulated and 3,875 downregulated genes. At 48 vs. 0 hours, we detected 10,017 upregulated and 8,755 downregulated genes.

(Figures 4A–D). These results suggest that exogenous melatonin can reduce the amplitude of circadian gene expression in placental tissue.

3.4 Oscillatory ratios reveal phase relationships between clock genes

To further capture phase relationships among clock genes, we calculated BMAL1/PER1 and BMAL1/PER2 ratios across timepoints. To further evaluate gene oscillations, we calculated the expression ratios *BMAL1/PER1* and *BMAL1/PER2* (Figure 5). The circadian oscillation circuits are dependent on the transcriptional/translational feedback loop of clock genes, which act as positive and negative regulators, inducing/inhibiting their expression. *BMAL1/PER1* ratios showed non-significant variation but tended to peak at 15:00 and 23:00 hours on the second day of incubation (Figure 5A).

Moreover, *BMAL1/PER2* ratios exhibited significant oscillation, peaking between 03:00 and 11:00 hours and declining between 15:00 and 23:00 hours ($p < 0.05$; Figure 5B), fitting a sine-wave function ($r^2 = 0.7368$). In contrast, melatonin treatment inhibited the *BMAL1/PER2* peaks (Figures 5C, D).

These findings support the existence of an antiphase rhythm between *BMAL1* and *PER2*, a circadian pattern that is disrupted by melatonin.

3.5 BMAL1/WEE1 ratio suggests a circadian regulation of the cell cycle

To assess circadian gating of the cell cycle, we analyzed the ratio of *BMAL1* to *WEE1* expression across the culture period. The *BMAL1/WEE1* expression ratio revealed a peak at 03:00–11:00

10.3389/fendo.2025.1640635

TABLE 1 Volcano data of differentially expressed genes in the circadian system and cell cycle GEO datasets.

GEO dataset	Gene	0–3 hours log2(fold change) and −log10(p-value)	3–15 hours log2(fold change) and −log10(p-value	15–39 hours log2(fold change) and −log10(p-value)	39–0 hours log2(fold change) and −log10(p-value)
GSE86171	*Per1*	n.d	n.d	n.d	n.d
	Per2	−0.492	2.623	0.767*	3.558*
	Per3	n.d	n.d	n.d	n.d
	BMAL1	−0.88	2.479	0.990*	2.884*
	BMAL2	n.d	n.d	−1.794*	6.259*
	Clock	n.d	n.d	n.d	n.d
	Cry1	−1.942	9.112	1.673	8.208
	Cry2	n.d	n.d	n.d	n.d
	TP53	0.498*	2.848*	−1.099	6.48*
	CIPC	n.d	n.d	0.95	5.198
	WEE1	n.d	n.d	n.d	n.d
GSE60433	*Per1*	3.12	6.69	n.d	n.d
	Per2	3.114*	6.844*	−2.719*	6.002*
	Per3	1.957	4.331	−1.868	3.939
	BMAL1	1.468	5.996	1.226	4.895
	BMAL2	n.d	n.d	n.d	n.d
	Clock	n.d	n.d	n.d	n.d
	Cry1	2.433	9.05	n.d	n.d
	Cry2	1.602	6.211	−1.115	4.262
	TP53	n.d	n.d	n.d	n.d
	CIPC	n.d	n.d	n.d	n.d
	WEE1	n.d	n.d	n.d	n.d
GSE40182	Per1	n.d	n.d	n.d	n.d
	Per2	0.219	1.833	n.d	n.d
	Per3	n.d	n.d	n.d	n.d
	BMAL1	n.d	n.d	n.d	n.d
	BMAL2	−2.048*	16.226*	n.d	n.d
	Clock	0.408*	4.975*	−0.403*	3.20*
	Cry1	n.d	n.d	n.d	n.d
	Cry2	n.d	n.d	n.d	n.d
	TP53	−0.336	2.587	n.d	n.d
	CIPC	0.938	7.955	n.d	n.d
	WEE1	0.552	1.95	n.d	n.d

We used four timepoints for data analysis. Clock- and cell cycle-related DEGs selected from the set of 391 time-regulated genes identified across GEO datasets. Values show log2(fold change) and −log10(p-value) at the indicated timepoint contrasts. These genes were prioritized to illustrate circadian–cell cycle crosstalk within the broader DEG set.
n.d, not detected; GEO, Gene Expression Omnibus; DEGs, differentially expressed genes.
(*) Mean of several data.

10.3389/fendo.2025.1640635

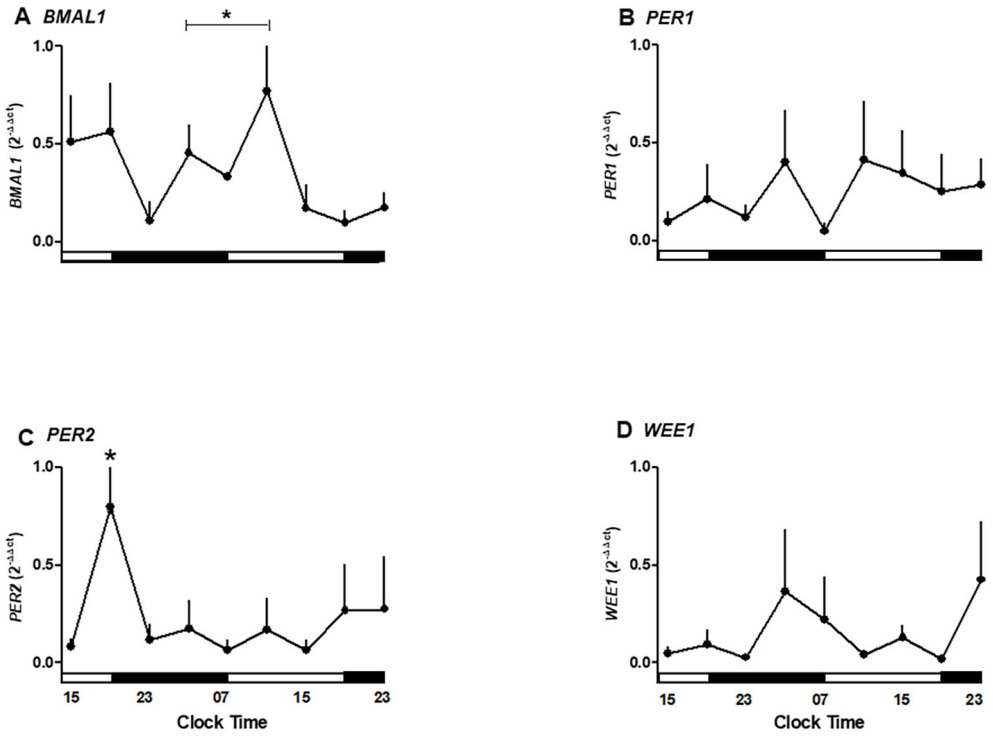

FIGURE 3
Temporal expression of clock and cell cycle genes in human placental explants cultured for 36 hours. **(A)** BMAL1 mRNA expression showing significant variation between 03:00–11:00 h and 15:00–23:00 h. **(B)** PER1 mRNA expression showing no significant oscillation but a trend toward higher levels in the evening. **(C)** PER2 mRNA expression peaking at 19:00 h during the first day of culture ($p < 0.05$). **(D)** WEE1 mRNA expression showing a mild, non-significant increase during nighttime hours.Data are expressed as mean ± SEM (n = 3 per timepoint). Statistical analysis by one-way ANOVA followed by Newman–Keuls post hoc test; $p < 0.05$ considered significant.

hours, followed by a decline during the night hours of the second day of culture ($p < 0.05$; Figure 6A). This antiphase relationship between *BMAL1* and *WEE1* was lost in melatonin-treated explants (Figure 6B). The pattern is consistent with the transcriptional regulation of *WEE1* by the CLOCK/BMAL1 complex.

3.6 Sustained melatonin production in placental explants

Finally, it was assessed whether placental explants produce melatonin endogenously and whether supplementation alters secretion levels. Endogenous melatonin was quantified in supernatants from untreated cultures (Figure 7A), while apparent exogenous levels were assessed in melatonin-supplemented cultures (Figure 7B). Values in treated conditions were interpreted relative to the standard curve and to paired untreated controls to distinguish secretion from supplemented hormone.

These findings confirm that the human placenta can produce melatonin autonomously and suggest a regulatory feedback loop between melatonin and the placental clock.

4 Discussion

The placenta exhibits a circadian production of critical hormones required for a healthy pregnancy (41–43, 68, 82, 83). In agreement with these findings, Diallo et al. (68) demonstrated that the human placenta displays circadian oscillations in its metabolism and is capable of synthesizing the melatonin hormone, suggesting the presence of a functional circadian clock in the placenta. Importantly, impaired circadian rhythms in the placental physiology due to the inhibition of melatonin production (e.g., shiftwork and night-time light exposure) have been associated with pregnancy complications and adverse outcomes (31, 84–89). We selected a low nanomolar concentration (10 nM) of melatonin, consistent with prior studies in several tissues, where nanomolar doses are biologically active while avoiding potential pharmacological effects (74–79). Using bioinformatics analyses, we detected time-dependent variation in the expression of cell cycle genes *TP53*, *CIPC*, and *WEE1* and clock genes *PER2*, *PER3*, *CRY1*, and *BMAL1*. These results suggest that such genes may serve as markers to study the intrinsic oscillatory capacity of placental

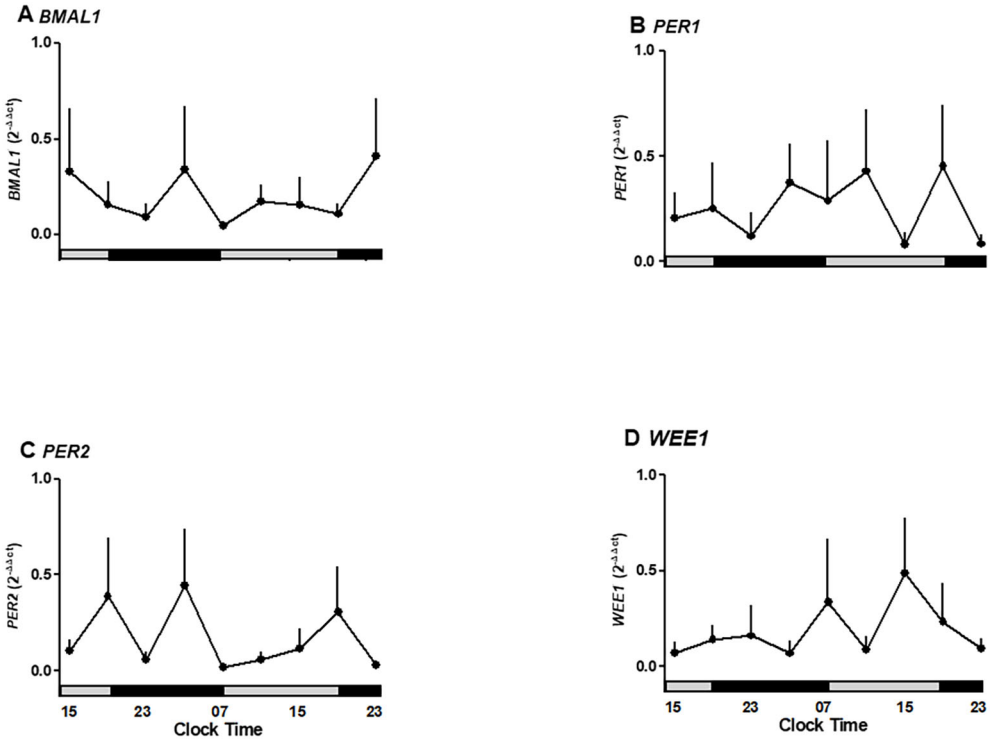

FIGURE 4
Oscillatory expression of clock genes BMAL1, PER1-2, and WEE1, a cell cycle gene in human placenta explants cultured for 36 hours in medium alone or plus melatonin. **(A)** BMAL1 expression under control and melatonin showing suppression of rhythmic peaks. **(B)** PER1 expression unaffected by melatonin treatment. **(C)** PER2 expression showing inhibition of oscillatory peaks by melatonin. **(D)** WEE1 expression showing a non-significant reduction under melatonin treatment.Profiles are representative of three placentas and expressed as Mean ± SE from 2-ΔΔCt. The bars on the X-axis indicate the relative hours of light (gray) and the hours of darkness (black).

tissue *in vitro*. To further explore this capacity, we performed culture experiments with human placental explants. Also, we provided complementary *in silico* and *ex vivo* evidence that human placental tissue displays intrinsic circadian dynamics involving *BMAL1*, *PER2*, and *WEE1* and that melatonin reduces the amplitude of these rhythms.

In culture, explants of the placenta can maintain the cellular function between 24 and 72 hours, synthesizing critical factors such as human placental lactogen (72, 90), human chorionic gonadotropin (CG) (71), prorenin (91), angiogenin (92), placental 24,25$(OH)_2D_3$ (93), and NO (94), and also showing the capacity of L-tryptophan transport and indoleamine 2,3-dioxygenase activity (95). Similarly, in our explants of the human placenta, we detected the expression of clock genes *BMAL1* and *PER1-2*. We observed a peak for *BMAL1* between 03:00 and 11:00 hours, with a local peak at 11:00 hours on the second day of culture, like that observed in rat liver (96), which was delayed 4 hours to the lungs and adrenal glands of rats (97, 98), or 9 hours in the adrenal gland of monkeys (17). The antiphase of approximately 12 hours observed for *BMAL1* and *PER2* is similar to that of trophoblasts synchronized by serum shock (51). Alternatively, the circadian expression of the clock gene *PER1* is not detected during culture. Despite the above, we speculated that the expression of *PER1* must be high during the hours of the night and at the end of the day, different from what was reported in rat liver (96) or vascular smooth muscle cells (99), where maximum expression was observed during the night.

Our data suggest that the human placenta shows the same expression pattern as the peripheral oscillator-like lung (97) and a delay of 5–7 hours from the adrenal (17, 98). However, we observed an advanced phase of approximately 4 hours from the rat's liver (96), and *PER2* expression is similar to that of the mouse placenta *ex vivo*. This pattern, after serum shock, is maintained in the culture of trophoblast cells (51). These data show the oscillation of the clock genes *BMAL1* and *PER2* in antiphase, which is related to the detected expression ratios of the *BMAL1/PER2* genes, and suggest that in the human placenta, there is an endogenous circadian clock with an autonomous capacity to work.

We showed the effect of melatonin on clock gene expression in the human placenta, similar to that reported over *BMAL1* and *PER2* in the pars tuberalis (100) and the adrenal gland (17, 101). Thus, our results suggest that melatonin has early effects on the expression of the clock genes as a chronobiotic agent, possibly via *BMAL1* inhibition and the posterior decrease of *PER1* and *PER2* expression. Another limitation of this approximation is that only

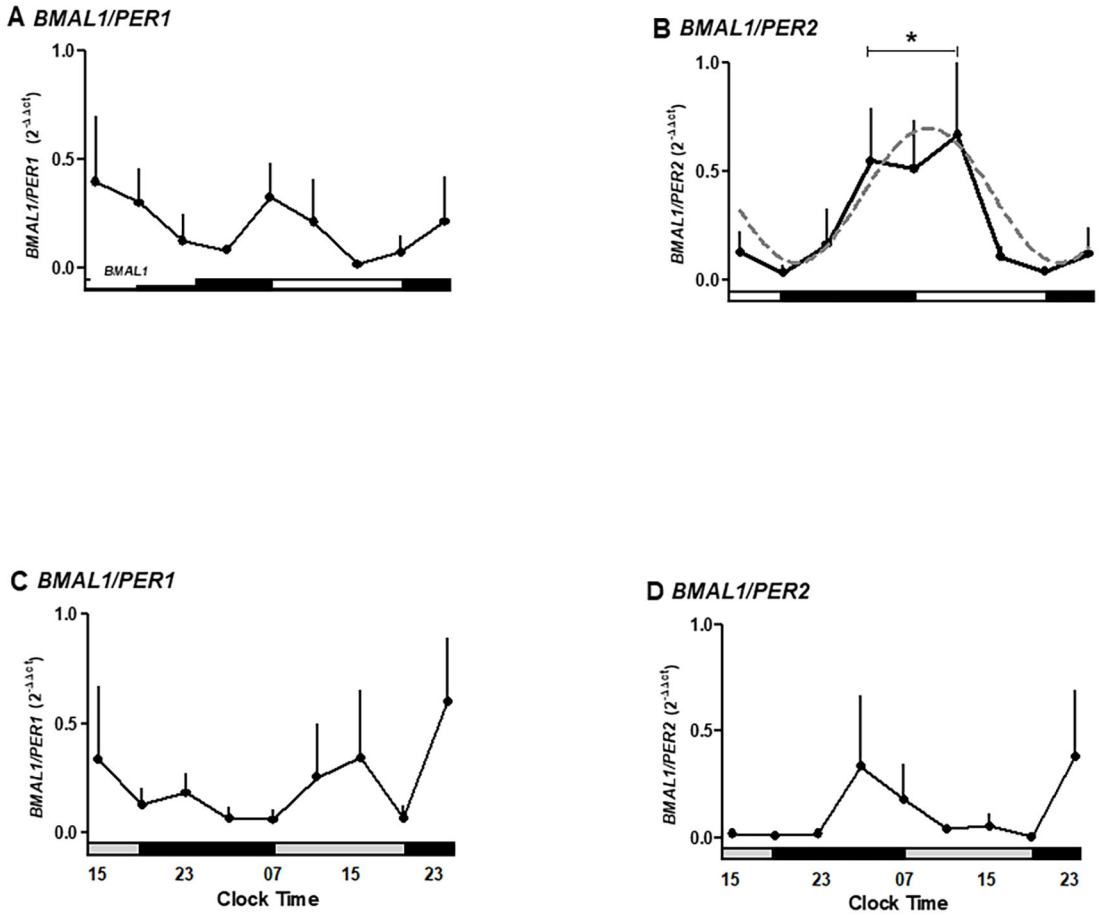

FIGURE 5
The ratio for expression of clock genes *BMAL1*, *PER1-2*, and *WEE1*, a cell cycle gene, in human placental explants cultured for 36 hours in medium alone **(A, B)** or medium plus melatonin **(C, D)**. Profiles are representative of three placentas and expressed as mean ± SE from $2^{-\Delta\Delta Ct}$. The dashed line in panel B represents the theoretical sine-wave function determined by equation Y = Baseline + Amplitude * Sine (Frequency X + Phaseshift), where Baseline = 0.39, Amplitude = 0.3, Frequency = 0.26, and Phaseshift = −0.8 for *BMAL1/PER-2* (r^2 = 0.7368). The data were normalized, considering the highest individual value within the experiment as 1 and the lowest value as 0. The bars on the X-axis indicate the hours of light (white), the hours of darkness (black), and relative hours of light (gray, **A, B**). * Different from other hours, one-way ANOVA, n = 3.

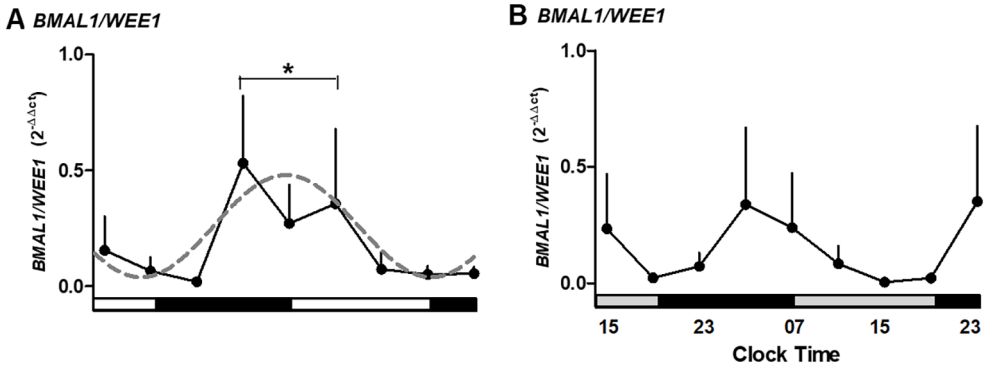

FIGURE 6
The ratio for expression of *BMAL1/WEE1* in medium alone **(A)** or medium alone plus melatonin **(B)** in human placental explants cultured for 36 hours. The dashed line in panel A represents the theoretical sine-wave function determined by equation Y = Baseline + Amplitude * Sine (Frequency X + Phaseshift), where Baseline = 0.26, Amplitude = 0.22, Frequency = 0.25, and Phaseshift = −0.08 for *BMAL1/WEE1* (r^2 = 0.5304). Profiles are representative of three placentas and expressed as mean ± SE from $2^{-\Delta\Delta Ct}$. The data were normalized, considering the highest individual value within the experiment as 1 and the lowest value as 0. The bars on the X-axis indicate the hours of light (white), the hours of darkness (black), and the relative hours of light (gray, in panel B). * Different from other hours, one-way ANOVA, n = 3.

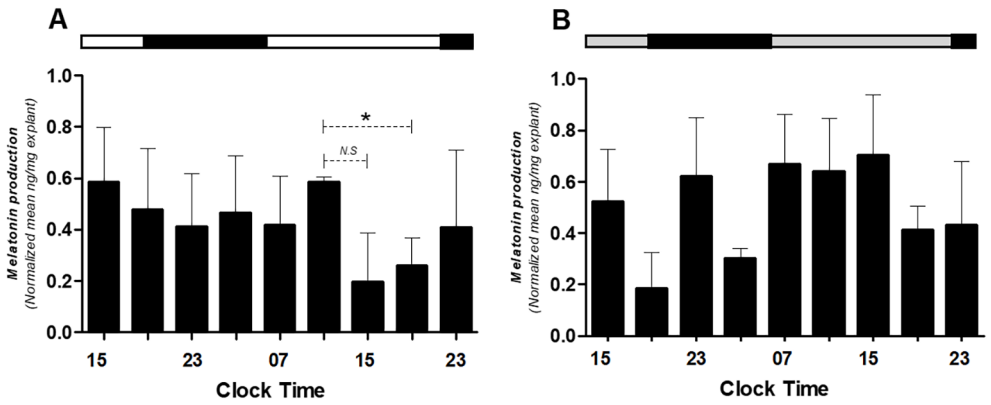

FIGURE 7
Melatonin production in medium alone **(A)** or medium alone plus melatonin **(B)** in human placental explants cultured for 36 hours. The average of each bar represents the average measurement of the melatonin concentrations obtained from the supernatant of each explant. The bar at the upper side of the graph indicates the hours of light (white), the hours of darkness (black), and relative hours of light (gray, in panel B). * Different from other hours, t-test, n = 3. N.S., non-significant difference.

a single concentration of melatonin (10 nM) was tested. Although this dose was selected based on its reported physiological relevance in placental and adrenal models, further dose–response studies will be necessary to fully establish the modulatory role of melatonin on placental circadian gene expression.

The circadian clock regulates the osteogenic potential by inhibiting BMAL1 expression (102), and the impaired expression of BMAL1 and PER1–2 causes tumor growth in mouse embryonic tissue (103). Alternatively, the knockdown of the clock gene *BMAL1* in carcinoma cells induces tumor growth when cells are injected subcutaneously, which may be mediated by the inhibition of apoptosis and reduction in the time that the cells remain in the G2/M phase (39). These antecedents suggest that the circadian system is closely related to the cell cycle in several peripheral tissues.

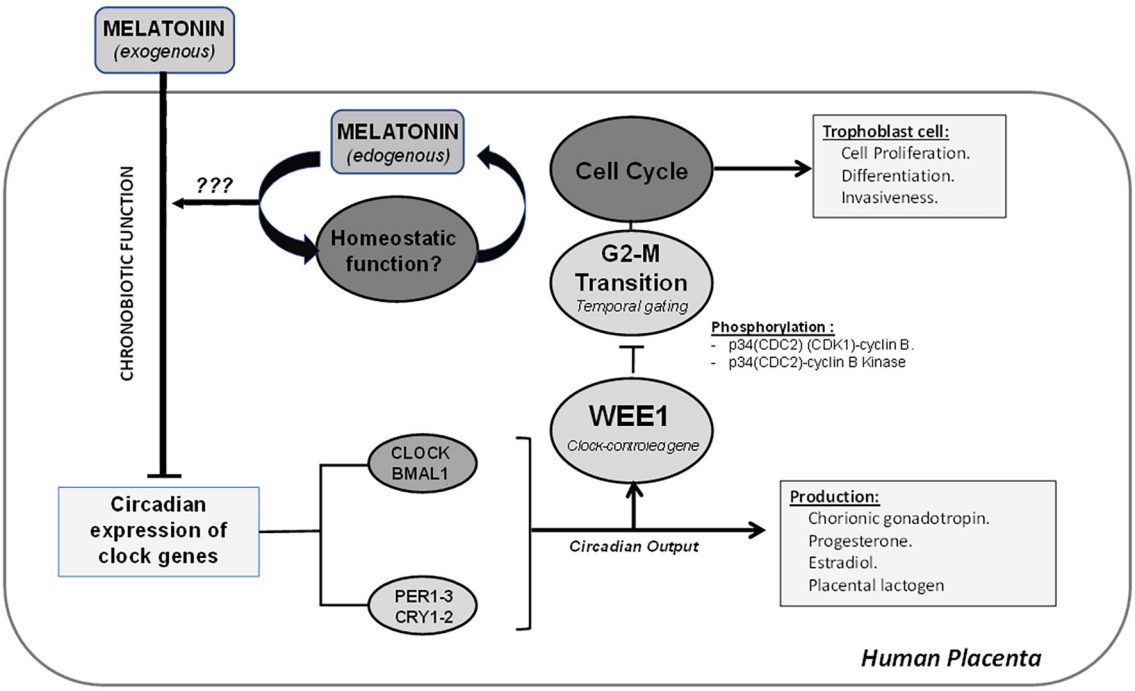

FIGURE 8
The placenta shows a circadian expression of clock genes, which can regulate the temporal gating of the cell cycle via modulation of mRNA expression of *WEE1* and inactivation of transition G2–M by phosphorylation of p34(CDC2) (CDK1)–cyclin B and p34(CDC2)–cyclin B kinase complex. The disruption of the circadian system of the placenta can modify critical processes, such as cell proliferation, differentiation, and invasiveness from trophoblast cells. Additionally, the placenta has the endogenous ability to produce melatonin, and it may play a homeostatic and antioxidant role in the placenta.

The *BMAL1/WEE1* ratio suggests that the circadian expression of *WEE1* increases at 03:00 hours, similar to a negative regulator of clock genes. The antiphase expression of *BMAL1* and *WEE1* detected here has been reported previously in the liver, with a peak for *WEE1* expression during the day/night transition and a peak for *BMAL1* during the night/day transition (96). Our results showed an antiphase of expression in the placenta for approximately 8 hours, suggesting the interplay of both clocks.

A limitation of our study is that clock gene expression was evaluated in whole placental explants rather than in isolated cells. While this approach allowed us to identify rhythmicity at the tissue level, it does not exclude the possibility that specific placental cell types, such as cytotrophoblasts or syncytiotrophoblasts, may exhibit distinct circadian dynamics. Future studies using isolated cell populations will be required to define cell type-specific rhythms and to clarify how melatonin modulates these cellular clocks.

Our data suggest that variations in the expression levels of the clock genes *BMAL1*, *PER1-2*, and the cell cycle gene *WEE1* would correspond to a self-sustained placental capacity. The entry into mitosis by human placenta cells would be regulated by the clock genes, which would modulate *WEE1* expression levels by inhibiting the cell cycle. Furthermore, we showed an agonist role of melatonin in the cell cycle, decreasing the expression of clock genes *BMAL1*, *PER1*, and *PER2* and lowering the expression of *WEE1*. Similar to what was previously reported by Lanoix et al., we detected melatonin production in the human placenta (67). However, our results show that this production is sustained for at least 36 hours, suggesting a homeostatic role or protector against oxidative stress (31, 104) in the placenta that requires further investigation. These results support the existence of a circadian system–cell cycle interaction, modulated by the melatonin hormone. A graphical summary of the proposed mechanism is shown in Figure 8. This model may help explain how chronodisruption or the disruption of melatonin secretion could impact placental development and fetal health during pregnancy.

Our experimental limitation is that the explant culture-based approach assessed gene expression at the tissue level and did not directly measure functional cell cycle outcomes, such as those that occur with measurements of proliferation indices, BrdU incorporation, and flow cytometry. Future work should incorporate these readouts and include validation in human placental cell lines (e.g., BeWo and JEG-3) to define cell type-specific responses and determine whether melatonin suppresses clock gene expression at the cellular level. Another limitation is that we did not directly evaluate cell cycle progression or proliferation indices. This prevents us from linking the transcriptional changes of *WEE1* and other genes to functional outcomes. Future work should address this gap to strengthen the biological interpretation of our findings.

Data availability statement

The datasets presented in this study can be found in online repositories. The names of the repository/repositories and accession number(s) can be found in the article/supplementary material.

Ethics statement

The studies involving humans were approved by Ethics Committee of Herminda Martin Hospital (Chillan) and the University of the Bío-Bío. The studies were conducted in accordance with the local legislation and institutional requirements. The participants provided their written informed consent to participate in this study.

Author contributions

CV: Formal Analysis, Writing – original draft, Investigation, Conceptualization. KJ-M: Writing – review & editing, Formal Analysis. NC: Formal Analysis, Visualization, Writing – review & editing. GC-G: Writing – review & editing, Data curation, Software. CL: Formal Analysis, Methodology, Writing – review & editing. LL: Formal Analysis, Writing – review & editing. FV-M: Software, Funding acquisition, Writing – review & editing, Supervision, Writing – original draft, Formal Analysis, Project administration, Validation, Methodology, Conceptualization.

Funding

The author(s) declare financial support was received for the research and/or publication of this article. This study was funded by Conicyt 79112027 (Chile) and Beca Investigación Postgrado UBB-2015 (Chile).

Acknowledgments

We wish to highlight the valuable collaboration of Dr. Luis Lillo and Dr. Carlos Escudero for their help in the final experiments. Finally, we want to acknowledge the valuable technical assistance of Arlette Constenla and Sonia Nuñez.

Conflict of interest

The authors declare that the research was conducted in the absence of any commercial or financial relationships that could be construed as a potential conflict of interest.

Generative AI statement

The author(s) declare that no Generative AI was used in the creation of this manuscript.

Any alternative text (alt text) provided alongside figures in this article has been generated by Frontiers with the support of artificial intelligence and reasonable efforts have been made to ensure accuracy, including review by the authors wherever possible. If you identify any issues, please contact us.

Publisher's note

References

1. Matsuo T, Yamaguchi S, Mitsui S, Emi A, Shimoda F, Okamura H. Control mechanism of the circadian clock for timing of cell division *in vivo*. *Sci (New York N.Y.)*. (2003) 302:255–59. doi: 10.1126/science.1086271

2. Schibler U. Circadian rhythms. Liver regeneration clocks on. *Sci (New York N.Y.)*. (2003) 302:234–35. doi: 10.1126/science.1090810

3. Gengatharan A, Malvaut S, Marymonchyk A, et al. Adult neural stem cell activation in mice is regulated by the day/night cycle and intracellular calcium dynamics. *Cell*. (2021) 184:709–722.e13. doi: 10.1016/j.cell.2020.12.026

4. Lim GB. Surgery: circadian rhythms influence surgical outcomes. *Nat Rev Cardiol*. (2018) 15:5. doi: 10.1038/nrcardio.2017.186

5. Montaigne D, Marechal X, Modine T, et al. Daytime variation of perioperative myocardial injury in cardiac surgery and its prevention by rev-erbα Antagonism: A single-centre propensity-matched cohort study and a randomised study. *Lancet (London England)*. (2018) 391:59–69. doi: 10.1016/S0140-6736(17)32132-3

6. Kwon YS, Jang SU, Hwang SMI, Tark H, Kim JH, Lee JJ. Effects of surgery start time on postoperative cortisol, inflammatory cytokines, and postoperative hospital day in hip surgery: randomized controlled trial. *Medicine*. (2019) 98:e158205. doi: 10.1097/MD.0000000000015820

7. Ruby CL, Major RJ, Hinrichsen RD. "Regulation of tissue regeneration by the circadian clock. *Eur J Neurosci*. (2021) 53:3576–975. doi: 10.1111/ejn.15244

8. IARC Monographs Vol 124 group. Carcinogenicity of night shift work. *Lancet Oncol*. (2019) 20:1058–59. doi: 10.1016/S1470-2045(19)30455-3

9. Feillet C, van der Horst GTJ, Levi F, Rand DA, Delaunay F. Coupling between the circadian clock and cell cycle oscillators: implication for healthy cells and Malignant growth. *Front Neurol*. (2015) 6:96. doi: 10.3389/fneur.2015.00096

10. Arafa K, Emara M. Insights about circadian clock and molecular pathogenesis in gliomas. *Front Oncol*. (2020) 10:199. doi: 10.3389/fonc.2020.00199

11. Crespo M, Leiva M, Sabio G. Circadian clock and liver cancer. *Cancers*. (2021) 13:36315. doi: 10.3390/cancers13143631

12. Reid KJ, Abbott. SM. "Jet lag and shift work disorder. *Sleep Med Clinics*. (2015) 10:523–355. doi: 10.1016/j.jsmc.2015.08.006

13. Valenzuela FJ, Vera J, Venegas C, et al. Evidences of polymorphism associated with circadian system and risk of pathologies: A review of the literature. *Int J Endocrinol*. (2016) 2016:2746909. doi: 10.1155/2016/2746909

14. Liang Y, Wang S, Huang X, et al. Dysregulation of circadian clock genes as significant clinic factor in the tumorigenesis of hepatocellular carcinoma. *Comput Math Methods Med*. (2021) 2021:8238833. doi: 10.1155/2021/8238833

15. Wendeu-Foyet M, Cénée S, Koudou Y, et al. Circadian genes polymorphisms, night work and prostate cancer risk: findings from the EPICAP study. *Int J Cancer*. (2020) 147:3119–29. doi: 10.1002/ijc.33139

16. Bonmati-Carrion MA, Arguelles-Prieto R, Martinez-Madrid MJ, et al. Protecting the melatonin rhythm through circadian healthy light exposure. *Int J Mol Sci*. (2014) 15:23448–500. doi: 10.3390/ijms151223448

17. Valenzuela FJ, Torres-Farfan C, Richter HG, et al. Clock gene expression in adult primate suprachiasmatic nuclei and adrenal: is the adrenal a peripheral clock responsive to melatonin? *Endocrinology*. (2008) 149:1454–61. doi: 10.1210/en.2007-1518

18. Lu Q, Kim JY. Mammalian circadian networks mediated by the suprachiasmatic nucleus. *FEBS J*. (2021) 289(21):6589–604. doi: 10.1111/febs.16233

19. Finger A-M, Kramer A. Peripheral clocks tick independently of their master. *Genes Dev*. (2021) 35:304–6. doi: 10.1101/gad.348305.121

20. Sinturel F, Gos P, Petrenko V, et al. Circadian hepatocyte clocks keep synchrony in the absence of a master pacemaker in the suprachiasmatic nucleus or other extrahepatic clocks. *Genes Dev*. (2021) 35:329–34. doi: 10.1101/gad.346460.120

21. Finger A-M, Kramer A. Mammalian circadian systems: organization and modern life challenges. *Acta Physiol (Oxford England)*. (2021) 231:e135485. doi: 10.1111/apha.13548

22. Baydas G, Gursu MF, Cikim G, et al. Effects of pinealectomy on the levels and the circadian rhythm of plasma homocysteine in rats. *J Pineal Res*. (2002) 33:151–55. doi: 10.1034/j.1600-079x.2002.02901.x

23. Cassone VM. The pineal gland influences rat circadian activity rhythms in constant light. *J Biol Rhythms*. (1992) 7:27–40. doi: 10.1177/074873049200700103

24. Farias TdSM, de Oliveira AC, Andreotti S, et al. Pinealectomy interferes with the circadian clock genes expression in white adipose tissue. *J Pineal Res*. (2015) 58:251–61. doi: 10.1111/jpi.12211

25. Hartley S, Dauvilliers Y, Quera-Salva M-A. Circadian rhythm disturbances in the blind. *Curr Neurol Neurosci Rep*. (2018) 18:655. doi: 10.1007/s11910-018-0876-9

26. Liu J, Clough SJ, Hutchinson AJ, Adamah-Biassi EB, Popovska-Gorevski M, Dubocovich ML. MT1 and MT2 melatonin receptors: A therapeutic perspective. *Annu Rev Pharmacol Toxicol*. (2016) 56:361–83. doi: 10.1146/annurev-pharmtox-010814-124742

27. Matsumoto T, Hess DL, Kaushal KM, Valenzuela GJ, Yellon SM, Ducsay CA. Circadian myometrial and endocrine rhythms in the pregnant rhesus macaque: effects of constant light and timed melatonin infusion. *Am J Obstetrics Gynecol*. (1991) 165:1777–84. doi: 10.1016/0002-9378(91)90032-m

28. Meyer-Bernstein EL, Jetton AE, Matsumoto SI, Markuns JF, Lehman MN, Bittman EL. Effects of suprachiasmatic transplants on circadian rhythms of neuroendocrine function in golden hamsters. *Endocrinology*. (1999) 140:207–18. doi: 10.1210/endo.140.1.6428

29. Molinero P, Soutto M, Benot S, Hmadcha A, Guerrero JM. Melatonin is responsible for the nocturnal increase observed in serum and thymus of thymosin alpha1 and thymulin concentrations: observations in rats and humans. *J Neuroimmunol*. (2000) 103:180–88. doi: 10.1016/s0165-5728(99)00237-4

30. Paul MA, Gray GW, Lieberman HR, et al. Phase advance with separate and combined melatonin and light treatment. *Psychopharmacology*. (2011) 214:515–23. doi: 10.1007/s00213-010-2059-5

31. Valenzuela FJ, Vera J, Venegas C, Pino F, Lagunas C. Circadian system and melatonin hormone: risk factors for complications during pregnancy. *Obstetrics Gynecol Int*. (2015) 2015:825802. doi: 10.1155/2015/825802

32. Ko CH, Takahashi JS. Molecular components of the mammalian circadian clock. *Hum Mol Genet*. (2006) 15:R271–277. doi: 10.1093/hmg/ddl207

33. Murakami H, Nurse P. DNA replication and damage checkpoints and meiotic cell cycle controls in the fission and budding yeasts. *Biochem J*. (2000) 349:1–12. doi: 10.1042/bj3490001

34. Weissbein U, Benvenisty N, Ben-David U. Quality control: genome maintenance in pluripotent stem cells. *J Cell Biol*. (2014) 204:153–635. doi: 10.1083/jcb.201310135

35. Hunt T, Sassone-Corsi P. Riding tandem: circadian clocks and the cell cycle. *Cell*. (2007) 129:461–645. doi: 10.1016/j.cell.2007.04.015

36. Gérard C, Gonze D, Goldbeter A. Effect of positive feedback loops on the robustness of oscillations in the network of cyclin-dependent kinases driving the mammalian cell cycle. *FEBS J*. (2012) 279:3411–315. doi: 10.1111/j.1742-4658.2012.08585.x

37. Masri S, Cervantes M, Sassone-Corsi P. The circadian clock and cell cycle: interconnected biological circuits. *Curr Opin Cell Biol*. (2013) 25:730–345. doi: 10.1016/j.ceb.2013.07.013

38. Kelleher FC, Rao A, Maguire A. Circadian molecular clocks and cancer. *Cancer Lett*. (2014) 342:9–185. doi: 10.1016/j.canlet.2013.09.040

39. Zeng Z-L, Wu M-W, Sun J, et al. Effects of the biological clock gene bmal1 on tumour growth and anti-cancer drug activity. *J Biochem*. (2010) 148:319–26. doi: 10.1093/jb/mvq069

40. Rotmensch S, Celentano C, Elliger N, et al. Diurnal variation of human chorionic gonadotropin beta-core fragment concentrations in urine during second trimester of pregnancy. *Clin Chem*. (2001) 47:1715–17. doi: 10.1093/clinchem/47.9.1715

41. Díaz-Cueto L, Barrios-de-Tomasi J, Timossi C, Méndez JP, Ulloa-Aguirre A. More *In-Vitro* Bioactive, Shorter-Lived Human Chorionic Gonadotrophin Charge Isoforms Increase at the End of the First and during the Third Trimesters of Gestation. *Mol Hum Reprod*. (1996) 2:643–50. doi: 10.1093/molehr/2.9.643

42. Serón-Ferré M, Ducsay CA, Valenzuela GJ. Circadian rhythms during pregnancy. *Endocrine Rev*. (1993) 14:594–609. doi: 10.1210/edrv-14-5-594

43. Lee CK, Moon DH, Shin CS, et al. Circadian expression of mel1a and PL-II genes in placenta: effects of melatonin on the PL-II gene expression in the rat placenta. *Mol Cell Endocrinol*. (2003) 200:57–66. doi: 10.1016/s0303-7207(02)00414-8

44. Doridot L, Miralles F, Barbaux S, Vaiman D. Trophoblasts, invasion, and microRNA. *Front Genet*. (2013) 4:248. doi: 10.3389/fgene.2013.00248

45. Frost JM, Moore GE. The importance of imprinting in the human placenta. *PloS Genet*. (2010) 6:e10010155. doi: 10.1371/journal.pgen.1001015

46. Gillespie AM, Liyim D, Goepel JR, Coleman RE, Hancock BW. Placental site trophoblastic tumour: A rare but potentially curable cancer. *Br J Cancer*. (2000) 82:1186–90. doi: 10.1054/bjoc.1999.1061

47. Shoni M, Nagymanyoki Z, Vitonis AF, et al. P-21-activated kinase-1, -4 and -6 and estrogen receptor expression pattern in normal placenta and gestational trophoblastic diseases. *Gynecologic Oncol*. (2013) 131:759–63. doi: 10.1016/j.ygyno.2013.09.010

48. Kobayashi Y, Ye Z, Hensch TK. Clock genes control cortical critical period timing. *Neuron*. (2015) 86:264–755. doi: 10.1016/j.neuron.2015.02.036

49. Luiza JW, Taylor SE, Gao FF, Edwards RP. Placental site trophoblastic tumor: immunohistochemistry algorithm key to diagnosis and review of literature. *Gynecologic Oncol Case Rep*. (2014) 7:13–5. doi: 10.1016/j.gynor.2013.11.001

50. Frigato E, Lunghi L, Ferretti ME, Biondi C, Bertolucci C. Evidence for circadian rhythms in human trophoblast cell line that persist in hypoxia. *Biochem Biophys Res Commun*. (2009) 378:108–15. doi: 10.1016/j.bbrc.2008.11.006

51. Demarez C, Assis LVMD, Krohn M, et al. The trophoblast clock controls transport across placenta in mice. *Dev (Cambridge England)*. (2021) 148:dev197673. doi: 10.1242/dev.197673

52. Wharfe MD, Mark PJ, Waddell BJ. "Circadian variation in placental and hepatic clock genes in rat pregnancy. *Endocrinology*. (2011) 152:3552–605. doi: 10.1210/en.2011-0081

53. Akiyama S, Ohta H, Watanabe S, et al. The uterus sustains stable biological clock during pregnancy. *Tohoku J Exp Med*. (2010) 221:287–98. doi: 10.1620/tjem.221.287

54. Pérez S, Murias L, Fernández-Plaza C, et al. Evidence for clock genes circadian rhythms in human full-term placenta. *Syst Biol Reprod Med*. (2015) 61:360–66. doi: 10.3109/19396368.2015.1069420

55. Mark PJ, Crew RC, Wharfe MD, Waddell BJ. Rhythmic three-part harmony: the complex interaction of maternal, placental and fetal circadian systems. *J Biol Rhythms*. (2017) 32:534–495. doi: 10.1177/0748730417728671

56. Tamura H, Nakamura Y, Pilar Terron M, et al. Melatonin and pregnancy in the human. *Reprod Toxicol (Elmsford N.Y.)*. (2008) 25:291–303. doi: 10.1016/j.reprotox.2008.03.005

57. Lanoix D, Ouellette R, Vaillancourt C. Expression of melatoninergic receptors in human placental choriocarcinoma cell lines. *Hum Reprod (Oxford England)*. (2006) 21:1981–895. doi: 10.1093/humrep/del120

58. Soliman A, Lacasse AA, Lanoix D, Sagrillo-Fagundes L, Boulard V, Vaillancourt C. Placental melatonin system is present throughout pregnancy and regulates villous trophoblast differentiation. *J Pineal Res*. (2015) 59:38–465. doi: 10.1111/jpi.12236

59. Lanoix D, Beghdadi H, Lafond J, Vaillancourt C. Human placental trophoblasts synthesize melatonin and express its receptors. *J Pineal Res*. (2008) 45:50–605. doi: 10.1111/j.1600-079X.2008.00555.x

60. Clarkson-Townsend DA, Bales KL, Hermetz KE, Burt AA, Pardue MT, Marsit CJ. Developmental chronodisruption alters placental signaling in mice. *PloS One*. (2021) 16:e02552965. doi: 10.1371/journal.pone.0255296

61. Hong Y, Won J, Lee Y, et al. Melatonin treatment induces interplay of apoptosis, autophagy, and senescence in human colorectal cancer cells. *J Pineal Res*. (2014) 56:264–74. doi: 10.1111/jpi.12119

62. Talib WH. Melatonin and cancer hallmarks. *Molecules (Basel Switzerland)*. (2018) 23. doi: 10.3390/molecules23030518

63. Su S-C, Hsieh M-J, Yang W-E, Chung W-H, Reiter RJ, Yang S-F. Cancer metastasis: mechanisms of inhibition by melatonin. *J Pineal Res*. (2017) 62. doi: 10.1111/jpi.12370

64. Bejarano I, Redondo PC, Espino J, et al. Melatonin induces mitochondrial-mediated apoptosis in human myeloid HL-60 cells. *J Pineal Res*. (2009) 46:392–400. doi: 10.1111/j.1600-079X.2009.00675.x

65. Hill SM, Belancio VP, Dauchy RT, et al. Melatonin: an inhibitor of breast cancer. *Endocrine-Rel Cancer Endocrine-Rel Cancer*. (2015) 22:R183–204. doi: 10.1530/ERC-15-0030

66. Blask DE, Brainard GC, Dauchy RT, et al. Melatonin-depleted blood from premenopausal women exposed to light at night stimulates growth of human breast cancer xenografts in nude rats. *Cancer Res*. (2005) 65:11174–84. doi: 10.1158/0008-5472.CAN-05-1945

67. Lanoix D, Guérin P, Vaillancourt C. Placental melatonin production and melatonin receptor expression are altered in preeclampsia: new insights into the role of this hormone in pregnancy. *J Pineal Res*. (2012) 53:417–255. doi: 10.1111/j.1600-079X.2012.01012.x

68. Diallo A, Coiffard B, Desbriere R, et al. Disruption of the expression of the placental clock and melatonin genes in preeclampsia. *Int J Mol Sci*. (2023) 24:2363. doi: 10.3390/ijms24032363

69. Huang D, Sherman BT, Zheng X, et al. Extracting biological meaning from large gene lists with DAVID. *Curr Protoc Bioinf*. (2009) 13. doi: 10.1002/0471250953.bi1311s27

70. Huang D, Sherman BT, Lempicki RA. "Systematic and integrative analysis of large gene lists using DAVID bioinformatics resources. *Nat Protoc*. (2009) 4:44–575. doi: 10.1038/nprot.2008.211

71. Cemerikic B, Zamah R, Ahmed MS. Opioid tolerance in human placenta due to *in vitro* methadone administration. *J Pharmacol Exp Ther*. (1995) 273:987–94. doi: 10.1016/S0022-3565(25)09689-2

72. Thordarson G, Forsyth IA. Dopamine reduces the receptor binding activity and not the secretion rate of placental lactogen *in vitro*. *J Reprod Fertil*. (1984) 72:261–67. doi: 10.1530/jrf.0.0720261

73. Ilan J, Pierce DR, Hochberg AA, Folman R, Gyves MT. Increased rates of polypeptide chain elongation in placental explants from human diabetics. *Proc Natl Acad Sci United States America*. (1984) 81:1366–70. doi: 10.1073/pnas.81.5.1366

74. Nadri P, Ansari-Mahyari S, Jafarpour F, et al. Melatonin accelerates the developmental competence and telomere elongation in ovine SCNT embryos. *PloS One*. (2022) 17:e0267598. doi: 10.1371/journal.pone.0267598

75. Torres-Farfan C, Richter HG, Rojas-Garcia P, et al. Mt1 melatonin receptor in the primate adrenal gland: inhibition of adrenocorticotropin-stimulated cortisol production by melatonin. *J Clin Endocrinol Metab*. (2003) 88:450–58. doi: 10.1210/jc.2002-021048

76. Torres-Farfan C, Richter HG, Germain AM, et al. Maternal melatonin selectively inhibits cortisol production in the primate fetal adrenal gland. *J Physiol*. (2004) 554:841–56. doi: 10.1113/jphysiol.2003.056465

77. Torres-Farfan C, Valenzuela FJ, Mondaca M, et al. Evidence of a role for melatonin in fetal sheep physiology: direct actions of melatonin on fetal cerebral artery, brown adipose tissue and adrenal gland. *J Physiol*. (2008) 586:4017–27. doi: 10.1113/jphysiol.2008.154351

78. Martín M, Macías M, León J, Escames G, Khaldy H, Acuña-Castroviejo Daríos. Melatonin increases the activity of the oxidative phosphorylation enzymes and the production of ATP in rat brain and liver mitochondria. *Int J Biochem Cell Biol*. (2002) 34:348–575. doi: 10.1016/s1357-2725(01)00138-8

79. Roth JA, Rabin R, Agnello K. Melatonin suppression of PC12 cell growth and death. *Brain Res*. (1997) 768:63–705. doi: 10.1016/S0006-8993(97)00549-0

80. Chomczynski P, Nicoletta S. "Single-Step Method of RNA Isolation by Acid Guanidinium Thiocyanate-Phenol-Chloroform Extraction." *Analytical Biochemistry*. (1987) 162 (1):156–59. doi: 10.1016/0003-2697(87)90021-2

81. Filali S, Bergamelli C, Lamine Tall M, et al. Formulation, stability testing, and analytical characterization of melatonin-based preparation for clinical trial. *J Pharm Anal*. (2017) 7:237–43. doi: 10.1016/j.jpha.2017.04.001

82. Bates K, Herzog ED. Maternal-fetal circadian communication during pregnancy. *Front Endocrinol*. (2020) 11:198. doi: 10.3389/fendo.2020.00198

83. McCarthy R, Jungheim ES, Fay JC, Bates K, Herzog ED, England SK. Riding the rhythm of melatonin through pregnancy to deliver on time. *Front Endocrinol*. (2019) 10:616. doi: 10.3389/fendo.2019.00616

84. Galdames HA, Torres-Farfan C, Spichiger C, et al. Impact of gestational chronodisruption on fetal cardiac genomics. *J Mol Cell Cardiol*. (2014) 66:1–11. doi: 10.1016/j.yjmcc.2013.10.020

85. Roman E, Karlsson O. Increased Anxiety-like Behavior but No Cognitive Impairments in Adult Rats Exposed to Constant Light Conditions during Perinatal Development. *Upsala J Med Sci*. (2013) 118:222–75. doi: 10.3109/03009734.2013.821191

86. Fontanetti PA, Nervegna MT, Vermouth NT , Mandalunis PM. Prenatal exposure to continuous constant light alters endochondral ossification of the tibiae of rat pups. *Cells Tis Org*. (2014) 200:278–86. doi: 10.1159/000433520

87. Yajima M, Matsumoto M, Harada M, Hara H, Yajima T. Effects of Constant Light during Perinatal Periods on the Behavioral and Neuronal Development of Mice with or without Dietary Lutein. *Biomed Res (Tokyo Japan)*. (2013) 34:197–2045. doi: 10.2220/biomedres.34.197

88. Olcese JM. Melatonin and female reproduction: an expanding universe. *Front Endocrinol*. (2020) 11:85. doi: 10.3389/fendo.2020.00085

89. Dou Y, Lin B, Cheng H, et al. The reduction of melatonin levels is associated with the development of preeclampsia: A meta-analysis. *Hyperten Preg*. (2019) 38:65–72. doi: 10.1080/10641955.2019.1581215

90. Warren WC, Keisler DH, Anthony RV. Synthesis and secretion of ovine placental lactogen and its biochemical properties. *Domest Anim Endocrinol*. (1990) 7:331–42. doi: 10.1016/0739-7240(90)90039-3

91. Downing GJ, Maulik D, Poisner AM. Human chorionic gonadotropin stimulates placental prorenin secretion: evidence for autocrine/paracrine regulation. *J Clin Endocrinol Metab*. (1996) 81:1027–30. doi: 10.1210/jcem.81.3.8772570

92. Rajashekhar G, Loganath A, Roy AC, Wong YC. Expression and Localization of Angiogenin in Placenta: Enhanced Levels at Term over First Trimester Villi. *Mol Reprod Dev*. (2002) 62:159–66. doi: 10.1002/mrd.10116

93. Rubin LP, Yeung B, Vouros P, Vilner LM, Reddy GS. Evidence for human placental synthesis of 24,25-dihydroxyvitamin D3 and 23,25-dihydroxyvitamin D3. *Pediatr Res*. (1993) 34:98–104. doi: 10.1203/00006450-199307000-00023

94. Zheng J, Li Y, Weiss AR, Bird IM, Magness RR. Expression of endothelial and inducible nitric oxide synthases and nitric oxide production in ovine placental and uterine tissues during late pregnancy. *Placenta*. (2000) 21:516–24. doi: 10.1053/plac.1999.0504

95. Kudo Y, Boyd CA. The role of L-tryptophan transport in L-tryptophan degradation by indoleamine 2,3-dioxygenase in human placental explants. *J Physiol*. (2001) 531:417–23. doi: 10.1111/j.1469-7793.2001.0417i.x

96. Yamajuku D, Inagaki T, Haruma T, et al. Real-time monitoring in three-dimensional hepatocytes reveals that insulin acts as a synchronizer for liver clock. *Sci Rep*. (2012) 2. doi: 10.1038/srep00439

97. Hwang J-W, Sundar IK, Yao H, Sellix MT, Rahman I. Circadian clock function is disrupted by environmental tobacco/cigarette smoke, leading to lung inflammation and injury via a SIRT1-BMAL1 pathway. *FASEB J: Off Publ Fed Am Soc Exp Biol*. (2014) 28:176–945. doi: 10.1096/fj.13-232629

98. Torres-Farfan C, Mendez N, Abarzua-Catalan L, Vilches N, Valenzuela GJ, Seron-Ferre M. A circadian clock entrained by melatonin is ticking in the rat fetal adrenal. *Endocrinology*. (2011) 152:1891–900. doi: 10.1210/en.2010-1260

99. Chalmers JA, Martino TA, Tata N, Ralph MR, Sole MJ, Belsham DD. Vascular circadian rhythms in a mouse vascular smooth muscle cell line (Movas-1). *Am J Physiol Regul Integr Comp Physiol*. (2008) 295:R1529–1538. doi: 10.1152/ajpregu.90572.2008

100. Dardente H, Menet JérômeS, Poirel VJ, et al. Melatonin induces cry1 expression in the pars tuberalis of the rat. *Brain Res Mol Brain Res*. (2003) 114:101–6. doi: 10.1016/S0169-328X(03)00134-7

101. Campino C, Valenzuela FJ, Torres-Farfan C, et al. Melatonin exerts direct inhibitory actions on ACTH responses in the human adrenal gland. *Hormone Metab Res = Horm Und Stoffwechselforschung = Horm Et Métaboli*. (2011) 43:337–42. doi: 10.1055/s-0031-1271693

102. Gambardella A, Nagaraju CK, O'Shea PJ, et al. Glycogen synthase kinase-3α/β Inhibition promotes *in vivo* amplification of endogenous mesenchymal progenitors with osteogenic and adipogenic potential and their differentiation to the osteogenic lineage. *J Bone Min Res: Off J Am Soc Bone Min Res*. (2011) 26:811–21. doi: 10.1002/jbmr.266

103. Lee J, Kim M-S, Li R, et al. Loss of bmal1 leads to uncoupling and impaired glucose-stimulated insulin secretion in β-cells. *Islets*. (2011) 3:381–88. doi: 10.4161/isl.3.6.18157

104. Richter HG, Hansell JA, Raut S, Giussani DA. Melatonin improves placental efficiency and birth weight and increases the placental expression of antioxidant enzymes in undernourished pregnancy. *J Pineal Res*. (2009) 46:357–645. doi: 10.1111/j.1600-079X.2009.00671.x

frontiers | Frontiers in Endocrinology

TYPE Original Research
PUBLISHED 17 November 2025
DOI 10.3389/fendo.2025.1657453

OPEN ACCESS

EDITED BY
Leonardo Ermini,
University of Siena, Italy

REVIEWED BY
Dazhi Fan,
Foshan Women and Children Hospital, China
Tian Xia,
First Teaching Hospital of Tianjin University of Traditional Chinese Medicine, China

*CORRESPONDENCE
Fang Wang
ery_fwang@lzu.edu.cn

RECEIVED 01 July 2025
ACCEPTED 24 September 2025
PUBLISHED 17 November 2025

CITATION
Wei Y, Wei X, Mu F and Wang F (2025) Estradiol trajectories and early pregnancy loss: a retrospective study.
Front. Endocrinol. 16:1657453.
doi: 10.3389/fendo.2025.1657453

Estradiol trajectories and early pregnancy loss: a retrospective study

Yanling Wei, Xue Wei, Fangxiang Mu and Fang Wang*

Department of Reproductive Medicine, Lanzhou University Second Hospital, Lanzhou, China

Objective: To investigate the association between early pregnancy estradiol (E2) trajectory patterns and the risk of early miscarriage in women with natural conception.

Methods: This retrospective study included 527 women aged 18–45 years with natural conception and at least three E2 measurements within the first 12 gestational weeks, from March 2023 to August 2024. Group-based trajectory modeling identified four distinct E2 trajectories. Demographic and clinical data were extracted from medical records, and pregnancy outcomes were obtained through follow-up. Multivariate logistic regression and subgroup analyses were performed to evaluate the association between E2 trajectories and early miscarriage.

Results: Among the four identified E2 trajectories, women in Trajectory 3 ("High Level with Steady Increase") showed a significantly reduced risk of early miscarriage compared to those in Trajectory 2 ("Low Level with Slow Increase") (adjusted OR = 0.24, 95% CI: 0.12–0.46, $p < 0.001$). Subgroup analyses stratified by age and number of previous miscarriages confirmed the robustness of this association, while no significant associations were found for the other trajectories. The highest miscarriage rate (42.03%) and lowest baseline E2 level (300.29 ± 194.23) were observed in Trajectory 2.

Conclusion: A steadily increasing high estradiol trajectory in early pregnancy is associated with a lower risk of early miscarriage, highlighting the potential value of E2 monitoring for early pregnancy risk assessment.

KEYWORDS

early pregnancy estradiol, trajectory patterns, early miscarriage, natural conception, risk assessment

1 Introduction

Early pregnancy loss, especially miscarriage occurring within 12 weeks of gestation (1), is the most common form of pregnancy failure and severely impacts women's reproductive health and psychological well-being. Its etiology is complex and not yet fully understood (2, 3). In recent years, with the continuous advancement of assisted reproductive technologies and natural pregnancy management, there has been widespread attention on the

prevention and intervention of early pregnancy failure (4, 5). Estrogen hormones, particularly estradiol (E2), play a critical role in maintaining early pregnancy and embryonic development (6, 7). E2 not only directly affects the functional remodeling of the endometrium (8) to facilitate embryo implantation (9) but also participates in regulating the bioactivity of progesterone (10) to ensure a proper developmental environment for the embryo (11).

Although prior studies have found that serum E2 levels are generally lower in patients with miscarriage (12, 13), suggesting that E2 levels may be closely related to pregnancy outcomes, these studies mainly rely on static measurements at single or limited time points, which fail to reflect the dynamic trends of estradiol variation, thereby limiting the accuracy of predicting pregnancy outcomes. Estradiol levels during early pregnancy exhibit nonlinear changes and significant individual variability; thus, a single time-point measurement cannot fully reveal its comprehensive effects on the pregnancy process. Therefore, elucidating the specific trajectories of E2 changes in early pregnancy and their associations with miscarriage risk is crucial for early risk assessment and clinical intervention.

In recent years, group-based trajectory modeling (GBTM) has been applied in biomedical research to identify disease progression patterns and hormonal variation trends among potential subtypes (14–16). Compared with traditional cross-sectional analyses, GBTM can accurately capture diverse temporal change patterns within different subgroups, providing a powerful tool for studies in personalized medicine (17). Applying this method to analyze dynamic changes of estradiol during early pregnancy can not only reveal the dynamic structure of hormone levels but also clarify the relationship between different trajectory types and pregnancy outcomes, facilitating the identification of potential high-risk subgroups and optimization of clinical management protocols.

This study is based on the clinical retrospective data of naturally conceived patients from the Department of Reproductive Medicine, Lanzhou University Second Hospital. We established a dynamic trajectory model of estradiol changes measured at multiple points within the first 12 weeks of pregnancy. Using GBTM, we analyzed serum E2 level patterns in 527 patients and explored the associations between different trajectory groups and the risk of early pregnancy miscarriage.

2 Methods

2.1 Study population

This retrospective study included 1,865 outpatients who visited the Reproductive Center of the Department of Reproductive Medicine, Lanzhou University Second Hospital between March 2023 and August 2024. The inclusion criteria were (1): age between 18 and 45 years; and (2) natural conception. The exclusion criteria were as follows (1): chromosomal abnormalities in either spouse or embryo (2); congenital uterine malformations (such as septate uterus, unicornuate uterus, bicornuate uterus, or uterus didelphys) (3); multiple pregnancies; and (4) fewer than three estradiol measurements within the first 12 weeks of pregnancy. Ultimately, 527 patients meeting the criteria were included and categorized into four groups based on estradiol level trajectories: Group 1 (n=35), Group 2 (n=364), Group 3 (n=88), and Group 4 (n=40) (see Figure 1).

2.2 Data collection

Demographic variables were extracted from medical records and included maternal age, weight, height, age at menarche, menstrual regularity, and history of previous pregnancy loss. Body mass index (BMI) was calculated by dividing weight in kilograms by height in meters squared. The number of previous miscarriages was categorized into three groups: one, two, and three or more. Pregnancy outcomes were obtained through follow-up or review of hospital medical records.

2.3 Primary outcomes

Early pregnancy loss was defined as miscarriage occurring before 12 weeks of gestation, including biochemical pregnancies. Ongoing pregnancy was defined as continuation of pregnancy at 12 weeks gestation or later. Gestational age was calculated in weeks from the date of conception to the date of the outcome event.

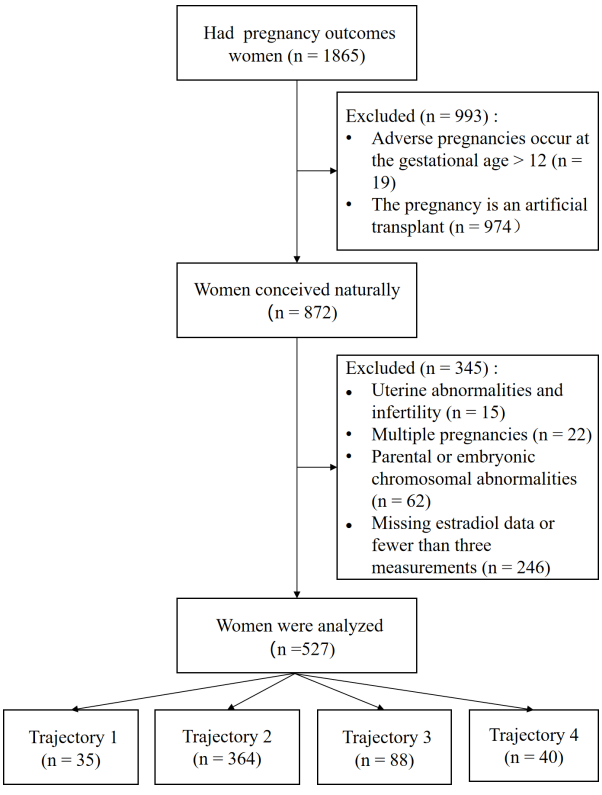

FIGURE 1
Flow chart.

2.4 Estradiol measurement

E2 levels were measured using a commercial automated electrochemiluminescence immunoassay system (DxI 800 Immunoassay System, Beckman Coulter, USA). All assays were performed by experienced technicians following the manufacturer's instructions precisely.

2.5 Statistical analysis

Sample size was estimated for a multiple logistic regression analysis. We aimed for 90% power to detect an OR of 0.24 at a two-sided α level of 0.05. The assumptions included a baseline event rate (pregnancy loss) of 42.03%, a 16.7% sample proportion for Trajectory Group 3, and an R-squared of 0.3 from other covariates. Based on these parameters, the calculation using PASS software yielded a required sample size of 286 participants. As our final cohort consisted of 527 patients, the study was adequately powered.

E2 level trajectories were modeled for the 527 patients using Group-Based Trajectory Modeling (GBTM) to identify latent subgroups with similar patterns of E2 changes. Trajectory shapes were explored using linear, quadratic, and cubic polynomial forms to capture different nonlinear trends. Gestational week was used as the time scale, and the number of trajectory groups was varied progressively from two to five. For each number of groups, models were initialized with parameters derived from the one-group model and run multiple times with random starting values to avoid convergence to local maxima.

The best-fitting model was selected based on the following criteria (1): minimum values of Akaike Information Criterion (AIC) and Bayesian Information Criterion (BIC) (2); average posterior probability (APP) greater than 0.70 for each group; and (3) minimum sample size of 5% in any trajectory group. Ultimately, a cubic polynomial model with four trajectory classes was chosen as the optimal fit. Model construction was performed using the "lcmm" package in R version 4.3.1.

Descriptive statistical analyses were conducted for the trajectory groups. Continuous variables were compared using the Kruskal-Wallis test or Student's t-test, while categorical variables were assessed by Chi-square test or Fisher's exact test and presented as counts (percentages). Further, multivariate logistic regression models were used to evaluate the association between E2 trajectory groups and pregnancy outcomes: Model 1 was unadjusted; Model 2 adjusted for age; Model 3 further adjusted for age, BMI, number of E2 measurements, and history of previous miscarriage. Subgroup analyses stratified by age and number of previous miscarriages were conducted to assess the consistency of these associations across different population characteristics.

All statistical analyses were performed using R software (version 4.3.1) and EmpowerStats (version 4.2). All hypothesis tests were two-sided, with a significance threshold set at $p < 0.05$.

3 Results

3.1 Baseline characteristics

The baseline characteristics of the 527 participants are presented in Table 1. All participants had at least three estradiol tests during early pregnancy. The cohort comprised 335 women with a 12-week ongoing pregnancy and 192 women with early

TABLE 1 Baseline characteristics of participant.

Characteristics	Total	Ongoing pregnancy	Pregnancy loss	*P*-value
N	527	335	192	
Age, years,mean ± SD	30.92 ± 3.72	30.54 ± 3.64	31.58 ± 3.77	**0.002**
Basic estradiol, pg/ml, mean ± SD	408.40 ± 378.61	408.62 ± 394.23	408.01 ± 350.70	0.986
BMI, kg/m2, mean ± SD	21.82 ± 3.01	21.57 ± 2.95	22.27 ± 3.07	**0.010**
Age at menarche, years, mean ± SD	13.02 ± 1.27	13.05 ± 1.27	12.97 ± 1.27	0.492
Count total occurrences, mean ± SD	8.07 ± 3.65	8.93 ± 3.59	6.57 ± 3.23	**<0.001**
Regularity of menstruation, n (%)				0.584
No	122 (23.15%)	75 (22.39%)	47 (24.48%)	
Yes	405 (76.85%)	260 (77.61%)	145 (75.52%)	
Previous miscarriage				**0.001**
1:1	199 (37.76%)	128 (38.21%)	71 (36.98%)	
2:2	205 (38.90%)	145 (43.28%)	60 (31.25%)	
3:≥3	123 (23.34%)	62 (18.51%)	61 (31.77%)	

SD, standard deviation; BMI, body mass index.
Bold values indicate statistical significance.

pregnancy loss. The overall mean age and mean age at menarche were 30.92 and 13.02 years, respectively. The two groups differed significantly in age, BMI, total number of measurements, and history of miscarriage ($p< 0.05$). All other baseline characteristics were comparable between the groups.

3.2 Identification of number of trajectories

Supplementary Table 1 summarizes the model fitting process for group-based trajectories with 1 to 5 latent classes using linear, quadratic, and cubic polynomial forms. Although the cubic model with five latent groups had the lowest Bayesian Information Criterion (BIC), one trajectory group included less than 5% of the sample. Therefore, the cubic model with four latent groups was selected as the optimal Group-Based Trajectory Model (GBTM). Supplementary Table 2 presents the comprehensive parameter estimates for the best-fitting four-class cubic trajectory model.

Based on the four estradiol trajectories shown in Figure 2, participants were classified into four groups:

Trajectory 1: "High Level with Sharp Increase" — characterized by a relatively high initial estradiol level, followed by a decline, and then a rapid increase in later stages.

Trajectory 2: "Low Level with Slow Increase" — characterized by consistently low estradiol levels with a gradual upward trend.

Trajectory 3: "High Level with Steady Increase" — characterized by an initial decline in estradiol levels followed by a faster rise reaching a relatively high level.

Trajectory 4: "Fluctuating Increase" — characterized by an estradiol level that rises initially, then falls, and rises again.

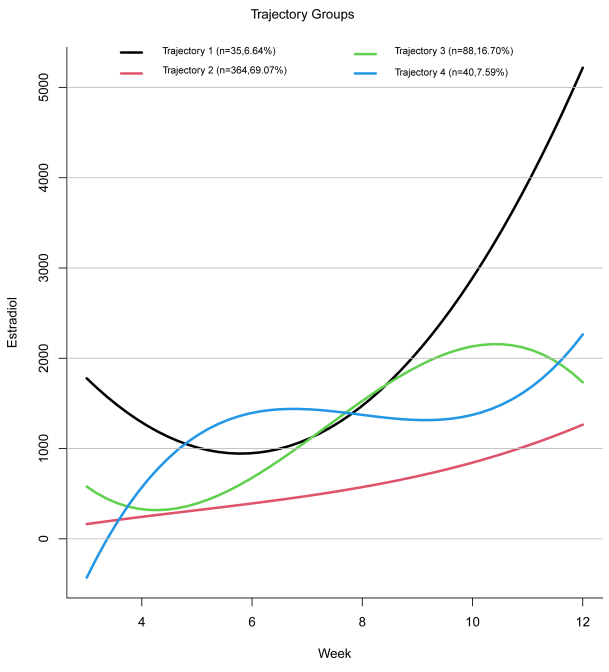

FIGURE 2
Mean trajectories of estradiol increasing.

3.3 Characteristics of trajectory subgroups

Table 2 presents the baseline characteristics of participants in each trajectory group. A total of 4,255 estradiol measurements were included in the study, distributed as follows: 259 measurements in Trajectory 1, 2,927 in Trajectory 2, 749 in Trajectory 3, and 320 in Trajectory 4. The four trajectory groups were similar in terms of age, BMI, age at menarche, number of measurements, and menstrual regularity. However, significant differences were observed among the groups in baseline estradiol levels and pregnancy outcomes. Compared with Trajectories 1, 3, and 4, Trajectory 2 showed the highest miscarriage rate (42.03%) and the lowest average baseline estradiol level (300.29 ± 194.23).

3.4 Association between estradiol trajectory groups and pregnancy outcomes

In the unadjusted Model 1, estradiol levels in Trajectory 3 were negatively associated with early miscarriage (OR = 0.26, 95% CI: 0.14–0.48, $p < 0.001$). This association remained significant after adjusting for age in Model 2 (OR = 0.26, 95% CI: 0.14–0.48, $p < 0.001$). In Model 3, which further adjusted for age, BMI, number of measurements, and number of previous miscarriages, no significant association was found between early miscarriage and Estradiol Trajectory 1 (OR = 0.74, 95% CI: 0.35–1.58, $p = 0.440$) or Trajectory 4 (OR = 0.49, 95% CI: 0.22–1.07, $p = 0.072$). However, the negative association between Trajectory 3 and early miscarriage remained significant, with the risk of miscarriage in Trajectory 3 being 0.24 times that of Trajectory 2 (OR = 0.24, 95% CI: 0.12–0.46, $p < 0.001$) (see Table 3).

3.5 Subgroup analysis

To assess whether the association between estradiol trajectories and pregnancy outcomes was consistent across different population characteristics, subgroup analyses were conducted stratified by age and number of previous miscarriages. Among participants aged 20–29 and 30–44 years, estradiol levels in Trajectory 3 were significantly negatively associated with early miscarriage ($p < 0.05$). Similarly, in participants with one or two previous miscarriages, Trajectory 3 estradiol levels showed a significant negative association with early miscarriage ($p < 0.05$), whereas other trajectory groups did not show significant associations. The subgroup analyses indicated no significant interaction effects of age or history of miscarriage on the relationship between estradiol trajectories and early miscarriage (p for interaction > 0.05) (see Supplementary Table 3).

4 Discussion

In this study of early pregnancies, we identified distinct patterns of serum E2 rise and found that they were associated with miscarriage risk. The trajectory characterized by high E2 levels with a steady rise

TABLE 2 Baseline characteristics of the total sample and the sample by the different trajectory groups.

Characteristics	Total (n = 527)	Trajectory 1 (n = 35)	Trajectory 2 (n = 364)	Trajectory 3 (n = 88)	Trajectory 4 (n = 40)	*P*-value
Total No.[b]	4255	259	2927	749	320	
Maternal age (years), mean ± SD	30.92 ± 3.72	31.89 ± 3.49	30.93 ± 3.70	30.76 ± 3.75	30.35 ± 3.93	0.326
Initial E2 (pg/ml), mean ± SD	408.40 ± 378.61	1036.25 ± 634.28	300.29 ± 194.23	422.76 ± 368.30	811.29 ± 546.90	**<0.001**
BMI (kg/m^2), mean ± SD	21.82 ± 3.01	22.01 ± 3.56	21.75 ± 2.99	22.31 ± 3.10	21.29 ± 2.39	0.272
Age at menarche (years), mean ± SD	13.02 ± 1.27	12.49 ± 1.12	13.00 ± 1.24	13.18 ± 1.24	13.32 ± 1.59	**0.018**
Total E2 assay, mean ± SD	8.07 ± 3.65	7.40 ± 2.33	8.04 ± 3.81	8.51 ± 3.44	8.00 ± 3.44	0.475
Regularity of menstruation, n (%)						0.076
Irregular	122 (23.15%)	13 (37.14%)	84 (23.08%)	14 (15.91%)	11 (27.50%)	
Regular	405 (76.85%)	22 (62.86%)	280 (76.92%)	74 (84.09%)	29 (72.50%)	
Number of previous pregnancy losses, n (%)						0.430
1	199 (37.76%)	10 (28.57%)	141 (38.74%)	37 (42.05%)	11 (27.50%)	
2	205 (38.90%)	14 (40.00%)	140 (38.46%)	35 (39.77%)	16 (40.00%)	
≥3	123 (23.34%)	11 (31.43%)	83 (22.80%)	16 (18.18%)	13 (32.50%)	
Pregnancy outcomes, n (%)						**<0.001**
Ongoing pregnancy	335 (63.57%)	21 (60.00%)	211 (57.97%)	74 (84.09%)	29 (72.50%)	
Pregnancy loss	192 (36.43%)	14 (40.00%)	153 (42.03%)	14 (15.91%)	11 (27.50%)	

SD, standard deviation; BMI, body mass index.
[b] Total number of estradiol assay.
Bold values indicate statistical significance.

(Trajectory 3) was associated with the lowest early miscarriage rate, whereas the low-level, slowly rising trajectory (Trajectory 2) carried the highest loss rate. This finding is novel in stratifying risk by dynamic endocrine profiles, and it underlines the critical importance of a robust estrogenic environment in early gestation.

4.1 High-level, steadily rising estradiol and low miscarriage risk

Women in Trajectory 3 – those with high initial estradiol and a sustained rise – had very favorable outcomes. This profile likely reflects an optimally functioning corpus luteum (CL) and timely luteal–placental transition. Early pregnancy estradiol is initially produced exclusively by the CL (18) and adequate levels indicate strong ovarian steroidogenic capacity (19, 20). A plentiful estradiol supply would also maintain progesterone secretion and placental growth factors, ensuring a healthy endocrine milieu (21, 22). In fact, predictive modeling in a separate Danish cohort showed estradiol to be the strongest serum predictor of viability, even outperforming hCG and progesterone (23). Taken together, these observations suggest that Trajectory 3 pregnancies experience the "normal" physiologic cascade of endometrial preparation and placentation, thereby minimizing loss.

Estradiol acts on the endometrium to promote proliferation and prepare for the secretory phase (24). In the proliferative (pre-

TABLE 3 The association of different trajectory with early pregnancy loss.

Trajectory	Model 1 OR (95% CI)	*P* value	Model 2 OR (95% CI)	*P* value	Model 3 OR (95% CI)	*P* value
Trajectory 2	ref		ref		ref	
Trajectory 1	0.92 (0.45, 1.87)	0.816	0.85 (0.42, 1.75)	0.667	0.74 (0.35, 1.58)	0.440
Trajectory 3	0.26 (0.14, 0.48)	**<0.001***	0.26 (0.14, 0.48)	**<0.001***	0.24 (0.12, 0.46)	**<0.001***
Trajectory 4	0.52 (0.25, 1.08)	0.080	0.54 (0.26, 1.12)	0.098	0.49 (0.22, 1.07)	0.072

OR, odds ratio; CI, confidence interval.
Asterisks indicate p values *P≤ 0.05.
Model 1: no adjusted.
Model 2: adjusted for age.
Model 3: adjusted for age, body mass index, total E2 assay, and number of previous pregnancy losses.

implantation) phase, estrogen induces mucosal growth and upregulates progesterone receptor expressionpmc (24). High, rising estradiol therefore primes the endometrium to respond fully to progesterone, a prerequisite for decidualization and implantation. Parisi et al. emphasize that even during the luteal phase, adequate estrogens are required to activate paracrine signaling for endometrial receptivity (25). By ensuring a thick, well-vascularized lining and sufficient progesterone sensitivity, Trajectory 3 pregnancies likely achieve optimal conditions for embryo embedding.

Furthermore, robust estradiol supports early placental angiogenesis and immune adaptation. Estrogen modulates angiogenic factor expression and helps remodel uterine natural killer (uNK) and T-helper cell function. Thus, a strong estradiol trajectory may foster a healthy, immune-tolerant microenvironment at the maternal-fetal interface (25). Altogether, the data indicate that Trajectory 3 represents a physiologically optimal endocrine pattern, and this aligns with the low observed miscarriage rate in this group.

4.2 Low-level, slowly rising estradiol and high miscarriage risk

In stark contrast, pregnancies following Trajectory 2 (low initial estradiol with a sluggish rise) showed the highest loss rate. This pattern likely reflects insufficient luteal support or failing trophoblast function. Low early estradiol has been repeatedly linked to miscarriage. In our cohort, the Trajectory 2 profile essentially replicates the endocrine state seen in many pregnancies that miscarry. Indeed, retrospective studies report that women with persistently low first-trimester estradiol have markedly elevated miscarriage rates. For example, Deng et al. (2022) found significantly lower mean E2 in women who miscarried versus those who did not (13). Likewise, Li et al. confirmed that low E2 values and poor E2 growth rates in the first trimester are strong warning signs of impending loss (26). The clinical importance of Trajectory 2 is underscored by interventional data. Boyle et al. observed that among women with low early pregnancy E2 (below the 50% percentile for gestational age), supplementing with dehydroepiandrosterone (DHEA) (which raises E2) significantly reduced miscarriage rates (27). In their cohort, untreated women with low estradiol had a 45.5% miscarriage rate, whereas those receiving DHEA (which boosted E2) had only a 17.5% loss rate. These findings imply that the high-risk Trajectory 2 does not merely mark failure, but may also be potentially modifiable by improving the hormonal milieu. In practice, our data suggest that patients in the low-E2 trajectory could benefit from closer surveillance or experimental therapies aimed at bolstering luteal steroidogenesis.

4.3 Findings from subgroup analyses

In this study, subgroup analyses were performed based on age and the number of previous miscarriages to explore the consistency of the association between estradiol trajectories and the risk of early miscarriage in different populations. The results showed that, regardless of the 20–29 or 30–44 years age groups, the estradiol pattern represented by Trajectory 3 (high level with steady increase) was significantly associated with a reduced risk of early miscarriage. Similarly, in subgroups with one or two previous miscarriages, the association between Trajectory 3 and lower risk of early miscarriage remained stable. These findings suggest that the predictive value of estradiol trajectory for early pregnancy outcomes is generally applicable and is not substantially affected by maternal age or previous history of miscarriage. Notably, no significant associations were observed for the other trajectory groups across different subgroups, further highlighting the unique protective effect of Trajectory 3. However, the sample size in some subgroups was limited, which may have reduced the statistical power.

4.4 Limitations

This study has several major limitations. First, as a single-center retrospective study, the sample consisted of outpatients from the Reproductive Center of the Department of Reproductive Medicine, Lanzhou University Second Hospital, which may have introduced selection bias, and the results have limited generalizability and may not be representative of a broader population. Second, although the inclusion and exclusion criteria were relatively strict, the clinical data relied on extraction from hospital electronic medical records, which may have resulted in incomplete information or inaccurate records. In addition, some confounding factors [such as lifestyle (28), smoking (28), diet (29), stress levels (30), vitamin D levels (28),and environmental exposures (31)] were not fully controlled in this study, which may have affected the relationship between estradiol trajectories and pregnancy outcomes. Third, since all participants conceived naturally and patients undergoing assisted reproductive technologies (such as IVF-ET) were not included, the findings may not be directly applicable to those populations. Fourth, the trajectory grouping resulted in a significant imbalance in sample sizes among the four groups. Future research should therefore employ a multi-center, large-sample prospective design to increase the sample size within each group. Fifth, there were individual differences in the number and timing of estradiol measurements, which may have influenced the accuracy of trajectory classification. While batch-level E2 intra- and inter-assay CVs were unavailable, which may constrain a completeassessment of analytical precision, the standardized Dxl 800 procedures and the physiologicallyplausible, directionally consistent links between E2 trajectories and early pregnancy outcomes offersome reassurance about result reliability. Finally, this study describes the association between E2 trajectories and miscarriage risk but lacks synchronous data on other biological markers (such as progesterone or placental growth factors), thus failing to clarify the specific biological pathways underlying this association. Future studies should use multicenter, large-sample, prospective cohort designs to further validate these findings and explore additional factors that may contribute to dynamic changes in estradiol during early pregnancy.

4.5 Conclusion

In summary, this study identified distinct estradiol trajectory patterns during early pregnancy and demonstrated that a high and steadily increasing estradiol level is associated with a significantly lower risk of early miscarriage. These findings highlight the potential value of monitoring estradiol dynamics for early pregnancy risk assessment. Further multicenter, prospective studies are needed to validate these results and explore the underlying mechanisms of estradiol's role in pregnancy outcomes.

Data availability statement

The original contributions presented in the study are included in the article/Supplementary Material. Further inquiries can be directed to the corresponding author.

Ethics statement

The studies involving humans were approved by The Ethics Committee of Lanzhou University Second Hospital (Approval No. 2019A-231). The studies were conducted in accordance with the local legislation and institutional requirements. The participants provided their written informed consent to participate in this study. Written informed consent was obtained from the individual(s) for the publication of any potentially identifiable images or data included in this article.

Author contributions

YW: Supervision, Conceptualization, Resources, Writing – original draft. XW: Methodology, Formal analysis, Data curation, Writing – original draft. FM: Validation, Visualization, Data curation, Writing – review & editing. FW: Writing – review & editing, Conceptualization.

Funding

The author(s) declare financial support was received for the research and/or publication of this article. This study was supported by the Science Foundation of Lanzhou University Second Hospital (Grant No. YJS-BD-19).

Conflict of interest

The authors declare that the research was conducted in the absence of any commercial or financial relationships that could be construed as a potential conflict of interest.

Generative AI statement

The author(s) declare that no Generative AI was used in the creation of this manuscript.

Any alternative text (alt text) provided alongside figures in this article has been generated by Frontiers with the support of artificial intelligence and reasonable efforts have been made to ensure accuracy, including review by the authors wherever possible. If you identify any issues, please contact us.

Publisher's note

Supplementary material

The Supplementary Material for this article can be found online at: https://www.frontiersin.org/articles/10.3389/fendo.2025.1657453/full#supplementary-material

References

1. Kim C, Barnard S, Neilson JP, Hickey M, Vazquez JC, Dou L. Medical treatments for incomplete miscarriage. *Cochrane Database Syst Rev*. (2017) 1:Cd007223. doi: 10.1002/14651858.CD007223.pub4

2. Bender Atik R, Christiansen OB, Elson J, Kolte AM, Lewis S, Middeldorp S, et al. ESHRE guideline: recurrent pregnancy loss: an update in 2022. *Hum Reprod Open*. (2023) 2023:hoad002. doi: 10.1093/hropen/hoad002

3. Quenby S, Gallos ID, Dhillon-Smith RK, Podesek M, Stephenson MD, Fisher J, et al. Miscarriage matters: the epidemiological, physical, psychological, and economic costs of early pregnancy loss. *Lancet*. (2021) 397:1658–67. doi: 10.1016/S0140-6736(21)00682-6

4. Haas DM, Hathaway TJ, Ramsey PS. Progestogen for preventing miscarriage in women with recurrent miscarriage of unclear etiology. . *Cochrane Database Syst Rev*. (2018) 10:Cd003511. doi: 10.1002/14651858.CD003511.pub4

5. Lim CE, Ho KK, Cheng NC, Wong FW. Combined oestrogen and progesterone for preventing miscarriage. *Cochrane Database Syst Rev*. (2013) 2013:Cd009278. doi: 10.1002/14651858.CD009278.pub2

6. Imudia AN, Goldman RH, Awonuga AO, Wright DL, Styer AK, Toth TL. The impact of supraphysiologic serum estradiol levels on peri-implantation embryo development and early pregnancy outcome following *in vitro* fertilization cycles. *J Assist Reprod Genet*. (2014) 31:65–71. doi: 10.1007/s10815-013-0117-8

7. Fatum M, Gyo Y, Diana P, Laufer N, Simon A. Is estradiol mandatory for an adequate follicular and embryo development? A mouse model using aromatase inhibitor (anastrozole). *J Assist Reprod Genet*. (2006) 23:407–12. doi: 10.1007/s10815-006-9089-2

8. Russo LA, Peano BJ, Trivedi SP, Cavalcanto TD, Olenchock BA, Caruso JA, et al. Regulated expression of matrix metalloproteinases, inflammatory mediators, and endometrial matrix remodeling by 17beta-estradiol in the immature rat uterus. *Reprod Biol Endocrinol*. (2009) 7:124. doi: 10.1186/1477-7827-7-124

9. Xie Y, Cui D, Kong Y. FoxM1 influences embryo implantation and is regulated by 17 beta-estradiol and progesterone in mouse uteri and endometrium cells. *Int J Clin Exp Pathol*. (2014) 7:6585–95.

10. Quadros PS, Wagner CK. Regulation of progesterone receptor expression by estradiol is dependent on age, sex and region in the rat brain. *Endocrinology*. (2008) 149:3054–61. doi: 10.1210/en.2007-1133

11. Haiyan L, Gang Y, Yu L, Lin L, Xiaoli C, Qingxue Z. Does serum progesterone level impact the ongoing pregnancy rate in frozen embryo transfer under artificial preparation with vaginal progesterone? Study protocol for a randomized controlled trial. *Trials*. (2022) 23:3. doi: 10.1186/s13063-021-05953-8

12. Su R, Wang Y, Lu Y, Lin B, An J. Weekly changes in serum β-human chorionic gonadotropin, estradiol, and progesterone levels for pregnancy assessment in women with unexplained recurrent miscarriage. *J Int Med Res*. (2025) 53:3000605251327478. doi: 10.1177/03000605251327478

13. Deng W, Sun R, Du J, Wu X, Ma L, Wang M, et al. Prediction of miscarriage in first trimester by serum estradiol, progesterone and β-human chorionic gonadotropin within 9 weeks of gestation. *BMC Pregnancy Childbirth*. (2022) 22:112. doi: 10.1186/s12884-021-04158-w

14. Grub J, Willi J, Süss H, Ehlert U. The role of estrogen receptor gene polymorphisms in menopausal symptoms and estradiol levels in perimenopausal women - Findings from the Swiss Perimenopause Study. *Maturitas*. (2024) 183:107942. doi: 10.1016/j.maturitas.2024.107942

15. Nagin DS, Odgers CL. Group-based trajectory modeling (Nearly) two decades later. *J Quant Criminol*. (2010) 26:445–53. doi: 10.1007/s10940-010-9113-7

16. Chien TY, Lee ML, Wu WL, Ting HW. Exploration of medical trajectories of stroke patients based on group-based trajectory modeling. *Int J Environ Res Public Health*. (2019) 16:3472. doi: 10.3390/ijerph16183472

17. Nagin DS. Group-based trajectory modeling: an overview. *Ann Nutr Metab*. (2014) 65:205–10. doi: 10.1159/000360229

18. Devoto L, Henríquez S, Kohen P, Strauss JF 3rd. The significance of estradiol metabolites in human corpus luteum physiology. *Steroids*. (2017) 123:50–4. doi: 10.1016/j.steroids.2017.05.002

19. Hamilton KJ, Arao Y, Korach KS. Estrogen hormone physiology: reproductive findings from estrogen receptor mutant mice. *Reprod Biol*. (2014) 14:3–8. doi: 10.1016/j.repbio.2013.12.002

20. Taghizabet N, Bahmanpour S, Fard NZ, Rezaei-Tazangi F, Hassanpour A, Nejad EK, et al. *In vitro* growth of the ovarian follicle: taking stock of advances in research. *JBRA Assist Reprod*. (2022) 26:508–21. doi: 10.5935/1518-0557.20210076

21. Trotter A, Kipp M, Schrader RM, Beyer C. Combined application of 17beta-estradiol and progesterone enhance vascular endothelial growth factor and surfactant protein expression in cultured embryonic lung cells of mice. *Int J Pediatr*. (2009) 2009:170491. doi: 10.1155/2009/170491

22. Jiang JY, Pan YY, Cui Y, Fan JF, Li Q, Yu SJ. Effects of estradiol and progesterone on secretion of epidermal growth factor and insulin-like growth factor-1 in cultured yak endometrial epithelial cells. *Tissue Cell*. (2018) 52:28–34. doi: 10.1016/j.tice.2018.03.008

23. Petersen JF, Friis-Hansen LJ, Bryndorf T, Jensen AK, Andersen AN, Løkkegaard E. A novel approach to predicting early pregnancy outcomes dynamically in a prospective cohort using repeated ultrasound and serum biomarkers. *Reprod Sci*. (2023) 30:3597–609. doi: 10.1007/s43032-023-01323-8

24. Yu K, Huang ZY, Xu XL, Li J, Fu XW, Deng SL. Estrogen receptor function: impact on the human endometrium. *Front Endocrinol*. (2022) 13:827724. doi: 10.3389/fendo.2022.827724

25. Parisi F, Fenizia C, Introini A, Zavatta A, Scaccabarozzi C, Biasin M, et al. The pathophysiological role of estrogens in the initial stages of pregnancy: molecular mechanisms and clinical implications for pregnancy outcome from the periconceptional period to end of the first trimester. *Hum Reprod Update*. (2023) 29:699–720. doi: 10.1093/humupd/dmad016

26. Li Y, Zhang J, Zhang K, Wang E, Shu J. Significance of dynamically monitoring serum estrogen and β-human chorionic gonadotropin in early pregnancy assessment. *J Clin Lab Anal*. (2021) 35:e23559. doi: 10.1002/jcla.23559

27. Boyle P, Andralojc K, van der Velden S, Najmabadi S, de Groot T, Turczynski C, et al. Restoration of serum estradiol and reduced incidence of miscarriage in patients with low serum estradiol during pregnancy: a retrospective cohort study using a multifactorial protocol including DHEA. *Front Reprod Health*. (2023) 5:1321284. doi: 10.3389/frph.2023.1321284

28. Lin S, Li J, Zhang Y, Song X, Chen G, Pei L. Maternal passive smoking, vitamin D deficiency and risk of spontaneous abortion. *Nutrients*. (2022) 14:3674. doi: 10.3390/nu14183674

29. Mu F, Liu L, Wang W, Wang M, Wang F. Dietary factors and risk for adverse pregnancy outcome: A Mendelian randomization analysis. *Food Sci Nutr*. (2024) 12:8150–8. doi: 10.1002/fsn3.4412

30. Wang Y, Meng Z, Pei J, Qian L, Mao B, Li Y, et al. Anxiety and depression are risk factors for recurrent pregnancy loss: a nested case-control study. *Health Qual Life Outcomes*. (2021) 19:78. doi: 10.1186/s12955-021-01703-1

31. Ha S, Sundaram R, Buck Louis GM, Nobles C, Seeni I, Sherman S, et al. Ambient air pollution and the risk of pregnancy loss: a prospective cohort study. *Fertil Steril*. (2018) 109:148–53. doi: 10.1016/j.fertnstert.2017.09.037

Frontiers in Endocrinology

Explores the endocrine system to find new therapies for key health issues

The second most-cited endocrinology and metabolism journal, which advances our understanding of the endocrine system. It uncovers new therapies for prevalent health issues such as obesity, diabetes, reproduction, and aging.

Discover the latest Research Topics

See more →

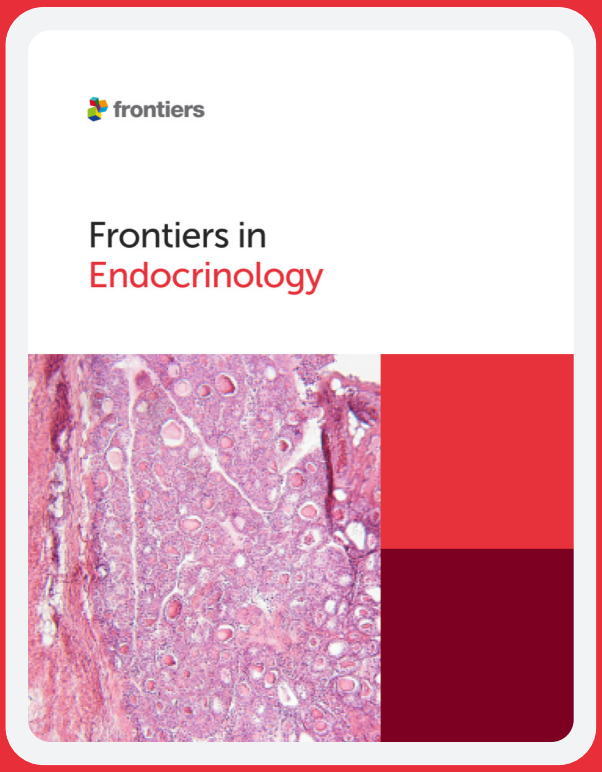

Frontiers

Avenue du Tribunal-Fédéral 34
1005 Lausanne, Switzerland
frontiersin.org

Contact us

+41 (0)21 510 17 00
frontiersin.org/about/contact